PEPTIDE NANOCONJUGATES FOR TISSUE DIAGNOSTICS AND MOLECULAR IMAGING

A Dissertation

Presented to

The Faculty of the Graduate School

At the University of Missouri-Columbia

In Partial Fulfillment

Of the Requirements for the Degree

Doctor of Philosophy

---

by

CHARLES W. CALDWELL, JR

Dr. Raghuraman Kannan, Doctoral Supervisor

DECEMBER 2016

The undersigned, appointed by the dean of the Graduate School, have examined the dissertation entitled

PEPTIDE NANOCONJUGATES FOR TISSUE

DIAGNOSTICS AND MOLECULAR IMAGING

presented by Charles W. Caldwell jr,

a candidate for the degree of doctor of philosophy

and hereby certify that, in their opinion, it is worthy of acceptance.

Professor Raghuraman Kannan

Professor Anandhi Upendran

Professor Jinglu Tan

Professor Li-Qun Gu

ACKNOWLEDGEMENTS

I would like to thank Dr. Kannan for his mentorship in research and ensuring his students are well prepared for their professional future. He encourages individual thinking and works with his group as a peer. Dr. Kannan ensures his students are included and given credit in all areas of research, including them in grant writing, pitch presentations, patent applications, and collaborative meetings. Dr. Kannan holds high standards for research and publication while also teaching students how to translate research in to marketable technologies. He continues to challenge his lab, department, and university to innovate.

I would also thank all my colleagues in Dr. Kannan's group for their friendship, help in improving my research methods, and helping with lab work: Dr. Anandhi Upendran, Dr. Henry White, Dr. Ajit Zambre, Dr. Soumavo Mukherjee, Dr. Abilash Gangula, Dhananjay Suresh, Shreya Ghoshdastidar, and Sairam Yadavilli.

I thank all my collaborators in the Department of Pathological and Anatomical Sciences: my former committee member Dr. Gerald Arthur, who I wish well in his retirement; Dr. Richard Hammer, who has provided invaluable clinical insights in pathology; Cory Johnson who aided me in gathering flow cytometry data.

I would like to thank my committee for overseeing my dissertation research and providing their insights. Dr. Upendran has been a second mentor in the lab, and has provided valuable opinion on my research and collaborated on a number of projects separate from my dissertation work. Dr. Gu has been an excellent researcher and professor in Biological

Engineering, and his courses taught me many of the methods I have applied in the nanotechnology field. Dr. Tan has been instrumental in overseeing my research under the Coulter Translational Partnership, which has funded all my work and continues to fund innovative projects at the University of Missouri. I also thank the rest of the Coulter Translational Partnership group for funding my research at the University of Missouri.

Table of Contents

Abstract

The rise of targeted therapy in cancer treatment has created a strong need for characterization of a patient's tumor before receiving treatment. Many effective cancer drugs are now being targeted to specific proteins present in the tumor, thus only patients who have tumors that express these proteins in appreciable amounts will respond to these kinds of therapy. The most popular method of diagnosing patients is through the practice of immunohistochemistry (IHC), where biopsied patient tissue is subjected to testing for specific protein expression. IHC works by incubating a primary antibody towards the target protein, followed by detection with a secondary antibody containing a reactive enzyme – most commonly, horseradish peroxidase (HRP). IHC procedures are expensive, comprises several steps, involves varying amounts of amplification due to enzyme reactivity, and is only as specific as the primary antibody. Patients receiving treatment using popular drugs targeted at common proteins such as EGFR, c-MET, and PD-L1 have shown varying degrees of responses based on initial IHC diagnosis, even when using FDA-approved diagnostic kits.

Due to the discrepancies seen between diagnosis and drug efficacy, we have developed new methods utilizing gold nanoparticles that utilize peptides to target protein biomarkers in human tissues. Peptides which are targeted towards receptors contain only the amino acid sequences which are sufficient for protein binding. Due to their tailored specificity, low cost, scalable production, and ease of modification, peptides can be an attractive method of investigating protein content in human tissues. We investigated the use of peptides combined with imaging agents as diagnostic methods to compare with standard immunohistochemistry procedures. Gold nanorods (GNR) scatter light efficiently in the dark field, and their high

surface-area-to-volume ratio allows each nanorod to be coated with many targeting peptides, enhancing specificity of each nanoparticle for the receptor of interest. We first investigated attachment of peptides to GNR that can be used to diagnose common biomarkers EGFR and c-MET in tumor tissues. EGFR is one of the most commonly overexpressed proteins in human cancers, and many EGFR-targeted drugs have shown improvement of progression-free survival in patients. During the course of EGFR-targeted treatment it is common that a patient will eventually develop resistance to the EGFR-targeted drugs. One such mechanism is the circumventing of EGFR pathway through upregulation of the c-MET protein on the tumor surface. Once EGFR is internalized and c-MET is the dominant pathway, patients will stop responding to EGFR-targeted drug and the tumor will continue proliferation. There are numerous c-MET drugs on the market for second or third line therapy when resistance occurs with this mechanism, however diagnosis of the c-MET biomarker has become controversial due to poor diagnostic results using the current standard IHC methods. We thus followed up our EGFR diagnostic study by investigating the c-MET protein using the same GNR platform with a c-MET-targeted peptide. The GNR-based histochemistry platform shows specificity for the targeted receptors in tumor cell lines and patient tissues, and is able to detect a range of protein expression, rather than relying on binary pathology grades of 1+,2+, or 3+ expression.

EGFR and c-MET are two popular biomarkers targeted by pharmaceuticals, and have seen recent success when combined with immune checkpoint inhibitors. The current surge in immuno-oncology has shown excellent response of patients to drugs that inhibit common immune checkpoints such as the interaction between immune receptor Programmed Death 1 (PD-1), expressed on immune cells, and its ligand, PD-L1, expressed on tumor cells. The binding

of PD-1 on T cells to PD-L1 on tumor cells will stop the T cells from destroying the tumor. Inhibition of immune checkpoints restore lost host immune function by allowing T-cells to recognize tumor cells as foreign. As with EGFR and c-MET, there has been much debate over whether current methods of diagnosing PD-L1 levels in patients are sufficient due to patient responses varying with respect to the diagnostic recommendation. We extended our peptide-based diagnostic method to investigate PD-L1 by analyzing the crystal structures of PD-L1 and PD-1 and synthesizing a peptide that is specific for the binding region of PD-L1. Using this sequence, we combined our PD-L1 peptide with a biotin molecule, to allow for conventional IHC, and a Cy5 fluorophore to conduct fluorescent investigations of PD-L1 levels in patient tumor tissues. When compared head-to-head with the current FDA-approved PD-L1 diagnostic standard, the peptide-based method shows high specificity for tumors in patient tissues that the FDA-approved diagnostic kits fail to recognize. Due to these results, we believe that peptide-based histochemistry can be used as a specific, cheap alternative to conventional antibody-based IHC.

1.0 Quantifiable Determination of EGFR in Human Tissues Using Peptide Conjugated Gold Nanorods

1.1 Introduction

The Epidermal Growth Factor Receptor (EGFR) is overexpressed on the cell membrane of a variety of malignant neoplasms, including colorectal adenocarcinoma, non-small cell lung carcinoma, head and neck carcinoma, and glioblastoma[1, 2]. EGFR is responsible for cell signaling that causes proliferation, and has been identified as an oncogene [3]. Many targeted anticancer therapeutic approaches are aimed at the inhibition of EGFR [4], such as the widely used EGFR inhibitor *Cetuximab*[5], which is currently used for treating colorectal carcinoma in humans. For any anti-EGFR therapy to be effective, precise determination of the EGFR expression levels within the cell membrane is important, since only EGFR-dependent (EGFR positive) tumors respond to these therapeutic approaches. [6, 7] Similarly, patients with tumors that do not express EGFR (EGFR negative) are more likely to be unaffected by the treatment [8]. Since the patient response to EGFR-targeted therapy depends on the levels of EGFR expressed in the tumor, accurate diagnosis of EGFR levels is crucial to the physician in order to make an appropriate therapeutic recommendation. Targeted therapies are expensive, and as a result many insurance companies have begun mandating EGFR testing before they will agree to reimburse the patient[9]. Currently, one of the most widely accepted method of patient diagnosis is through antibody-based immunohistochemistry (IHC). The antibody IHC method involves incubating the tissue first with a primary antibody, followed by detection using a secondary antibody specific to the primary. The secondary antibody is often conjugated to a substrate such as horseradish peroxidase that will react with the chromogen, 3, 3' Diethyl

aminobenzidine (DAB) to produce a visible color change that is interpreted and scored by pathologists. Due to many factors, including variable human interpretation, difficulty of digital interpretation, and variation of staining intensity, EGFR IHC has shown to be an unreliable method of diagnosis[10], with up to 70% difference in EGFR diagnosis based on the kit used.

In recent years, gold nanorods (GNRs) have been used as contrast agents for molecular imaging using technologies such as dark-field microscopy, near-infrared (NIR) transmission, photoacoustic tomography (PAT), two-photon excited luminescence (TPL), and surface-enhanced Raman spectroscopy (SERS) imaging[11]. In these techniques, GNRs are functionalized with receptor-specific proteins to create a contrast agent specific to the target of interest. Due to the high surface area to volume ratio of GNRs, many targeting molecules can be attached to the surface to enhance specificity [12]. Interestingly, metallic nanoparticles such as GNR have shown to scatter light up to 1,000 times more efficiently than quantum dots when viewed using dark field microscopy[13]. Due to the asymmetric illumination of dark field microscopy, non-spherical GNR can enhance this contrast more than their spherical counterparts[14]. Their shape can also allow for visualization using cross-polarized microscopy[15]. Due to the light-scattering properties of GNR and their ability to specifically target cellular receptors[16], we believe that GNR conjugated with target specific proteins can be used to evaluate biomarker levels in a method similar to IHC. Indeed, El Sayed *et al.* demonstrated the specificity and efficacy of EGFR-targeted gold nanorods for photothermal therapy in human cell lines[17]. To the best of our knowledge, utilization of GNR for identifying and quantifying receptors in tumor cells or tissues has not been attempted.

To design a GNR-based diagnostic imaging agent, we have conjugated a peptide (1070) with EGFR-avid properties to GNR functionalized with a polyethylene glycol (PEG) surface modification (Fig. 1). The binding sequence of 1070 is similar to GE-11 peptide, that has shown previous success in vivo EGFR targeting [18], but has been modified by addition of lysine residues and a short polyethylene glycol chain to improve solubility upon conjugation with gold nanorods. In our studies, we have performed systematic investigation to demonstrate GNR-1070 as a new class of IHC agent to identify EGFR expression in human tumor cells and tissues. GNR-1070 shows reliable success in diagnosing EGFR-expressing tumor cell lines and paraffin-embedded tissue sections obtained from patients. GNR-1070 staining in tissues was compared with current gold standard Dako's EGFR PharmDX™ kit in 14 human patients. The results show that GNR-based IHC can be a reliable class of agents for examining biomarker expression in human tumor tissues. Additionally, by applying digital imaging techniques to quantify EGFR levels by both IHC and GNR methods, we show that GNR is more robust than conventional IHC staining methods based on choice of arbitrary thresholds selected for quantification.

1.2 Experimental Methods

1.2.1 Synthesis of Gold Nanorods

Gold nanorods (GNR) of aspect ratio 3:4 were prepared using an established seed-mediated growth method with minor modifications[19]. All solutions were made in fresh deionized water (DI H_2O). A seed solution was prepared by making a 10mL solution of .1 M Cetyltrimethylammonium Bromide (CTAB, Sigma Aldrich). The CTAB solution was slightly heated until the CTAB had dissolved, giving a clear solution. 250 μL of a .01 M solution of

chlorauric acid ($HAuCl_4$, Sigma Aldrich) was then added to the CTAB solution while stirring. Immediately after addition of chlorauric acid, 600μL of ice-cold .01 M sodium borohydride ($NaBH_4$, Sigma Aldrich) was added to the solution, which changed color from gold to light brown. The seed solution was then left to stir for 5 minutes. While the seed solution stirred, 500 mL of growth solution was then prepared. The first step was to make 250mL of a .1 M CTAB solution, then heat until the CTAB had dissolved as had been done with the seed solution. 250 mL of .01 M chlorauric acid was then added to this CTAB solution and stirred lightly by hand. 10 mL of .0043 M silver nitrate ($AgNO_3$, Sigma Aldrich) was added to the solution and again stirred gently by hand. 4 mL of .1 M ascorbic acid (Sigma Aldrich) was then added, and the solution was stirred very gently until the solution had turned from gold-orange to clear. This completed the growth solution. 0.5 mL of the seed solution was then added in to the growth solution. The solution was left undisturbed after this point due to the delicate nature of the synthesis. Minutes later the solution turned from clear to purple, indicating the formation of GNR.

The GNR solution was left undisturbed for 24 hours, then washed of CTAB. The GNR solution was twice filtered through filter paper to remove excess CTAB. To further remove excess CTAB, the solution was centrifuged at 16,000 RPM for 10 minutes at 25^{o}C. The supernatant was removed and replaced with fresh DI H_2O. The centrifuging step was then repeated once. The sample of GNR was then characterized using UV-Vis spectroscopy (Fig. 1c, S1), TEM imaging (Fig. 1a), and zeta potential measurements (Fig 1b, S2).

1.2.2 Synthesis of PEGylated Gold Nanorods (GNR-PEG)

GNR was surface coated with thiolated polyethylene glycol (PEG_{750}, JenKem Technology USA) prior to functionalization with the 1070 peptide. A solution of PEG750 was added to the GNR

solution at a molar ratio of 1:2 (GNR: PEG750) and was allowed to stir for 24 hours. The solution was centrifuged at 16,000 RPM for 10 minutes at 25^{o}C. The supernatant was removed and replaced with fresh DI H_2O. After washing, GNR-PEG was then characterized by UV-Vis spectroscopy (Fig. 1c), TEM imaging (Fig. 1a), and zeta potential measurements (Fig.1b, S3).

1.2.3 Synthesis of Peptide-Conjugated Gold Nanorods (GNR-1070)

A solution of 1070 peptide (CPC Scientific) was then added to the GNR-PEG solution while stirring at a molar ratio of 1:1 GNR-PEG:1070 peptide. Molarity of GNR was calculated using the UV-Vis absorbance of the longitudinal peak. This solution was stirred for 24 hours to ensure maximum binding of peptide to the GNR surface, and was centrifuged at 16,000 RPM for 10 minutes at 25^{o}C. The supernatant was discarded and replaced with fresh DI H_2O. GNR-1070 was then characterized using UV-Vis spectroscopy (Fig. 1c), TEM (Fig. 1a), and Zeta potential measurements (Fig. 1b, S4). HPLC was performed to estimate the amount of peptide bound to GNR at 39.3% conjugation (S6-11). HPLC on peptides was performed using a C18 column (0.1% TFA in water, 0-100% Acetonitrile, 1.0ml/min). HPLC characterization of GNR compounds was performed using a Sepharose column (0.1% TFA in water, 0-100% Acetonitrile, 1.0ml/min).

1.2.4 Cell Line Growth and Treatment

After achieving 80% confluence, $5x10^5$ SKBr3 or WiDr cells (ATCC) were seeded on to coverslips in a six-well plate, and allowed to adhere overnight in media (DMEM) containing 10%FBS. Prior to treatment with the GNR-1070 compound, the wells were first washed with cold 1x PBS solution 3 times to remove the growth media. The cells were then fixed with 4% paraformaldehyde for 10 minutes at room temperature (RT), followed by 3 more 1x PBS

washes. 1.5 mL of a blocking buffer containing 1% BSA was added to each well and left alone for 1 hour at RT. For the wells that were pre-blocked, 2 mg/mL of 1070 peptide was added to the buffer solution and left for 1 hour at RT. The blocking buffer solution was washed with cold 1x PBS (3 times). To treat the cells with the GNR agents, 10-times diluted blocking buffer solution was added to each well. To these wells, 50 µL GNR-1070 or GNR-PEG (98.5 µg Au/mL; 0.5 absorbance, as measured by the longitudinal peak), was added. The plate was then left undisturbed for 2 hours at RT. After 2 hours, the nanorod solution was washed from the wells 5 times with cold 1x PBS. The coverslips were removed from the wells, and mounted on to glass slides using a mounting media containing fluorescent DAPI nuclear stain. The cell slides were then viewed at 40x magnification on a Cytoviva modified Olympus BX41 using dual-mode dark field and fluorescence channels to view GNR binding and DAPI-stained nuclei.

1.2.5 Preparation of Paraffin-Embedded Cell and Tissue Sections

Control slides included in the Dako PharmDX™ kit and EGFR-graded cell arrays provided by Eli Lilly and Co. were treated with either antibody or GNR-1070. The same procedure was done for paraffin-embedded tissue sections received from the MU OneHealth Biorepository (IRB project number 1210307). Paraffin was removed from the tissues by immersing in 100% Xylene for 5 minutes, then rehydrated in graded ethanol and finally DI H_2O. Once prepared for staining, control slides were either treated according to Dako's PharmDX™ Kit manual, or stained using GNR-1070. For GNR staining, the slides were treated with a 2.5% BSA solution for 10 minutes prior to addition of the nanorod solution. After washing, the slides were treated with GNR-1070 (5 µg Au/mL) solution in a humid chamber for 2 hours. After this time, the slides were washed

thoroughly with PBS and DI H2O. The slides were air dried and stained with DAPI. The GNR-1070 treated cell pellet slides were viewed at 40x magnification on a Cytoviva modified Olympus BX41 using dual-mode dark field and fluorescence channels to view GNR binding and DAPI-stained nuclei, while the DAKO stained slides were imaged using a conventional bright field microscope. GNR-1070 stained tissue sections were imaged on a Leica DM5500 using an overlay of DAPI and dark field channels at 20x magnification. Dako stained tissues were imaged in the bright field at 10x and 20x.

1.3 Results

1.3.1 Characterization of GNR, GNR-PEG and GNR-1070

After synthesis (Scheme 1), we confirm the formation of uniform gold nanorods of 3:4 aspect ratio using UV-Vis spectral analysis, zeta potential measurement, and TEM images. In UV spectral measurements, gold nanorods are identified by their characteristic 2-peak absorption spectrum. Due to the rod shape of the nanoparticle, we see a smaller transverse peak, which coincides with the 15 nm width of the nanorods, at around 540 nm. A second longitudinal peak, which varies based on the length of the gold nanorods, is seen for 50 nm long rods at around 780 nm. The zeta potential of a material measures surface charge of a colloid at the slipping plane. In the case of gold nanorods, the zeta potential is highly positive, usually +40mV or higher due to

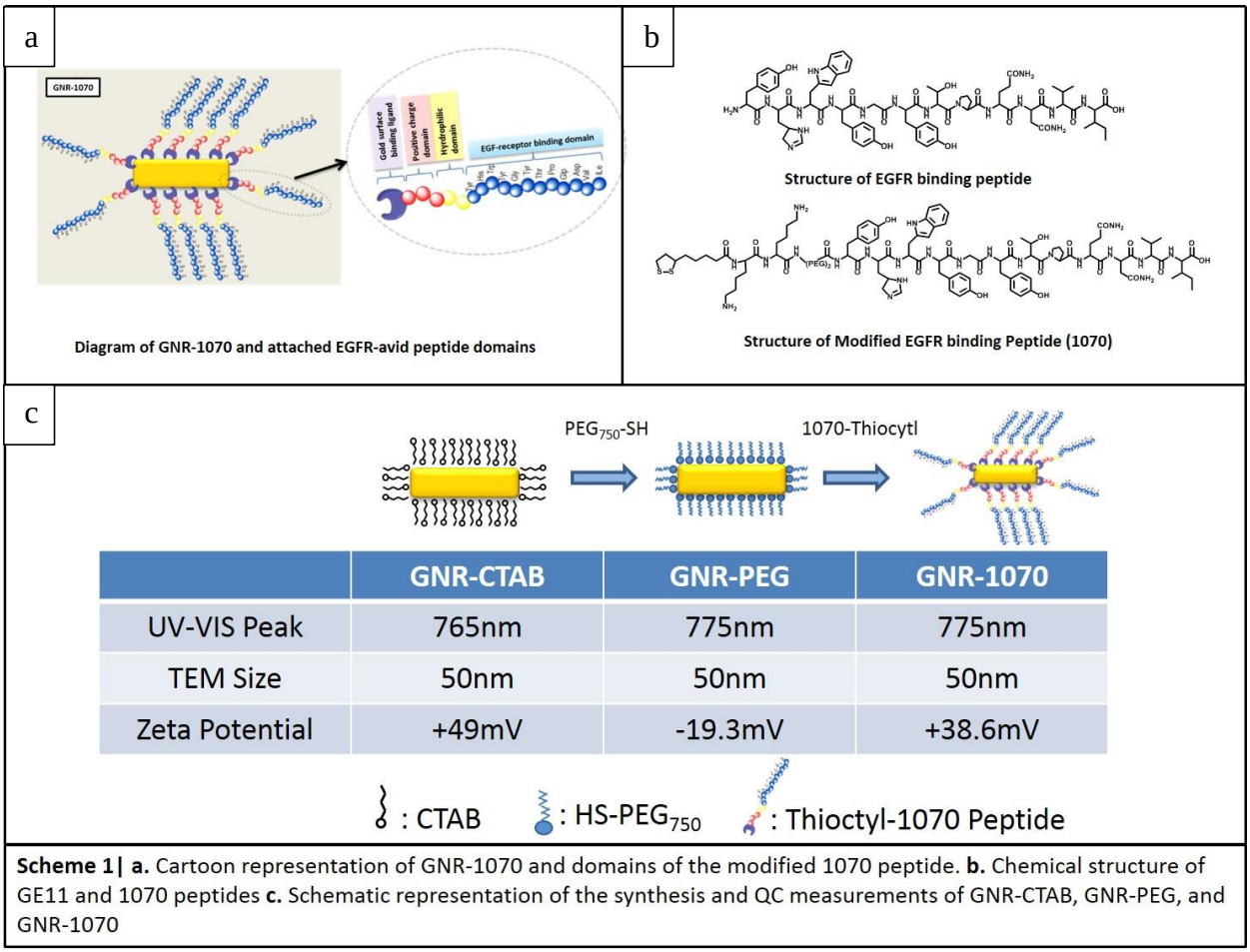

	GNR-CTAB	GNR-PEG	GNR-1070
UV-VIS Peak	765nm	775nm	775nm
TEM Size	50nm	50nm	50nm
Zeta Potential	+49mV	-19.3mV	+38.6mV

Scheme 1| a. Cartoon representation of GNR-1070 and domains of the modified 1070 peptide. **b.** Chemical structure of GE11 and 1070 peptides **c.** Schematic representation of the synthesis and QC measurements of GNR-CTAB, GNR-PEG, and GNR-1070

the presence of CTAB surfactant. TEM images confirm the presence of uniform gold nanorods. (Figure 1).

As an intermediate step in the conjugation of the 1070 peptide to GNR, we exchange the CTAB surfactant on the surface of the GNR with 750 KD polyethylene glycol (PEG_{750}) by utilizing thiol present at one end of the PEG chain, since sulfur has a known strong affinity for gold. The

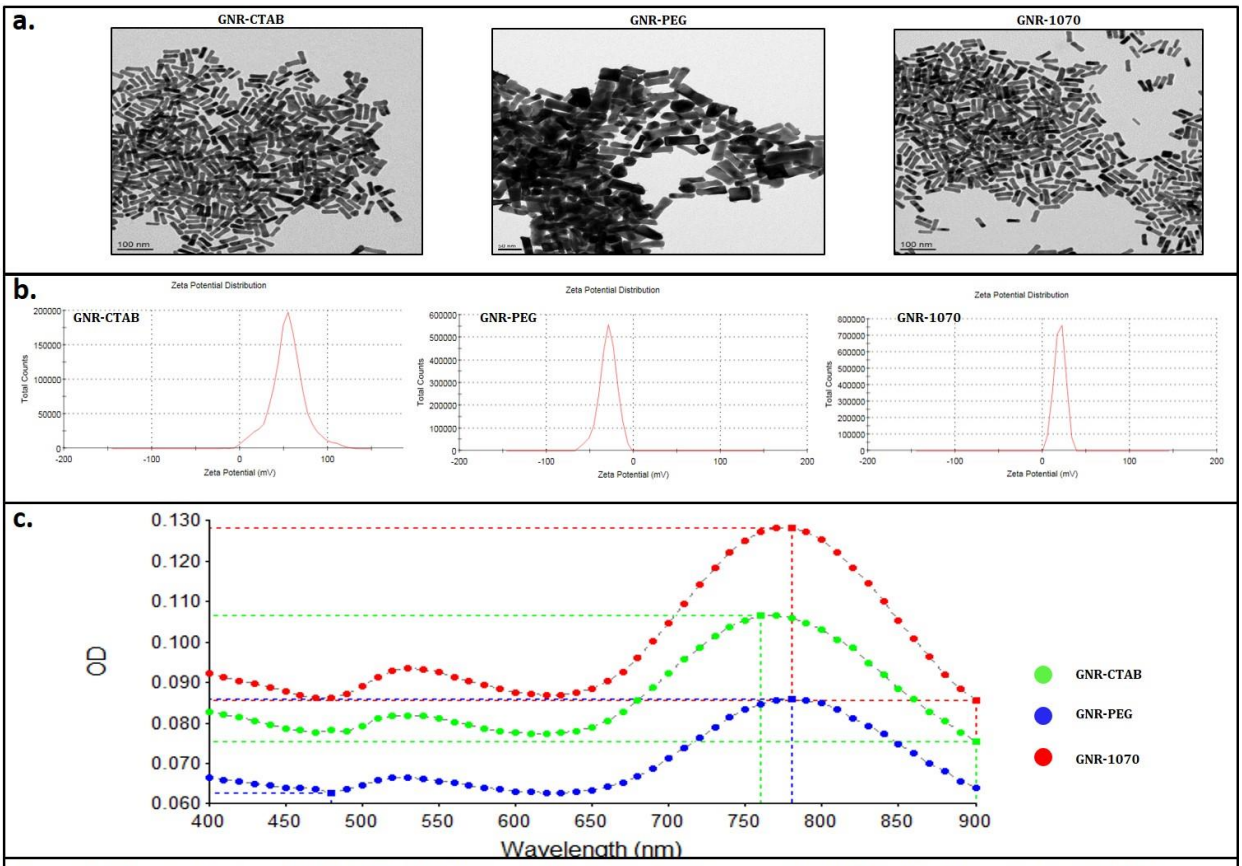

Figure 1 | Characterization of GNR-CTAB, GNR-PEG, and GNR-1070 a. TEM images of GNR-CTAB, GNR-PEG, and GNR-1070. **b.** Zeta potential of GNR-CTAB (+54.2 mV), GNR-PEG (-29.5 mV), and GNR-1070 (+19.6 mV) **c.** UV-Vis of GNR-CTAB, GNR-PEG, and GNR-1070

exchange of CTAB with PEG shifts the UV peaks only slightly, but the retention of two distinct peaks confirm that the nanorods still maintain their shape. The zeta potential measurement of GNR-PEG is the most reliable method of confirming the complete exchange of PEG for CTAB due to GNR-PEG having a characteristic negative zeta potential of -20mV or below, as seen in previous studies. Similar to the addition of PEG, the 1070 peptide was conjugated to the surface of GNR-PEG utilizing dithiol present in the 1070 peptide (Figure 1). The addition of 1070 peptide to the surface of GNR results in minimal change in UV-Vis peaks, however, the zeta potential changes to a positive value (15mV or higher). We further characterized the three constructs (GNR-CTAB, GNR-PEG, GNR-1070) using HPLC on a sepharose column; GNR-CTAB has the highest retention time of 16.1 minutes, followed by GNR-PEG at 15.5 minutes, and GNR-1070 at

15.3 minutes. The minimal change in retention time between GNR-PEG and GNR-1070 is anticipated, as the surface molecules are similar on both constructs, thus the size of the compound does not change much. We also used HPLC using a C18 column to compare the naked peptide retention time of 13.3 minutes with that of the bound construct. Using these methods of characterization as quality control, we confirm that GNR functionalized with PEG and EGFR-targeting peptide 1070 can be reproducibly synthesized. An accelerated stability study of GNR-1070 was performed resuspension of the conjugate in NaCl, BSA, HSA, Cysteine, Histidine, and 1x PBS and measuring UV and zeta potential at 1hr, 24hr, and 48hr (S12, S13). Appropriate staining of EGFR using GNR-1070 was seen after storage of GNR-1070 in -80°C for 6 months and 1 year time periods. GNR-1070 is stable in solutions of water, PBS, and BSA for 6 months-1 year.

1.3.2 EGFR Targeting in Fixed Cell Lines – SKBr3, WiDr, MCF-7

Specific binding of GNR-1070 to the EGF receptor was investigated in human cell lines purchased from ATCC. Cell lines with varying degrees of EGFR on the surface were chosen for this study. The SKBr3 cell line was the first cell line selected due to previously reported overexpression of the EGF receptor in this cell line[20]. A moderate EGFR-expressing colorectal cell line, WiDr[21], was compared to that of SkBr3. MCF-7 cells which do not express EGFR at a meaningful level were also included as negative control[22]. To examine specificity and efficacy, cell lines grown on coverslips were treated with GNR-1070 agent in a six-well plate for 2 hours. As controls, the remaining wells were either pre-blocked with free 1070 peptide, or incubated with GNR-PEG, which does not contain the EGFR-targeting 1070 peptide (S17-23). We used a

combination of dark field microscopy and fluorescence to visualize GNR and the DAPI-stained cell nuclei. We further confirmed the presence of GNR using hyperspectral imaging and identifying characteristic spectrum of GNR (S24-27). The samples treated with

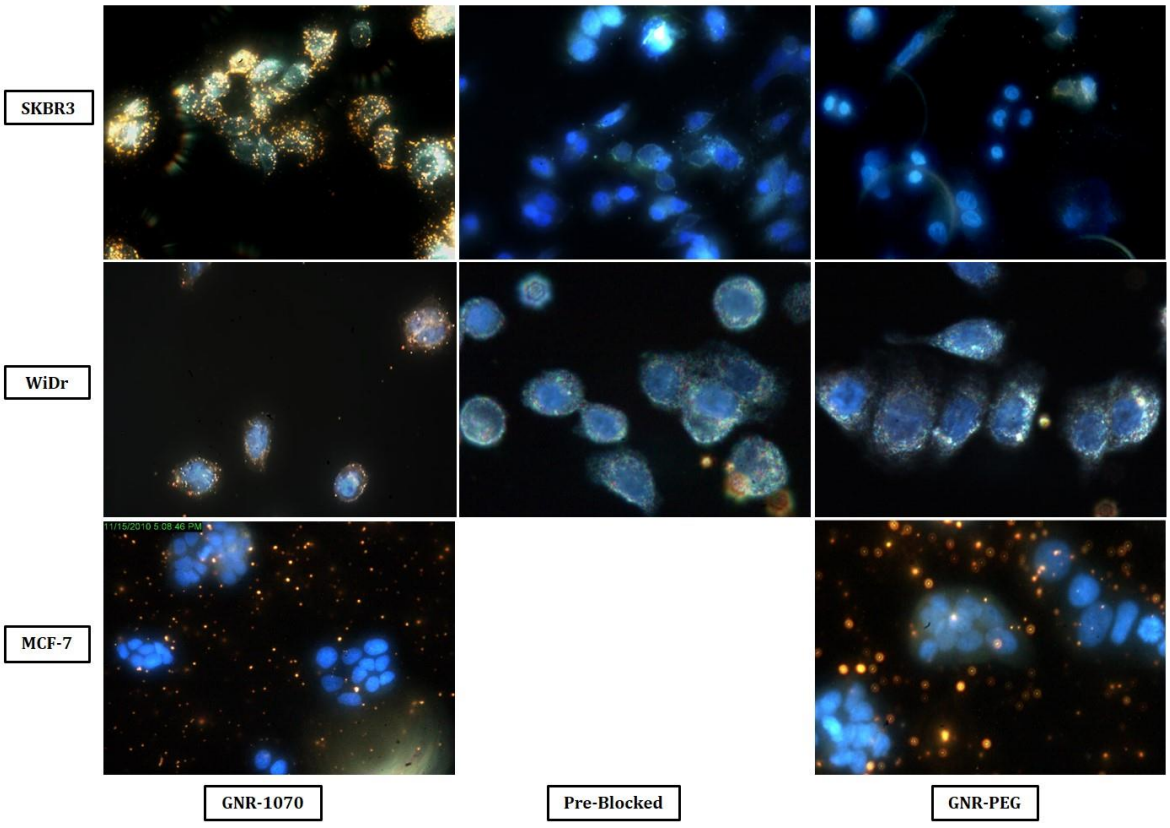

Figure 2 | GNR-1070 binds EGFR-expressing cell lines. EGFR-expressing cell lines SkBr3 (top) and WiDr fixed and incubated with GNR-1070 for 2h. As controls, cell lines were also pre-blocked with 1070 peptide before treatment (middle) and treated with non-targeted GNR-PEG (right). Also shown is negative control line MCF-7, which does not overexpress EGFR

GNR-1070 showed a high localization of gold nanorods on the membranes of the SKBr3 cells, with little background gold signals (Figure 2). In contrast, those cell samples that were pre-blocked with 1070 peptide or treated with GNR-PEG showed little affinity for the cells, and most bright signals can be attributed to non-specific binding of GNR. This experiment was repeated using the colon cell line WiDr, which shows moderate EGFR expression. As expected, less binding of GNR-1070 was observed in the WiDr cells compared to SKBr3, however both cell lines showed little to no gold signals when pre-blocked or treated with GNR-PEG. The MCF-7

lines showed no meaningful surface binding of GNR-1070 as expected. Due to the negative results from the unblocked treatment, MCF-7 was not used in blocking studies. Based on the results from the cell lines, we confirm that GNR-1070 is specific for EGFR, and binds to membranes at varying levels based on the amount of EGFR protein expressed on the surface of the cells.

1.3.3 EGFR Targeting in Paraffin-Embedded Cell Lines

To establish use of GNR-1070 for EGFR detection in histological samples, the specificity in paraffin-embedded cell lines was examined. The FDA-approved Dako EGFR PharmDX™ Kit for EGFR IHC contains paraffin-embedded control slides that stain for EGFR expression. The cell lines on these slides are HT-29, a WiDr derivative which stains as 2+ for EGFR according to Dako, and CAMA-1, which stains lightly, but not enough to warrant an EGFR diagnosis (EGFR 0). We examined the staining of GNR-1070 compared to Dako's own PharmDX™ IHC on these control slides (Figure 3). In the HT-29 section, the staining is much more intense with both Dako and GNR-1070 (Figure 3a, b). In the CAMA-1 cell section, light staining can be seen with both GNR-1070 as well as with the Dako IHC stain (Figure 3c, d). The gold signal is much brighter in the HT-29 section, and more clusters of GNR are seen than in the treated CAMA-1. As controls, the HT-29 samples were either treated with non-specific GNR-PEG, or pre-blocked with 1070

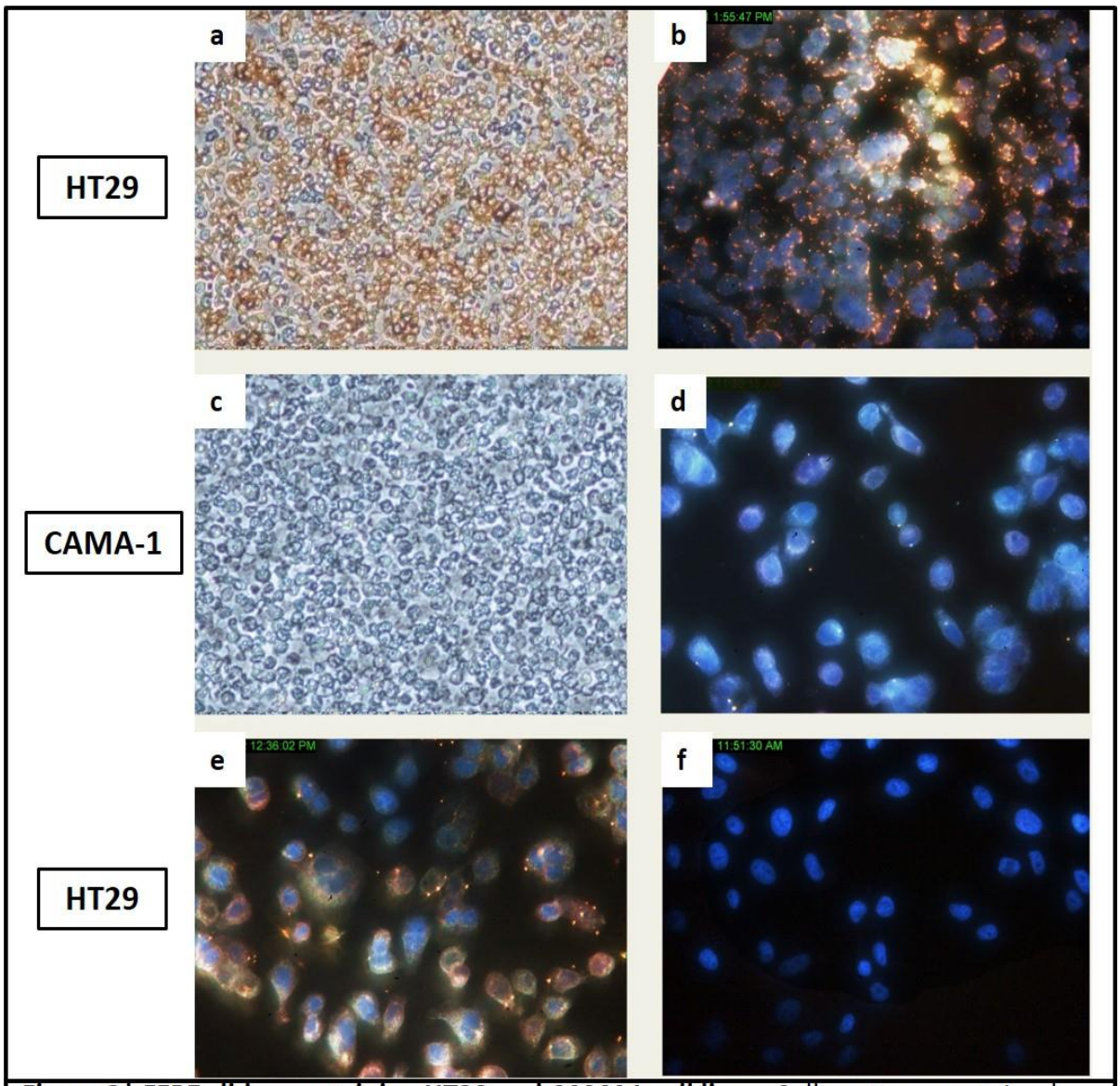

Figure 3| FFPE slides containing HT29 and CAMA1 cell lines. Cell spots were stained with Dako PharmDx (**a,c**) or GNR-1070 (**b,d**) according to established protocols. EGFR-positive cell line HT29 was also blocked with 1070 peptide before treatment (**e**) and treated with nonspecific GNR-PEG (**f**)

peptide and then treated with targeted GNR-1070 (Figure 3e, f). Each control sample only shows non-specific gold signals, with only a small amount of surface binding in the pre-blocked group.

To further validate and quantify GNR-1070 binding in paraffin-embedded cell lines, GNR-1070 was used to stain paraffin-embedded EGFR cell arrays provided by Eli Lilly and Company's

Diagnostic and Experimental Pathology department (S28-30). These cell arrays contain cell samples previously graded internally at Lilly labs as being EGFR 1+, 2+, and 3+ based on internal methods. These samples were treated with GNR-1070 using the method previously

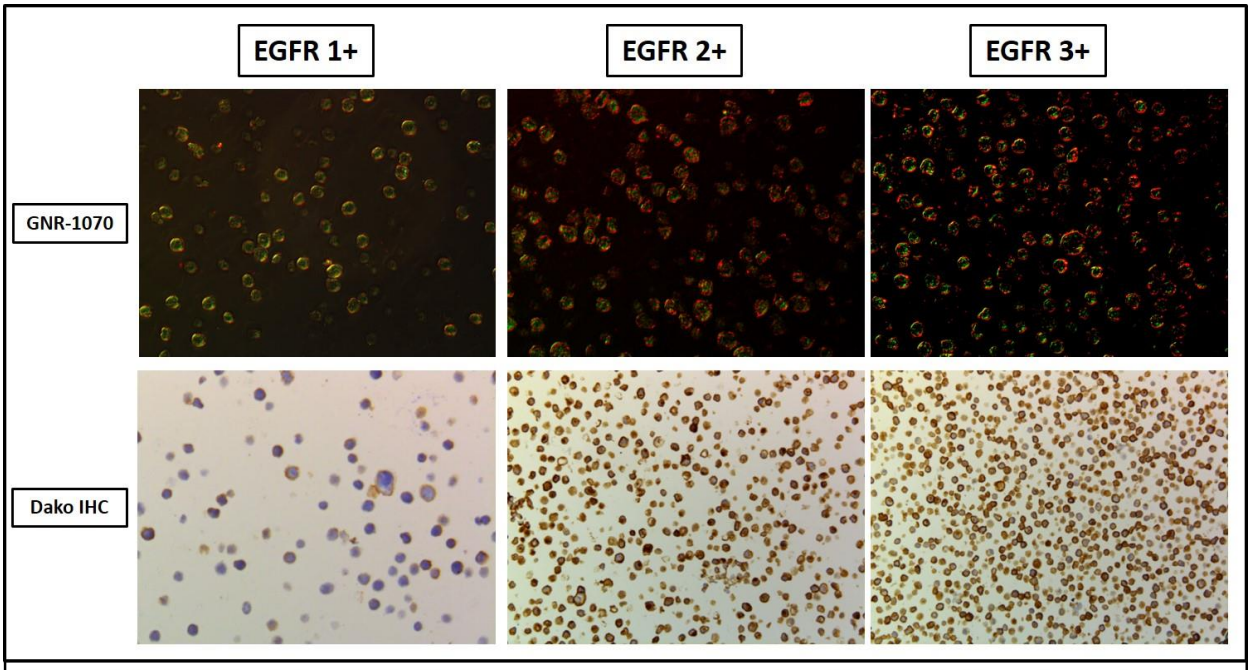

Figure 4| Dako and GNR staining of EGFR Cell Line Array. Analysis of EGFR-expressing cell lines obtained from Lilly Labs shows that EGFR levels can be quantified with the GNR-1070 EGFR stain. Cell lines ranging from 1+ to 3+ EGFR expression were stained with either Dako PharmDx Kit or GNR-1070

established with the Dako control slides (Figure 4). In this case, we did not stain nuclei with fluorescence in order to refine our image analysis. As expected, the expression of gold nanorods on the cell membranes increased with the grading of EGFR levels. The correlation of GNR expression and histological grade in these samples was evaluated using image analysis to quantify GNR signals. Images of each stained EGFR cell line were analyzed on a per-cell basis by finding the boundaries of cell nuclei and counting the number of Red/Green pixels associated with each nucleus (S31-37). Arranging the samples by EGFR grade on a log scale of relative pixels per cell shows a linear increase in the number of GNR-related pixels as the grading of

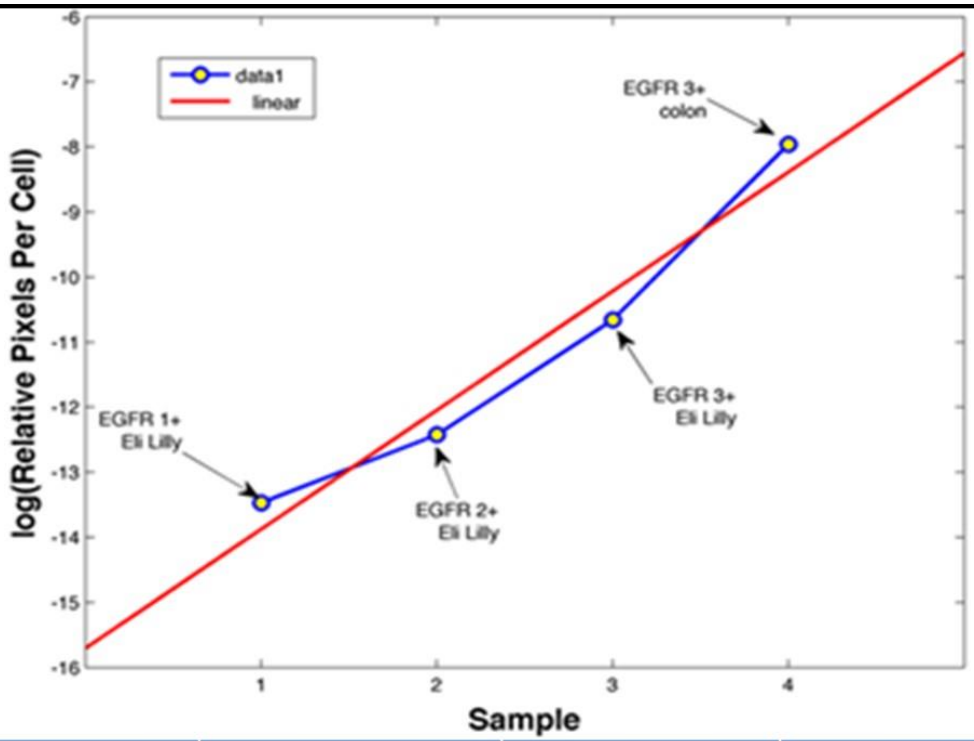

Parameter	EGFR 1+	EGFR 2+	EGFR 3+
Number of nuclei	128	199	271
RG pixels total	892	3,935	27,835
RG pixels/ nucleus	6.97	19.8	102.7
Mean nuclear area	3,198	3,486	2,993
Median nuclear area	2,192	1,039	2,091

Figure 5| Analysis of EGFR Cell Line Array. Analysis of EGFR-expressing cell lines obtained from Lilly Labs shows that EGFR levels can be quantified with the GNR-1070 EGFR stain. Cell lines ranging from 1+ to 3+ EGFR expression were stained with GNR-1070 and analyzed by RG pixels/nucleus and show a meaningful increase in GNR staining as EGFR levels increase.

EGFR increases (Figure 5). The plot allows us to examine EGFR expression on a per-cell basis and analyze the amount of protein present in any given field of view. The correlation between nanorods present and EGFR pathology grade establishes a basis for grading nanorod-based immunohistochemistry in human tissues. This method is not limited to integer values of 1+,2+, and 3+, but rather can distinguish any number of EGFR expression within the diagnostic ranges.

1.3.4 Efficacy in Paraffin-Embedded Human Tissues

Once confidence in EGFR staining was established for paraffin-embedded cell lines, a comparison between GNR-1070 and gold standard Dako EGFR PharmDX™ staining was performed using paraffin-embedded tissue sections acquired from the Mizzou One Health Biorepository (S39-56). These studies were conducted after obtaining proper IRB approval (number). Serial Sections of ten colorectal patient samples were quantified using Dako's EGFR PharmDX™ kit to examine EGFR levels and compared with GNR-1070

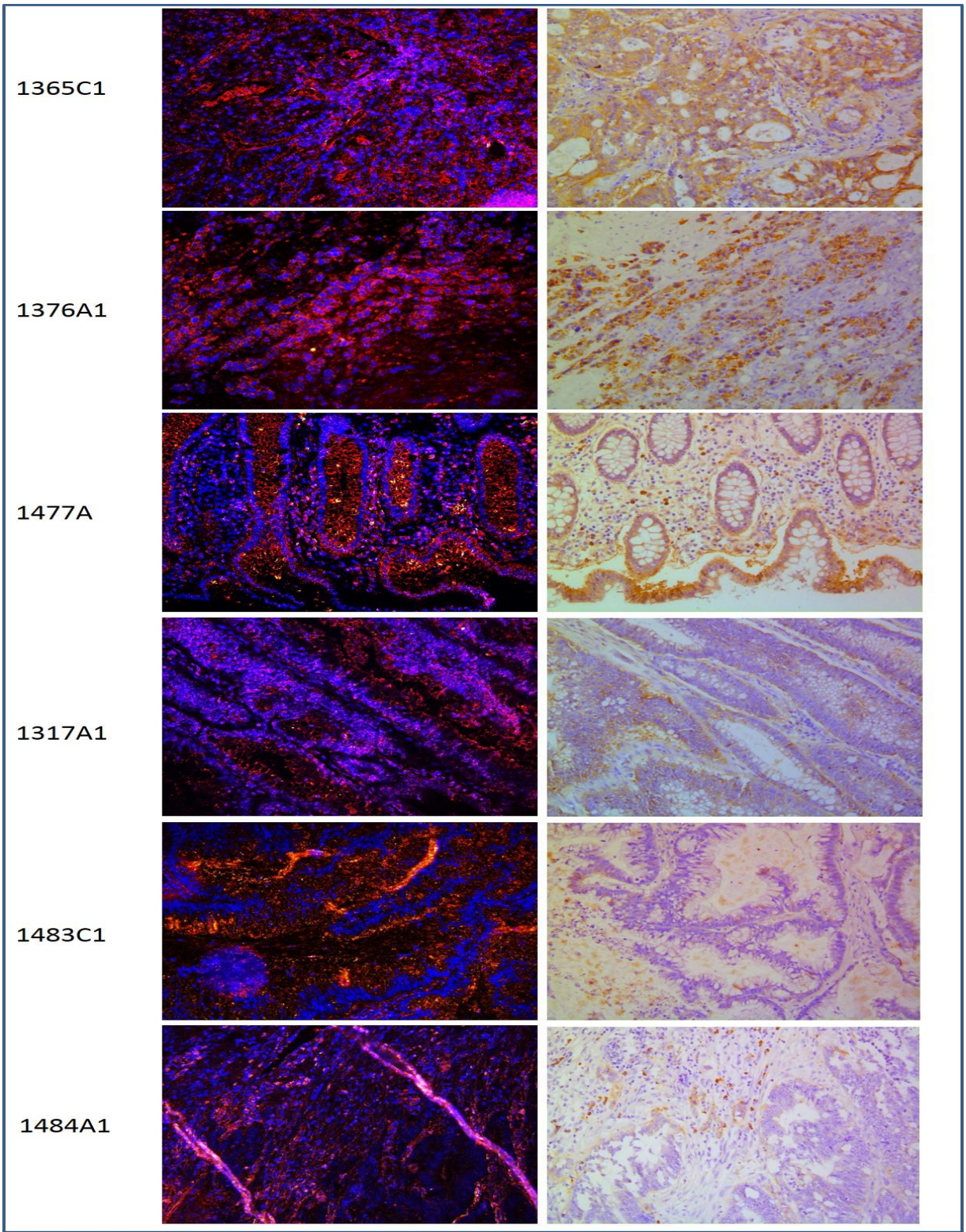

Figure 6| Visual Comparison Between GNR and IHC Staining. EGFR detection using both GNR-1070 and Dako's EGFR PharmDX kit was analyzed using watershed algorithms. Show here are representative image from selected patients. GNR can be seen as bright red/gold dots on the DAPI-stained nuclei, while IHC staining is marked by the brown enzyme amplification from interaction between DAB and HRP.

(S57). Tissues were stained using either the protocol required by Dako's EGFR PharmDX™ Kit™ or by treating slides with 5µg Au/mL solution of GNR-1070 compound for 2 hours followed by washing. Images were taken of Dako stained samples using conventional bright field microscopy, while images of the GNR-1070 stain were taken using an overlay of DAPI fluorescent nuclear stain and dark field imaging for nanorod scattering (Figure 6). The staining seen in the GNR samples is much more resolved than in the histochemically stained sections due to there being no enzyme-based amplification of the signal and less variance in the intensity of staining. What is seen instead is the reflection of light given off by each nanorod that can then be quantified using refined versions of our algorithms that were explored in the previous cell line samples.

The quantification of GNR staining is done on a per-cell basis using a watershed algorithm to predict cytoplasmic area and membrane location based on nuclear shape (Figure 7). Briefly,

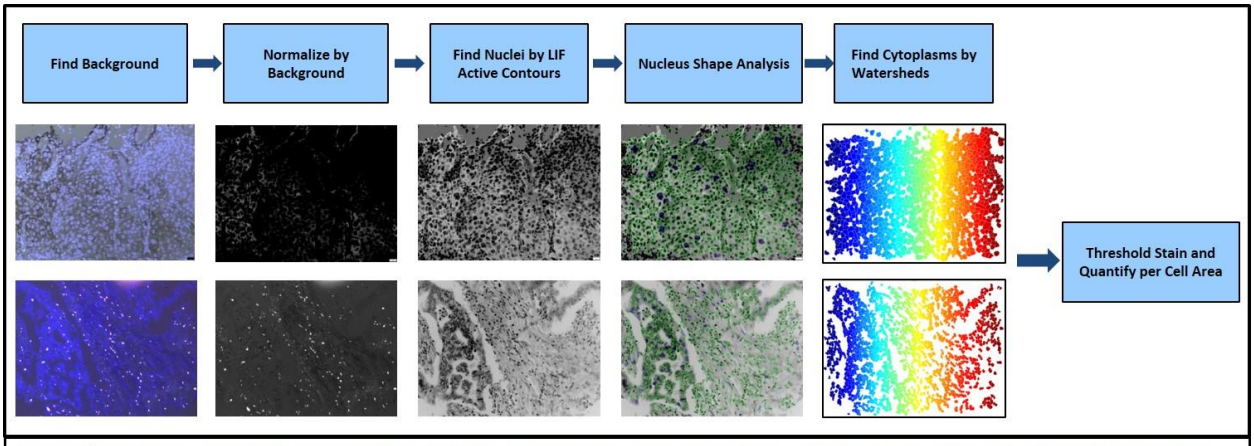

Figure 7|Tissue Image Analysis. Quantification of GNR and Dako staining was achieved by segmenting cells and counting stained pixels within the cytoplasm as a percentage of cell area. Once cytoplasms are found, staining can be quantified on a per-cell basis using the desired threshold selected as the cutoff for a positive stain.

analysis of an image is done by first finding a background and normalizing the image based on the background. The nuclei are then found by local image fitting the active contours. The nuclear shapes are then analyzed and the cytoplasmic area can be predicted based on

watershed methods. Once the location and cytoplasmic area of each cell are found, the amount of gold staining can be quantified by analyzing the amount of bright red/gold color given off in the images. Since quantification of any histochemical stain can vary based on the threshold selected for staining, we did a comparison of the variability of both DAKO IHC and GNR-1070 given an arbitrary threshold (Figure 8). Using conventional IHC, the percentage of stained cells decreases drastically as the selection of the staining threshold changes. Using GNR-1070 we see that the percentage of cells stained does not vary in a meaningful way as the threshold increases until we

Threshold	Dako IHC	GNR-HC
15%	0.250	0.132
25%	0.219	0.123
35%	0.199	0.122
45%	0.178	0.124
55%	0.157	0.131
65%	0.138	0.136
75%	0.121	0.090
stdev	**0.0456**	**0.0154**

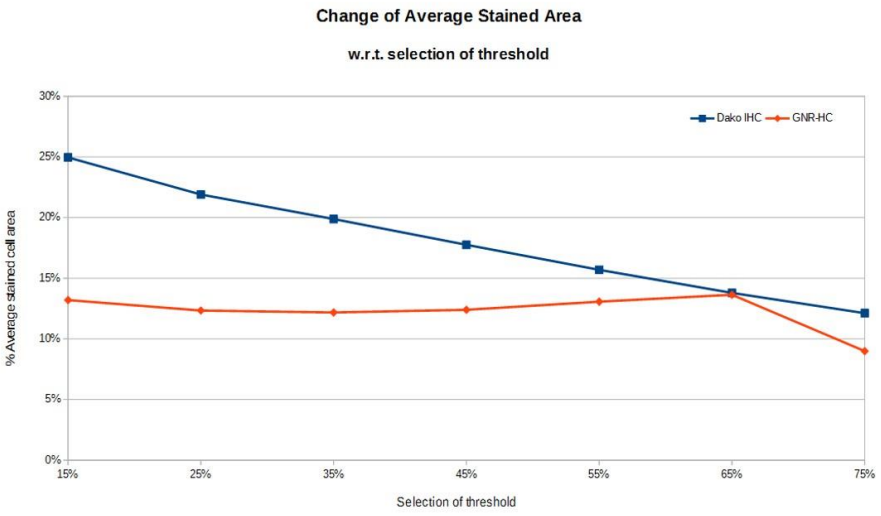

Figure 8| Change In Staining Based on Threshold Selection. Selected images of cancer cells stained with Dako IHC and GNR-1070 are processed in order to study robustness of both tests with respect to quantifiability. Cell nuclei and cytoplasms are automatically delineated by using a combination of level set active contours and watershed algorithms. The amount of stains and GNR are computed as a percentage of cytoplasm area on a per cell basis. We show that the GNR distribution is narrower than Dako IHC stain distribution, and is steady across a wide range of threshold parameters whereas IHC stain distribution is heavily dependent on the choice of an arbitrary threshold for quantification.

select a very high threshold. GNR distribution is narrower than the Dako IHC stain distribution, and is steady across a wide range of threshold parameters, whereas the IHC distribution is much more dependent on the arbitrary threshold selected.

Each of the ten colorectal tissues analyzed was graded for EGFR expression based on the Dako staining by a board certified pathologist (Figure 9). These grades can range from 0 (normal) to 3+ (very high) expression, and each pathologist graded the cases independently based on the criteria in the Dako EGFR PharmDX™ manual with no input from the others. For the ten

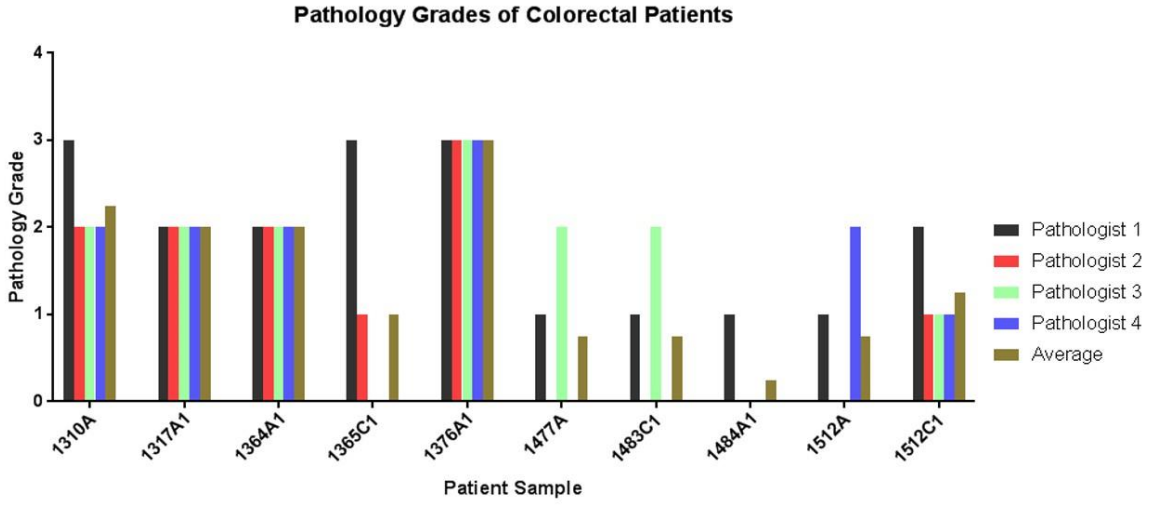

	1310A	1317A1	1364A1	1365C1	1376A1	1477A	1483C1	1484A1	1512A	1512C1
Pathologist 1	3+	2+	2+	3+	3+	1+	1+	1+	1+	2+
Pathologist 2	2+	2+	2+	1+	3+	0	0	0	0	1+
Pathologist 3	2+	2+	2+	0	3+	2+	2+	0	0	1+
Pathologist 4	2+	2+	2+	0	3+	0	0	0	2+	1+
Agreement	3/4	4/4	4/4	2/4	4/4	2/4	2/4	3/4	2/4	3/4
Average	2.25	2	2	1	3	.75	.75	.25	.75	1.25

Figure 9| Pathologist Grades for Selected Colorectal Samples. Four pathologists independently graded ten different colorectal cases for EGFR expression using Dako's EGFR PharmDX kit and scored using criteria from the Dako PharmDX manual. Six of the cases had at least 3 pathologists agreeing on the EGFR grade, while the other four samples showed major disagreement over grading.

colorectal cases examined, there were only three cases in which all four pathologists agreed with one another on the EGFR grade (1317A1, 1364A1, and 1376A1). Three cases (1310A, 1484A1, 1512C1) had at least three pathologists agreeing with one another. The other four cases had agreement from only two pathologists. There is a large discrepancy in agreement

between the pathologists in many cases, with as large as a three-grade increase of 0 to 3+ seen in case 1365C1. Each tissue was then quantified for GNR or IHC expression based on images of numerous fields of each tissue and compared to that of the pathology grade based on immunohistochemistry. The pathology grades were then given arbitrary numerical numbers to fit our scale – 0, 0.1, 0.2, and 0.3 for their corresponding grades of 0, 1+, 2+, and 3+. For every case

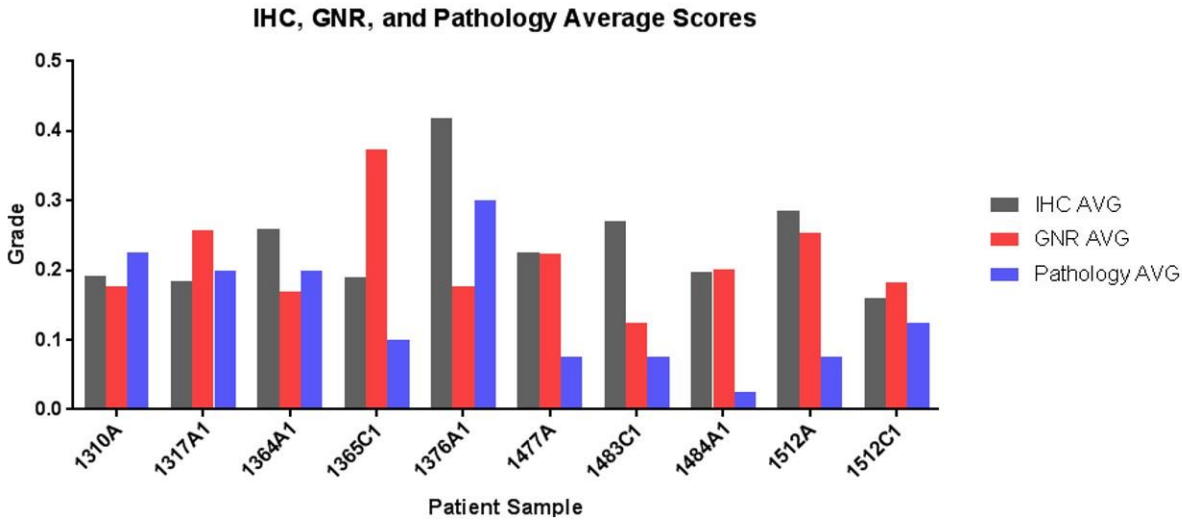

Figure 10| Average Quantification Scores. GNR and IHC quantification scores were averaged using 40, 50, and 60% thresholds and matched up with average pathology grades from four pathologists. Pathology grades were assigned arbitrary values of 0, 0.1, 0.2, and 0.3 to correspond with 0, 1+, 2+, or 3+ scale. Large discrepancies in pathology grading led to many pathology scores disagreeing with both IHC and GNR quantification. Though there is some large disagreement between IHC and GNR quantification in some cases, the majority of the cases showed GNR and IHC grading matching with each other closely.

we took numerous images of different areas of the tissue stained with both IHC and GNR-1070 and had them analyzed using the aforementioned watershed algorithm. Based on the threshold data in Figure 8, we quantified GNR and IHC signals using the most closely agreeing thresholds between GNR and IHC by averaging the 40, 50, and 60% threshold values. The resulting values were compared against the averages of the four pathologist grades for each case (Figure 10).

The scores shown indicate that both GNR and IHC quantification methods disagree with pathology in many of the samples (Figure 11), where a difference of less than 0.1 is taken as an agreeing score. IHC quantification only agreed with the pathology grade in 4 out of the 10 cases, while GNR performed marginally better with 5 out of 10 cases in agreement with pathology grading. The pathology cases which were agreed upon by at least 3 of the 4 pathologists also showed the most agreement with both IHC and GNR, with GNR giving more consistent values of agreement. Interestingly, the cases which disagree with pathology the most using GNR quantification

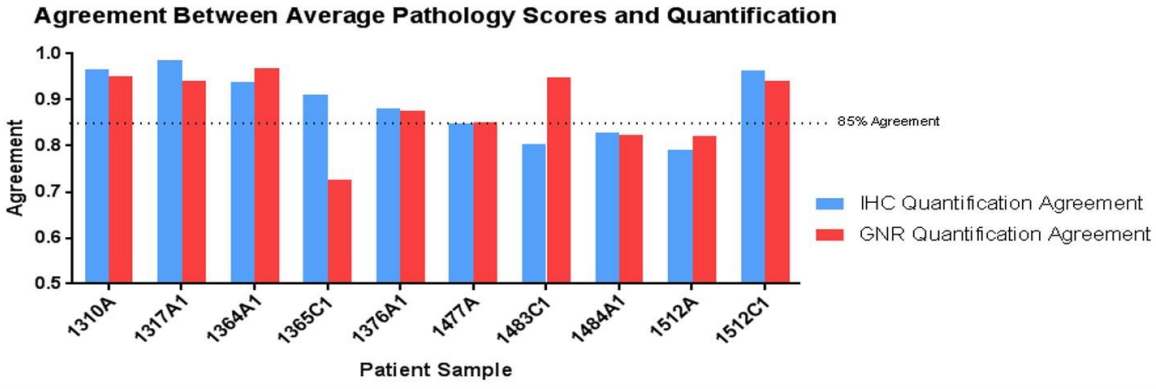

	Pathology and IHC Agreement					Pathology and GNR Agreement					IHC and GNR Agreement
	Path 1	Path 2	Path 3	Path 4	AVG	Path 1	Path 2	Path 3	Path 4	AVG	AVG
1310A	0.108	0.008	0.008	0.008	0.033	0.123	0.023	0.023	0.023	0.048	0.015
1317A1	0.015	0.015	0.015	0.015	0.015	0.058	0.058	0.058	0.058	0.058	0.043
1364A1	0.06	0.06	0.06	0.06	0.060	0.03	0.03	0.03	0.03	0.030	0.030
1365C1	0.11	0.09	0.19	0.19	0.145	0.073	0.273	0.373	0.373	0.273	0.128
1376A1	0.119	0.119	0.119	0.119	0.119	0.123	0.123	0.123	0.123	0.123	0.004
1477A	0.125	0.225	0.025	0.225	0.150	0.124	0.224	0.024	0.224	0.149	0.001
1483C1	0.171	0.271	0.071	0.271	0.196	0.025	0.125	0.075	0.125	0.088	0.109
1484A1	0.097	0.197	0.197	0.197	0.172	0.101	0.201	0.201	0.201	0.176	0.004
1512A	0.185	0.285	0.285	0.085	0.210	0.154	0.254	0.254	0.054	0.179	0.031
1512C1	0.039	0.061	0.061	0.061	0.056	0.017	0.083	0.083	0.083	0.067	0.011

Figure 11| Quantification Agreement Between Grading Methods. Difference between each pathology grading score and IHC or GNR quantification are shown. Average agreement scores below 0.1 are accepted as an agreement. GNR quantification agrees with the pathology score 5/10 cases, while the IHC quantification agrees with pathologists 4/10 cases. IHC and GNR quantification methods showed agreement in 8/10 cases. The two disagreeing cases between GNR and IHC were also the most disagreed upon pathology graded samples.

methods (1365C1, 1376A1, 1477A, 1484A1, 1512A) also disagree using IHC quantification. Total average disagreement of all cases was 0.116 using IHC quantification, and 0.119 using GNR

quantification. Arbitrary quantification scoring of pathology grades may need to be refined in order to properly compare them to the numbers given by GNR and IHC quantification. A larger sample size study that includes patient response data will need to be performed in order to know which pathology grading are the most appropriate for patient treatment.

While pathology grading was largely disagreed with using both quantification methods, we also see a large amount of agreement between only IHC quantification and GNR quantification. Eight out of the ten cases were in agreement between the two quantification methods, showing a low average disagreement across all ten cases of 0.038. Interestingly, the two cases which did not agree between IHC and GNR quantification were also the two cases which showed the highest amount of disagreement among the pathologists (1365C1, 1483C1). Case 1365C1 showed two pathologists agreeing on a score of 0, and showed surprising disagreement – pathologist 1 had graded this case as 3+, and pathologist 2 had graded the case as 1+. GNR quantification of this case actually showed a value of a 3+, agreeing with pathologist 1, while IHC quantification also showed a higher score nearing 2+. Pathology notes indicate 1365C1 shows heavy cytoplasmic staining of EGFR, which could have been picked up by the GNR quantification method. Case 1483C1 also showed very large disagreement, with two pathologists grading it as a 0, while the other pathologists gave grades of 1+ and 2+. GNR score showed this case as a 1+, which agrees more closely with the pathology grade of ~1+. IHC quantification showed a score nearer to 2-3+. Pathology notes indicate that there was heavy edge artifact in case 1483C1, which could be the reason the IHC quantification is so much higher than the GNR score. Given these results, GNR-1070 shows highly comparable EGFR quantification to IHC staining using conventional IHC quantification techniques. Since GNR

staining is less reliant on the threshold selection compared to IHC quantification, GNR-based tissue diagnosis is an attractive method of quantifying tissue proteins at all levels of staining criteria.

1.4 Discussion

The synthesis of gold nanorods (GNR), pegylated gold nanorods (GNR-PEG), and GNR functionalized with EGFR-targeting peptide 1070 (GNR-1070) was achieved and reproduced numerous times. GNR themselves are stable for months to years, and are an attractive platform for targeting biomarkers. Like fluorescent markers, we can quantify the signal given off by the gold stain, but unlike fluorescence, the reflectance of the GNR seen in the dark field images will never fade. GNR-1070 combines the specific targeting of peptides with the imaging capabilities of the gold nanorod, making GNR-based histological detection an attractive alternative to traditional IHC that uses a 2 or 3 step antibody-enzyme process. One of the biggest hurdles with quantification of GNR-1070 is comparing the differences between the nanorod-based histological procedure and the traditional enzyme-based IHC, which has been the preferred method for decades. The disagreement shown between four pathologists in the ten patient samples stained for EGFR highlights the urgent need for a more robust, quantifiable method of protein detection. Disagreement was high among the pathologists themselves, and this caused much disagreement in the comparison of both IHC and GNR staining to pathology diagnosis. In the cases where there was most agreement among pathologists, quantification methods showed grading very similar to that of the pathology grade. Due to the lack of patient diagnosis, treatment, and response data we cannot say which pathologist grading is most correct.

Given the varying stain intensity of the enzyme-reacted antibody IHC, we have shown that one of the most important criteria when quantifying IHC is the selection of an appropriate threshold of staining. The IHC quantification method used to compare IHC to GNR quantification averaged the thresholds of 40%, 50%, and 60% due to those thresholds giving values most similar to the GNR quantification values shown in Figure 8. Given this method, it is not surprising that GNR and IHC quantification values agreed in most of the colorectal samples stained for EGFR. Disagreement between the two methods is much higher at lower thresholds (S57). For example, in case 1310A the IHC quantification ranges from 0.523 at a 15% threshold to 0.127 at a 70% threshold (a difference of 0.396), whereas the GNR score ranges from 0.250 to 0.133 at the same threshold (difference of 0.117). Since GNR values do not vary as largely based on threshold selection, they are much more readily quantified and thus can be used to detect proteins that require lower thresholds as staining criteria. Further studies involving a larger number of patient samples, complete with treatment and response data, can be done to refine the quantification and diagnostic capabilities of GNR-based tissue diagnosis.

2.0 Peptide-Conjugated Gold Nanorods for Evaluation of c-MET Receptor Levels in NSCLC Tissues

2.1 Introduction

Anti-EGFR drugs have shown to improve progression-free survival for colorectal cancer and Non-small Cell Lung Cancer (NSCLC) patients alike[23]. The expression of the hepatocyte growth factor receptor (HGFR, c-MET) in tumors is linked to resistance of anti-EGFR therapies[24, 25], whereby the tumors will circumvent the EGFR pathway by internalizing the receptor and up regulating surface c-MET expression to proliferate[26]. Nearly 20 percent of cancers which are treated with EGFR inhibitors as first-line therapy will eventually develop resistance through this mechanism[27, 28]. c-MET has thus been previously reported to be upregulated in many of the same cancers as EGFR[29-31]. Normally, c-MET will only be expressed in stem and progenitor cells[32]. In cancers, the expression of the MET pathway affects the development of cancer through activation of oncogenic pathways such as RAS, PI3K, and STAT3, and also promotes angiogenesis in tumors (Figure 1) [33]. c-MET expression is also associated with brain metastasis in NSCLC[34]. Only patients who overexpress c-MET will benefit from anti-c-MET treatment, and as such only those who are appropriately diagnosed with c-MET expression will receive treatment[35]. Recently there has been debate about the role of c-MET diagnostics due to failure of combination therapy of EGFR inhibitor erlotinib and MET targeting drug Onartuzumab[36, 37]. A phase III trial that selected only high c-MET expressing patients using a companion diagnostic did not show any benefit of the combination therapy, leading to questions about whether the drug or the selection method is to blame. Due to resistance to EGFR targeted drugs being common during the course of therapy, and the

question of whether more sensitive diagnosis is needed, we have extended the gold nanorod IHC (GNR-IHC) diagnostic platform to investigate the expression of the c-MET protein in NSCLC tissues.

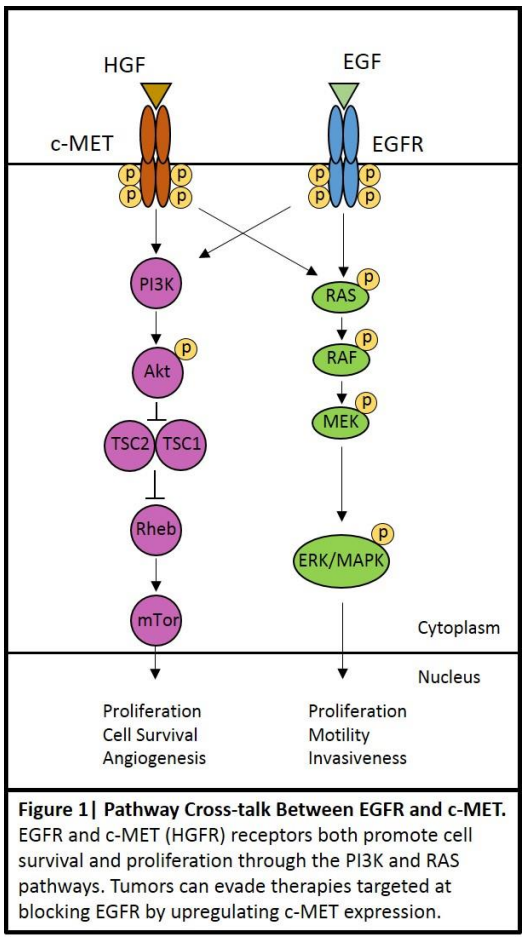

Figure 1| Pathway Cross-talk Between EGFR and c-MET. EGFR and c-MET (HGFR) receptors both promote cell survival and proliferation through the PI3K and RAS pathways. Tumors can evade therapies targeted at blocking EGFR by upregulating c-MET expression.

In chapter 1, the potential of a novel immunohistochemical test for EGFR that can increase sensitivity of IHC tests using peptide-conjugated gold nanorods (GNR) - a nanoconstruct made of cylindrical gold particles about 50nm long, has been shown. GNR are utilized for their excellent light scattering properties, especially when using dark field microscopy[17]. The image signal given by GNR is not chemically reliant on conversion and amplification of reporter molecules as is IHC, but rather the physical scattering of light given off by the metallic compounds which will not fade over time. This consistent signal allows GNR to be analyzed statistically and given a reliable output based on the amount of GNR in a given image. The surface of GNR is easily modifiable to be attached to a ligand of choice[16, 38]. To design a combined c-MET-targeted, GNR-based diagnostic and imaging agent, we have conjugated a peptide with c-MET-avid properties to GNRs functionalized with a polyethylene glycol (PEG) surface modification. The c-MET-binding portion of the peptide is comprised of 11 amino acid sequence YLFSVHWPPLKA. This peptide was previously identified to bind to c-MET specifically and efficiently by screening a phage display library[39]. Due to solubility issues, the peptide as such cannot be conjugated to GNR by

simply adding a thiol group and modified by incorporating lysine groups. The modification of c-MET peptide (1093) solves the solubility issues while leaving the binding sequence intact. In our studies we show the specific binding of the GNR-peptide compound (GNR-1093) to MET receptors in MET-overexpressing cells lines and tissues. The demonstrated efficacy and biocompatibility of MET receptor-targeted GNR-1093 combined with the numerous imaging techniques developed for in vivo imaging of GNR in the past few years gives promise that peptide-conjugated GNRs can be utilized as a specific diagnostic and imaging agent.

2.2 Materials and Methods

2.2.1 Synthesis of Gold Nanorods

Gold nanorods (GNR) of aspect ratio 3:4 were prepared using an established seed-mediated growth method with minor modifications[19]. All solutions were made in fresh deionized water (DI H_2O). A seed solution was prepared by making a 10mL solution of .1 M Cetyltrimethylammonium Bromide (CTAB, Sigma Aldrich). The CTAB solution was lightly heated until the CTAB had dissolved, giving a clear solution. 250 μL of a .01 M solution of chlorauric acid ($HAuCl_4$, Sigma Aldrich) was then added to the CTAB solution while stirring. Immediately after addition of chlorauric acid, 600μL of ice-cold .01 M sodium borohydride ($NaBH_4$, Sigma Aldrich) was added to the solution, which changed color from gold to light brown. The seed solution was then left to stir for 5 minutes. While the seed solution stirred, 500 mL of growth solution was then prepared. The first step was to make 250mL of a .1 M CTAB solution, then heat until the CTAB had dissolved as had been done with the seed solution. 250 mL of .01 M chlorauric acid was then added to this CTAB solution and stirred lightly by hand. 10 mL of .0043 M silver nitrate ($AgNO_3$, Sigma Aldrich) was added to the solution and again stirred gently by

hand. 4 mL of .1 M ascorbic acid (Sigma Aldrich) was then added, and the solution was stirred very gently until the solution had turned from gold-orange to clear. This completed the growth solution. 0.5 mL of the seed solution was then added in to the growth solution. The solution was left undisturbed after this point due to the delicate nature of the synthesis. Minutes later the solution turned from clear to purple, indicating the formation of GNR. The GNR solution was left alone for 24 hours, then washed of CTAB. The GNR solution was twice filtered through filter paper to remove excess CTAB. To further remove excess CTAB, the solution was then centrifuged at 16,000 RPM for 10 minutes at 25 C. The supernatant was removed and replaced with fresh DI H_2O. The centrifuging and washing step was then repeated. The sample of GNR was then characterized using UV-Vis spectroscopy, TEM imaging, and Zeta potential measurements.

2.2.2 Synthesis of PEGylated Gold Nanorods (GNR-PEG)

A 750 Dalton polyethylene glycol (PEG_{750}, JenKem Technology USA) linker modified with thiol was attached to the GNR before functionalization with the 1070 peptide. A solution of PEG_{750} was added to the GNR solution at a molar ratio of 1:2 (GNR: PEG_{750}). This solution was allowed to stir for 24 hours. The solution was then centrifuged at 16,000 RPM for 10 minutes at 25 C. The supernatant was removed and replaced with fresh DI H2O. After washing, GNR-PEG was then characterized through UV-Vis spectroscopy (Fig. 1c), TEM imaging (Fig. 1a), and Zeta potential measurements(Fig.1b, S3).

2.2.3 Synthesis of Peptide-Conjugated Gold Nanorods (GNR-1093)

A solution of 1093 peptide (CPC Scientific) was then added to the GNR-PEG solution while stirring at a molar ratio of 1:1 GNR-PEG:1093 peptide. This solution was stirred for 24 hours to ensure maximum binding of peptide to the GNR surface. The solution was then centrifuged at 16,000 RPM for 10 minutes at 25^{o} C. The supernatant was removed and replaced with fresh DI H2O. GNR-1093 was then characterized using UV-Vis spectroscopy, TEM, and Zeta potential.

2.2.4 Cell Line Growth and Treatment

After achieving confluence, 5x10^{5} H441 or MCF-7 cells (ATCC) were seeded on to coverslips in a six-well plate, and allowed to adhere overnight in media (DMEM) containing 10%FBS. Prior to treatment with the GNR-1070 compound, the wells were first washed with cold 1x PBS solution 3 times to remove the growth media. The cells were then fixed with 4% paraformaldehyde for 10 minutes at RT, followed by 3 more 1x PBS washes. 1.5 mL of a blocking buffer containing 1% BSA was added to each well and left alone for 1 hour at RT. For the wells that were pre-blocked, 2 mg/mL of 1093 peptide was added to the buffer solution and left for 1 hour at RT. The blocking buffer solution was removed with 3 more cold 1x PBS washes. To treat the cells with the GNR agents, 10-times diluted blocking buffer solution was added to each well. To these wells, 50 µL of 0.5 absorbance, as measured by the longitudinal peak (98.5 µg Au/mL), GNR-1093 or GNR-PEG was added. The welled plate was then left alone for 2 hours at RT. After 2 hours, the nanoparticle solution was washed from the wells 5 times with cold 1x PBS. The coverslips were removed from the wells, and mounted on to glass slides using a mounting media containing fluorescent DAPI nuclear stain. The cell slides were then viewed at 40x

magnification on a Leica DM5500 using fluorescence to visualize DAPI, and dark field to visualize gold nanorod scattering.

2.2.5 Preparation of Paraffin-Embedded Cell and Tissue Sections

Formalin fixed, paraffin-embedded (FFPE) c-MET expressing cell lines on glass slides were provided by Eli Lilly's Diagnostic and Experimental Pathology Department. Tissue sections were procured from the MU OneHealth Biorepository after obtaining IRB approval (IRB project number 1210307). Paraffin was removed from the slides by immersing in 100% Xylene for 5 minutes, then rehydrated in graded ethanol and finally DI H_2O. Citrate buffer antigen retrieval was performed on the slides using a Roche Benchmark Ultra autostainer. Once prepared for staining, IHC was performed on the samples with anti-MET antibody AbCam51067 or stained using GNR-1093. For GNR staining, the slides were treated with a 2.5% BSA solution for 10 minutes prior to addition of the nanorod solution. After washing, the slides were treated with 5 µg Au/mL GNR-1093 solution in a humid chamber for 2 hours. After this time, the slides were washed thoroughly with PBS and DI H2O. The slides were air dried and stained with DAPI fluorescent nuclear stain. The GNR-treated slides were viewed using a Leica DM5500 microscope, using fluorescence to visualize DAPI, and dark field to visualize gold nanorod scattering. Antibody stained slides were imaged using a conventional bright field microscope.

2.3 Results

2.3.1 Characterization of GNR, GNR-PEG and GNR-1093

The formation of uniform gold nanorods of 3:4 aspect ratio was confirmed by performing detailed physic-chemical characterization such as UV-Vis spectral analysis, TEM and zeta potential measurement. In UV spectral measurements, gold nanorods are identified by their characteristic 2-peak absorption spectrum. Due to the rod shape of the nanoparticle, we see a smaller transverse peak, which coincides with the 15 nm width of the nanorods, at around 540 nm. A second longitudinal peak, which varies based on the length of the gold nanorods, is seen for 50 nm long rods at around 780 nm. The zeta potential of a material measures surface charge of a colloid at the slipping plane. In the case of gold nanorods, the zeta potential is highly positive, usually 40mV or higher due to the presence of CTAB surfactant on the nanorod. TEM images confirm the presence of uniform gold nanorods.

As an intermediate step in the conjugation of the 1093 peptide to GNR, we exchange the CTAB surfactant on the surface of the GNR with a 750 kD polyethylene glycol (PEG_{750}) by utilizing thiol present at one end of the PEG chain, since sulfur has a known strong affinity for gold. The exchange of CTAB for PEG shifts the UV peaks only slightly, but the retention of two distinct peaks confirm that the nanorods still maintain their shape. The zeta potential measurement of GNR-PEG is the most reliable method of confirming the complete exchange of PEG for CTAB due to GNR-PEG having a characteristic negative zeta potential of -20mV or below, as seen in previous studies. Similar to the addition of PEG, the 1093 peptide was conjugated to the surface of GNR-PEG utilizing dithiol present in the 1093 peptide (Figure 2). The addition of 1093 peptide to the surface of GNR-PEG again shows only a very slight shift in the UV-Vis peaks, however the change in zeta potential to a positive value of +28mV confirms the conjugation of the peptide to GNR. Using these methods of characterization as quality control, we confirm that GNR

functionalized with PEG and peptide 1093 can be reproducibly synthesized. Percent conjugation and stability was not analyzed with HPLC for GNR-1093, but is expected to be comparable to HPLC characterization and stability of GNR-1070 shown in chapter 1.

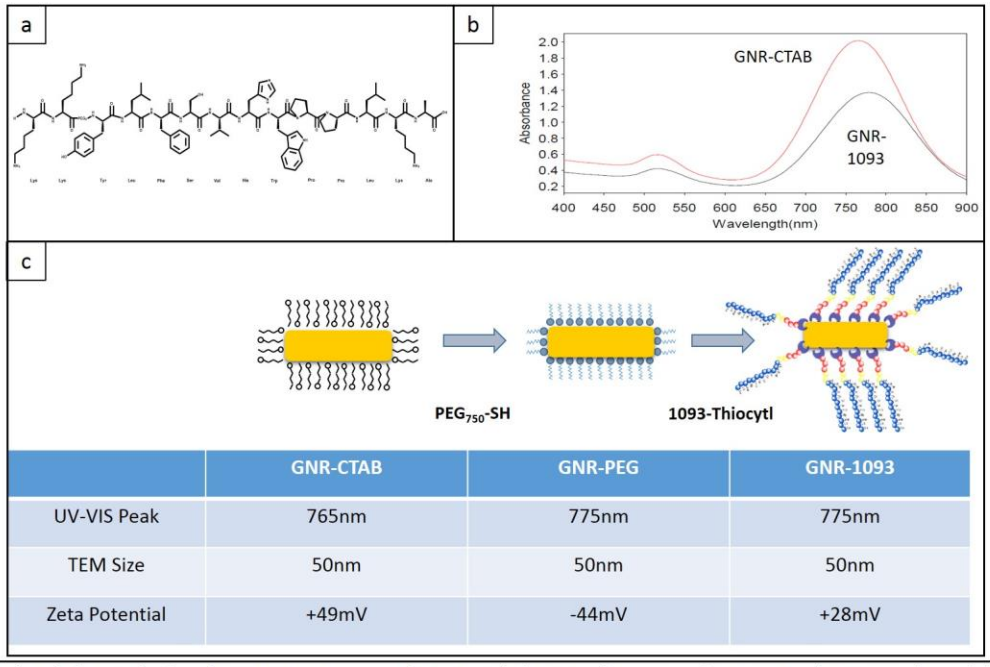

	GNR-CTAB	GNR-PEG	GNR-1093
UV-VIS Peak	765nm	775nm	775nm
TEM Size	50nm	50nm	50nm
Zeta Potential	+49mV	-44mV	+28mV

Figure 2| Synthesis and Characterization of GNR-1093. a. Structure of 1093 Peptide **b.** UV-Vis absorption of GNR-CTAB and GNR-1093 shows slight shift in the UV peak when PEG and 1093 are conjugated to the surface of the gold nanorod **c.** Schematic showing the synthesis process and quality control parameters for characterization of each compound. Zeta potential is most important, as it shifts from postitive to negative when PEG is added, and back to positive once the peptide is bound to the surface of the gold nanorod.

3.3.2 c-MET Targeting in Cultured Cell Lines

To investigate the specific binding of GNR-1093 to the c-MET receptor, we first incubated GNR-1093 with NSCLC cell line H441 (High c-MET expression)[40] and breast cancer cell line MCF-7 (low c-MET expression)[41]. To treat the cell lines, each cell line was grown to 80% confluency, removed from the flask using TrypIE (Sigma), then seeded $5x10^5$ cells per well on a glass coverslip placed in a six-welled plate, and allowed to adhere in serum-free media overnight. The following day, media was washed from the plates using 4 washes of cold 1x PBS, and cells were fixed using 4% paraformaldehyde (PFA). After 10 minutes, PFA was removed with cold PBS (4 times), and wells were treated with 2mL of 5µg Au/mL of GNR-1093 in PBS. The plates were

left undisturbed for 2 hours at RT, then excess GNR solution was washed off with PBS. The coverslips were removed from the wells, and mounted on a slide using DAPI fluorescent mount. We used the fluorescent DAPI channel to locate cell nuclei, and dark field to look for scattering due to presence of GNR (Figure 3). In the H441 cell line samples, the GNR signal was extremely bright. The majority of GNR scattering is localized on the membrane of the H441 cells that highly express c-MET. In contrast, the MCF-7 cell line that has lower c-MET expression, showed only minimal gold signals on their membrane. As a negative control, both these cell lines were incubated with GNR-PEG, which does not contain the c-MET-targeting peptide. As expected, the GNR signals in the samples treated with GNR-PEG showed only nonspecific GNR. Cell lines were then blocked using only the 1093 peptide, then incubated with 5µg Au/mL of GNR-1093. While the peptide did not block the receptors 100%, the amount of GNR seen in the cells was drastically reduced from what was seen in the unblocked samples.

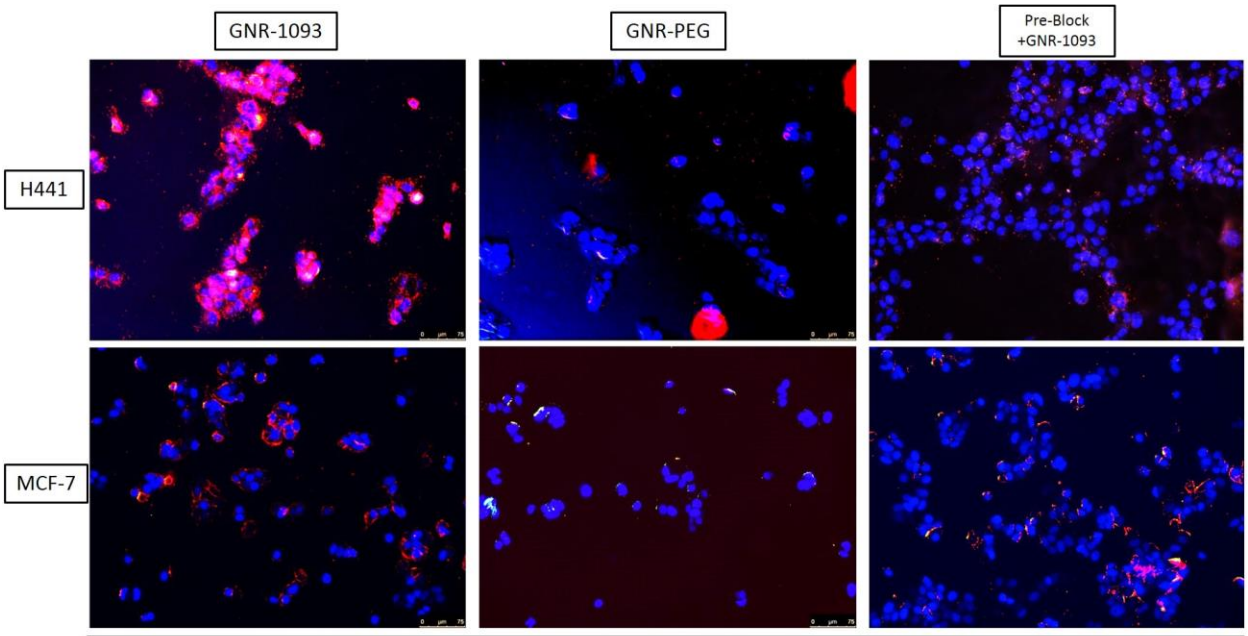

Figure 3| GNR-1093 Staining of Cultured Cell Lines. H441 (High cMET expression) and MCF-7 (low cMET expression) cell lines were fixed on coverslips and incubated with GNR-1093 for 2 hours in a 6-welled plate. Dark-field microscopy shows high red/orange GNR signals in the H441 sample, and low signal in the MCF-7 sample. Cell lines were treated with non-targeted GNR-PEG as a negative control, which showed no specific binding in either sample, as expected.

2.3.3 c-MET Targeting in FFPE Cell Lines

To investigate the efficacy of GNR-1093 in paraffin-embedded samples, we obtained slides from Eli Lilly and Company's Diagnostic and Experimental Pathology department which contained an array of c-MET-expressing cell lines. Each array contained paraffin-embedded cell spots which were graded as either 1+, 2+, or 3+ for c-MET expression, and were validated internally for use in c-MET diagnostic development. These slides were de-waxed according to standard IHC protocol and antigen retrieval was performed in a heated citrate buffer. Once this was done, slides were either stained using 5µg Au/mL of GNR-1093, or stained with conventional IHC using c-MET antibody (AbCam51067) at 1:200 dilution as the primary antibody. Antibody-stained IHC samples were imaged in the bright field, while the GNR-stained slides were imaged using an overlay of fluorescence to locate the nuclei and dark field to locate gold nanorod scattering (Figure 4). Comparing the two methods, we see an increase in both the brown stain from the antibody IHC and the red/orange light scattering seen from the gold nanorods as the grading increases. Images of each GNR-stained sample were then analyzed for gold intensity on a per-cell basis. Using Matlab algorithms we are able to isolate each cell based on the DAPI nuclear fluorescence and calculate the intensity of the GNR signal by counting the

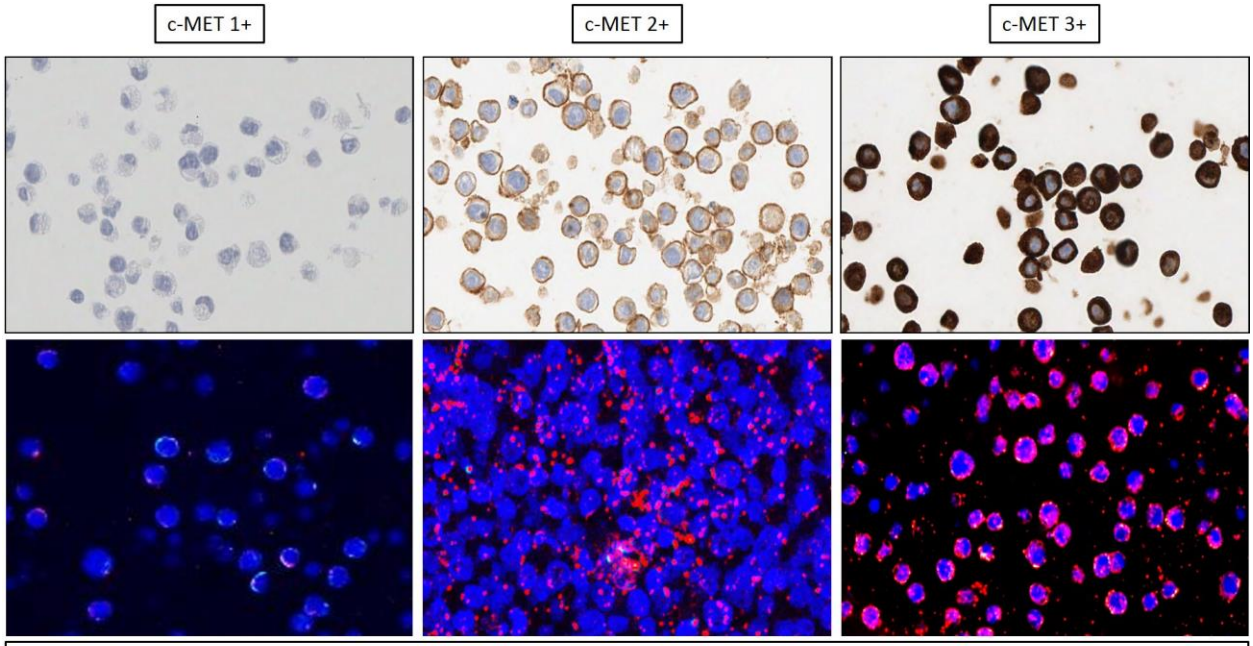

Figure 4| FFPE MET Graded Cell Lines. Paraffin-embedded cell arrays were treated on a glass slide using either AbCam 51067 or GNR-1093. Both the antibody and gold stains show a linear increase of signal on the cell membranes as the MET pathology grade increases

number and intensity of Red/Green pixels associated with each nucleus (Figure 5). Each data point was plotted on a log scale of relative Red/Green pixels per cell. This graph shows the linear increase in c-MET expression on a per-cell basis using GNR to quantify the MET levels. Each increasing data point corresponds with the appropriate pathology grade as MET expression increases.

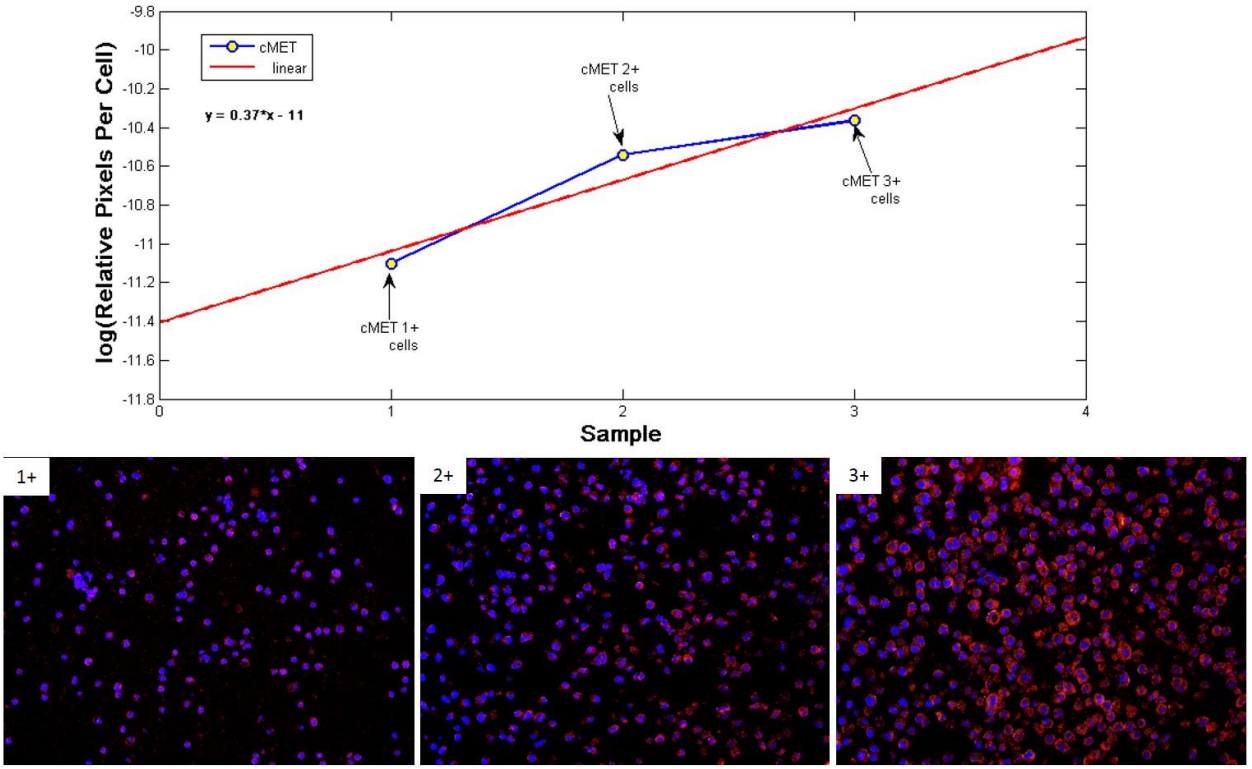

Figure 5| FFPE MET Graded Cell Lines. Gold staining of the graded FFPE cell lines were analyzed on a log scale of relative Red/Green pixels per nucleus. Using this analysis method, we see a linear increase in the gold signal as cMET expression increases, and can analyze cell staining on a continuous scale, rather than 1+, 2+, or 3+ grades

2.3.4 c-MET Targeting in FFPE Patient Tissues

Since we were able to identify GNR staining in Formalin fixed paraffin embedded (FFPE) cell samples, we then investigated the affinity of GNR-1093 for c-MET in five FFPE NSCLC tissue samples. To compare the histochemical staining of the c-MET receptor between the c-MET antibody (AbCam51067) and GNR-1093, we first used duodenum tissue, known to heavily express the c-MET protein[42], as a control. Antigen retrieval was performed on all samples using the Roche Benchmark Ultra autostainer. The antibody-stained (AbCam51067) tissues were also run on the autostainer at 1:200 dilution and counterstained with hematoxylin, whereas the GNR-stained samples were done by manually incubating GNR-1093 for 2 hours in a humid chamber, then counter-stained using DAPI fluorescent nuclear stain. The AbCam51067-

stained duodenum tissue shows heavy brown staining throughout the tissue, with the heaviest staining localized in the glandular cells (Figure 6). The same was true for the GNR-1093 stained samples, which showed very bright gold signals

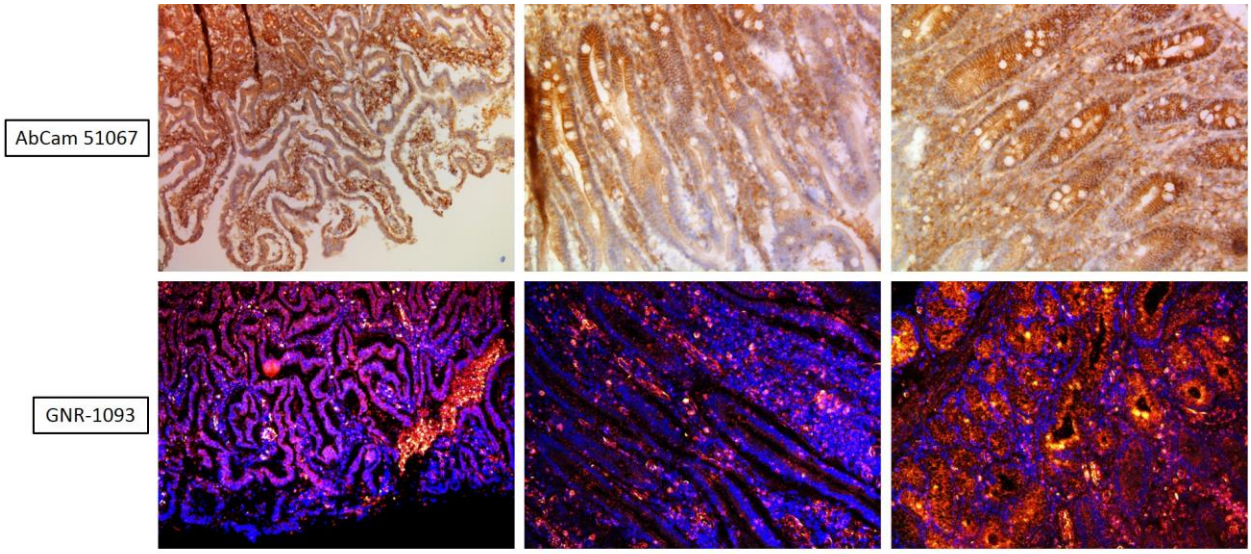

Figure 6| Duodenum Tissue as cMET Staining Control. Duodenum tissue, which has high cMET expression, was stained with either AbCam 51067 (1:200 dilution) or GNR-1093 (5ug Au/mL). Heavy membrane staining in the glandular cells was seen using both methods

that are localized on the cell membranes of the duodenum tissue. The duodenum tissue was also treated with GNR-PEG as a negative control, which showed no specific binding to the tissue. Once we had established c-MET specificity in the control tissue, we were then able to investigate NSCLC tissue samples which had been collected by the MU One Health Biorepository. Five patient tissues that had been previously been identified as EGFR-positive using both Dako PharmDX™ EGFR kit and our own GNR-1070 EGFR detection agent were stained for c-MET using both AbCam 51067 and GNR-1093. The five patients selected were chosen at random, and these patient samples had not previously been evaluated for c-MET expression. Interestingly, all five samples selected showed high c-MET expression according to both the antibody and GNR-1093 (Figure 7). c-MET expression was evaluated based on staining in the tumor cells, which showed very high expression. In most cases the c-MET expression was

mainly located in epithelial cells along the outer edges of the tissue (Figure 7 a, c, d), while other cases showed pockets of tumor cells which stained heavily for c-MET (Figure 7b). Some background staining was seen in other areas of the tissue using each method, however evaluating the tumor cells alone shows high affinity of GNR-1093 to the membranes of the tumor cells.

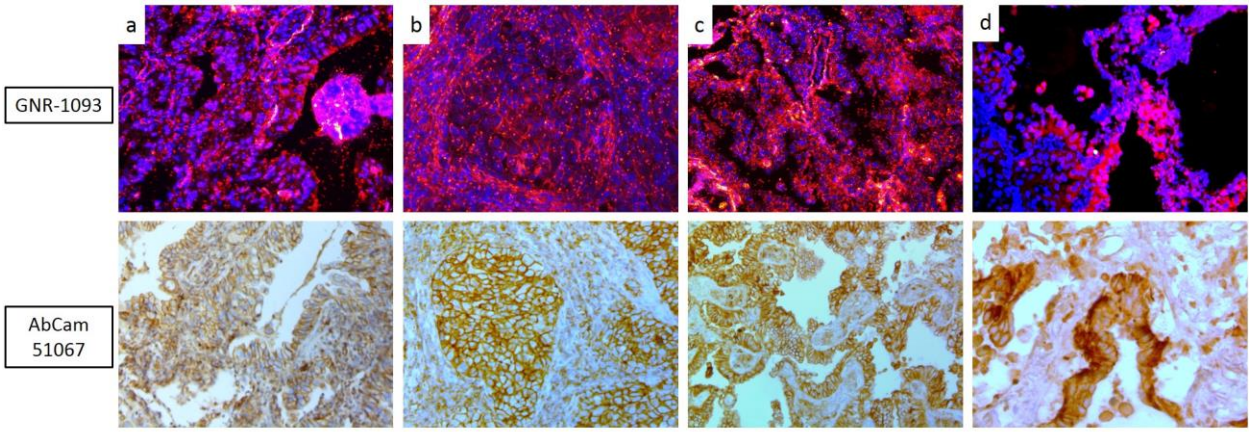

Figure 7| NSCLC Tissue Staining With AbCam 51067 and GNR-1093. Patient NSCLC tissue obtained from the MU OneHealth BioRepository was stained with both AbCam 51067 (1:200 dilution) and GNR-1093 (5ug Au/mL). Heavy staining of cMET was seen in all samples using both GNR and antibody-based methods.

c-MET expression was further examined using a tissue microarray from US Biomax (biomax.us) containing 18 cases of NSCLC - squamous cell carcinoma. After de-waxing and antigen retrieval as with the patient tissues, each microarray was stained using either GNR-1093 to look for c-MET expression, or GNR-PEG as a negative control. Cores were then imaged using the same method of fluorescent DAPI to stain the nucleus and dark field imaging to examine scattering from the gold nanorods. In all cases, GNR-PEG showed no specific binding to any of the tissues, leaving behind only small amounts of non-specific GNR after washing. The GNR-1093 stained samples, however, showed GNR binding to tumor cells in spots D2, F2, and B2, while the other samples showed little to no binding of GNR in the tumor cells (Figure 8, 9).

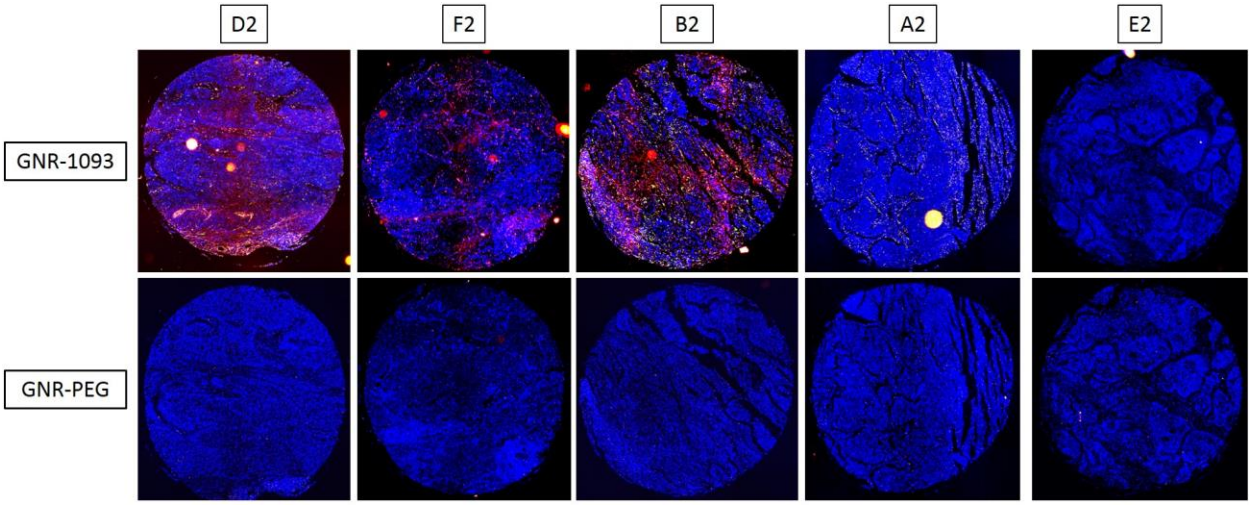

Figure 8| NSCLC Tissue Microarray stained with GNR-1093 and GNR-PEG. A NSCLC tissue microarray was examined for MET expression using either MET-targeted GNR-1093 or negative control GNR-PEG. Tumor cells were examined for MET staining by examination of red signals pertaining to gold nanorods. Using this method we were able to identify tissues which stained positively for MET expression (a-c) or negatively for MET expression (d,e).

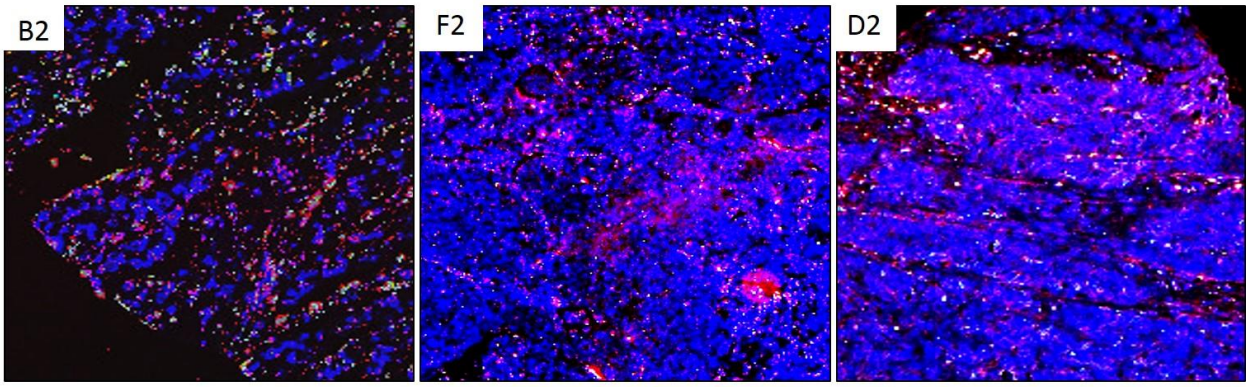

Figure 9| 20x Magnification of TMA Spots. Higher magnification images of TMA spots B2, F2, and D2 show GNR staining (Red) around the membranes of cMET expressing cells stained with fluorescent DAPI nuclear stain.

2.4 Discussion

We have synthesized and characterized a c-MET-specific gold nanorod conjugate GNR-1093, that utilizes a peptide for receptor targeting. GNR-1093's specificity for c-MET was evaluated in multiple cell lines and paraffin-embedded tissues. Gold nanorods have a high surface-area-to-volume ratio, allowing for conjugation of many peptides on the surface of just one gold nanorod, enhancing the sensitivity of the gold nanorod detection method. Due to the expression of c-MET being most likely in EGFR-positive tissues, we selected NSCLC tissues that

previously had been evaluated for EGFR expression using both gold nanorods and Dako's EGFR PharmDX™ kit. We found it interesting, though not surprising, that each tissue investigated had high amounts of c-MET. Every tissue investigated contained high amounts of c-MET according to both GNR based diagnostics and antibody based IHC. We saw background staining in both the antibody and GNR methods, and likely would need to titrate both further in order to eliminate the background seen outside the tumor cells. When diagnosing the tissues, however, it is important to look at the staining of the tumor cells themselves, which showed membrane staining for c-MET with both the antibody and the GNR-1093 stains. In these cases, the patients would likely acquire resistance to EGFR-targeted drugs through the c-MET pathway, and would be recommended for anti-c-MET therapy. The tissue microarray (TMA) showed high MET staining in 17% of the cases contained on the microarray (n=18). Interestingly, the cases that showed the highest amount of staining for c-MET were also among the highest grade tumors on the TMA. c-MET is known to be expressed at a much higher level (~43.3%)[43] in high-grade NSCLC squamous cell carcinoma and thus would be expected to be seen in some of the high grade cases contained in the TMA.

3.0 Identification and Validation of a PD-L1 Binding Peptide for Determination of PDL1 Expression in Tumors

3.1 Introduction

Immune checkpoint inhibition has become an important modality for treating cancers, and has demonstrated significant success in recent years [44]. By inhibiting immune checkpoints host immune response recover from tumor evasion. The innate immune response can potentially negate the tumor's ability to resist targeted therapy, eliminating the need for continuous lines of therapy [45]. There are numerous drugs either approved or in the pipeline that target dominant immune checkpoints such as PD-L1 or CTLA4[46, 47]. One immune checkpoint of particular interest in human cancers is the interaction between Programmed Cell Death Receptor 1 (PD-1) and its ligand, Programmed Cell Death Ligand 1 (PD-L1) [48]. Overexpression of PD-L1 has been reported in many different tumor types, such as melanoma (40-100%), Non-Small Cell Lung Carcinoma (NSCLC) (35%-95%), Glioblastoma (100%), ovarian cancer (33-80%), and colorectal adenocarcinoma (53%)[49]. PD-L1 expression is characteristic of immune checkpoint evasion, allowing tumor cells to go unrecognized by immune T-cells as foreign. When an activated T-cell recognizes an antigen through binding of T-cell receptor to major histocompatibility complex, other checkpoints such as PD-1: PD-L1 are checked before the T-cell can recognize the cancer cell as foreign. When PD-1 on the T-cell surface and PD-L1 on the tumor surface are allowed to interact, the T-cell will be inhibited from destroying the foreign cell[50] (Figure 1). Many approved drugs are aimed at binding to and blocking either PD-1 or PD-L1 that stops receptor-ligand binding and will allow the T-cell to continue with killing foreign

tumor cells. These drugs have shown therapeutic success in both primary and metastatic cancers[51, 52]; however, not all patients will respond to this kind of therapy based on initial diagnosis. In order to determine which patients should be selected for immune checkpoint therapy, the appropriate diagnostic must be used to determine levels of PD-L1 in the tumor. Patient selection for the therapy depend on the levels of PD-L1 staining in the tissue. Above a certain "cutoff" point on staining pattern, patient would be considered as PD-L1 positive and expected to respond to administered therapy. Some clinical trials confirm that patients with higher expression of PD-L1 levels show increased response to the drug[53]. In other trials, it is shown that the expression is not a clear predictor for patient's response [54]. Indeed, diagnosis of PD-L1 expression in patients has proven to be somewhat controversial due to proprietary methods and diagnostic interpretation[55, 56]. PD-L1 assays are being developed in a 'one drug – one assay' method, where assay scoring and guidelines can vary based on the type of drug and diagnostic method used [57], and companion diagnostic development is usually tied to the clinical outcome of the drug[58]. In drugs such as nivolumab, PD-L1 assay is

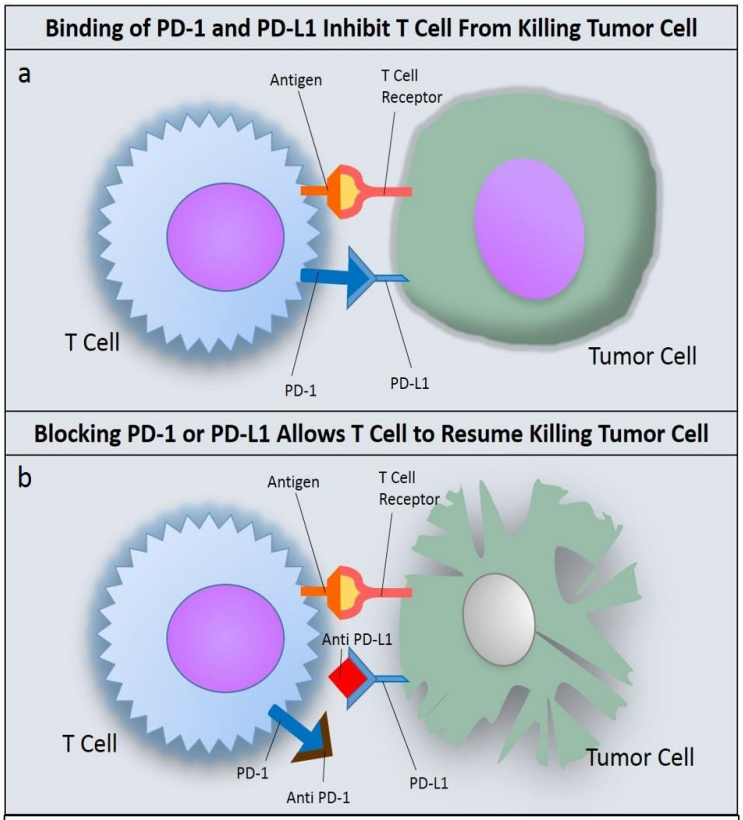

Figure 1| Blocking of PD-1 or PD-L1 Restores Host T Cell Function.
(a) Binding of PD-L1 to PD-1 will inhibit host T Cell from killing the tumor cell. (b) By drugging either PD-1 or PD-L1, receptor binding is blocked and the T Cell can resume normal tumor killing functions

used as complementary for patient selection. Based on several clinical studies, it is clear that current immunohistochemistry (IHC) diagnostic agents for detecting PD-L1 in patients' tissues suffer from three serious limitations. *First*, IHC agents for PD-L1 are based on antibodies raised against different clones of PD-L1; even though these IHC agents target the same marker they identify different parts of the marker. Therefore, these agents give different staining pattern based on the clone used. *Second,* the antibody used for detecting the primary IHC agent bound to the tissue would also be different in these assays resulting in varying performance based on the assay used for diagnosis. *Third,* the IHC agents were designed and developed by different companies and they would require the use of their own staining equipment and scoring algorithm. For example, Dako's IHC agents used for selecting patients for nivolumab and pembrolizumab, utilize Dako IHC autostainer and their own scoring algorithm. In a similar fashion, for selecting patients for treating with drugs such as Atezolizumab and Durvalumab, Ventana diagnostics utilize Ventana automated IHC platforms and their own scoring algorithm. The data comparing these IHC agents for patients' response, the Blueprint Project –a collaboration of 6 major pharmaceutical companies focused on comparing these tests with patient's response data, is still ongoing. It is worth to mention here that factors such as tumor heterogeneity would not play a role in predicting patient response, as this factor is common in both PD-L1 positive and PD-L1 negative patients. Furthermore, running a different test for each drug evaluated is impractical due to limited tissue from biopsy, turnaround time, and cost. Potential harm to patients can result if inappropriate tests or cutoff levels are used to make treatment decisions[59]. Among all, the PD-L1 marker itself is also somewhat labile and must be evaluated soon after the biopsy.[60]

In order to overcome the problems associated with PD-L1 IHC, we have identified a novel peptide sequence, RKC-10, which is specific for human PD-L1. RKC-10 has shown to bind optimally to the structure of PD-1 receptor using crystal structure analysis of the PD-L1:PD1 binding pocket. RKC-10 can be modified with reporter molecules of interest, such as biotin for IHC (RKC-10-Biotin), or fluorescent molecules for fluorescent analysis (RKC-10-Cy5, Cy5). As mentioned above, antibody based IHC agents recognizes different epitopes in PD-L1; in sharp contrast, the identified peptide sequence recognizes the unique binding site between PD-1 and PD-L1. Additionally, the peptide based assay developed in this study is standalone, that is secondary antibody is not necessary for staining. Peptide attached with fluorescent dye enable easy detection of the PD-L1 biomarker in the tissue. The data presented in this study, utilizes manual staining of RKC-10 in human tissues; therefore, the need for autostainer specific for this agent is not needed. Additional advantages include that the peptide is relatively inexpensive, easy to synthesize in laboratory, and can be mass produced in higher quantities. The results obtained demonstrate that RKC-10 is very specific in binding to tumor cells *in vitro*. For this study, the specificity of RKC-10 has been evaluated using IHC methods in over 200 different patient tissues (One placental tissue, Seven patient NSCLC cases, five Hodgkin's Lymphoma cases, and a TMA containing 78 cases of squamous cell carcinoma, 69 cases of adenocarcinoma, 3 cases of mucinous carcinoma, 7 cases of bronchioalveolar carcinoma, 5 cases of adenosquamous carcinoma, 4 cases of atypical carcinoid, 15 cases of small cell carcinoma, and 11 cases of large cell carcinoma). Further investigation of RKC-10 has been done in breast, retinoblastoma, and lung cancer cell lines using flow cytometry. Flow cytometry using RKC-10 was also performed in whole blood spiked with PD-L1 expressing cells, and squamous cell

carcinoma and metastatic melanoma obtained from patients. We used gold standard Ventana SP263 PD-L1 for IHC comparison, and commercially available CD274 for flow cytometry comparison.

3.2 Materials and Methods

3.2.1 Identification of RKC-10 Peptide

The RCSB protein data bank was searched for the complex of PD1 and PD-L1. Out of the results, the structure corresponding to the PDB ID "4ZQK" was selected for analysis because it represents the Structure of the complex of human programmed death-1 (PD-1) and its ligand PD-L1 in its non-mutated form with an X-ray resolution of 2.45 Å. The selected structure was visually examined using the open-source program PyMOL Molecular Graphics System Version 1.8.20. A proprietary Fortran program was developed and used to analyze interactions between residues within the binding region. If distance between two residues in the binding region was less than or equal to 1.2 times the sum of the Van der Waal's radii of the two atoms, it was regarded to be a contact and the residue-residue contact count was updated to +1. Number of occurrences for each sequence was calculated and used to identify the peptide sequences used in this study.

3.2.2 Flow Cytometry Using Cultured Cell Lines

Cell lines MDA-MB-231, Y79, and MCF-7 were purchased from ATCC, thawed, and grown in culture to confluency. When confluent, adherent cells were removed from the flask by scraping gently with a cell scraper and media removed using centrifugation. Suspension cells were pipetted from the flask and centrifuged to remove media. Cell lines were resuspended in Eppendorf tubes in 100 µL PBS at a concentration of $5x10^6$ cells per mL. Cy5-conjugated peptide

solution was then added to the tubes to make the desired concentration of peptide in 200 µL. Eppendorf tubes were then placed in the incubator for 1 hour and vortexed at the 30-minute mark. After 1 hour, cell lines were analyzed on a BD FACS Canto II, a 3-laser, 8-color flow cytometer (San Jose, CA) using Diva 8.0 acquisition and analysis software (San Jose, CA). The cells of interest were gated using Forward and Side scatter (FSC/SSC) and positive antibody expression. 10,000 singlet events were collected for each specimen.

3.2.3 Flow Cytometry Using Patient Tissues

All investigations using patient tissues were de-identified according to IRB protocol (IRB project number 2004603). Cases were evaluated using flow cytometry for suspected hematopoetic neoplasms. A portion of each fresh specimen was collected into RPMI. Each sample was prepared to create cell suspensions which were combined with neat amounts of the following antibodies (BD, San Jose, CA): CD15 FITC, CD34 PE, CD33 PerCP-Cy5-5, CD13 PE-Cy7, CD11B APC, HLA-DR APC-H7, CD16 V450, CD45 V500C, Kappa FITC, Lambda PE, CD5 PerCP-Cy5-5, CD19 PE-Cy7, CD23 APC, CD20 APC-H7, CD10 BV421 V450, CD4 FITC, CD8 PE, CD2 PE-Cy7, CD56 APC, CD3 APC-H7, CD7 V450, CD38 PerCP-Cy5-5, CD10 APC, CD5 BV421 V450, CD23 PE, CD8 PE-Cy7, CD200 APC, and CD138 PerCP-Cy5-5 (Dako, Carpinteria, CA) and incubated for 15 minutes in the dark. Any erythrocytes within the specimens were lysed with BD PharmLyse (San Jose, CA) and the specimens were washed with BD Staining Buffer with BSA (San Jose, CA). Each sample was evaluated using BD FACSC anto II, a three laser, eight-color flow cytometer (San Jose, CA) within 24 hours of collection. 50,000 events were collected for each sample. The expression data were analyzed using BD FACS Diva software, version 8.0 (San Jose, CA). Cases diagnosed as non-hematopoietic tumors were further subjected to evaluation with PDL-1

peptide if material was available combined with CK to identify the epithelial component. The cell suspensions were stained with 10µl of BD Cytokeratin FITC (clone CAM5.2), 20µl of Cy5-conjugated peptide solution, and 10µl of BD Pharmingen CD274 PE (clone MIH1), incubated in the dark for 30 minutes, washed with BD Stain Buffer with BSA, and reconstituted to 500µl with Stain Buffer with BSA in 500ml polystyrene tubes for analysis. The specimens were analyzed on the FACS Canto II using the same panel template, gating strategy, and collection events as the cell line specimens.

3.2.4 Immunohistochemistry Using Biotinylated Peptide

To detect PD-L1 in FFPE tissues we employed manual IHC techniques with a biotin-conjugated version of peptide RKC-10-Cy5 (CPC Scientific) and compared with Ventana PD-L1 (SP263) Rabbit monoclonal Primary Antibody stained on a Roche Benchmark Ultra autostainer. Seven PD-L1 expressing NSCLC patient tissues were obtained from the MU OneHealth tissue bank and de-identified according to IRB protocols. Paraffin-embedded patient tissue slides were baked overnight, then de-waxed and rehydrated according to standard protocols. Tissue sections were then subjected to antigen retrieval in EDTA at 95°C for 20 minutes in EDTA (pH 0.9). The solution is then cooled for an additional 20 minutes on the bench top prior to buffer rinse. Tissues were then incubated with 15 µM biotinylated peptide for 2 hours in a humid chamber at RT. After 2 hours, slides were washed with buffer and treated with Pierce™ High Sensitivity Streptavidin-HRP (1:200 dilution) (Sigma) for 30 minutes at RT in a humid chamber. Once this was complete, slides were again washed in buffer then treated with DAB (Sigma) for 10 minutes. Slides were again washed in buffer, then dehydrated using graded alcohol and xylene

and counterstained with hematoxylin. Slides were then imaged using brightfield microscopy on a Leica DM5500.

3.2.5 Immunohistochemistry Using Cy5 Fluorophore Conjugated Peptide

We investigated PDL1 in seven FFPE tissues and 192 lung cancer cases on a microarray using our peptide conjugated with Cy5 fluorophore (CPC Scientific). A lung cancer tissue microarray (TMA) was purchased from U.S. Biomax that contains 192 separate cases of various types of lung cancers (LC1923, biomax.us). In addition, seven NSCLC patient tissues were obtained from the Mizzou OneHealth tissue bank and de-identified according to IRB protocols. Paraffin-embedded tissue slides were baked overnight, then de-waxed and rehydrated according to standard protocols. Tissue sections were then subjected to antigen retrieval in EDTA at 95°C for 20 minutes in EDTA (pH 0.9). The solution is then cooled for an additional 20 minutes on the bench top prior to buffer rinse. Tissues were then incubated with 15 µM Cy5-conjugated peptide for 2 hours in a humid chamber in the dark at RT. After 2 hours, slides were washed with buffer. The slides were then mounted using nucleus-specific DAPI counterstain and cover slipped. Slides were then imaged using fluorescence microscopy on a Leica DM5500 and compared to the same sections which had been stained with the Ventana antibody. For fluorescent analysis, DAPI channels and Cy5 channels were overlaid to image cell nuclei and PD-L1 expression, respectively.

3.2.6 IHC Blocking Using PD-L1 Peptide or Ventana Antibody SP263

To test specificity of the PD-L1 peptide, we first blocked IHC signals of the SP263 antibody by treating the tissue with PD-L1 peptide for 1 hour prior to autostaining the tissue using the Roche autostainer with the Ventana PD-L1 kit according to Roche's specifications. We also

investigated blocking of the PD-L1 peptide using the SP263 antibody by first treating the tissue with SP263 antibody for 30 minutes prior to treating the tissue with peptide according to the previously mentioned protocol.

3.3 Results

3.3.1 Identification of PD-L1 Binding Peptide and Mock Peptide

We focused our initial research on understanding the interaction of PD-1 and PD-L1 based on X-ray crystal structure data (S1) with the goal of identifying the peptide sequence that is selectively mediating the interactions. After the crystal structure of each protein was identified, a proprietary Fortran program was used to analyze which amino acid sequences interact most closely between the two proteins. Number of occurrences for each sequence was calculated and used to identify the peptide sequences used in this study. (Figure 2). The calculations provided several sequences of peptide that could possess high-affinity for targeting PD-L1 in tumor. As a first step, we synthesized a library of peptides and studied the stability and PD-L1 affinity. The study resulted in identification of a high affinity peptide, RKC-10-Cy5 for targeting PD-L1. Data related to anti-PDL1 and mock peptide was used to synthesize peptides for this study. Binding sequences of each peptide were further modified to incorporate either

biotin or fluorophore for antigen detection, and to increase solubility of the peptide.

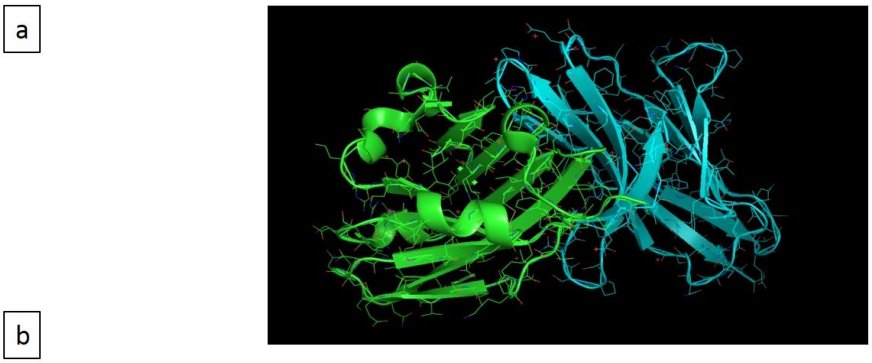

Figure 2| a. Protein structure of PD-1 (blue) and PD-L1 (green) **b.** Flowchart for identifying optimal peptide binding sequence

3.3.2 Fluorescent RKC-10-Cy5 as Marker for Flow Cytometry

RKC-10-Cy5 was then investigated for PD-L1 specificity using flow cytometry in cultured cell lines and patient tissues. The cell lines examined were breast cancer line MDA-MB-231, which shows very high PD-L1 expression[61], along with retinoblastoma line Y79 and breast cancer line MCF-7, which show no meaningful PD-L1 expression[62]. To set our conditions for flow cytometry, we first examined titrations of PD-L1 peptide using all three cell lines. Cultured cells were grown to confluency and removed from the flask using a cell scraper. Media was removed through centrifugation and 100 µL of Pharmingen Stain Buffer(BSA) containing 5x10^5 cells was resuspended in 5 separate 1.5 mL Eppendorf tubes. 100 µL of buffer containing RKC-10-Cy5 was added to the five tubes to make final concentrations of 0.1, 0.05, 0.01, 0.005, and 0.001 mg/mL of peptide per cell sample. The tubes were vortexed and allowed to remain at RT for 1 hour. 15 minutes prior to performing flow cytometry, 10 µL of cytokeratin-specific antibody

containing a FITC fluorophore was added to each cell solution. Cells were then examined using flow cytometry. In each of the samples we gate for double-positives by analyzing expression of both cytokeratin (FITC channel) and PD-L1 (Cy5 channel) (S2). For all three cell lines we see a decrease in mean fluorescence intensity (MFI) as the concentration of peptide decreases (Figure 3, S3-5). Samples containing 0.1 and 0.05 mg/mL concentrations were deemed to have fluorescence intensities too high for accurate analysis for each cell line. Y79 and MCF7 both have a much lower PD-L1 expression than MDA-MB-231, which correlates with expression

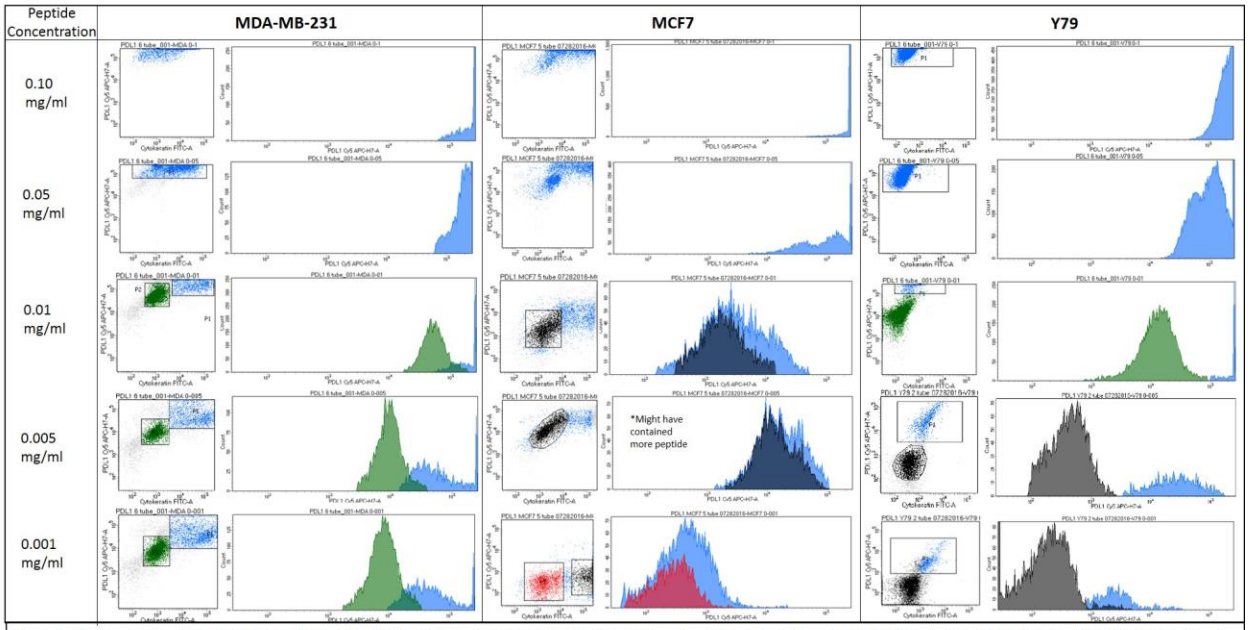

Figure 3| Flow Cytometry Titrations of RKC-10-Cy5 in Cell Lines. Cultured cell lines expressing high PD-L1 (MDA-MB-231) and low PD-L1 (MCF7, Y79) were incubated with fluorescent RKC-10-Cy5 peptide and anti-cytokeratin for 1 hour at shown concentrations, then analyzed for expression using flow cytometry. Higher concentrations of peptide were unable to distinguish expression, while lower concentrations of 0.005 and 0.001 mg/mL peptide were selected as ideal for flow cytometry.

seen using our Cy5 conjugated peptide and comparing the cell lines with flow cytometry. Y79 and MCF7 MFI is close to tenfold lower than that seen in MDA-MB-231 in all lower concentrations. The MCF7 sample containing 0.005mg/ml was much higher than anticipated due to this sample being treated twice with peptide. We selected 0.005 mg/mL as our optimal concentration based on these comparisons, and all subsequent flow cytometry experiments

were performed using this concentration. Lung cancer cell lines A549 (low PDL1) and HCC827 (high PDL1) were investigated for PD-L1 expression using both phycoerythrin-conjugated cd274 and RKC-10-Cy5 (Figure 4,S6). Cell lines were cultured as before and treated with either antibody or peptide in buffer. When run through the flow cytometer we see a much higher signal associated with PD-L1 expression in the HCC827 cell line than in the A549 samples. The antibody associated fluorescence was higher than the peptide associated fluorescence in both samples, which is attributed to differences in titrating peptide and antibody.

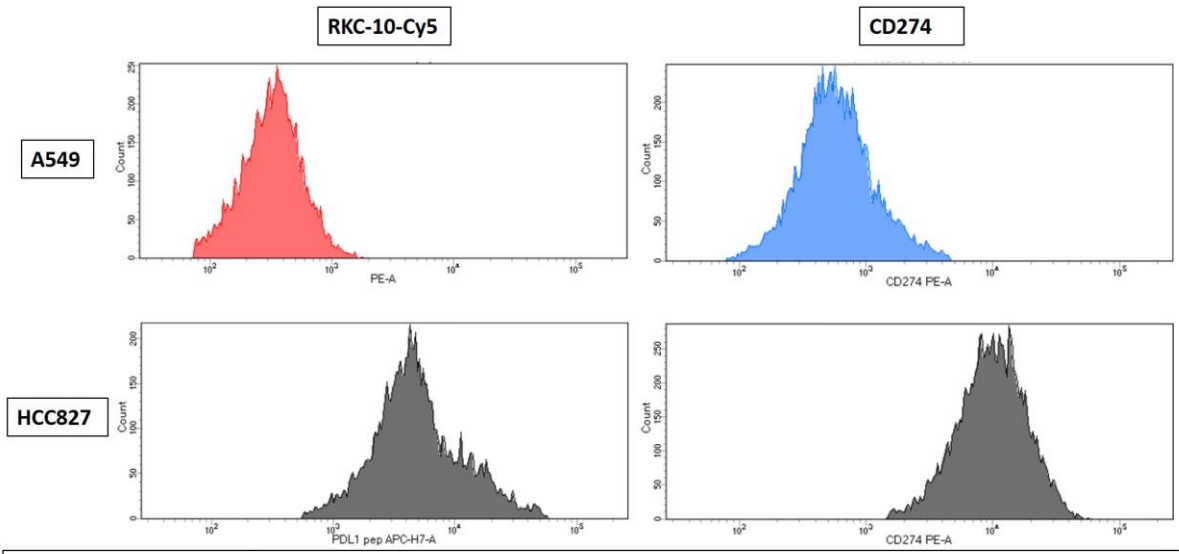

Figure 4| RKC-10-Cy5 and CD274 Antibody Compared in NSCLC Cell Lines. NSCLC cell lines A549 (PD-L1 low) and HCC827 (PD-L1 high) were incubated with either RKC-10-Cy5 peptide or CD274 antibody for 1 hour, then analyzed using flow cytometry. As expected, both antibody and peptide showed high MFI in HCC827, while A549 showed much lower MFI.

3.3.3 Detection of PD-L1 in Circulating Tumor Cells and Patient Tissues

PD-L1 expression in patient tissues was analyzed using RKC-10-Cy5 and compared to expression in MDA-MB-231 cells and a negative control of normal blood (Figure 5). The MFI of the MDA-MB-231 cells was 9,448, while the whole blood gave an MFI of -123 (S9). We investigated both a squamous cell carcinoma and metastatic melanoma sample for PD-L1

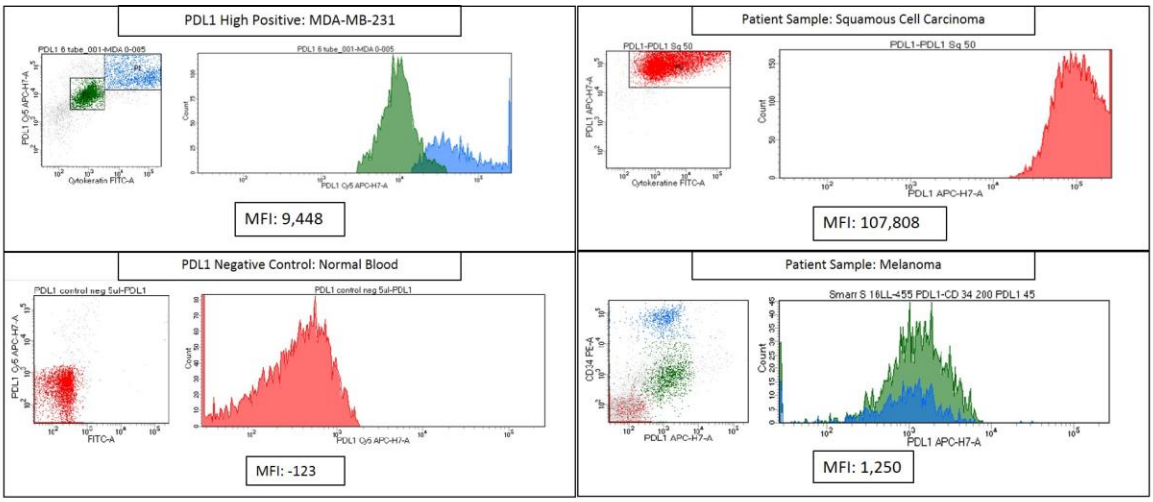

Figure 5| Flow Cytometric Analysis of PD-L1 Expression in Patient Tissues. RKC-10-Cy5 peptide was incubated with patient melanoma and squamous cell carcinoma samples for 1 hour according to clinical protocols. Patient tissues were compared to MDA-MB-231 (PD-L1 high positive) and normal blood (PD-L1 negative) in order to asses PD-L1 expression. The SCC sample showed very high PD-L1 expression, while the melanoma sample showed a moderate expression of PD-L1.

expression using those MFIs as high and negative, respectively. The squamous cell carcinoma was shown as having an MFI of 107,808, while the melanoma sample gave an MFI of 1,250. The squamous cell carcinoma PD-L1 expression was very high, while the melanoma sample was graded as 'moderate' PD-L1 expression (S10,11). The melanoma sample showed no expression of cytokeratin. Since loss of CK expression is consistent with circulating tumor cells, we believe we can use RKC-10-Cy5 to detect CTCs. To see whether detection of low cell counts was possible, whole blood samples were spiked with MDA-MB-231 cells. MDA-MB-231 were diluted with whole blood, then treated with RKC-10-Cy5 and cytokeratin before staining. These samples were also treated with a phycoerythrin-conjugated antibody (cd274) against PD-L1 to further verify PD-L1. We were indeed able to detect positive signals of cytokeratin and PDL1 expression at low counts of ~15 cells in the whole blood sample using both the peptide and the antibody (Figure 6).

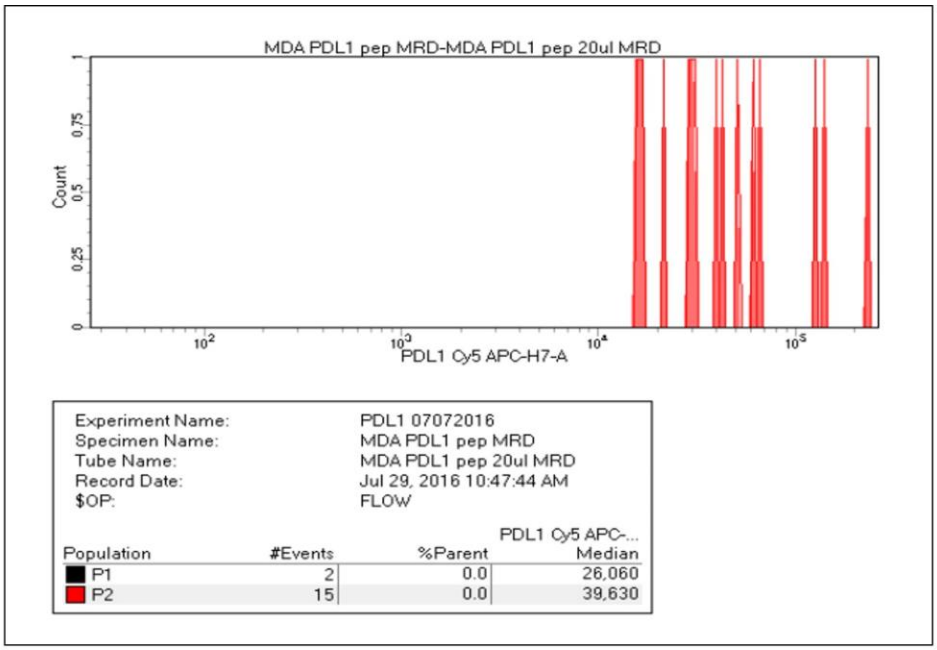

Figure 6| Whole Blood Spiked with MDA-MB-231. High PD-L1 expressing cell line MDA-MB-231 was serially diluted in 2mL of whole blood and treated with RKC-10-Cy5 peptide and anti-cytokeratin. Counts of cells as low as 15 cells were seen using RKC-10-Cy5 peptide, and confirmed using the cytokeratin stain.

3.3.4 Biotinylated RKC-10-Biotin as Immunohistochemistry Agent

Seven Patient NSCLC tissues were investigated for PD-L1 using either manual IHC with 15 µM RKC-10-Biotin peptide, or the Ventana PD-L1 (SP263) rabbit monoclonal primary antibody stained on a Roche Benchmark Ultra. In this study the peptide was conjugated with biotin, which was used to bind a secondary treatment of streptavidin-HRP. Formalin-Fixed Paraffin Embedded (FFPE) placenta tissue was used as the positive control, since PDL1 is expressed in placental trophoblasts[63]. In this study we also utilized biotinylated mock peptide RKC-11-Biotin as a negative control. This mock peptide was synthesized to have very low affinity to PD-L1. Both the PD-L1 peptide (RKC-10-Biotin) and Ventana clone SP263 stained the trophoblasts heavily in the placental tissue (Figure 7, S12-14). The SP263 antibody featured heavy edge staining but also showed membranous staining of the trophoblast cells. RKC-10-Biotin peptide showed heavy membrane staining of the trophoblast cells without the intense edge artifacts

seen when using the

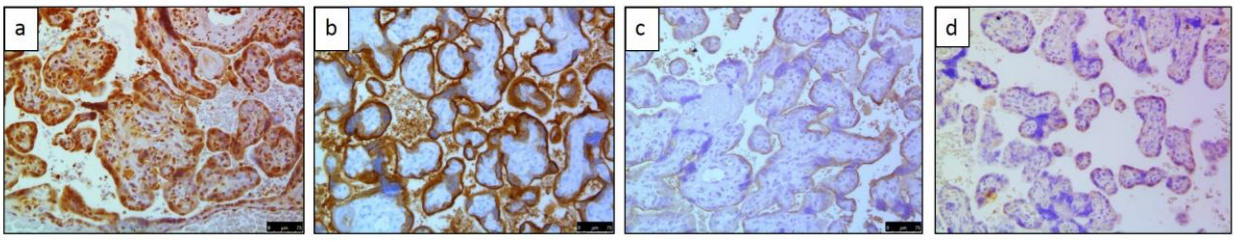

Figure 7| FFPE placenta tissue. Placenta tissue was treated with (a) 15 µM RKC-10-Biotin, (b) Ventana SP263 PDL-1 antibody, (c) pre-blocked with RKC-10-Biotin, then treated with Ventana PDL-1 antibody, (d) mock peptide RK-11-Biotin

SP263 antibody. Low-affinity mock peptide RKC-11-Biotin showed light staining at high concentrations, but did not achieve the heavy staining RKC-10-Biotin did (Fig 7d, S15). Higher concentrations of the peptide showed more staining in other parts of the placental tissue, but the heaviest staining is localized to the trophoblast cells (S2-S6). Blocking of the SP263 antibody was achieved by first treating the placenta tissue with RKC-10-Biotin for 30 minutes, washing, and treating on the Roche autostainer according to specifications. The pre-blocked tissue showed drastic reduction of staining, with mostly edge artifacts being seen (Figure 7c). Placenta tissue that was not pre-blocked was stained with the SP263 kit in parallel with the pre-blocked tissue, and showed the expected trophoblast staining as before (S16-18).

Once confidence in PD-L1 staining was established in repeated placenta tissues, we compared staining in seven NSCLC patient tissues (patients 'A' through 'G') with the SP263 antibody and RKC-10-Biotin (Figure 8, S21-29). When using the RKC-10-Biotin peptide we saw heaviest staining localized to the tumor regions of the tissues, which can be very intense based on the concentration of peptide used. In contrast, the SP263 antibody did not show heavy tumor staining in most tissue sections, showing only faint staining in these regions that could be interpreted as negative or faintly positive for PD-L1. The most intense staining from the SP263

kit was shown in the tumor cells of patient G. All areas of patient G that stained positive for PD-L1 using the SP263 antibody also stained positively using PD-L1 peptide.

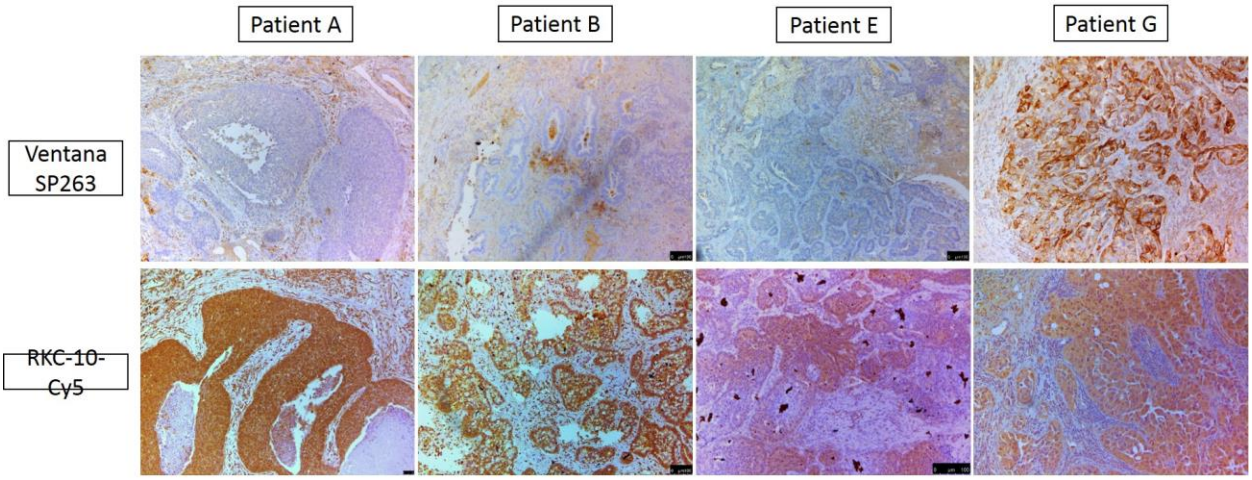

Figure 8| Biotinylated RKC-10-Cy5 Peptide in IHC Application. Patient tissues were stained using IHC protocols using either SP263 or biotinylated RKC-10-Cy5 and analyzed for tumor staining. RKC-10-Cy5 stains tumor specifically in all cases, whereas SP263 only showed significant staining in patient G

3.3.5 Fluorescent RKC-10-Cy5 as Immunohistochemistry Agent

We compared staining of the placenta and seven selected NSCLC patient tissues using the SP263 antibody and RKC-10-Cy5 conjugated with a Cy5 fluorophore. To stain with the fluorescent PD-L1 peptide, antigen retrieval was performed and tissue slides were treated with 15 µM fluorescent peptide in a dark, humid chamber for 2 hours, washed with buffer, then counter-stained and mounted with DAPI nucleus stain. Peptide-stained slides were imaged on a Leica DM5500 using channels specific for DAPI or Cy5, and channels were overlaid to examine PD-L1 expression. To confirm the data from the IHC stained tissues, the same seven patient tissues A-G were stained with RKC-10-Cy5 (Figure 9, S30-46). The Cy5 signal in these tissues was consistent with the HRP staining, where RKC-10-Cy5 peptide stained many areas of tumor that the SP263 antibody did not. Where the SP263 staining is positive, we see similar staining between both the antibody and peptide. However, many tumor areas not visibly stained by the

antibody were stained specifically when the peptide was used. To examine a larger range of tissues for PDL1 expression, fresh-cut lung cancer tissue microarrays containing 192 separate

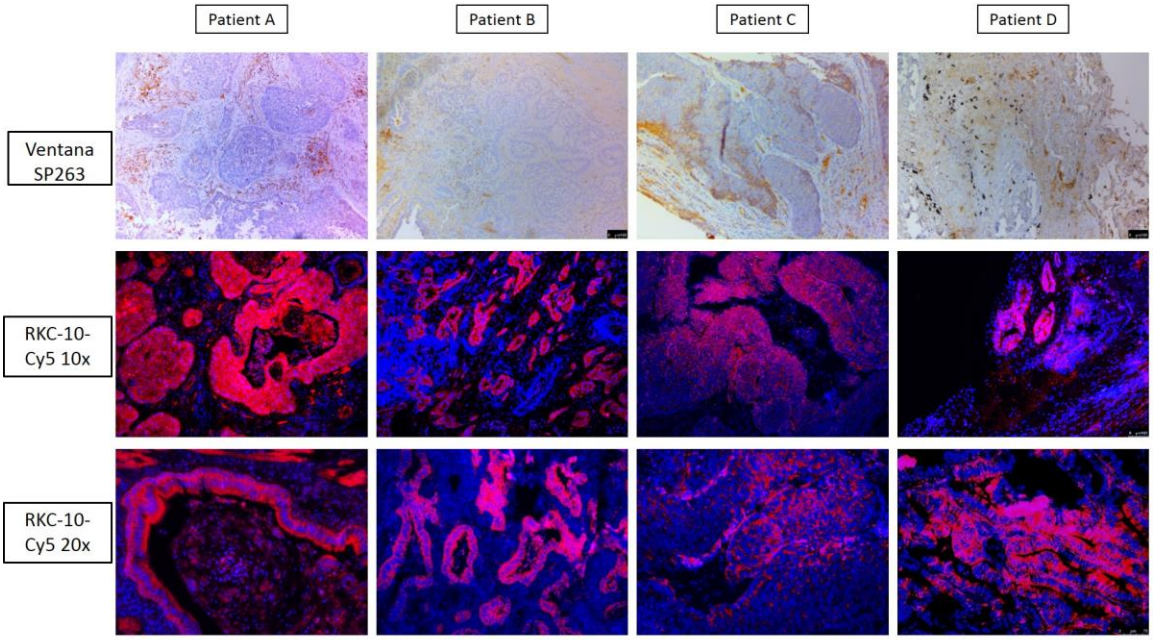

Figure 9| Comparison of PD-L1 Evaluation in Patient NSCLC Tissues. Seven patient NSCLC tissues were stained using either SP263 or RKC-10-Cy5 peptide. All cases stained using RKC-10-Cy5 showed high affinity for tumor, while SP263 only showed heavy tumor staining in patient G and some lighter staining in patients C and D.

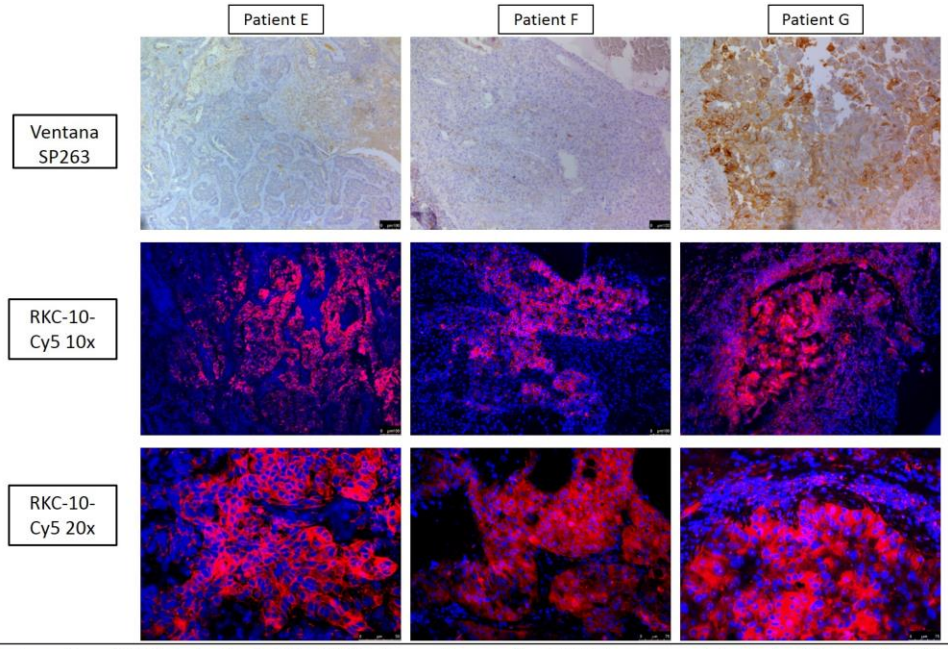

Figure 9| Comparison of PD-L1 Evaluation in Patient NSCLC Tissues. Seven patient NSCLC tissues were stained using either SP263 or RKC-10-Cy5 peptide. All cases stained using RKC-10-Cy5 showed high affinity for tumor, while SP263 only showed heavy tumor staining in patient G and some lighter staining in patients C and D.

cases of lung cancers were purchased from U.S. Biomax, Inc. This array (S47) contained 78 cases

of squamous cell carcinoma, 69 cases of adenocarcinoma, 3 cases of mucinous carcinoma, 7 cases of bronchioalveolar carcinoma, 5 cases of adenosquamous carcinoma, 4 cases of atypical carcinoid, 15 cases of small cell carcinoma, and 11 cases of large cell carcinoma. To analyze stained TMAs, the slides were scanned in at 10x magnification using the Leica DM5500 motorized stage and stitched together using Leica LAS X software (S48-56). Serial sectioned TMAs were then compared head to head when stained with either SP263 kit or the RKC-10-Cy5 peptide (Figure 10).

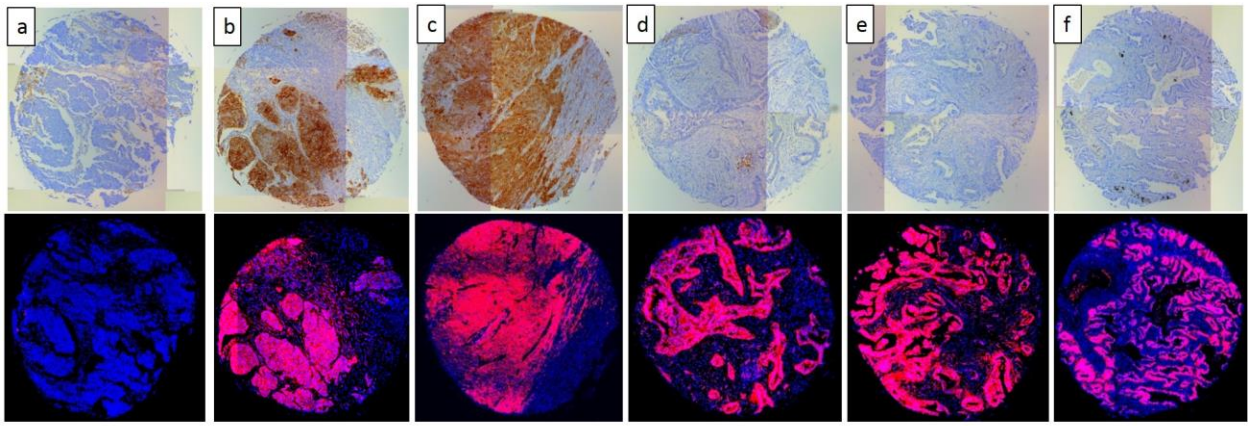

Figure 10| Select Cases From NSCLC TMA. Six of 192 cores from Biomax TMA LC1923 are shown which were stained using either Roche SP263 antibody (top) or RKC-10-Cy5 peptide (bottom). Shown are representative samples which show negative PD-L1 with both methods (a), positive PD-L1 with both methods (b,c), and samples which are negative using SP263 but stain positive in the tumor using RKC-10-Cy5.

In cases where the SP263 antibody was negative for tumor staining, the same is seen with the RKC-10-Cy5 peptide (Fig. 10a). Likewise, in cases where the SP263 antibody stained positively in tumor, RKC-10-Cy5 shows staining consistent with the SP263 stain (Fig. 10b,c). Interestingly, in the majority of cases, the SP263 antibody showed no tumor staining, while the RKC-10-Cy5 peptide showed consistent, specific staining in tumor cells and immune infiltrate (Fig. 10d, e, f). Analysis of individual spots at 40x confirms the presence of specific tumor cell staining (Figure 11). These results are consistent with the biotin-conjugated peptide IHC, where the PD-L1 peptide stained many large areas of tumor, while the SP263 antibody showed little to no

staining in many of these areas. The Cy5 channel was very intensely bright and we had to use a very low exposure in order to image the PD-L1. PD-L1 expression was specifically seen in tumor areas of the tissue, and staining of immune cells was also seen outside the tumor areas, as is expected.

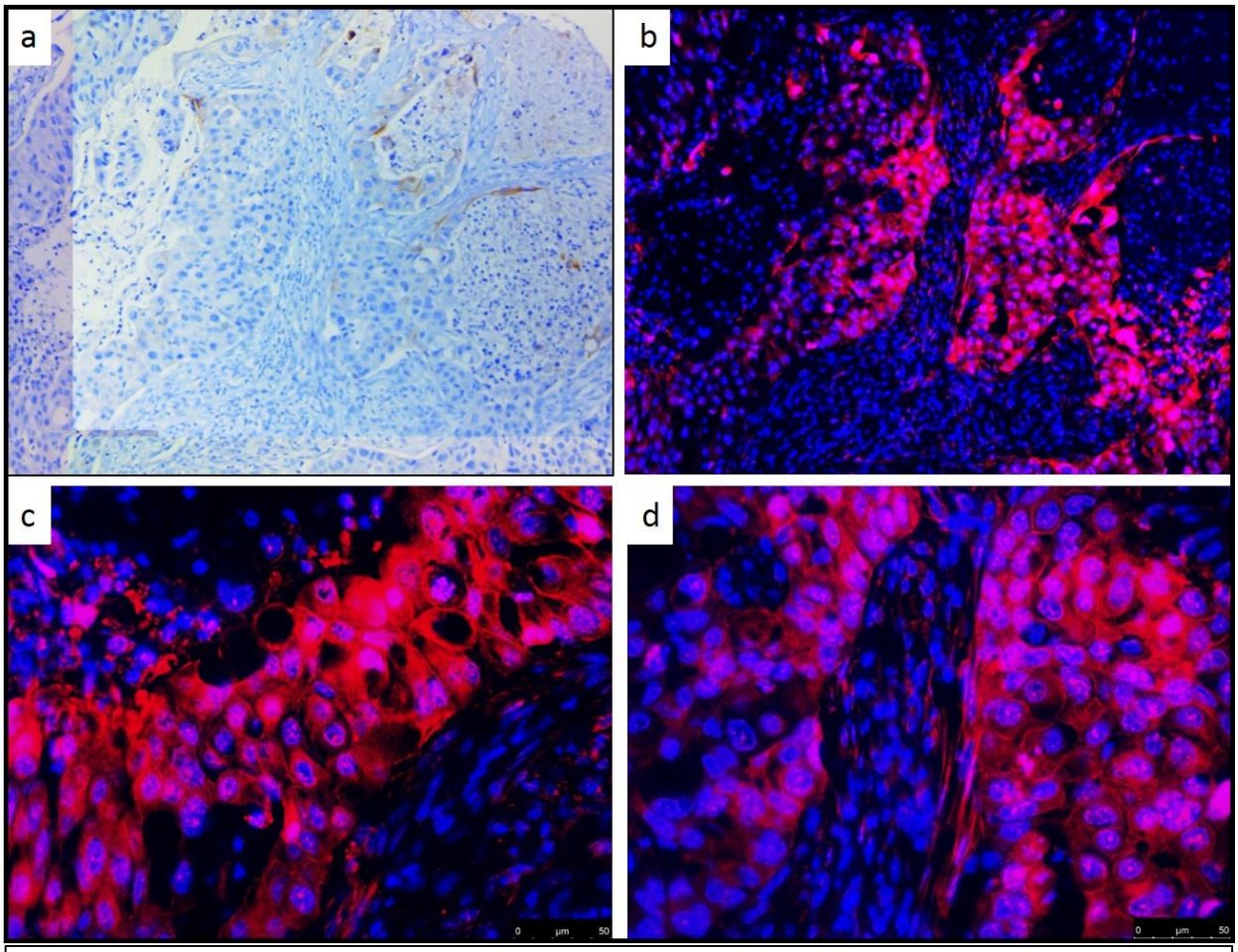

Figure 11| Peptide Positive Spot at 40x Magnification. A selected TMA core which stained negative using SP264 antibody (a) shows high membrane staining in the tumor using fluorescent RKC-10-Cy5 peptide at 10x (b) and 40x (c,d) magnifications.

3.3.6 Fluorescent RKC-10-Cy5 Detects PD-L1 on Reed-Sternberg Cells in Hodgkin's Lymphoma

In addition to the NSCLC patient tissues, we also investigated four different Hodgkin's Lymphoma cases for PD-L1 expression. Presence of Reed-Sternberg cells in a biopsied tissue is often the diagnostic indicator of a patient having Hodgkin's lymphoma. RS cells are large, often

multinucleated tumor cells that are derived from B-cell lymphocytes. RS cells heavily express PD-L1[64], to the point of PD-L1 being a diagnostic indicator of RS cells. Due to the characteristic expression of PD-L1 in RS cells, we examined PD-L1 levels in the four identified Hodgkin's lymphoma patient samples using the fluorescent RKC-10-Cy5 peptide and compared with the SP263 antibody (Figure 12). In each patient sample, the pathologist-identified RS cells showed PD-L1 staining with both RKC-10-Cy5 and SP263 antibody. When using the RKC-10-Cy5 peptide, RS cells were easily identified by the pathologist due to the heavy Cy5 fluorescent signal. These cells were additionally confirmed as RS cells by examining the multinucleate characteristic of the cells, shown clearly by staining the nuclei with fluorescent DAPI. The SP263 antibody IHC additionally confirmed the presence of PD-L1 in the RS cells. Using both methods, we also see some light staining of the tumor microenvironment besides the RS cells, which is expected as PD-L1 is often expressed on immune cells.

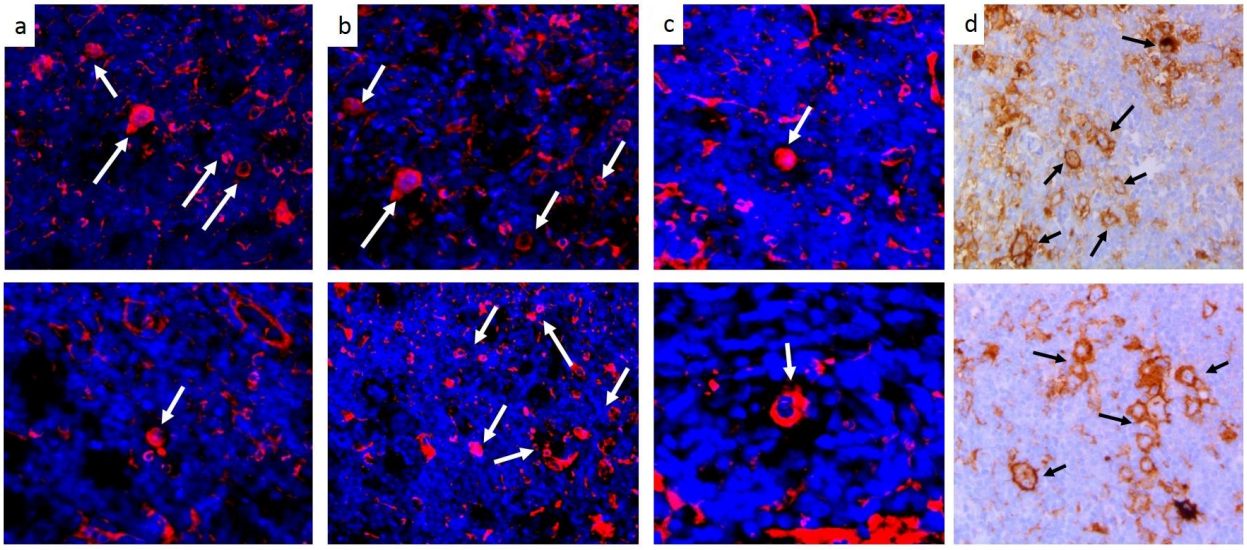

Figure 12| RKC-10-Cy5 Detects Presence of PD-L1 on Reed-Sternberg Cells in Hodgkin's Lymphoma. Hodgkin's Lymphoma tissues were incubated with either fluorescent RKC-10-Cy5 peptide (a-c) or SP263 antibody (d) to examine PD-L1 levels in Reed-Sternberg (RS) cells. RKC-10-Cy5 was able to specifically stain the RS cells (some but not all indicated by arrows), which are known to express high levels of PD-L1. PD-L1 expression in RS cells was also confirmed with the SP263 staining.

3.4 Discussion

The PD-L1 targeting peptide RKC-10-Cy5 was identified through structural analysis of PD-1: PD-L1 binding pocket structure. PD-L1 specific peptide RKC-10-Biotin has shown high specificity for tumor cells in 200 different cases of tissue – 192 lung cancer cases on a TMA, seven patient lung cancers, and one placenta tissue. Patient tissues stained specifically and reproducibly within the tumor and PD-L1 expressing immune cells using either a biotin-conjugated peptide for IHC, or a Cy5 fluorophore-labelled peptide for fluorescent microscopy. RKC-10-Cy5 staining showed a positive correlation with Ventana's FDA-approved PD-L1 diagnostic (SP263) where the SP263 kit stained tumor positively for PD-L1 expression. While there were some cases that were negative using both SP263 and RKC-10-Cy5, there were a large number of cases where RKC-10-Cy5 showed very specific tumor staining that were not stained by the SP263 antibody. This could either be due to higher specificity of RKC-10-Cy5 or due to a lower titration of SP263 to only detect PD-L1 above a clinical cutoff, since the SP263 kit is meant for clinical diagnosis for use with its companion therapeutic drug durvalumab. In the Hodgkin's lymphoma cases, PD-L1 expression as measured by the RKC-10-Cy5 peptide matched up well with the IHC staining shown by the SP263 antibody, especially in the Reed-Sternberg cells. Since pembrolizumab was recently fast-tracked by the FDA to treat Hodgkin's lymphoma cases, RKC-10-Cy5 will need to be compared with the pembrolizumab companion diagnostic 22C3. Due to the multinucleate characteristics of the RS cells, it would be easy to detect and quantify the number of RS cells in a given Hodgkin's tissue based on PD-L1 expression and nuclei. Since RKC-10-Cy5 shows such specificity for tumor, it could detect a wide range of PD-L1 expression and inform more precise diagnostic levels for treatment. It has been shown that there is an urgent need for a PD-L1

diagnostic that can precisely detect PD-L1 protein irrespective of the drug intended to be used – a sensitive assay such as RKC-10-Cy5 could be used to achieve this. Detection of PD-L1 expression in whole blood and metastatic melanoma suggests that RKC-10-Cy5 could also potentially be used to detect low amounts of circulating tumor cells that express PD-L1. Recent debates about the diagnosis of PD-L1 in patients highlight the need for refined methods of determining PD-L1 levels in the patient. By utilizing a peptide-based approach, we can detect all levels of PD-L1 with a high sensitivity and specificity. In a heterogeneous tumor, identification of PD-L1 expression using traditional methods may not be an accurate way of determining a binary IHC cutoff, but would rather require a wider range of diagnostic levels to determine optimal therapy. Recent studies have also shown tumors that express PD-L1 according to *in vivo* imaging methods, but upon excision for IHC no PD-L1 was detected[65]. Tumor mutations over a given period of treatment may lead to fluctuating PD-L1 levels, and as such may need to be monitored routinely.

3.5 Acknowledgements

We thank Jennifer Schnabel and Diane McConnell of the MU One Health Biorepository for all work related to immunohistochemistry, and Kruthi Murthy at the University of Missouri for work done related to flow cytometry.

4.0 References

1. Krasinskas, A.M., *EGFR Signaling in Colorectal Carcinoma.* Pathology Research International, 2011. **2011**.

2. Normanno, N., et al., *Epidermal growth factor receptor (EGFR) signaling in cancer.* Gene, 2006. **366**(1): p. 2-16.

3. Gazdar, A.F., *Activating and resistance mutations of EGFR in non-small-cell lung cancer: role in clinical response to EGFR tyrosine kinase inhibitors.* Oncogene, 0000. **28**(S1): p. S24-S31.

4. Dziadziuszko, R. and J. Jassem, *Epidermal growth factor receptor (EGFR) inhibitors and derived treatments.* Annals of Oncology, 2012. **23**(suppl 10): p. x193-x196.
5. Jonker , D.J., et al., *Cetuximab for the Treatment of Colorectal Cancer.* New England Journal of Medicine, 2007. **357**(20): p. 2040-2048.

6. Hartmann, S., et al., *Influence of epidermal growth factor receptor expression on the cetuximab and panitumumab response rates of head and neck carcinoma cells.* Journal of Cranio-Maxillofacial Surgery, 2014. **42**(7): p. 1322-1328.

7. Pirker, R., et al., *EGFR expression as a predictor of survival for first-line chemotherapy plus cetuximab in patients with advanced non-small-cell lung cancer: analysis of data from the phase 3 FLEX study.* Lancet Oncol, 2012. **13**(1): p. 33-42.

8. Sequist, L.V., et al., *Response to Treatment and Survival of Patients with Non-Small Cell Lung Cancer Undergoing Somatic EGFR Mutation Testing.* The Oncologist, 2007. **12**(1): p. 90-98.

9. Lynch, J.A., et al., *Utilization of epidermal growth factor receptor (EGFR) testing in the United States: a case study of T3 translational research.* Genet Med, 2013. **15**(8): p. 630-638.

10. Hutchinson, R.A., et al., *Epidermal growth factor receptor immunohistochemistry: new opportunities in metastatic colorectal cancer.* Journal of Translational Medicine, 2015. **13**(1): p. 1-11.

11. Stone, J., S. Jackson, and D. Wright, *Biological applications of gold nanorods.* Wiley Interdisciplinary Reviews: Nanomedicine and Nanobiotechnology, 2011. **3**(1): p. 100-109.

12. Sau, T.K. and D.V. Goia, *Biomedical Applications of Gold Nanoparticles*, in *Fine Particles in Medicine and Pharmacy*, E. Matijević, Editor. 2012, Springer US: Boston, MA. p. 101-145.

13. Xiao, L. and E.S. Yeung, *Optical Imaging of Individual Plasmonic Nanoparticles in Biological Samples.* Annual Review of Analytical Chemistry, 2014. **7**(1): p. 89-111.

14. Huang, X. and M.A. El-Sayed, *Gold nanoparticles: Optical properties and implementations in cancer diagnosis and photothermal therapy.* Journal of Advanced Research, 2010. **1**(1): p. 13-28.

15. Chen, Y., et al., *Selectively Imaging Single Gold Nanorods by Polarized Light Microscopy with Low Background.* Plasmonics, 2015. **10**(6): p. 1883-1888.

16. Gui, C. and D.-x. Cui, *Functionalized Gold Nanorods for Tumor Imaging and Targeted Therapy.* Cancer Biology & Medicine, 2012. **9**(4): p. 221-233.

17. Huang, X., et al., *Cancer Cell Imaging and Photothermal Therapy in the Near-Infrared Region by Using Gold Nanorods.* Journal of the American Chemical Society, 2006. **128**(6): p. 2115-2120.

18. Li, Z., et al., *Identification and characterization of a novel peptide ligand of epidermal growth factor receptor for targeted delivery of therapeutics.* The FASEB Journal, 2005. **19**(14): p. 1978-1985.

19. Nikoobakht, B. and M.A. El-Sayed, *Preparation and Growth Mechanism of Gold Nanorods (NRs) Using Seed-Mediated Growth Method.* Chemistry of Materials, 2003. **15**(10): p. 1957-1962.

20. Henjes, F., et al., *Strong EGFR signaling in cell line models of ERBB2-amplified breast cancer attenuates response towards ERBB2-targeting drugs.* Oncogenesis, 2012. **1**(7): p. e16.

21. Prahallad, A., et al., *Unresponsiveness of colon cancer to BRAF(V600E) inhibition through feedback activation of EGFR.* Nature, 2012. **483**(7388): p. 100-103.

22. Wang, K., et al., *Characterizing Breast Cancer Xenograft Epidermal Growth Factor Receptor Expression by Using Near-Infrared Optical Imaging.* Acta radiologica (Stockholm, Sweden : 1987), 2009. **50**(10): p. 1095-1103.

23. Cataldo , V.D., et al., *Treatment of Non–Small-Cell Lung Cancer with Erlotinib or Gefitinib.* New England Journal of Medicine, 2011. **364**(10): p. 947-955.

24. Engelman, J.A., et al., * MET Amplification Leads to Gefitinib Resistance in Lung Cancer by Activating ERBB3 Signaling .* Science, 2007. **316**(5827): p. 1039-1043.

25. Wheeler, D.L., et al., *Mechanisms of acquired resistance to cetuximab: role of HER (ErbB) family members.* Oncogene, 2008. **27**(28): p. 3944-3956.

26. Viticchiè, G. and P. Muller, *c-Met and Other Cell Surface Molecules: Interaction, Activation and Functional Consequences.* Biomedicines, 2015. **3**(1): p. 46.

27. Ma, C., S. Wei, and Y. Song, *T790M and acquired resistance of EGFR TKI: a literature review of clinical reports.* Journal of Thoracic Disease, 2011. **3**(1): p. 10-18.

28. Zucali, P.A., et al., *Role of cMET expression in non-small-cell lung cancer patients treated with EGFR tyrosine kinase inhibitors.* Annals of Oncology, 2008. **19**(9): p. 1605-1612.

29. Kawakami, H., et al., *Targeting MET Amplification as a New Oncogenic Driver.* Cancers, 2014. **6**(3): p. 1540-1552.

30. Takeuchi, H., et al., *c-MET Expression Level in Primary Colon Cancer.* A Predictor of Tumor Invasion and Lymph Node Metastases, 2003. **9**(4): p. 1480-1488.

31. Kammula, U.S., et al., *Molecular co-expression of the c-Met oncogene and hepatocyte growth factor in primary colon cancer predicts tumor stage and clinical outcome.* Cancer Letters, 2007. **248**(2): p. 219-228.

32. Ishikawa, T., et al., *Hepatocyte Growth Factor (HGF)/c-Met Signaling is required for Stem Cell Mediated Liver Regeneration.* Hepatology (Baltimore, Md.), 2012. **55**(4): p. 1215-1226.

33. Organ, S.L. and M.-S. Tsao, *An overview of the c-MET signaling pathway.* Therapeutic Advances in Medical Oncology, 2011. **3**(1 Suppl): p. S7-S19.

34. Benedettini, E., et al., *Met Activation in Non-Small Cell Lung Cancer Is Associated with de Novo Resistance to EGFR Inhibitors and the Development of Brain Metastasis.* The American Journal of Pathology, 2010. **177**(1): p. 415-423.

35. Koeppen, H., et al., *Biomarker Analyses from a Placebo-Controlled Phase II Study Evaluating Erlotinib ± Onartuzumab in Advanced Non–Small Cell Lung Cancer: MET Expression Levels Are Predictive of Patient Benefit.* Clinical Cancer Research, 2014. **20**(17): p. 4488-4498.

36. Hirsch, F.R., P.A. Bunn, and R.S. Herbst, *"Companion Diagnostics": Has Their Time Come and Gone?* Clinical Cancer Research, 2014. **20**(17): p. 4422-4424.

37. Rolfo, C., et al., *Onartuzumab in lung cancer: the fall of Icarus?* Expert Review of Anticancer Therapy, 2015. **15**(5): p. 487-489.

38. Locatelli, E., I. Monaco, and M. Comes Franchini, *Surface modifications of gold nanorods for applications in nanomedicine.* RSC Advances, 2015. **5**(28): p. 21681-21699.

39. Zhao, P., et al., *Identification of a Met-Binding Peptide from a Phage Display Library.* Clinical Cancer Research, 2007. **13**(20): p. 6049-6055.

40. Li, B., et al., *Higher Levels of c-Met Expression and Phosphorylation Identify Cell Lines With Increased Sensitivity to AMG-458, a Novel Selective c-Met Inhibitor With Radiosensitizing Effects.* International Journal of Radiation Oncology*Biology*Physics, 2012. **84**(4): p. e525-e531.

41. Dua, R., et al., *Detection of Hepatocyte Growth Factor (HGF) Ligand-c-MET Receptor Activation in Formalin-Fixed Paraffin Embedded Specimens by a Novel Proximity Assay.* PLOS ONE, 2011. **6**(1): p. e15932.

42. Ido, A., et al., *Mucosal repair and growth factors: recombinant human hepatocyte growth factor as an innovative therapy for inflammatory bowel disease.* Journal of Gastroenterology, 2005. **40**(10): p. 925-931.

43. Xu, Y., et al., *Expression and clinical significance of c-Met in advanced esophageal squamous cell carcinoma.* BMC Cancer, 2015. **15**(1): p. 6.

44. Postow, M.A., M.K. Callahan, and J.D. Wolchok, *Immune Checkpoint Blockade in Cancer Therapy.* Journal of Clinical Oncology, 2015. **33**(17): p. 1974-1982.

45. Tumeh, P.C., et al., *PD-1 blockade induces responses by inhibiting adaptive immune resistance.* Nature, 2014. **515**(7528): p. 568-571.

46. BHARDWAJ, G., A. AGRAWAL, and R. TYAGI, *COMBINATION THERAPIES OR STANDALONE INTERVENTIONS? INNOVATION OPTIONS FOR PHARMACEUTICAL FIRMS FIGHTING CANCER.* International Journal of Innovation Management, 2015. **19**(03): p. 1540003.

47. La-Beck, N.M., et al., *Immune Checkpoint Inhibitors: New Insights and Current Place in Cancer Therapy.* Pharmacotherapy: The Journal of Human Pharmacology and Drug Therapy, 2015. **35**(10): p. 963-976.

48. Zou, W., J.D. Wolchok, and L. Chen, *PD-L1 (B7-H1) and PD-1 pathway blockade for cancer therapy: Mechanisms, response biomarkers, and combinations.* Science Translational Medicine, 2016. **8**(328): p. 328rv4-328rv4.

49. Chen, D.S., B.A. Irving, and F.S. Hodi, *Molecular Pathways: Next-Generation Immunotherapy—Inhibiting Programmed Death-Ligand 1 and Programmed Death-1.* Clinical Cancer Research, 2012. **18**(24): p. 6580-6587.

50. Naidoo, J., D.B. Page, and J.D. Wolchok, *Immune Checkpoint Blockade.* Hematology/Oncology Clinics of North America, 2014. **28**(3): p. 585-600.

51. Mahoney, K.M., G.J. Freeman, and D.F. McDermott, *The Next Immune-Checkpoint Inhibitors: PD-1/PD-L1 Blockade in Melanoma.* Clinical Therapeutics, 2015. **37**(4): p. 764-782.

52. Aguiar, P.N., et al., *The role of PD-L1 expression as a predictive biomarker in advanced non-small-cell lung cancer: a network meta-analysis.* Immunotherapy, 2016. **8**(4): p. 479-488.

53. Garon, E.B., et al., *Pembrolizumab for the Treatment of Non–Small-Cell Lung Cancer.* New England Journal of Medicine, 2015. **372**(21): p. 2018-2028.

54. Spira, A., et al, *Efficacy, safety and predictive biomarker results from a randomized phase II study comparing MPDL3280A vs docetaxel in 2L/3L NSCLC (POPLAR).*
, in *2015 ASCO Annual Meeting*. 2015, Journal of Clinical Oncology: Chicago, IL.

55. Kerr, K.M. and F.R. Hirsch, *Programmed Death Ligand-1 Immunohistochemistry: Friend or Foe?* Archives of Pathology & Laboratory Medicine, 2016. **140**(4): p. 326-331.

56. Sholl, L.M., et al., *Programmed Death Ligand-1 Immunohistochemistry— A New Challenge for Pathologists: A Perspective From Members of the Pulmonary Pathology Society.* Archives of Pathology & Laboratory Medicine, 2016. **140**(4): p. 341-344.

57. Scheel, A.H., et al., *Harmonized PD-L1 immunohistochemistry for pulmonary squamous-cell and adenocarcinomas.* Mod Pathol, 2016. **29**(10): p. 1165-1172.

58. Cheng, S., W.H. Koch, and L. Wu, *Co-development of a companion diagnostic for targeted cancer therapy.* New Biotechnology, 2012. **29**(6): p. 682-688.

59. Kalia, M., *Biomarkers for personalized oncology: recent advances and future challenges.* Metabolism, 2015. **64**(3, Supplement 1): p. S16-S21.

60. Kerr, K.M., et al., *Second ESMO consensus conference on lung cancer: pathology and molecular biomarkers for non-small-cell lung cancer.* Annals of Oncology, 2014. **25**(9): p. 1681-1690.

61. Soliman, H., F. Khalil, and S. Antonia, *PD-L1 Expression Is Increased in a Subset of Basal Type Breast Cancer Cells.* PLOS ONE, 2014. **9**(2): p. e88557.

62. Usui, Y., et al., *Expression of Costimulatory Molecules on Human Retinoblastoma Cells Y-79: Functional Expression of CD40 and B7H1.* Investigative Ophthalmology & Visual Science, 2006. **47**(10): p. 4607-4613.

63. Veras, E., et al., *PD-L1 Expression in Human Placentas and Gestational Trophoblastic Diseases.* International Journal of Gynecological Pathology, 9000. **Publish Ahead of Print**.

64. Chen, B.J., et al., *PD-L1 Expression Is Characteristic of a Subset of Aggressive B-cell Lymphomas and Virus-Associated Malignancies.* Clinical Cancer Research, 2013. **19**(13): p. 3462-3473.

65. Ilie, M., et al., *Comparative study of the PD-L1 status between surgically resected specimens and matched biopsies of NSCLC patients reveal major discordances: a potential issue for anti-PD-L1 therapeutic strategies.* Annals of Oncology, 2016. **27**(1): p. 147-153.

5.0 Supporting Information

5.1 Supplementary Figures: Quantifiable Determination of EGFR in Human Tissues Using Peptide Conjugated Gold Nanorods

Supplementary Information: Characterization

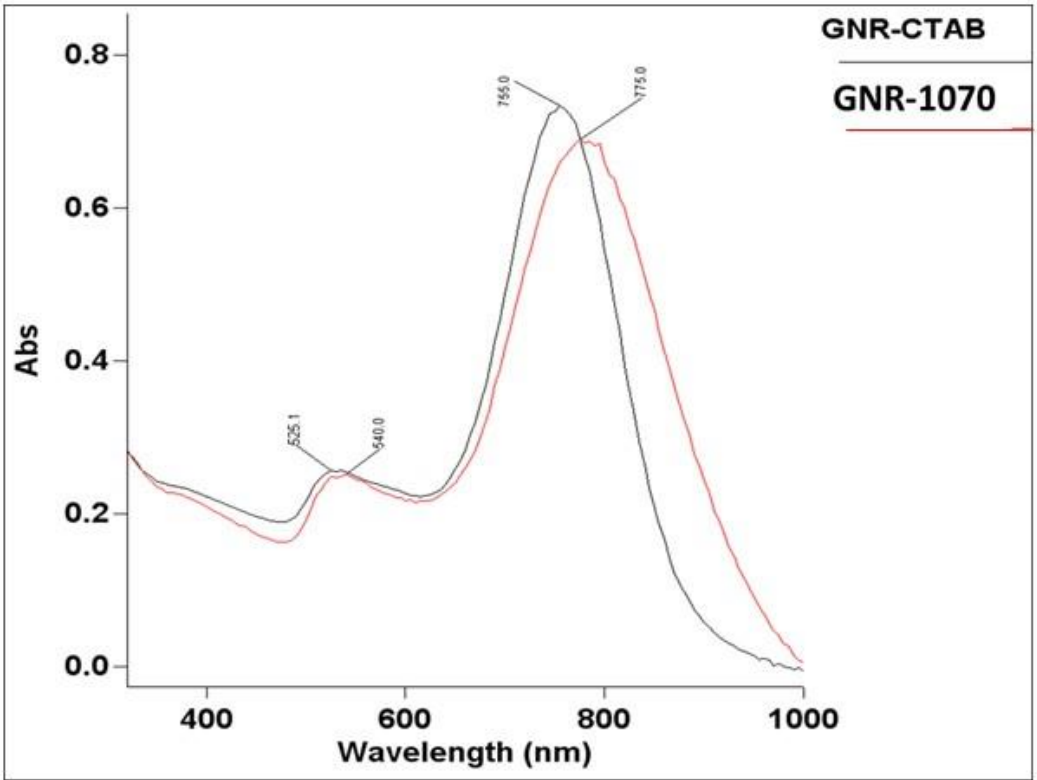

S1| UV-Vis comparison between GNR-CTAB and GNR-1070

Results

		Mean (mV)	Area (%)	St Dev (mV)
Zeta Potential (mV): 44.3	Peak 1:	43.6	95.5	13.7
Zeta Deviation (mV): 21.3	Peak 2:	78.7	4.5	4.67
Conductivity (mS/cm): 0.963	Peak 3:	0.00	0.0	0.00

Result quality : See result quality report

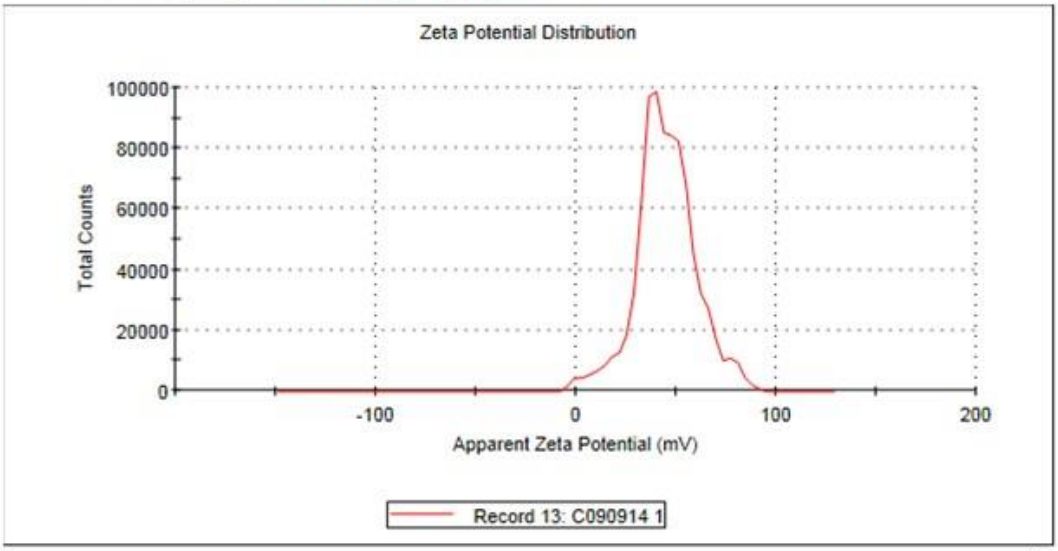

S2| Zeta Potential of GNR-CTAB

Results

		Mean (mV)	Area (%)	St Dev (mV)
Zeta Potential (mV): -42.2	Peak 1:	-42.2	100.0	7.28
Zeta Deviation (mV): 7.28	Peak 2:	0.00	0.0	0.00
Conductivity (mS/cm): 0.00596	Peak 3:	0.00	0.0	0.00

Result quality : See result quality report

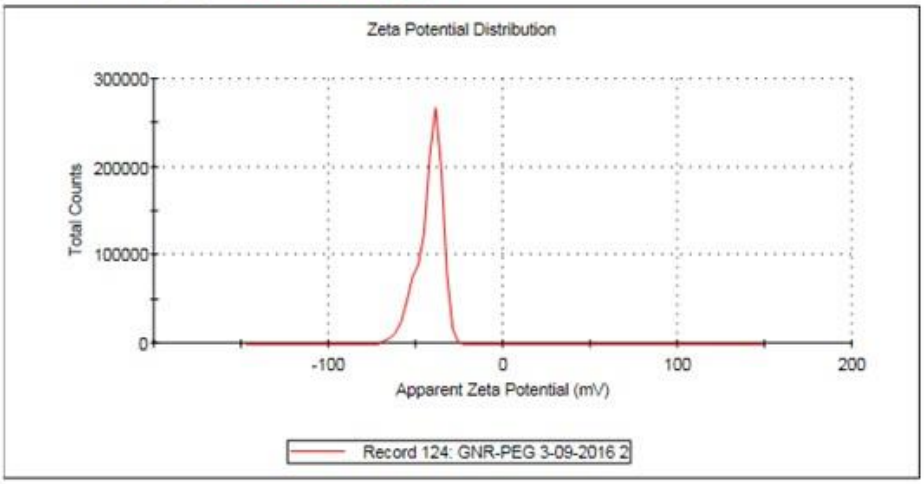

S3| Zeta Potential of GNR-PEG

Results

		Mean (mV)	Area (%)	Width (mV)
Zeta Potential (mV): 18.4	**Peak 1:**	18.4	100.0	8.13
Zeta Deviation (mV): 8.13	**Peak 2:**	0.00	0.0	0.00
Conductivity (mS/cm): 0.00555	**Peak 3:**	0.00	0.0	0.00

Result quality : Good

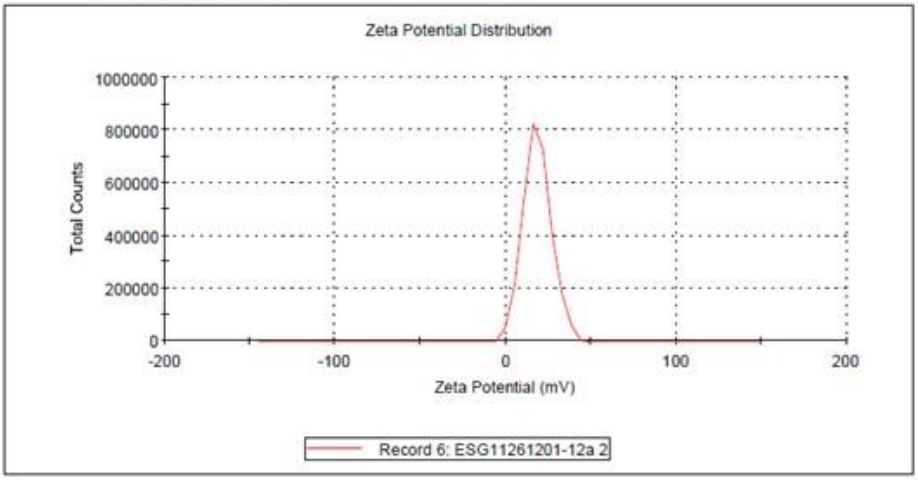

S4| Zeta Potential of GNR-1070

GE11 Peptide Structure

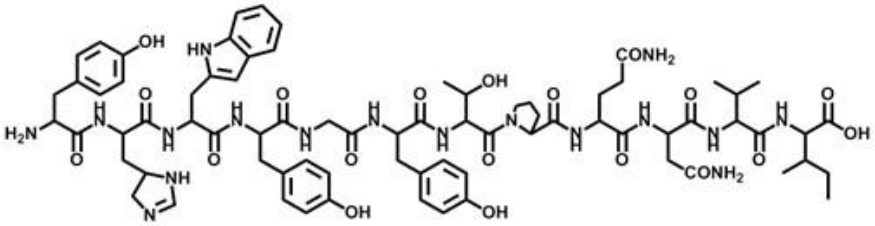

1070 Peptide Structure

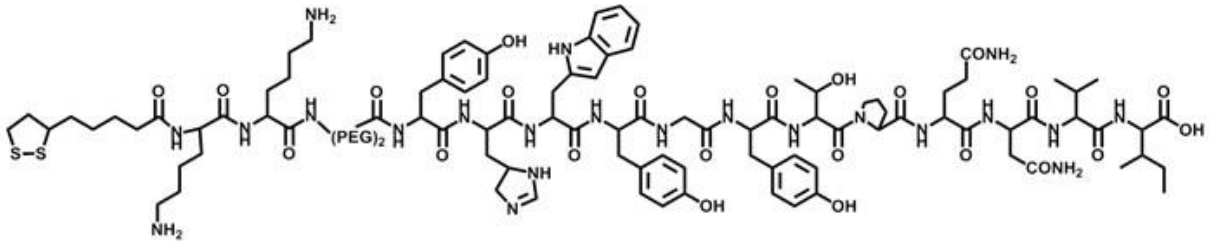

S5| Chemical structure of GE11 and 1070 peptides

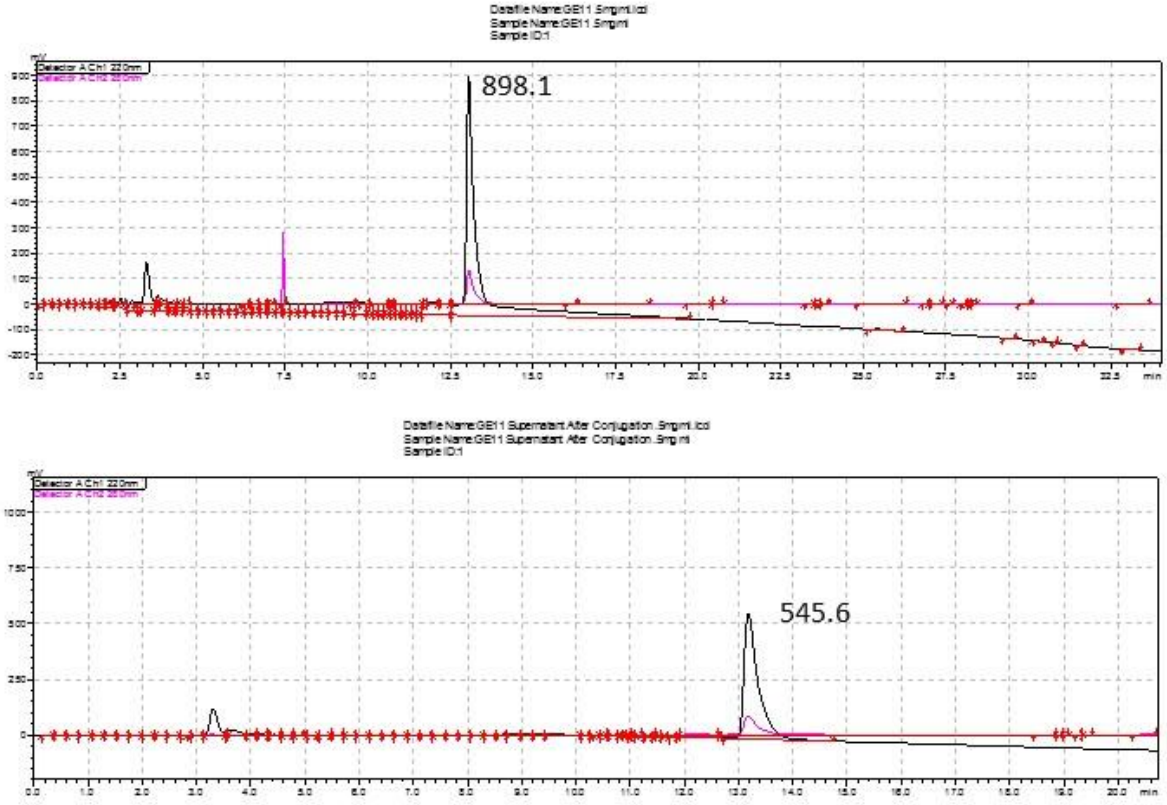

S6| HPLC chromatogram of peptide 1070 on C18 column (top) and supernatant after conjugation using the same concentration. Bound peptide of ~40%.

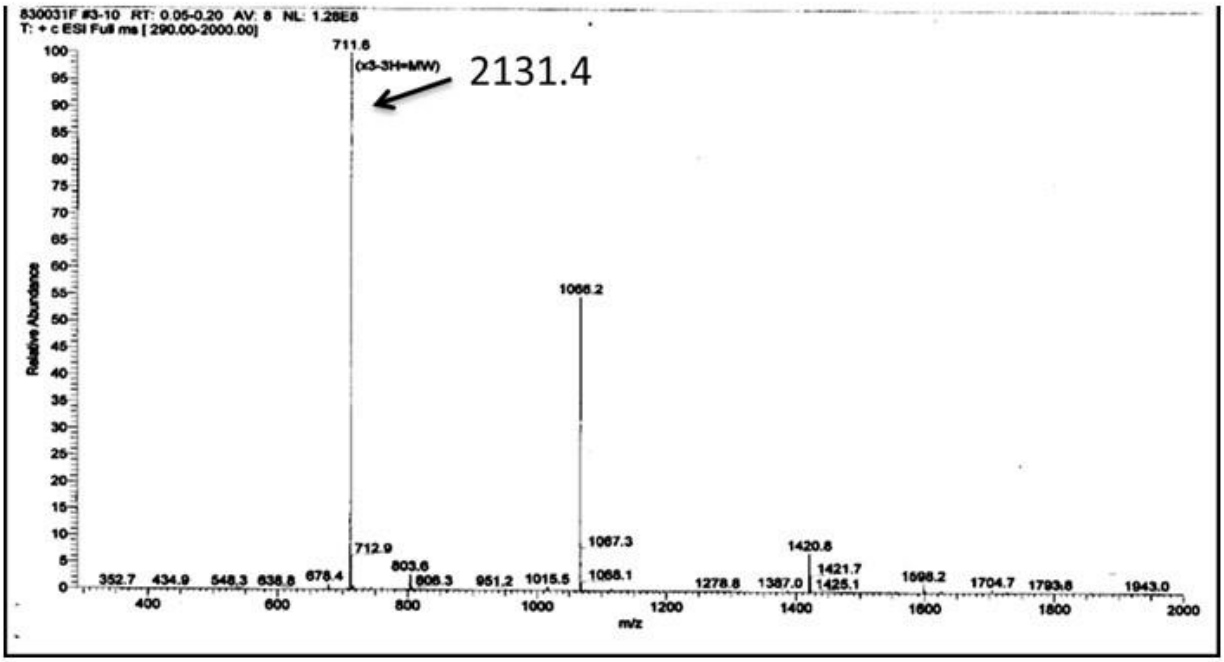

S7| Mass spectrum of 1070 peptide

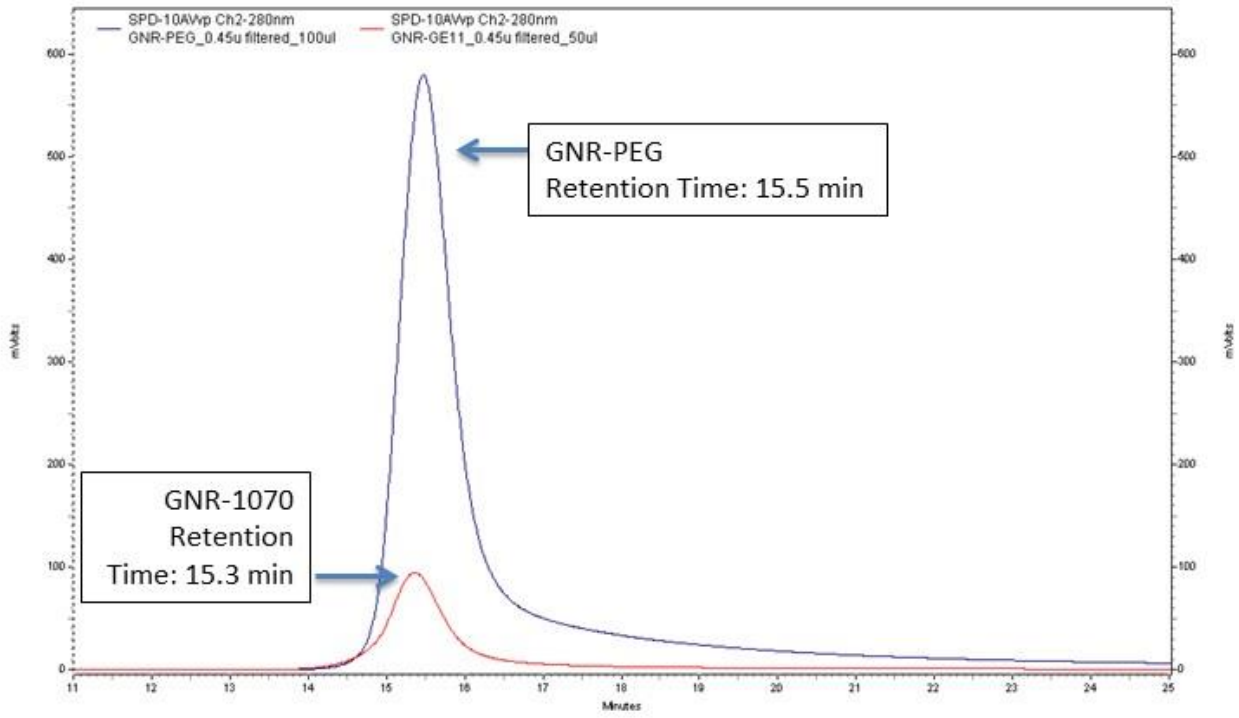

S8| HPLC chromatogram of GNR-1070 and GNR-PEG on Sepharose column

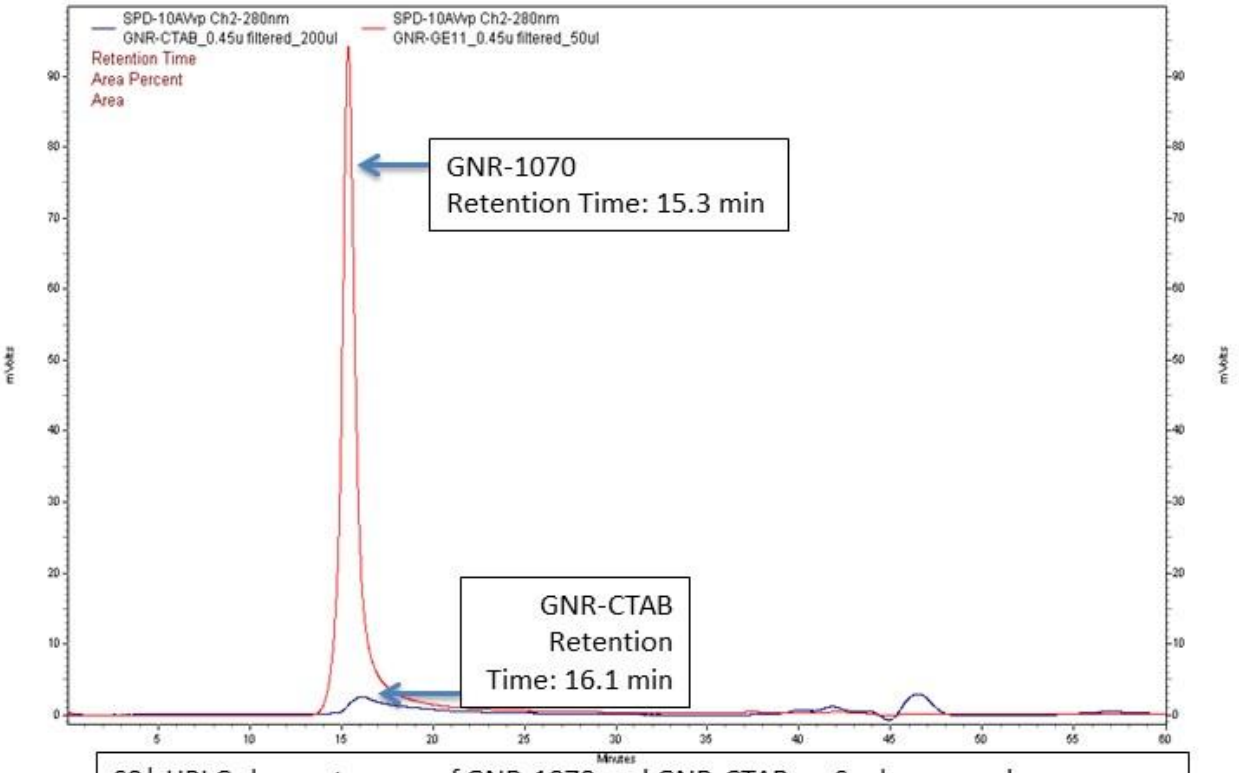

S9| HPLC chromatogram of GNR-1070 and GNR-CTAB on Sepharose column

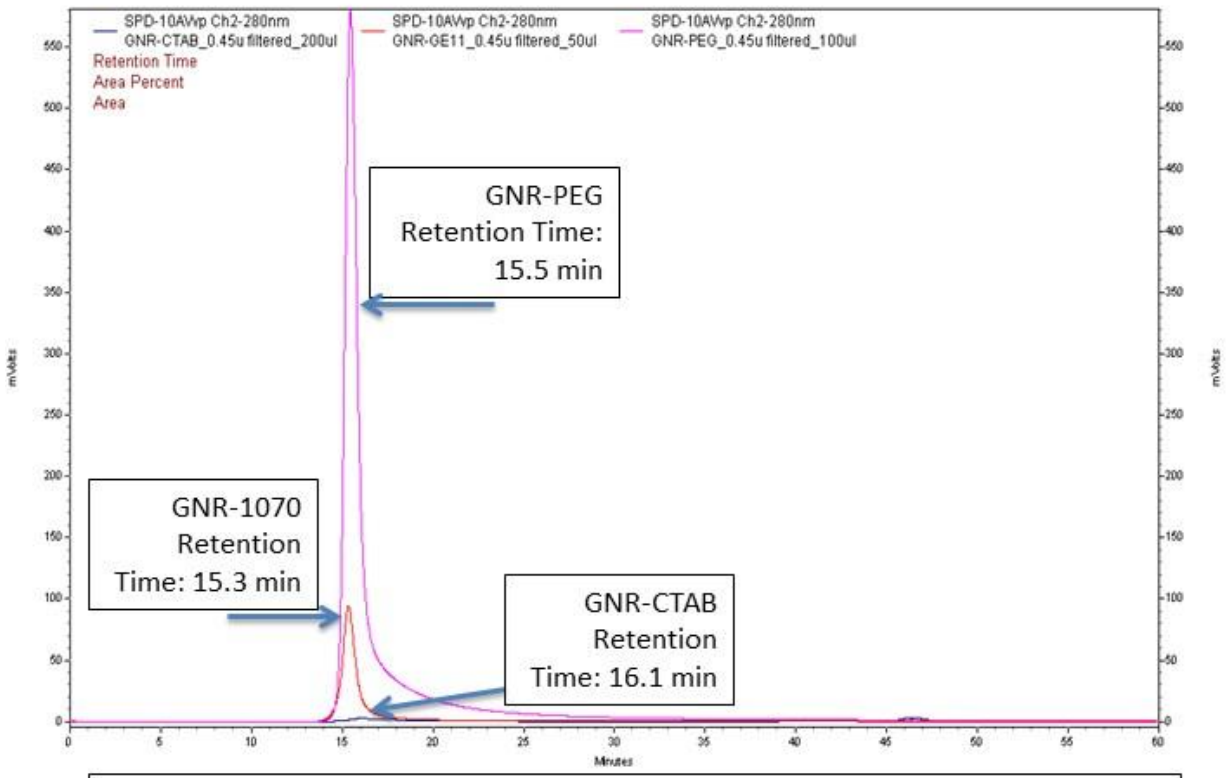

S10| HPLC chromatogram of GNR-1070 and GNR-CTAB on C18 column

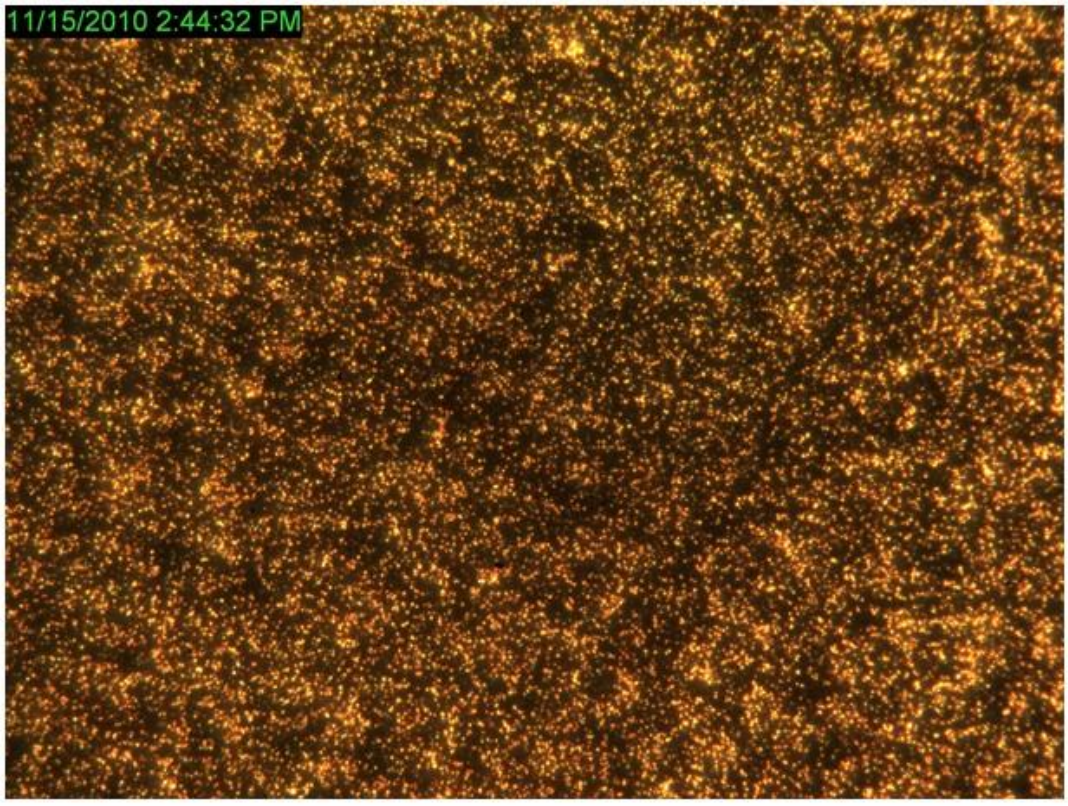

S11| Dark-field image of gold nanorods, 20x magnification

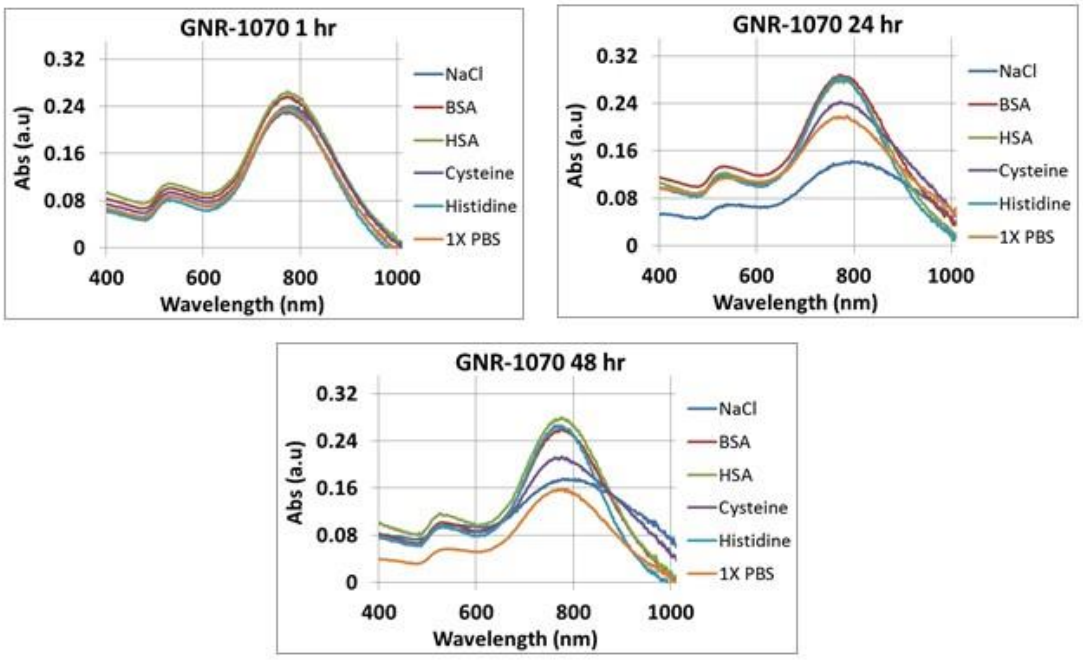

S12| Stability of GNR-1070 in the presence of NaCl, BSA, HSA, Cysteine, Histidine, and 1x PBS

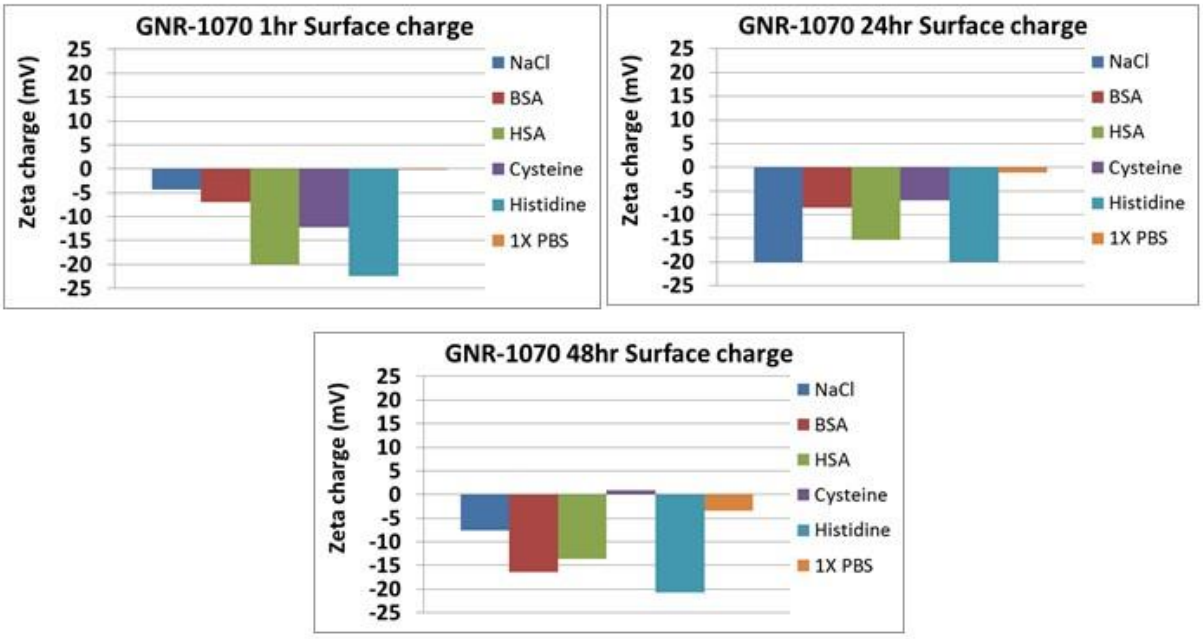

S13| Stability of GNR-1070 in the presence of NaCl, BSA, HSA, Cysteine, Histidine, and 1x PBS

Compound QC: BME Test

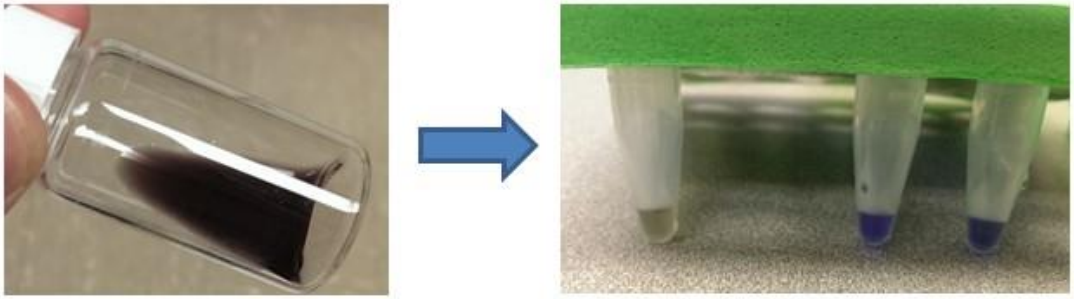

S14| Beta Mercaptoethanol (BME) binds to the surface of non-conjugated gold nanorods (GNR-CTAB). The addition of the blue laemmli dye mixed with BME will not change color when added to the peptide-conjugated GNR-1070, whereas GNR-CTAB shows a distinct color change from blue to green

GNR-1070 SDS-PAGE Gel Electrophoresis

1. Ladder
2. GE11 + Laemmli + BME
3. GNR-CTAB + Laemmli
4. GNR-CTAB + Laemmli + BME
5. GE11 + Laemmli
6. GNR-GE11 + Laemmli
7. GNR-GE11 + Laemmli + BME
8. GE11 + Laemmli + BME
9. GNR-CTAB + Laemmli + BME
10. GNR-GE11 + Laemmli + BME

S15| GNR-CTAB samples showed no presence of GE11 peptide, did not move in SDS-PAGE Gel

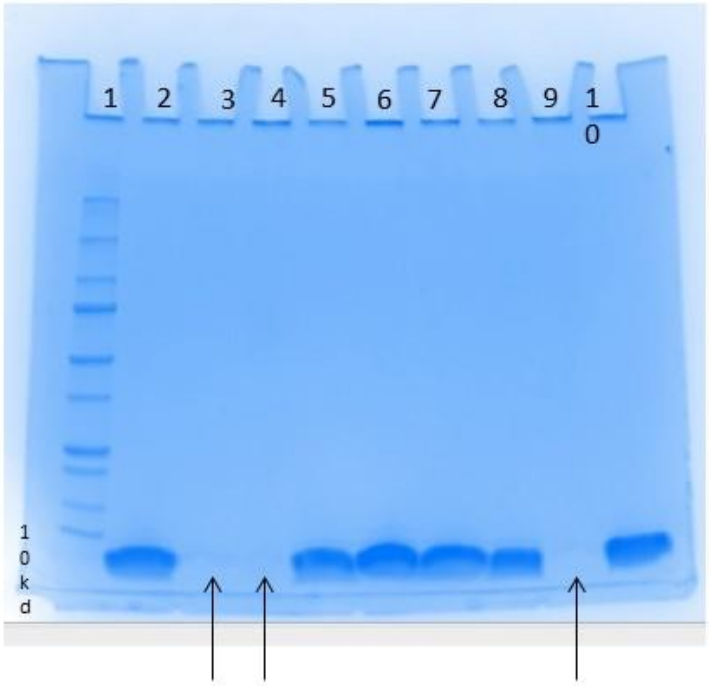

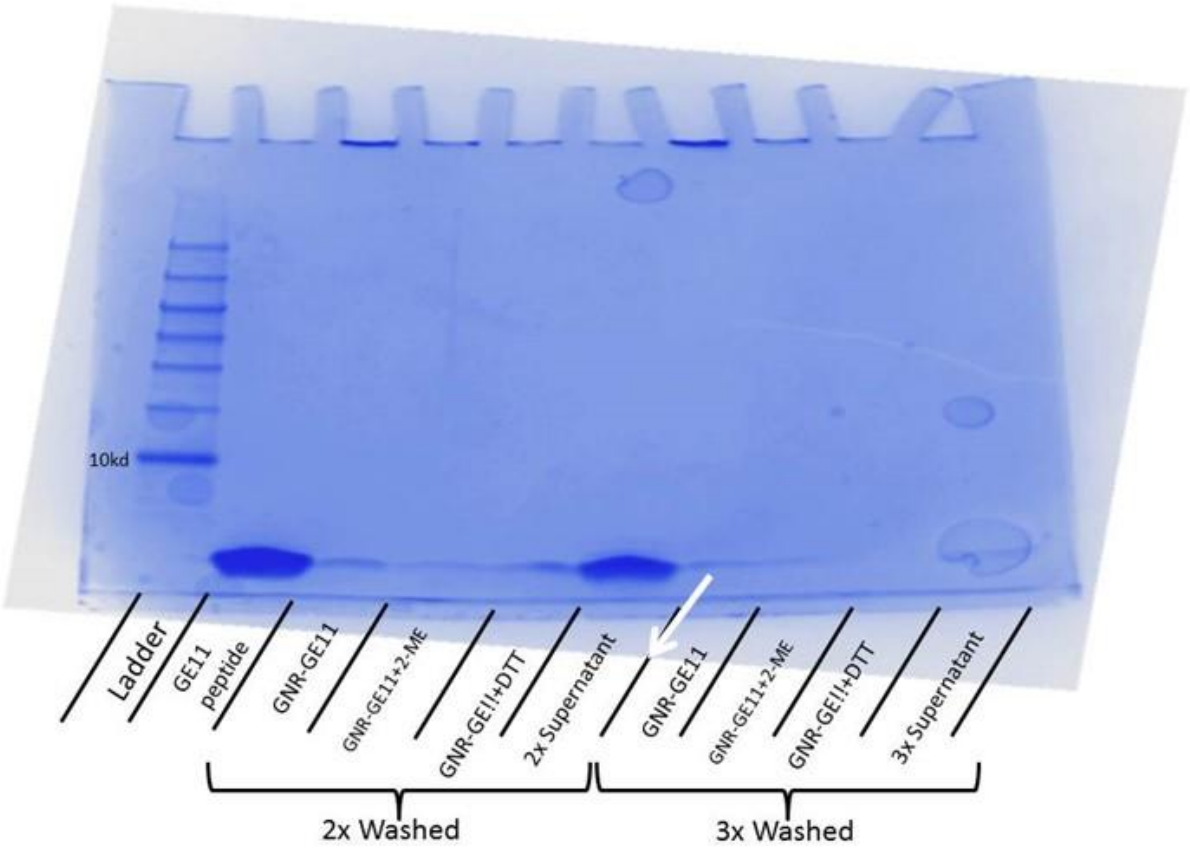

S16| 2 Washes is sufficient to remove unbound peptide.

S17| SkBr3: Unblocked, Treated with GNR-1070

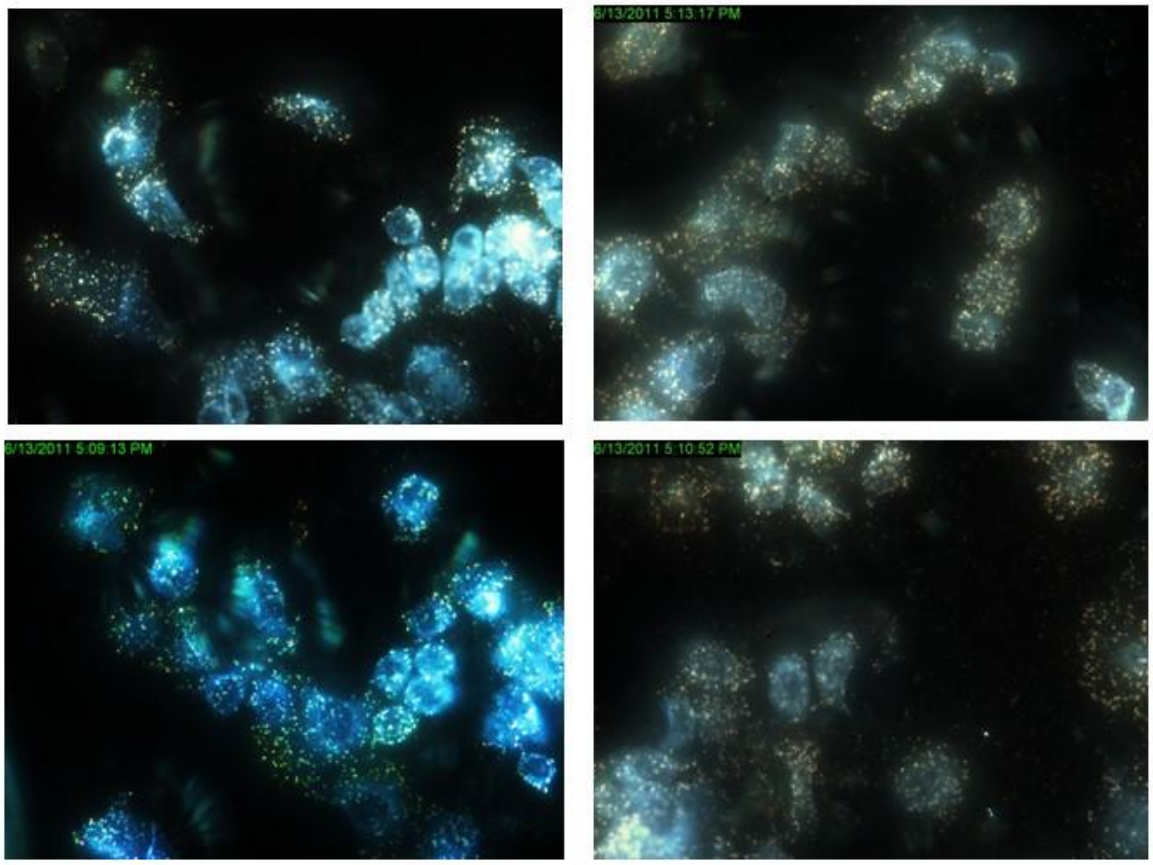

S18| SkBr3: Pre-blocked with Peptide 1070, Treated with GNR-1070

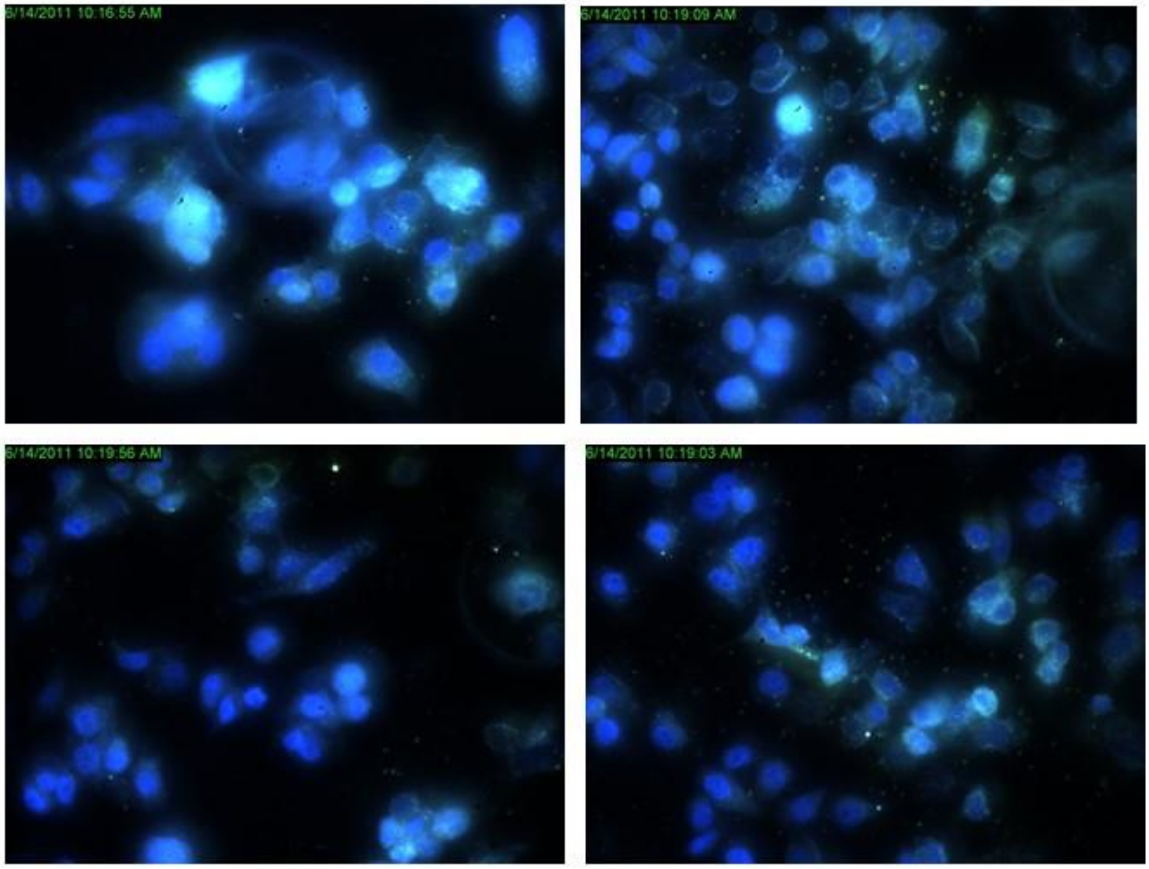

S19| SkBr3: Treated with GNR-PEG (No Peptide for Targeting)

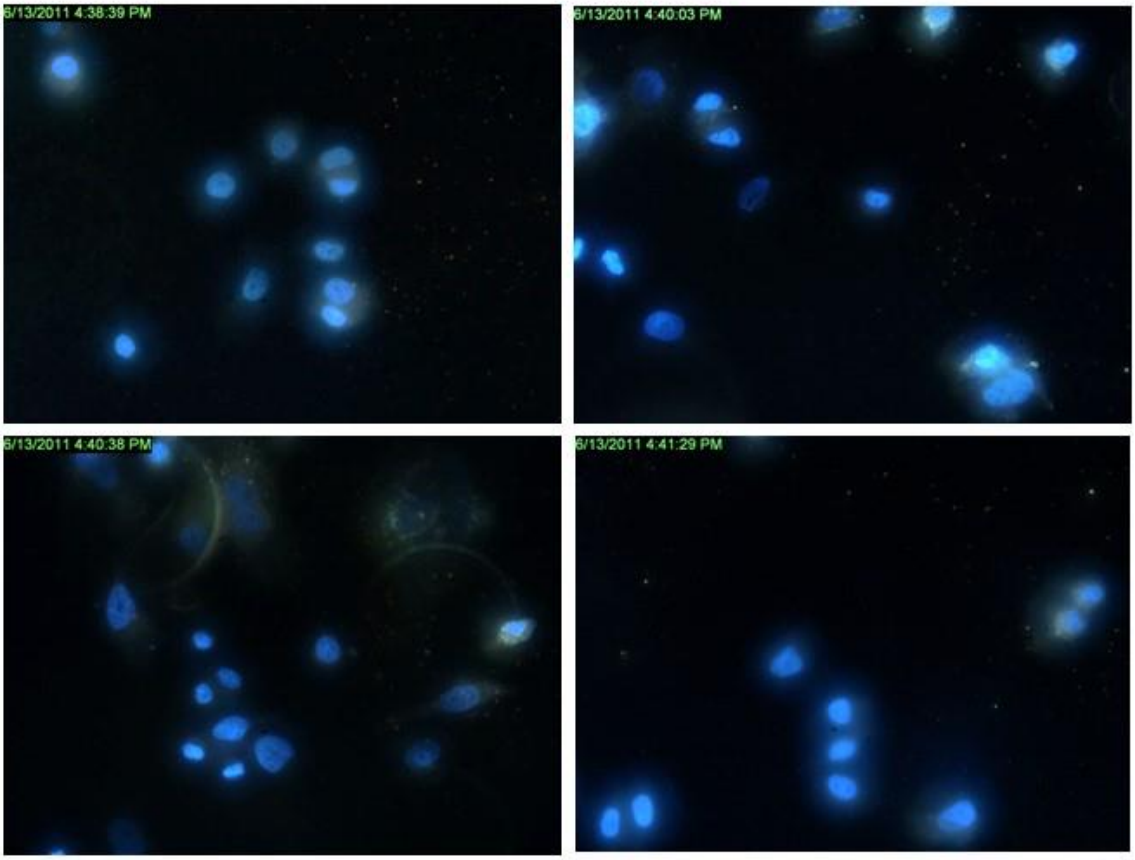

S20| WiDr: Not Blocked, Treated with GNR-1070

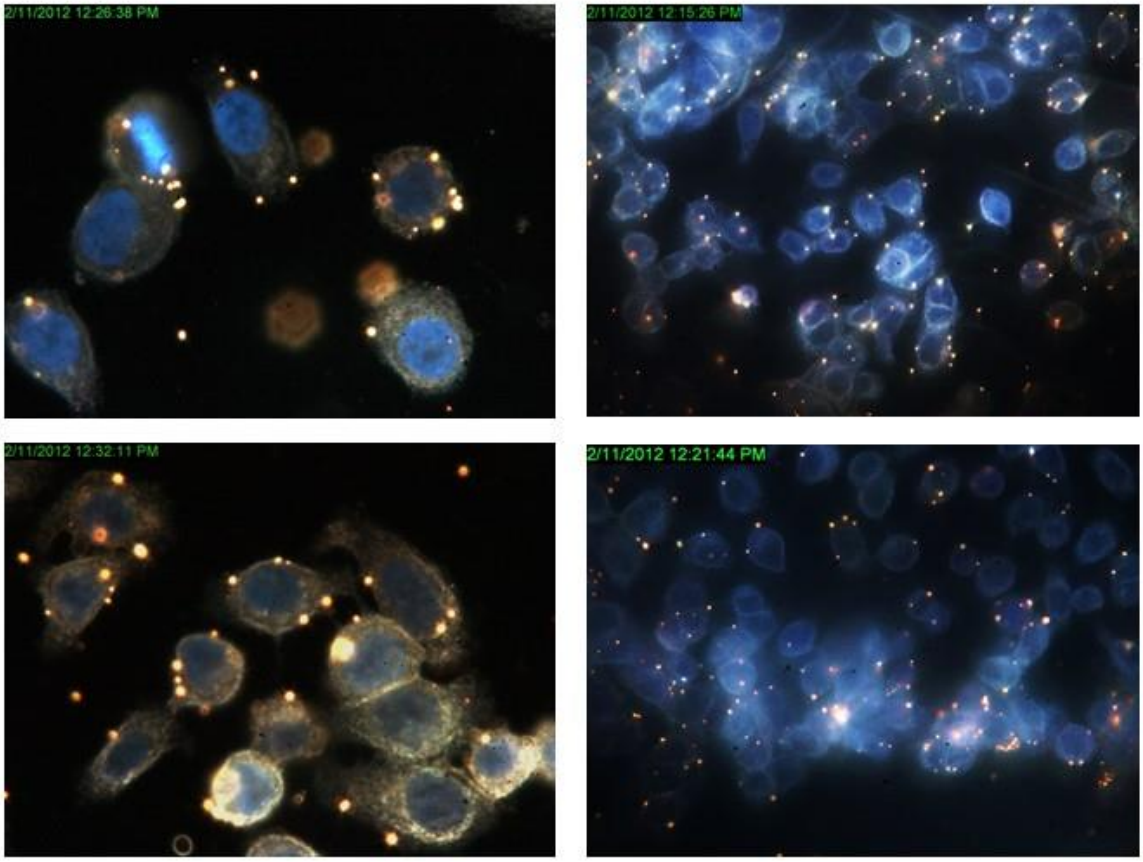

S21| WiDr: Pre-blocked with Peptide 1070, Treated with GNR-1070

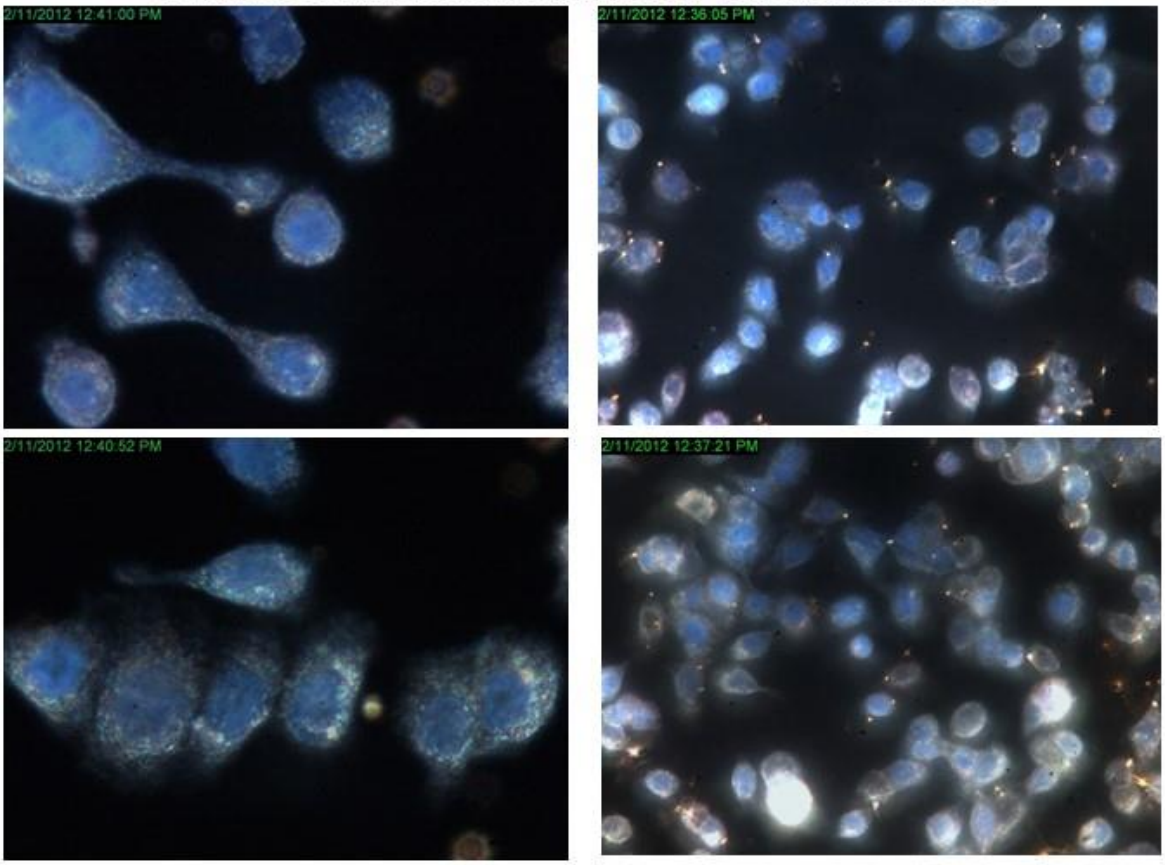

S22| WiDr: Treated with GNR-PEG (No Peptide for Targeting)

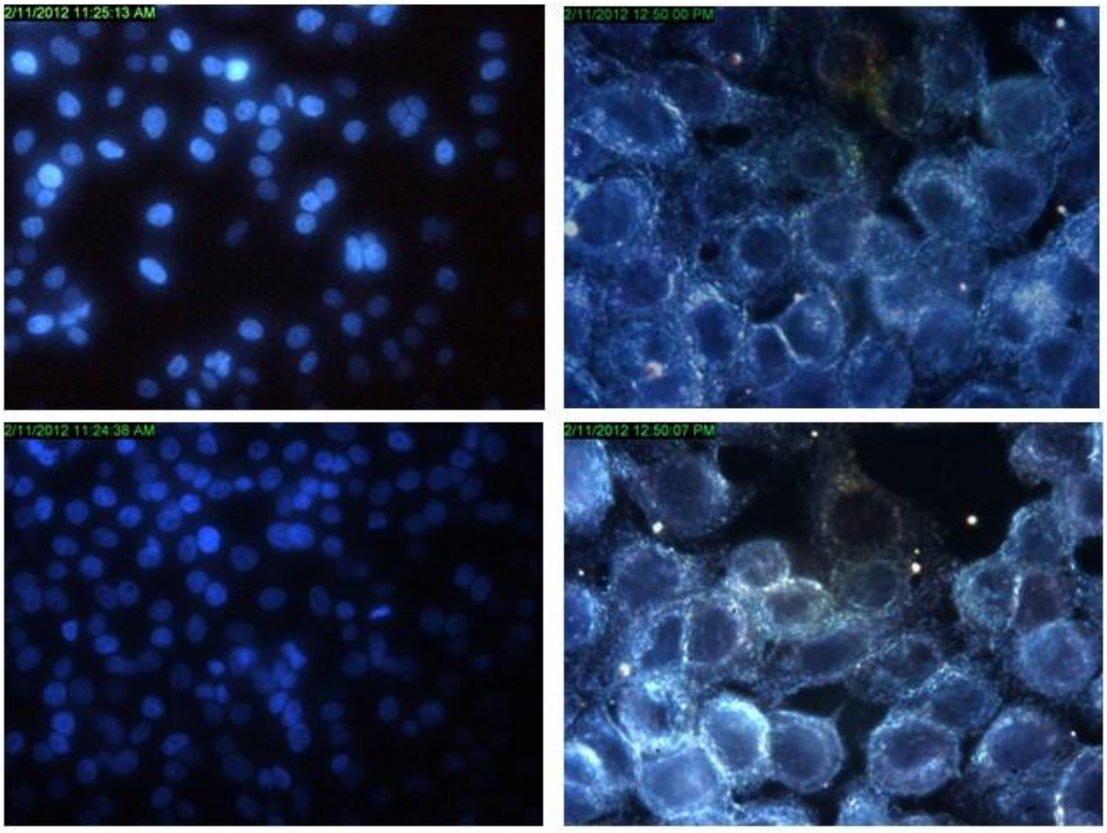

S23| MCF-7 (No EGFR Overexpression): Treated with GNR-1070

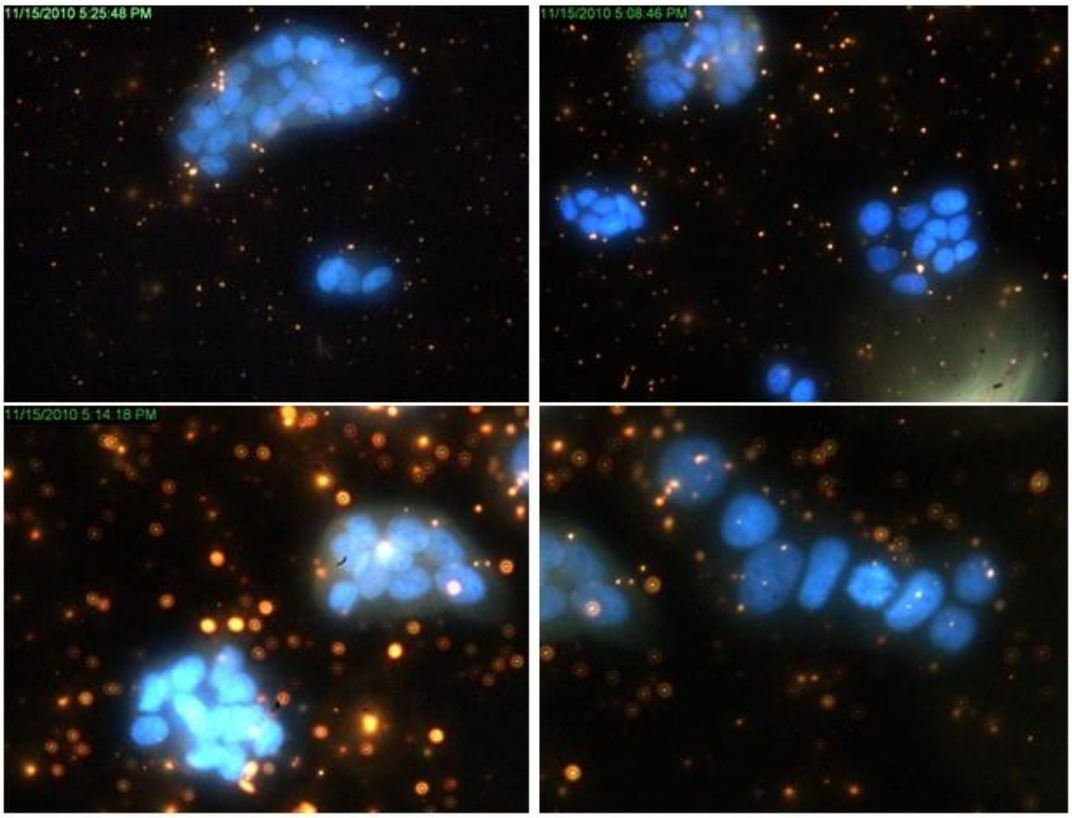

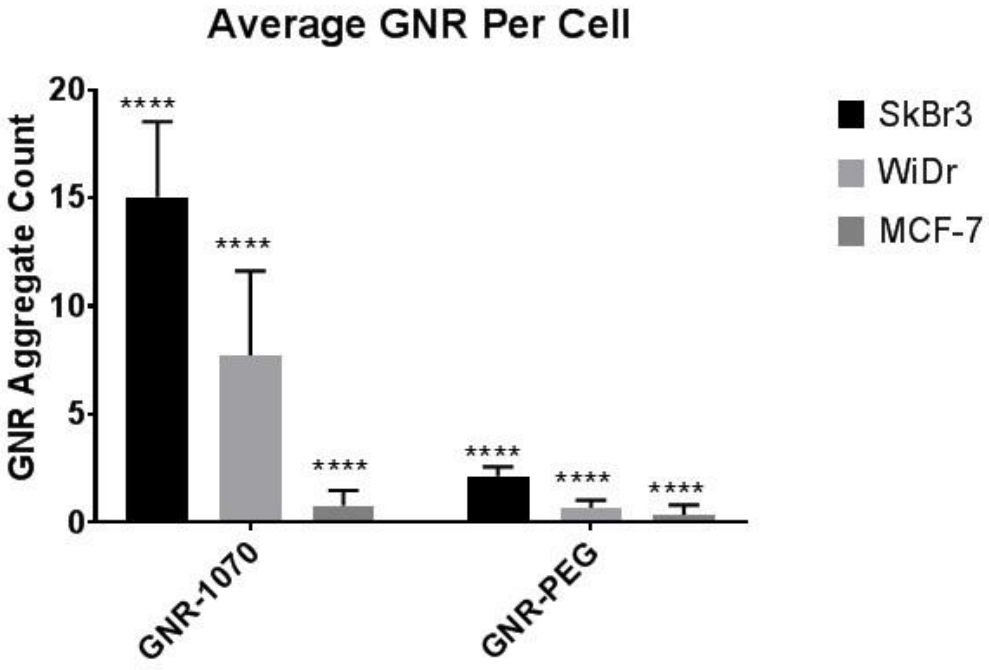
Average GNR Per Cell
GNR Aggregate Count
20
15
10
5
0
****
****
****
****
****
****
GNR-1070
GNR-PEG
SkBr3
WiDr
MCF-7

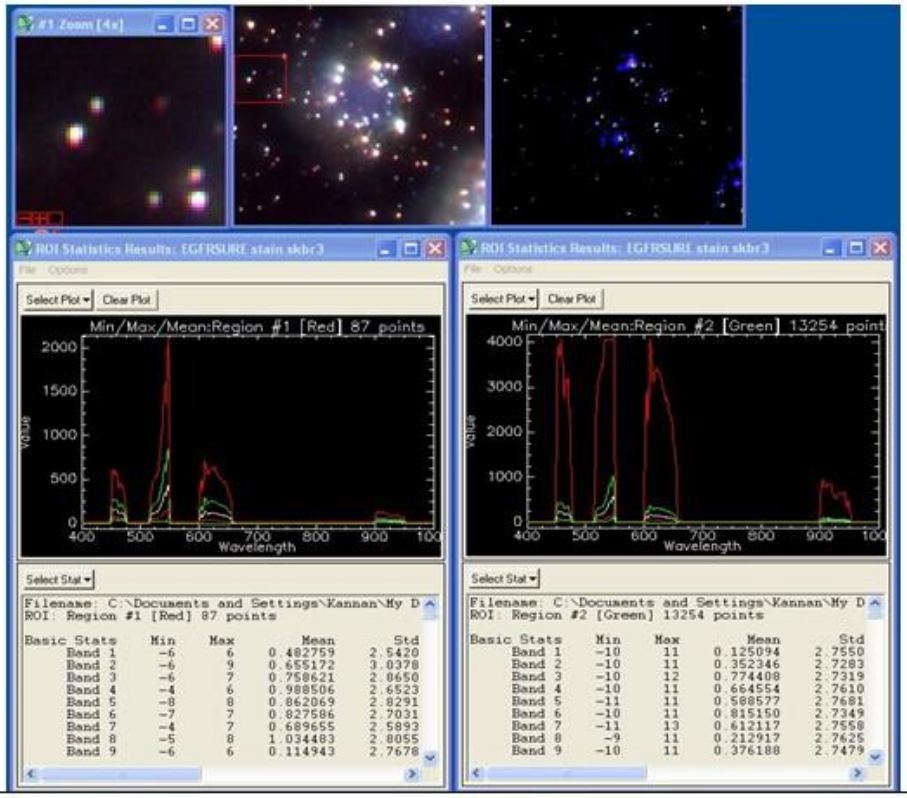

S24| The hyperspectral profile of GNR-GE11 can be used to confirm the presence of gold nanoparticles in the cell. We first Look at the profile of the individual nanorods, which show heavy red peaks at ~480, 540, and 630nm

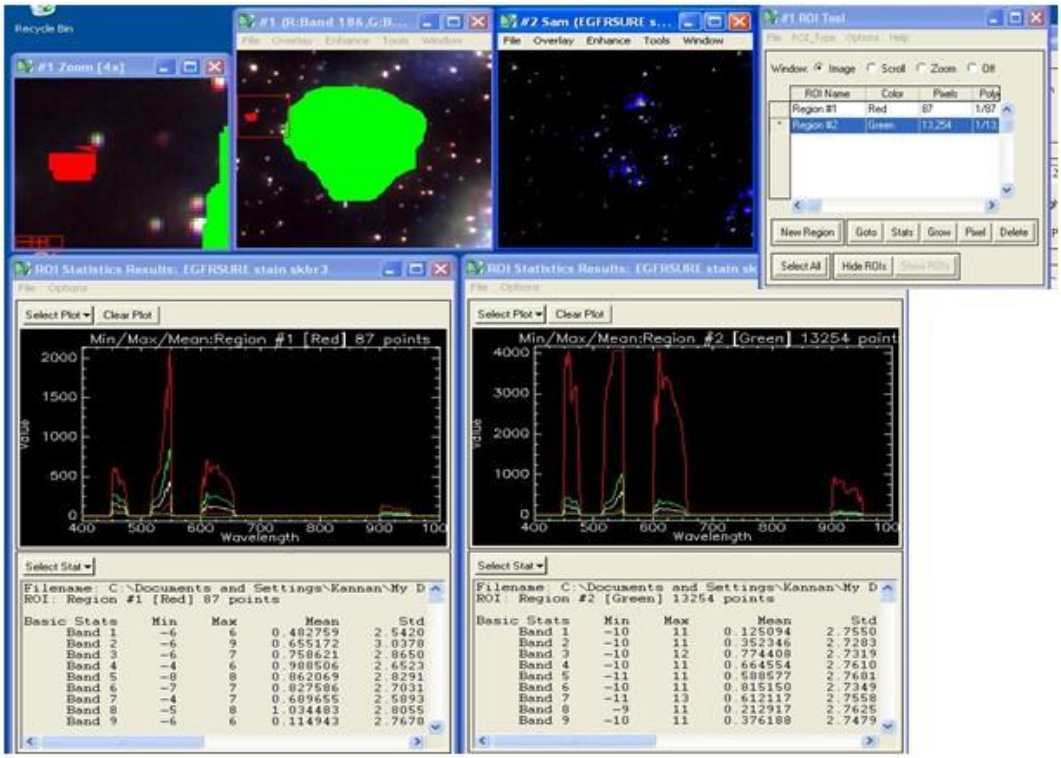

S25| Once spectral profile of lone nanorods (Red ROI) are established, a region of interest such as a cell (Green ROI) can be profiled. The cellular ROI is compared to the profile of the nanorods to confirm that the bright signals are indeed gold nanorods based on the characteristic red peaks.

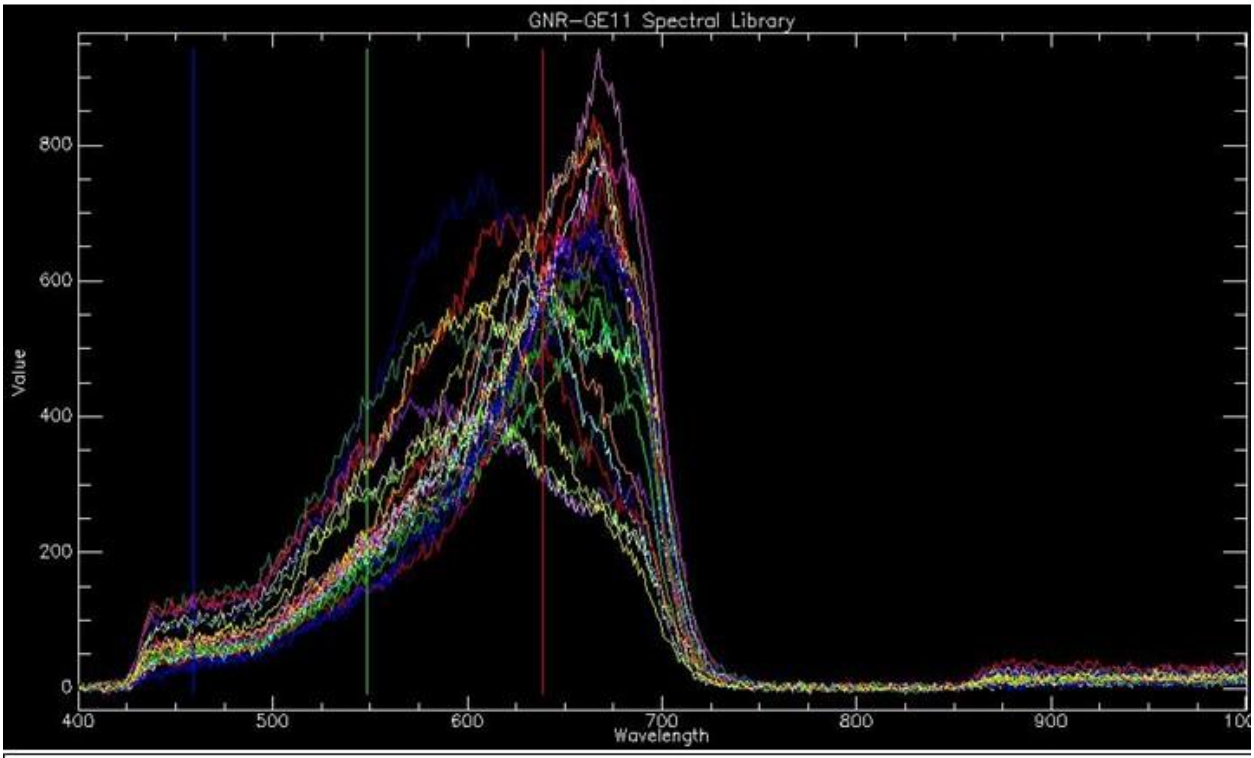

S26| By using the hyperspectral camera and selecting only the nanoparticles, we can build an average spectral profile of GNR-GE11, which peaks between 500nm and 700nm, corresponding to the UV profile of the gold nanorods. This spectral profile can be searched for in a given sample.

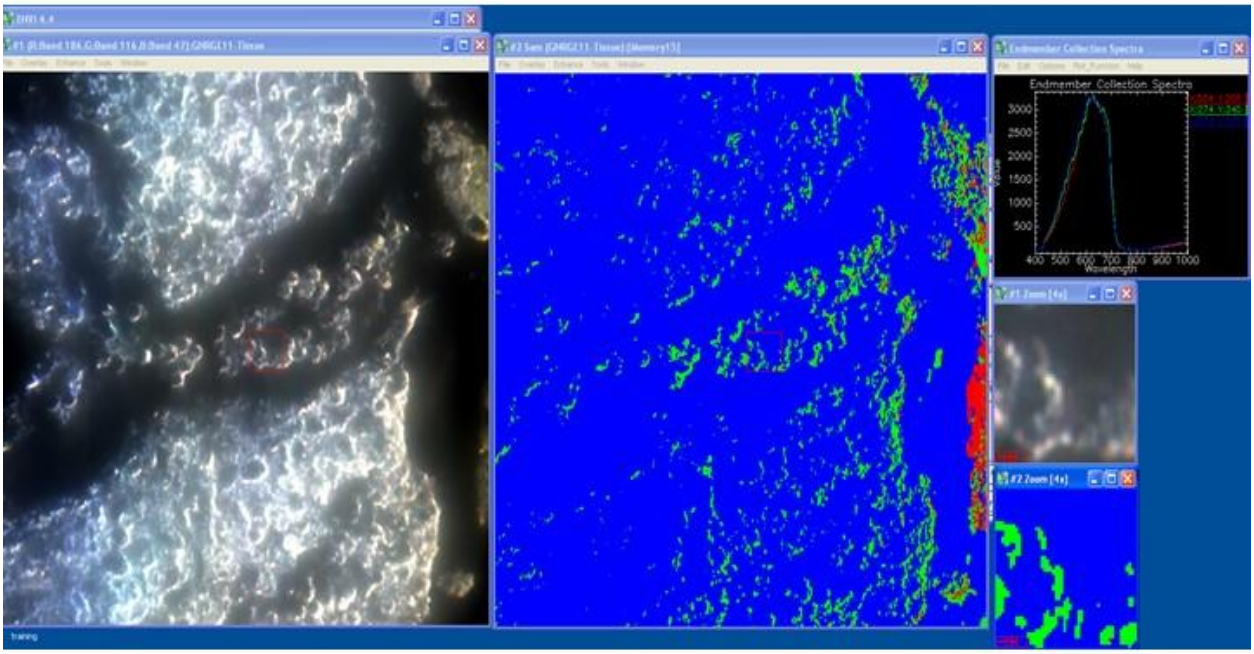

S27| The spectral profile of the gold nanorods can be used to find all areas of a given region which express this unique profile. In the above case, we can find where gold nanorods are staining a tissue section by searching for this spectral profile in the hyperspectral image, which takes a spectral profile image as opposed to a traditional RGB image.

S28| Eli Lilly Cell Lines: 1+ EGFR Expression

GNR-1070

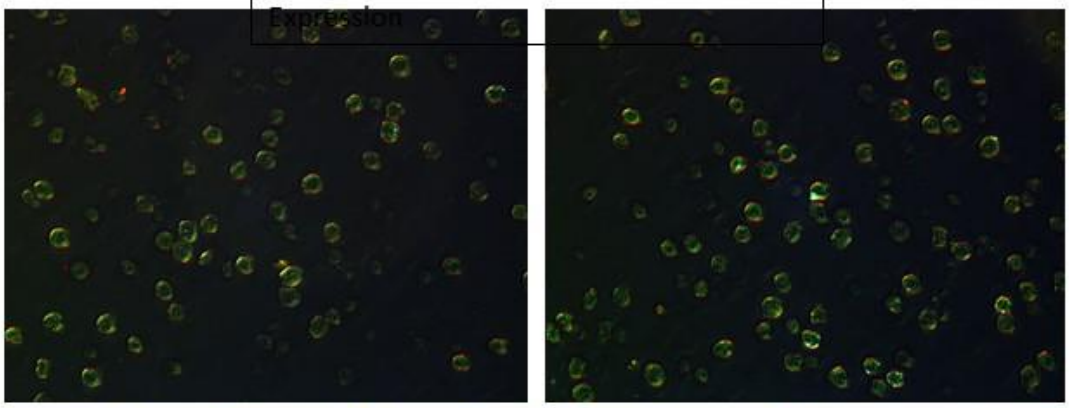

DAKO EGFR PharmDx

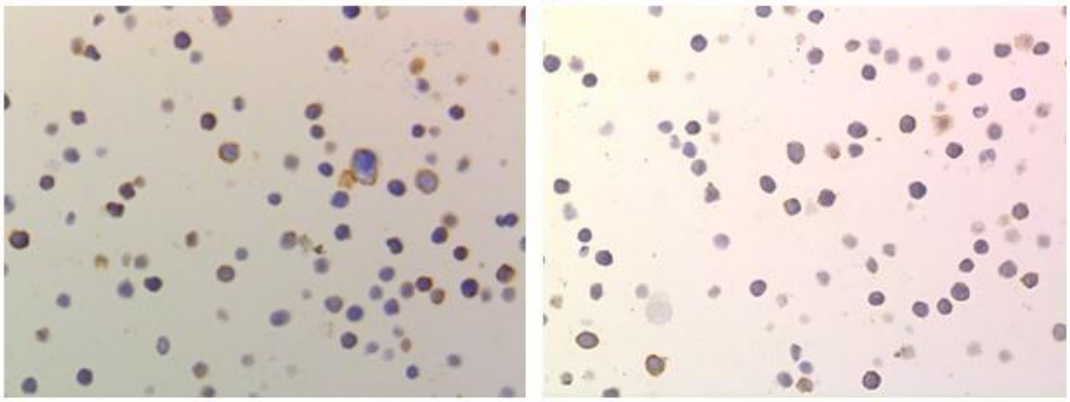

S29| Eli Lilly Cell Lines: 2+ EGFR Expression

GNR-1070

DAKO EGFR PharmDx

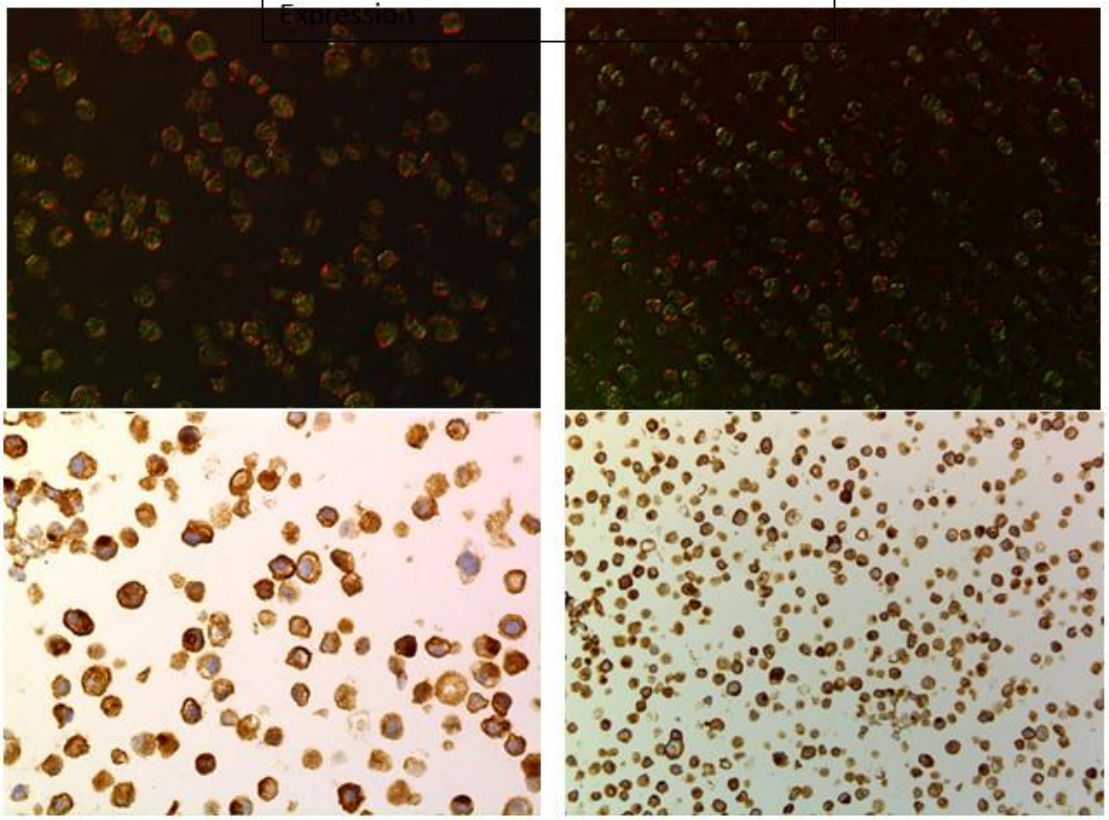

S30| Eli Lilly Cell Lines: 3+ EGFR

GNR-1070

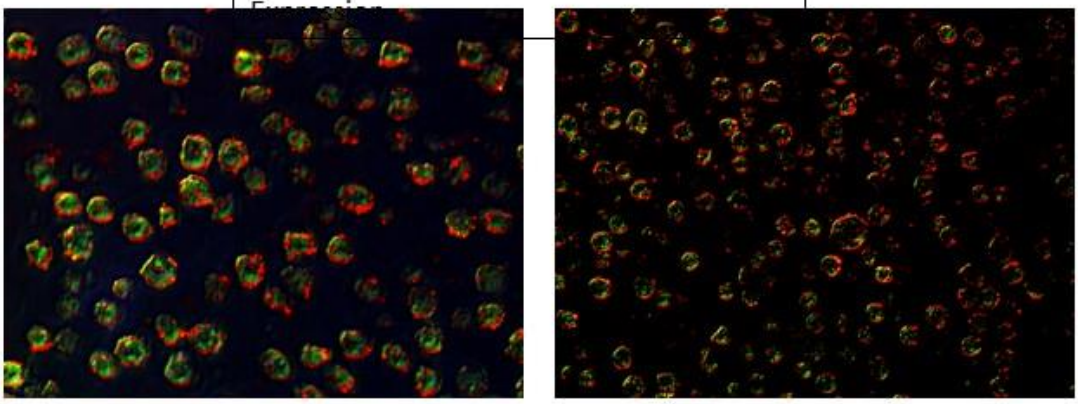

DAKO EGFR PharmDx

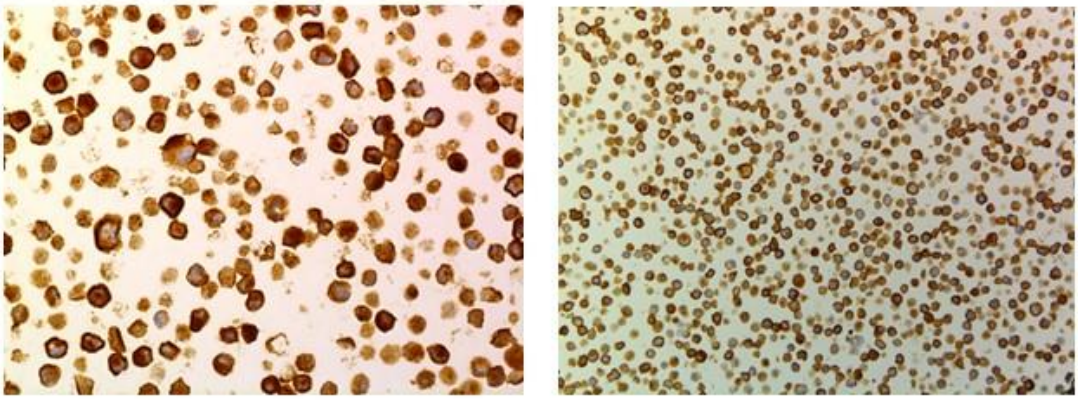

S31| Quantitation of Eli Lilly Cell Lines: 1^{+}-3^{+} EGFR Expression

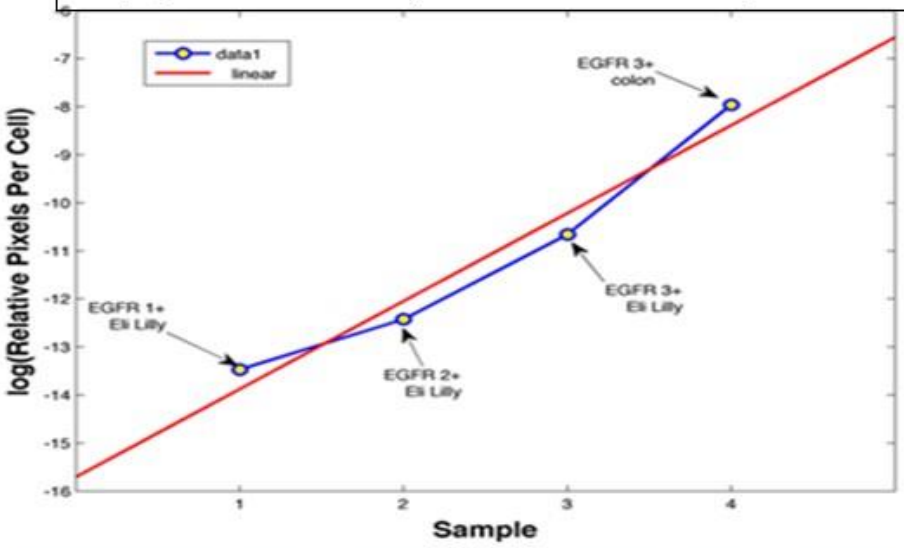

Parameter	EGFR 1+	EGFR 2+	EGFR 3+
Number of nuclei	128	199	271
RG pixels total	892	3,935	27,835
RG pixels/ nucleus	6.97	19.8	102.7
Mean nuclear area	3,198	3,486	2,993
Median nuclear area	2,192	1,039	2,091

EGFR 1+

EGFR 3+

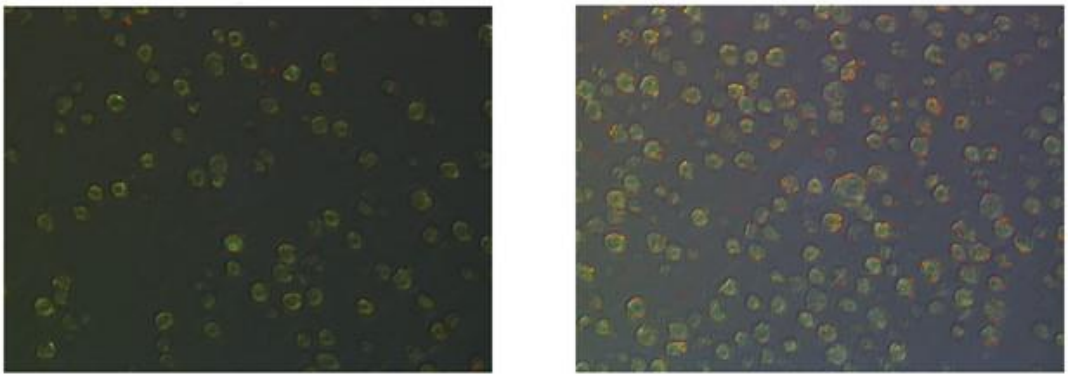

S32| Quantitation of Eli Lilly Cell Lines: 1^{+}-3^{+} EGFR Expression – Raw RBG Images

EGFR 3+: Identification of Nuclei

Enhanced Gray Scale

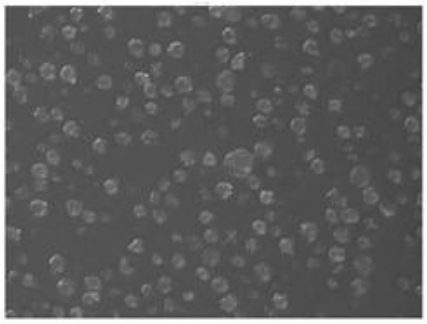

Nuclear Boundaries

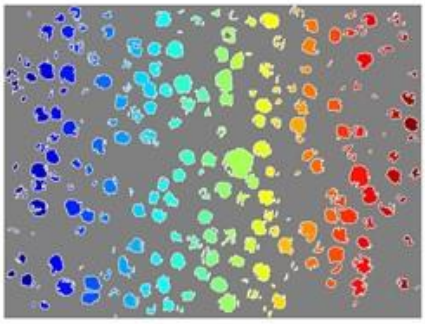

S33| Identification of Nuclei in EGFR3+ cell lines. Convert RGB image to gray scale image, enhance contrast and remove low intensity background objects. Then convert to binary image (not shown). Find boundaries of connected objects and apply colormap. Find object properties, particularly number and area in pixels. Count only nuclei with >150 pixels.

Image Analysis Results

Parameter	EGFR 1+	EGFR 2+	EGFR 3+
Number of nuclei	128	199	271
RG pixels total	892	3,935	27,835
RG pixels/ nucleus	6.97	19.8	102.7
Mean nuclear area	3,198	3,486	2,993
Median nuclear area	2,192	1,039	2,091

S34| Quantification of RG pixels per nucleus on cell samples

Distribution of Nuclear Area

EGFR 1+

EGFR 3+

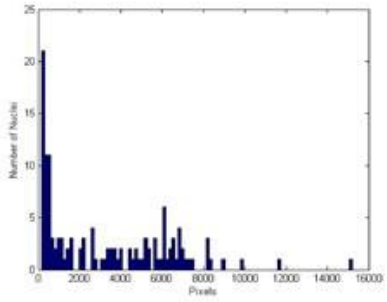

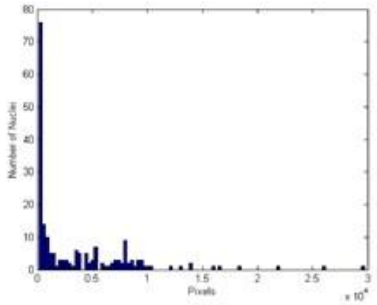

S34| Distribution of Nuclei in EGFR samples. Many more small nuclei in EGFR3+ suggesting that these are only nuclear fragments and should be removed. This can easily be done by adjusting the lower limit of acceptable nuclear area which, for this run, was set at 150 pixels.

EGFR 1+

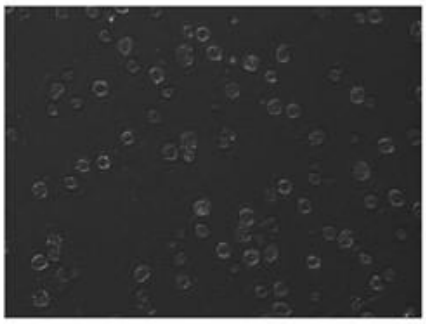

EGFR 3+

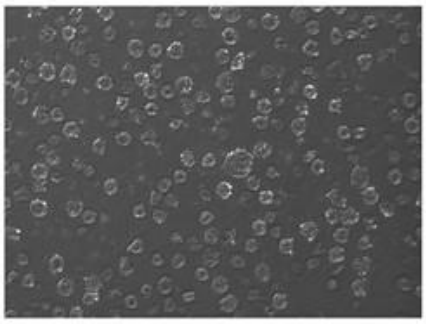

S35| Greyscale images of red layer of RGB images

EGFR 1+

EGFR 3+

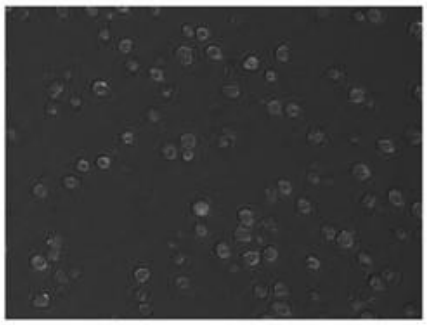

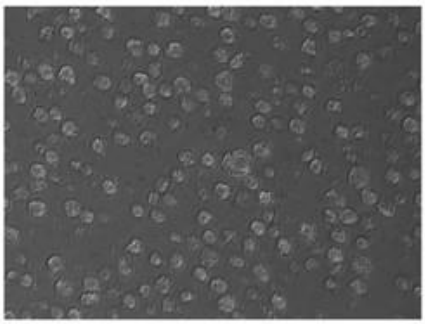

S36| Greyscale images of green layer of RGB images

EGFR 1+

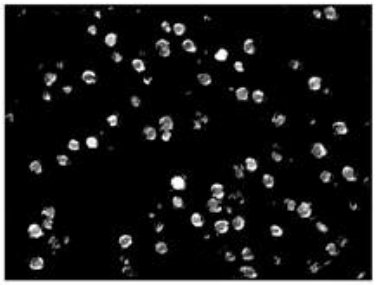

EGFR 1+

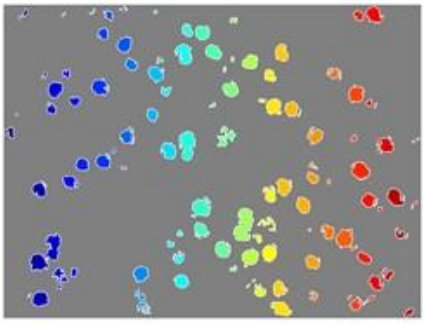

S37| Identifying nuclear boundaries in EGFR 1+ Cells

EGFR 2+

EGFR 2+

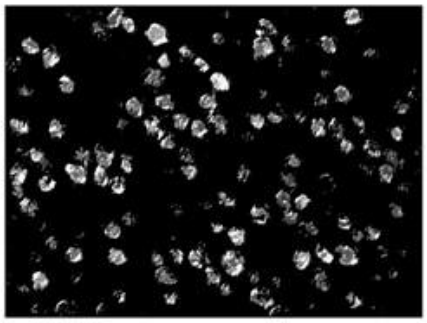

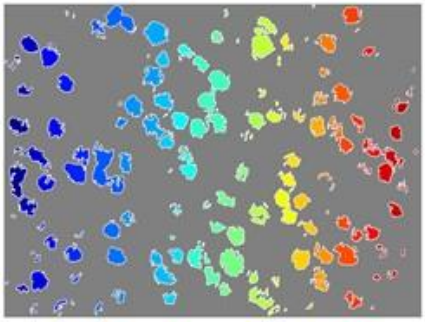

S38| Identifying nuclear boundaries in EGFR 3+ Cells

Other Patient Tissues

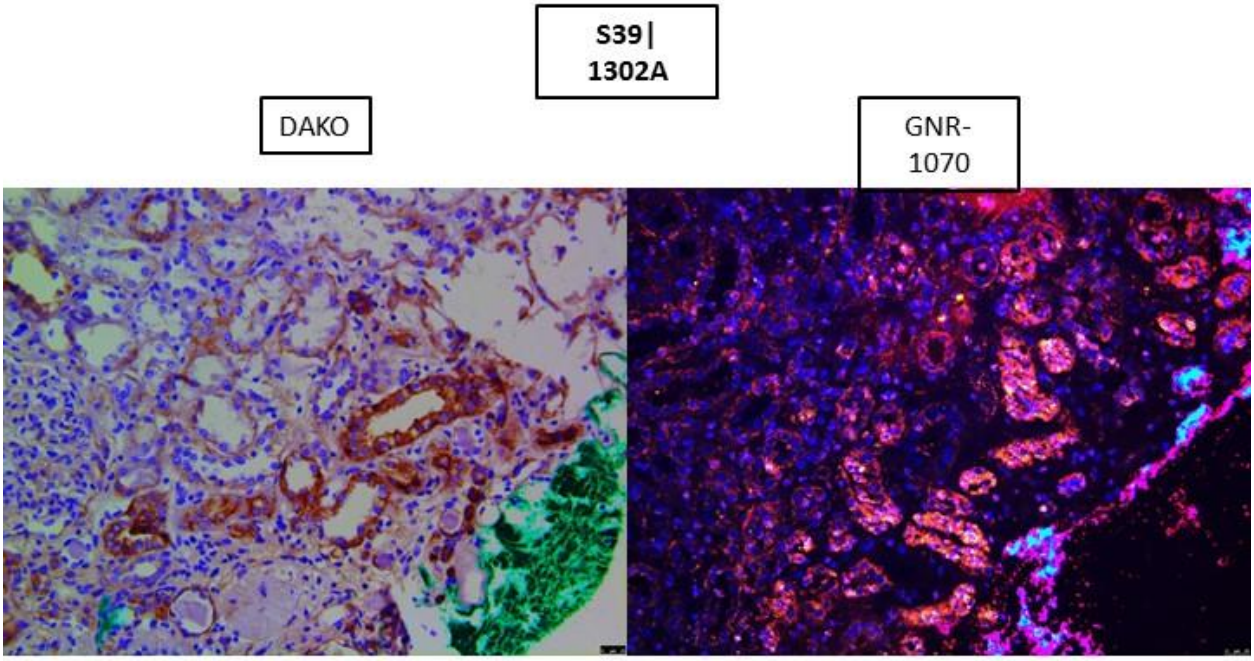
S39|
1302A
DAKO
GNR-
1070

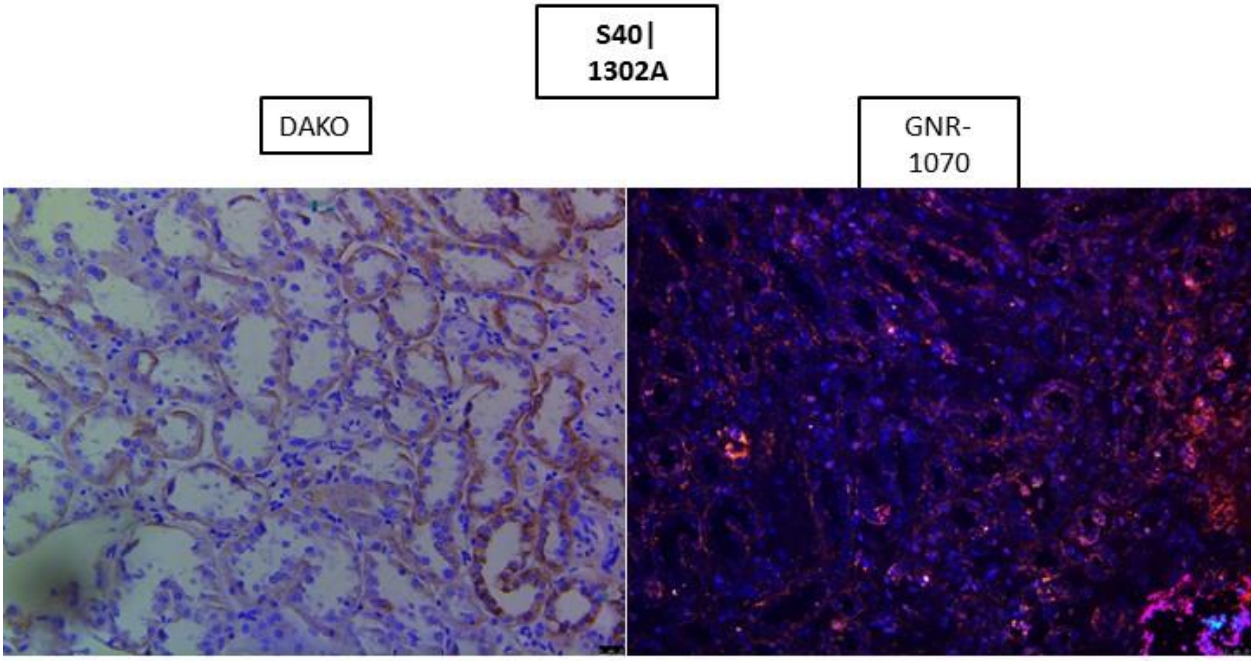
S40|
1302A
DAKO
GNR-
1070

S41|1304A

DAKO

GNR-1070

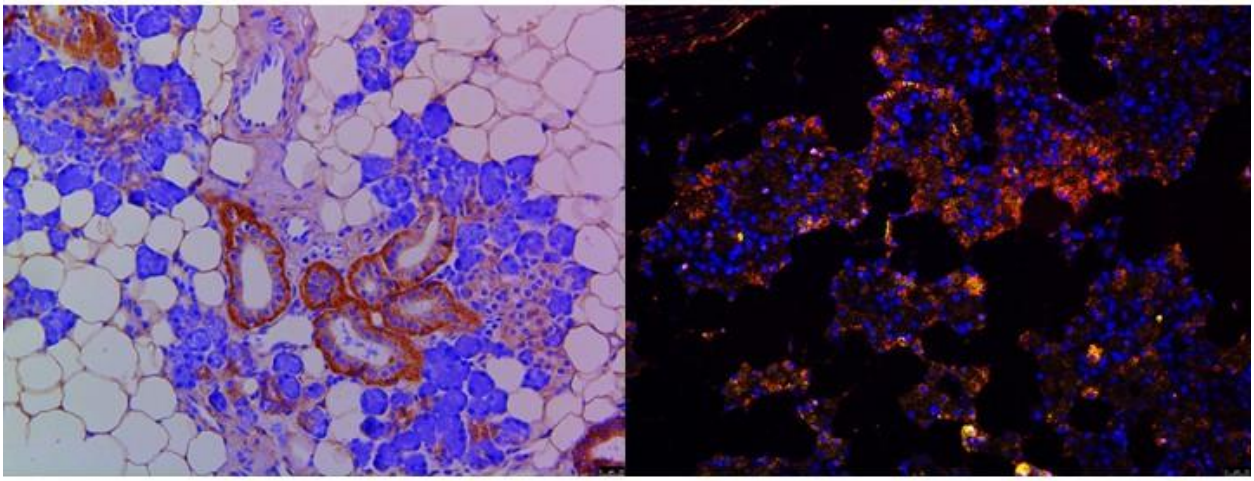

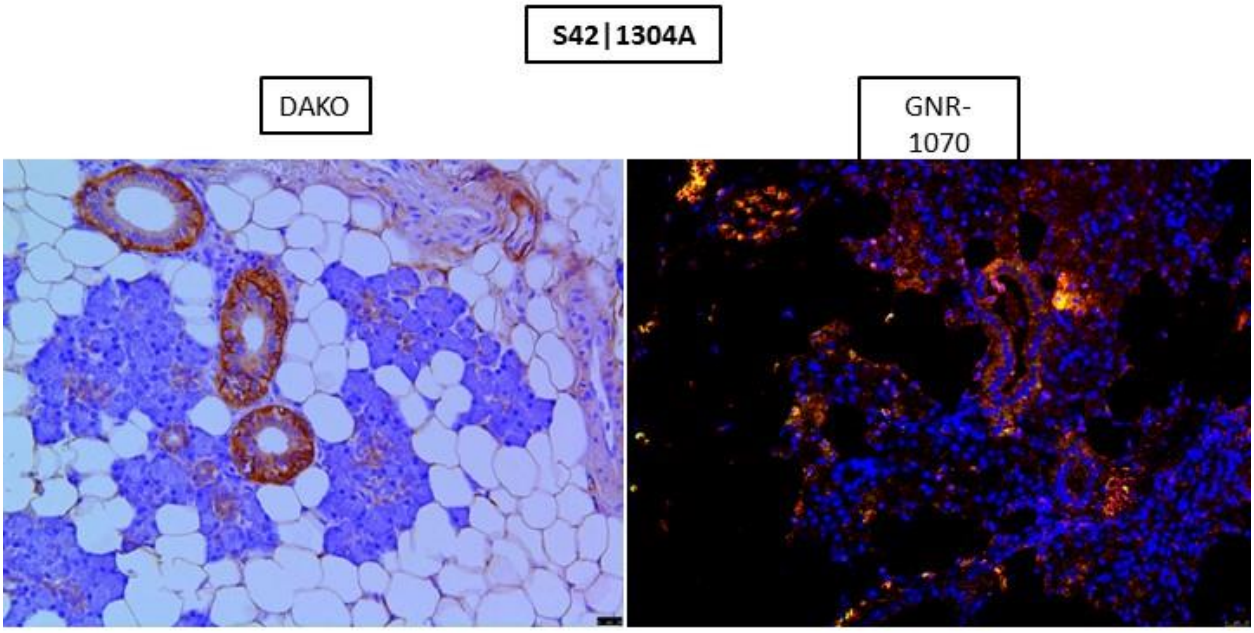
S42|1304A
DAKO
GNR-1070

S43| 1235A

DAKO

GNR-1070

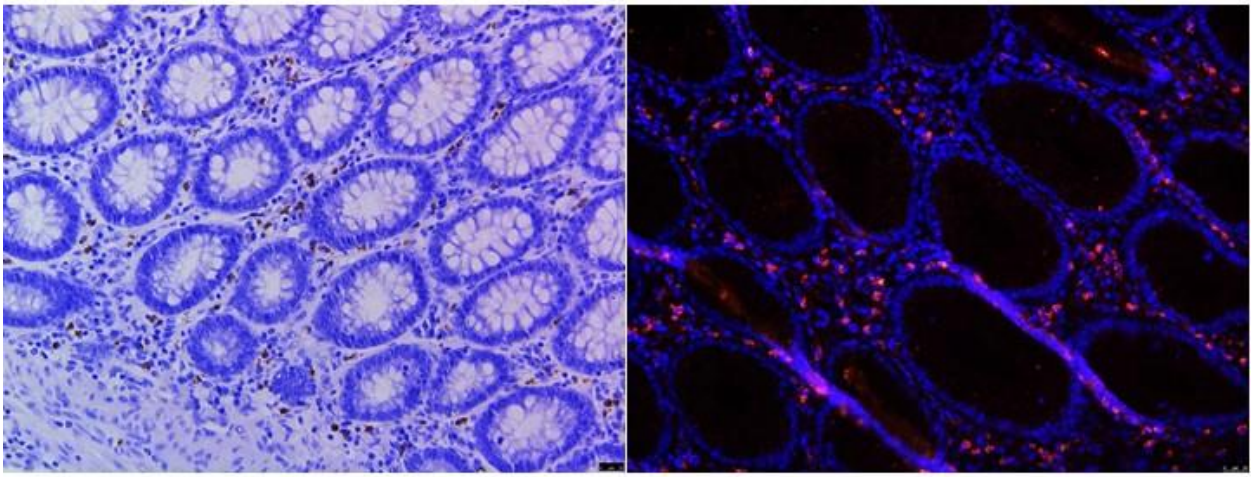

S44| 1235A

DAKO

GNR-1070

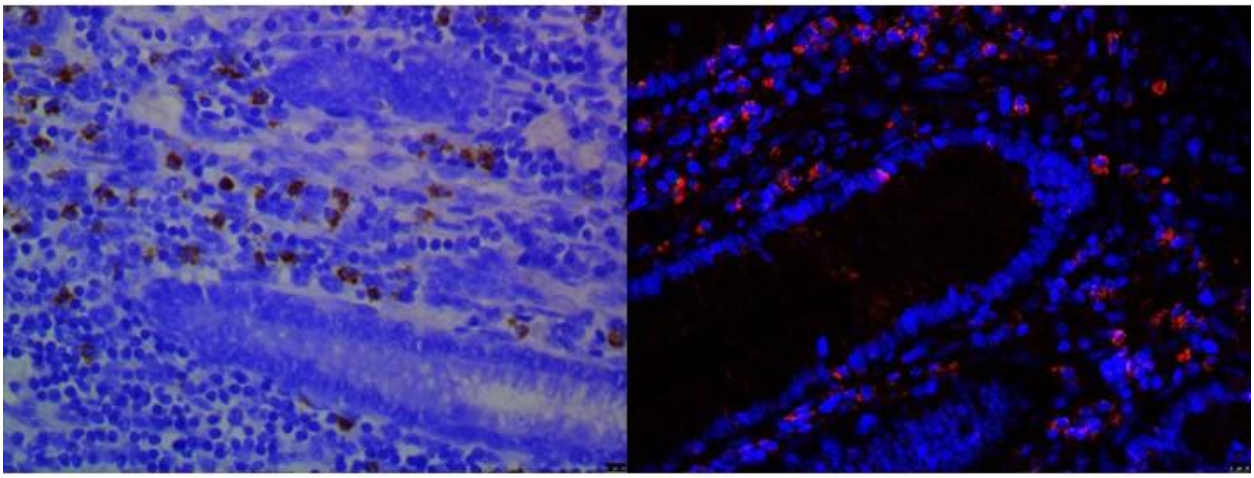

S45 | 1150E2

DAKO

GNR-1070

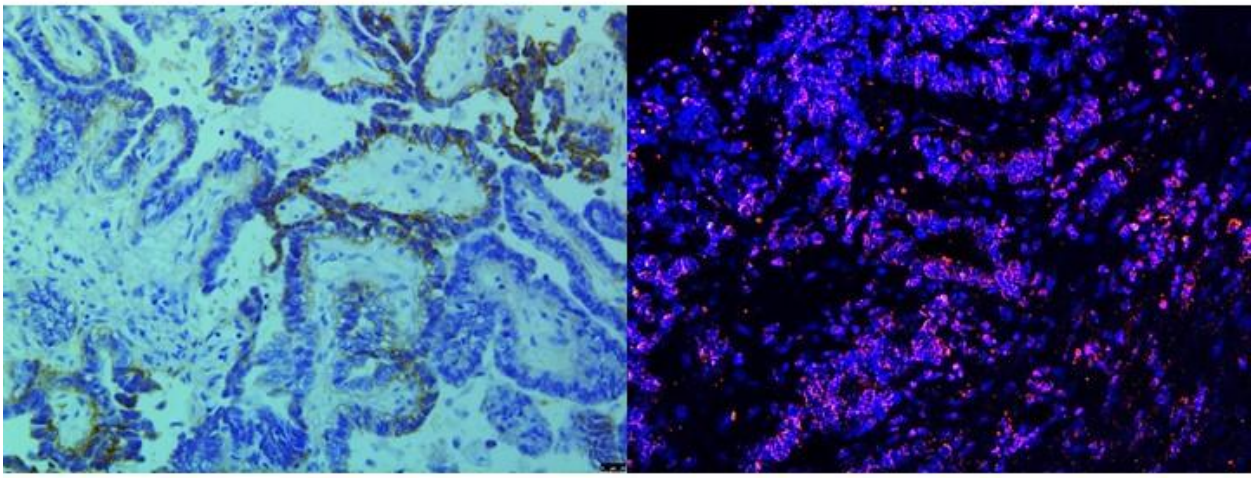

S46| 1150E2

DAKO

GNR-1070

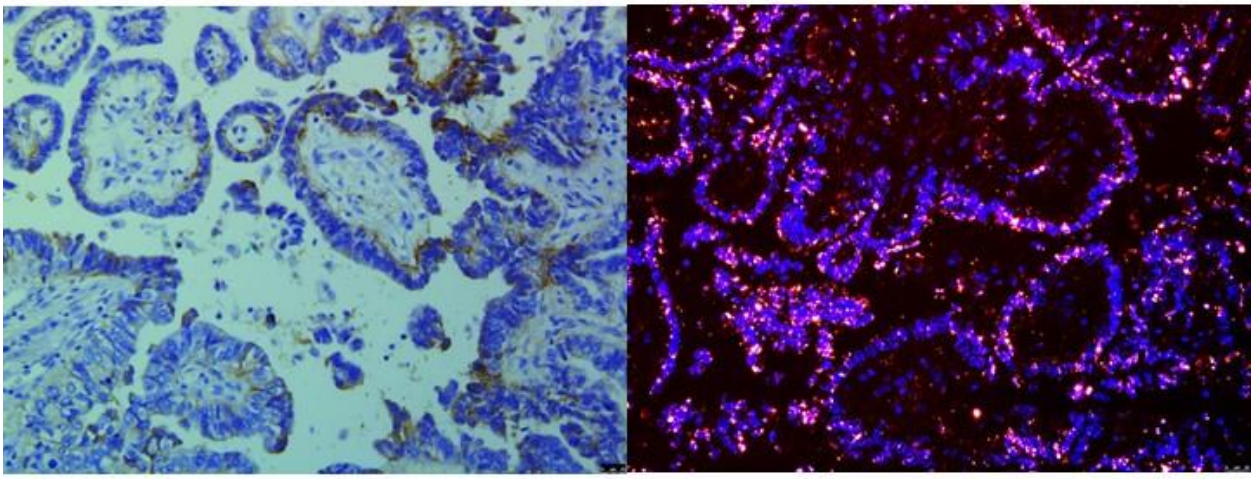

S47|1128E 1

DAKO

GNR-1070

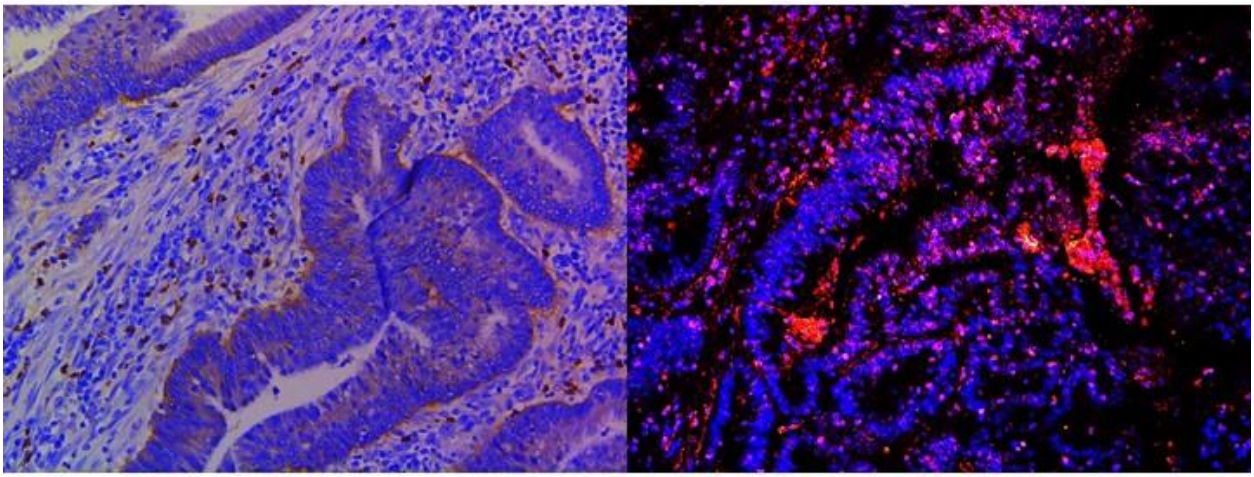

S48|
1128E1

DAKO

GNR-
1070

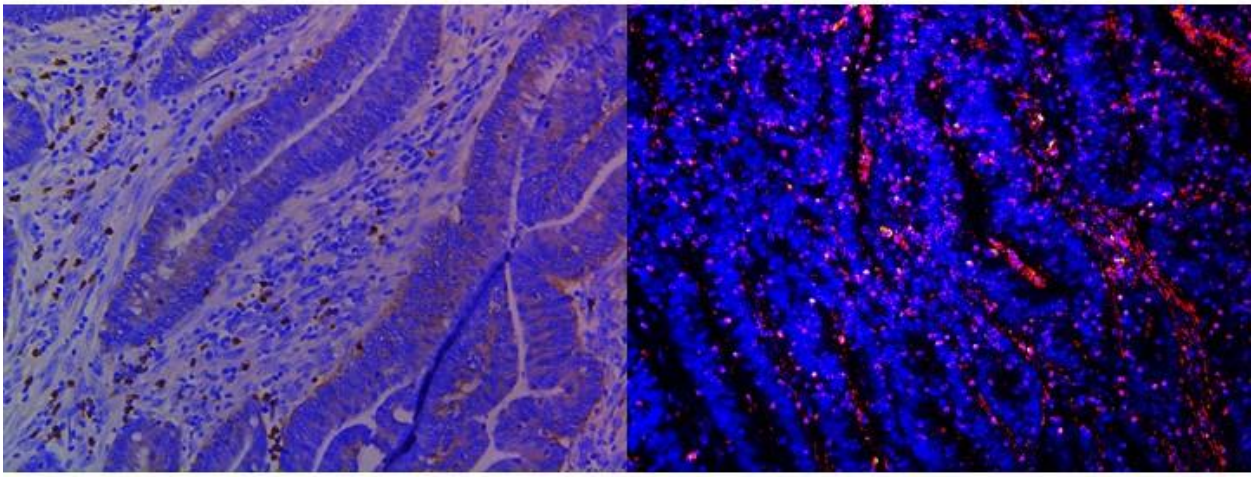

S49| 1132B2

DAKO

GNR-1070

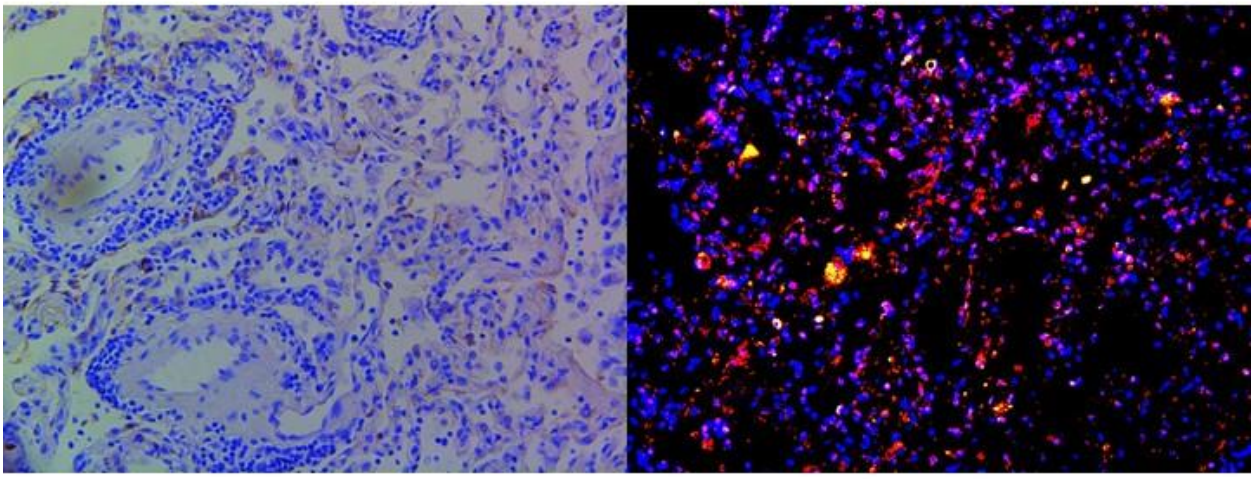

S50| 1132B2

DAKO

GNR-1070

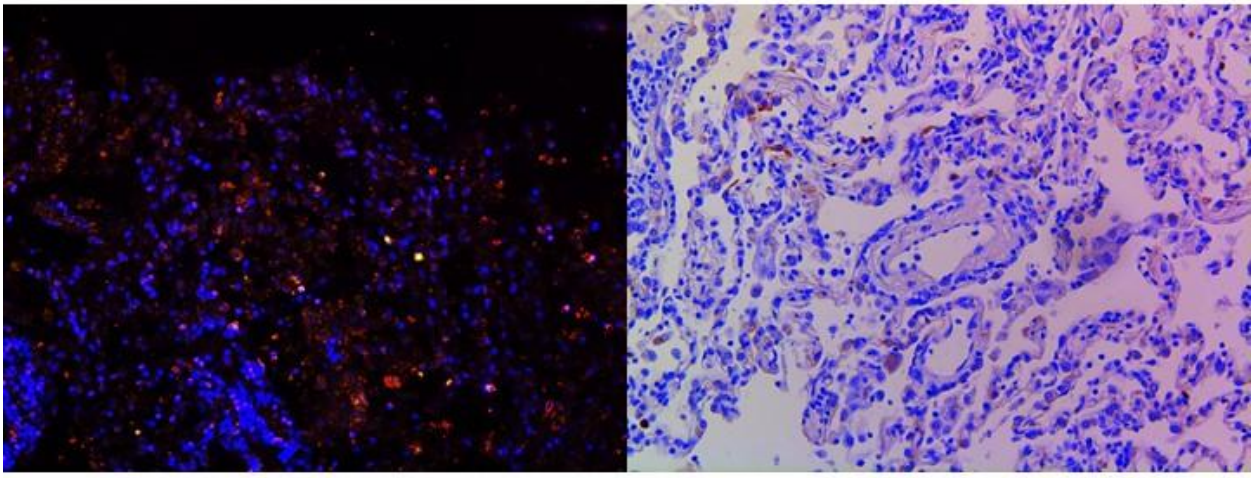

S51|
1216F1

DAKO

GNR-
1070

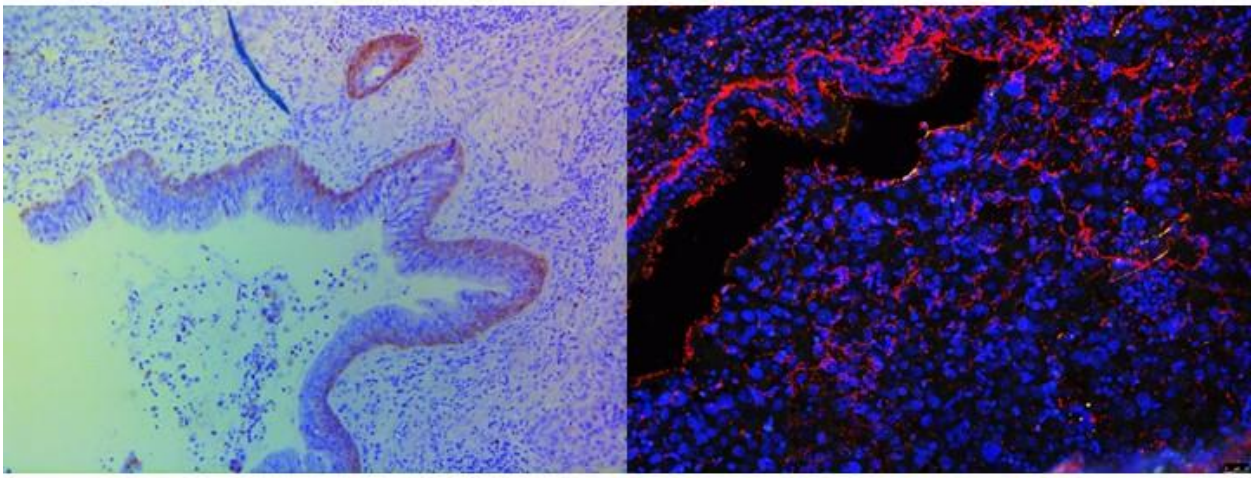

S52| 1216F1

DAKO

GNR-1070

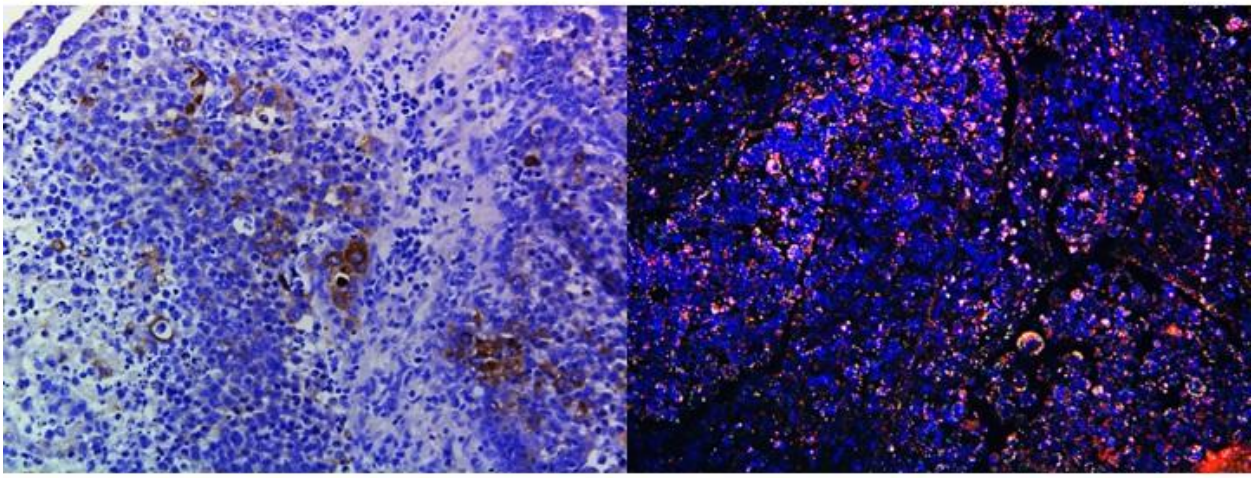

S531233A

DAKO

GNR-1070

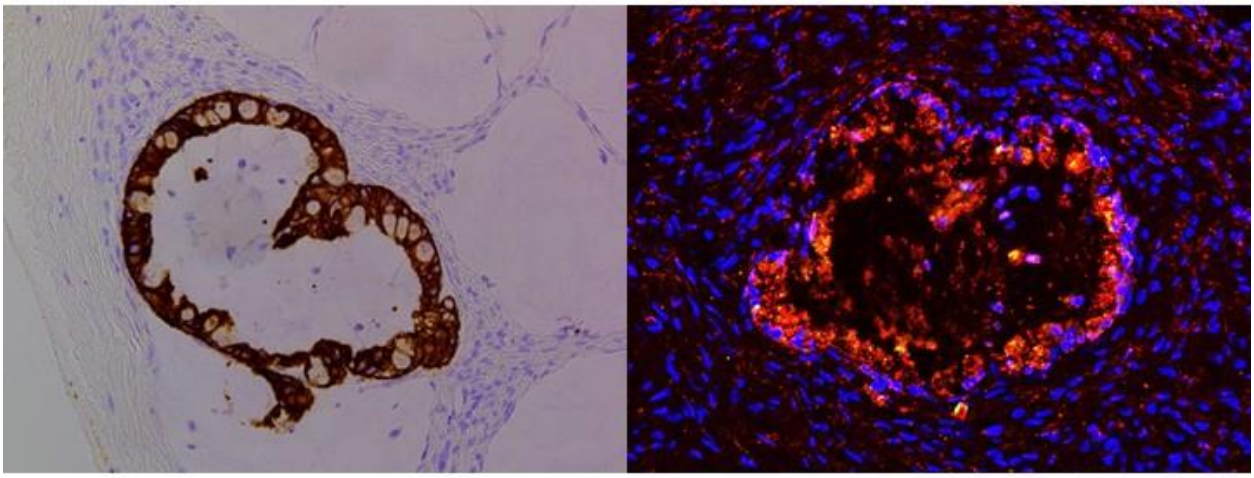

S54| 1233A

DAKO

GNR-1070

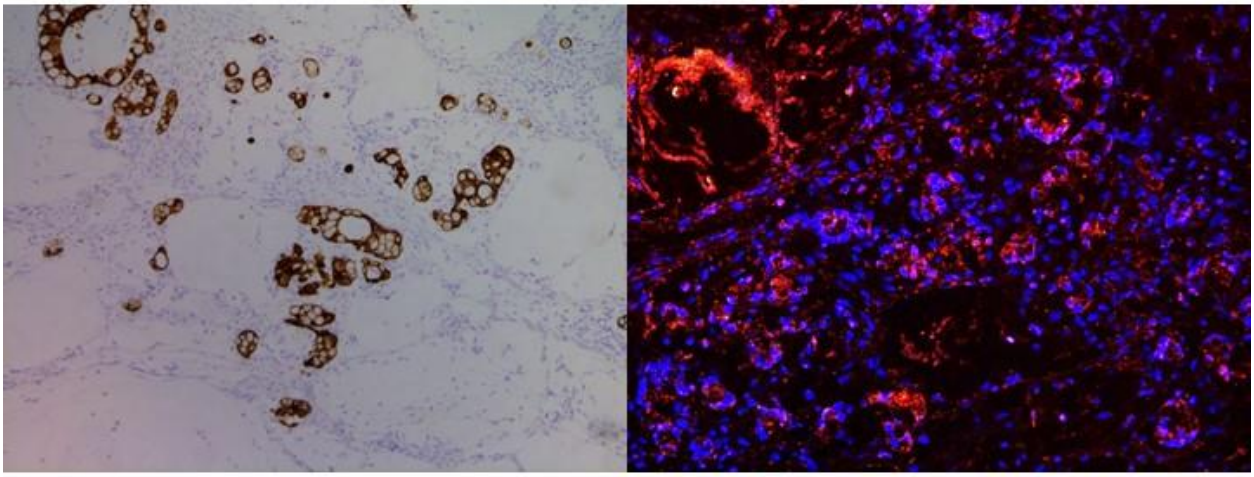

S55 | 1094B1

DAKO

GNR-1070

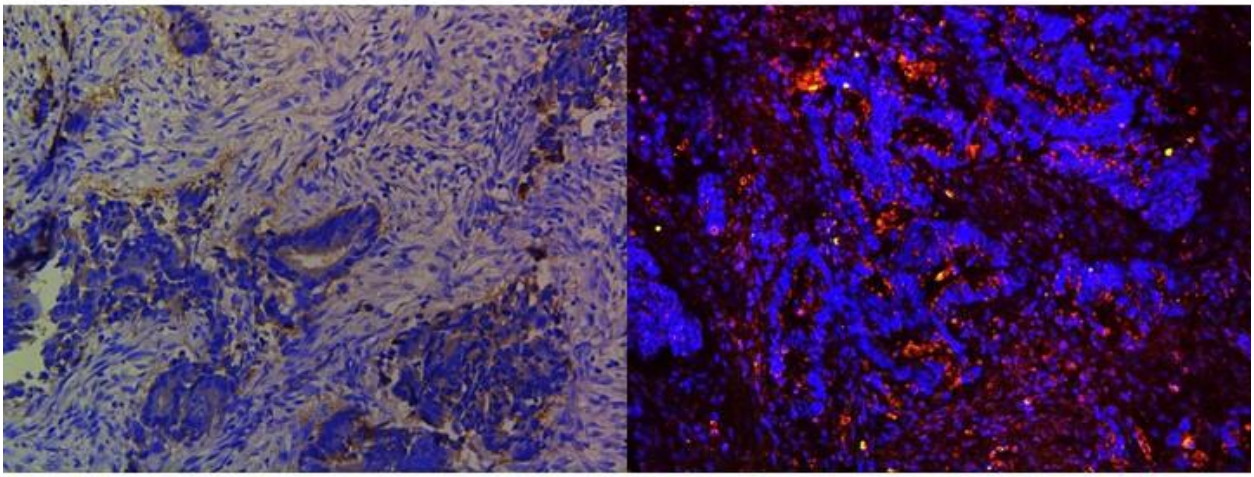

S56|
1094B1

DAKO

GNR-
1070

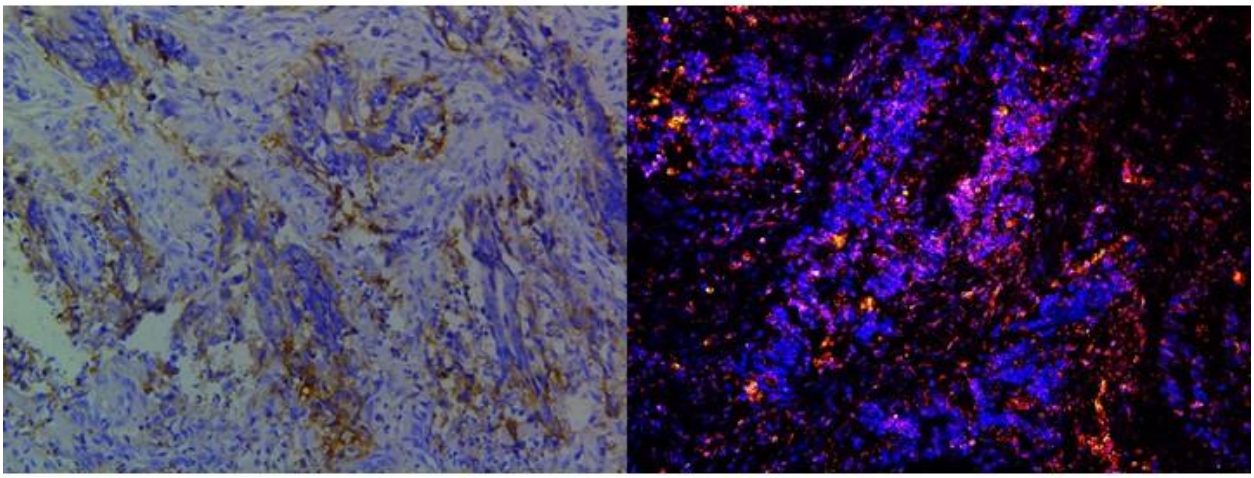

S57| Quantification of GNR and DAB percentages with arbitrary numerical representations of pathology grading. “Normal” cases removed in final evaluation.

5.2 Supplementary Figures: Peptide-Conjugated Gold Nanorods for Evaluation of c-MET Receptor Levels in NSCLC Tissues

S1: HPLC – Peptide 1093

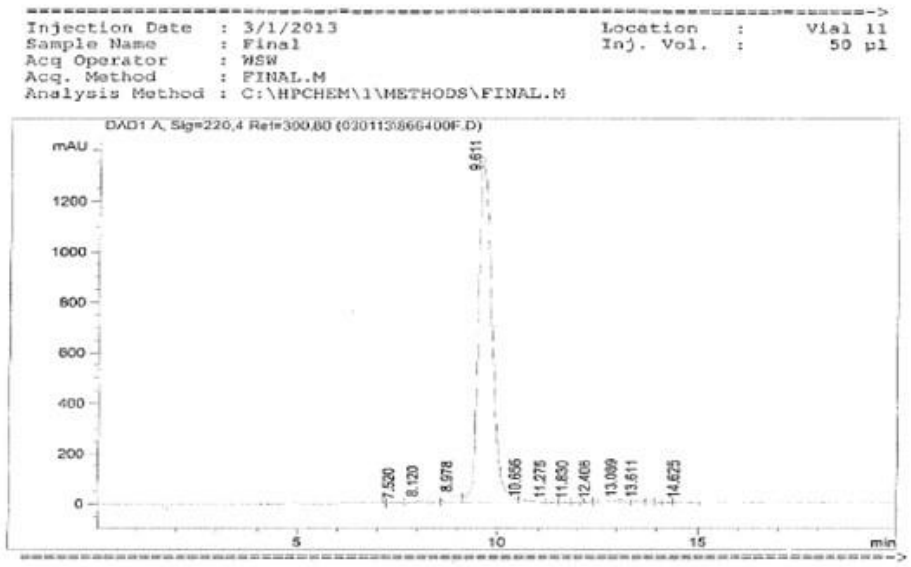

S2: Mass Spectrometry – Peptide 1093

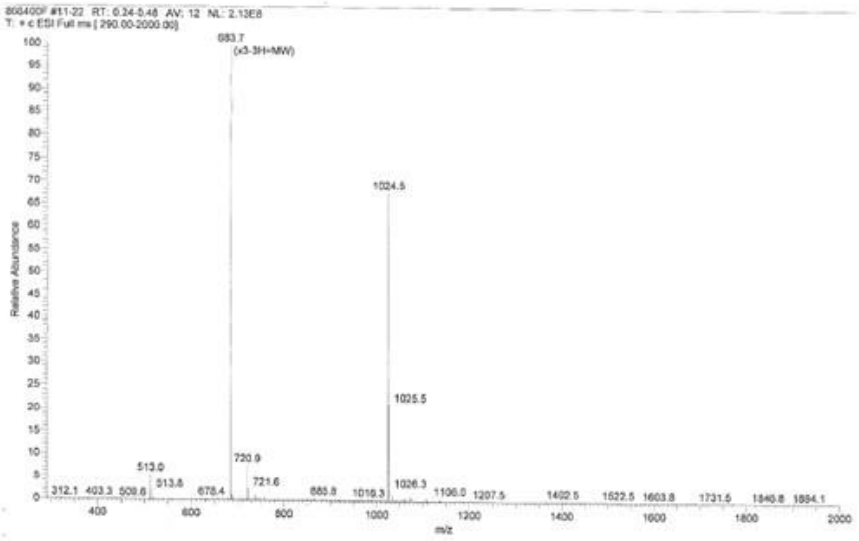

S3: Structure of Peptide 1093 Binding Sequence

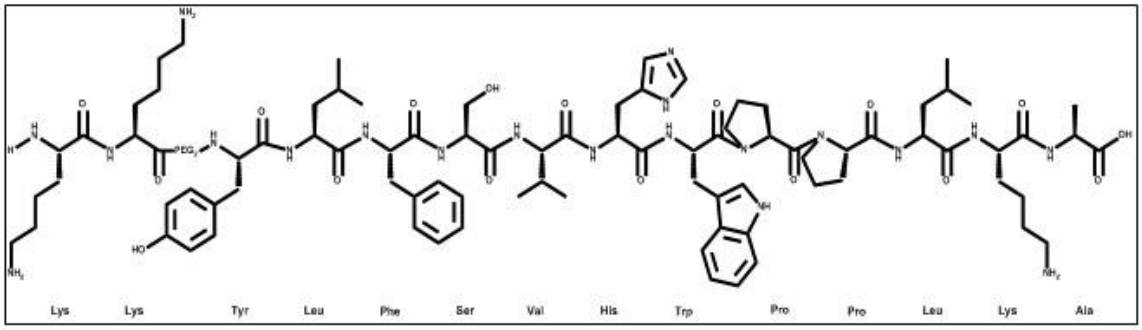

S4:H441 Cell Line Treated with GNR-PEG

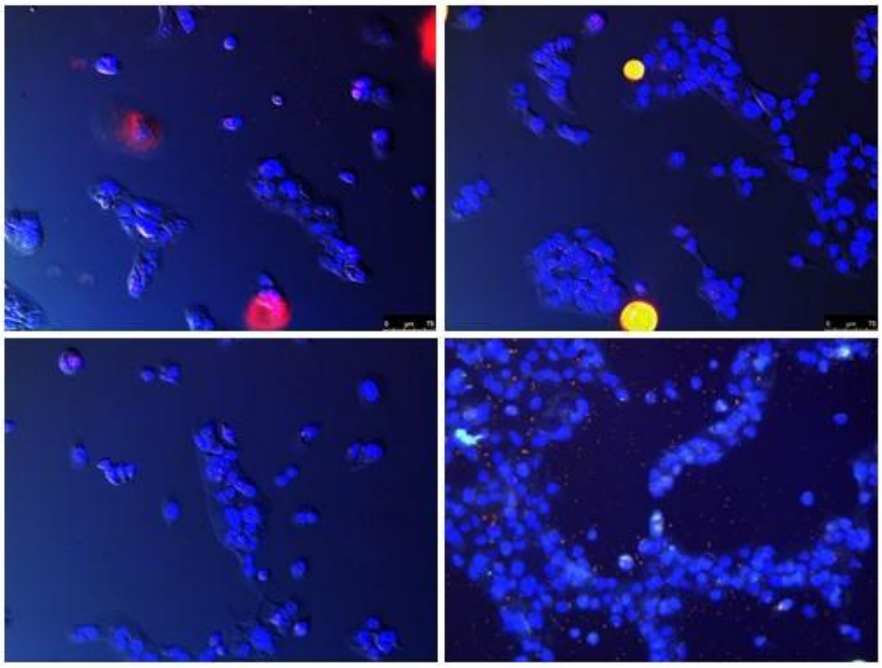

S5: H441 Cell Line Pre-Blocked with 1093 Peptide and Treated with GNR-1093

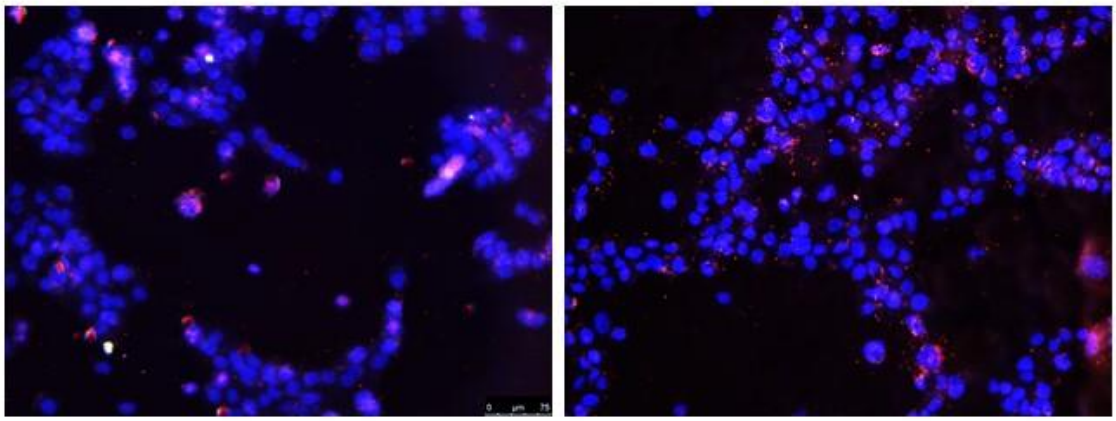

S6: H441 Cell Line Treated with GNR-1093

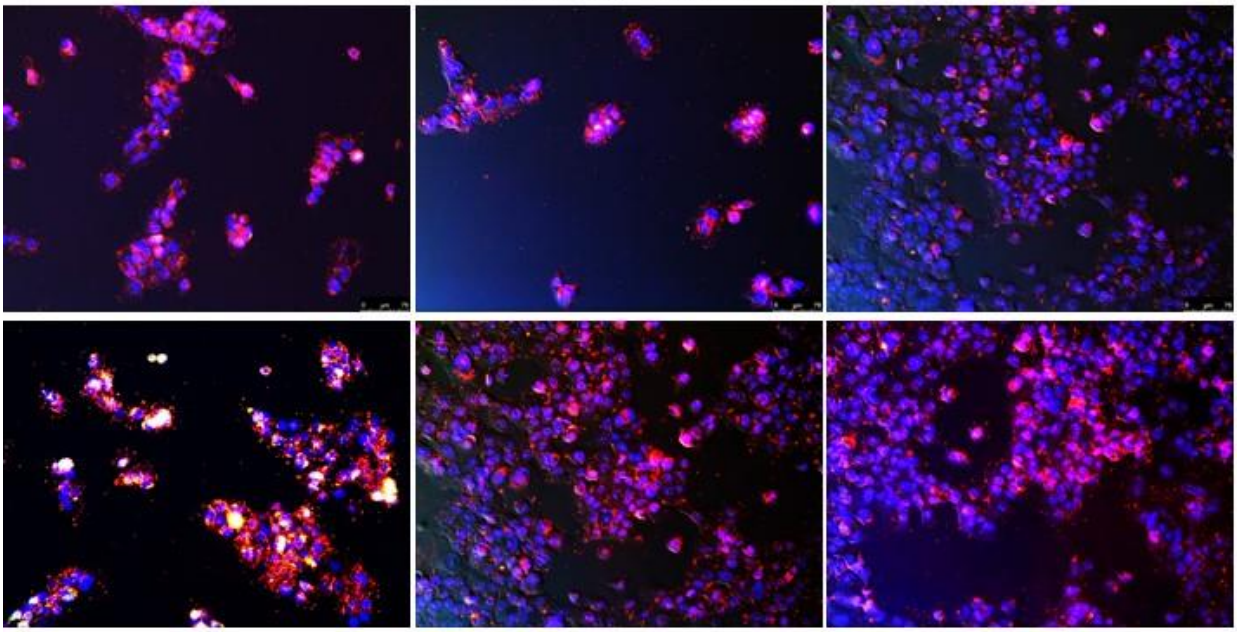

S7: MCF7 Cell Line Treated with GNR-PEG

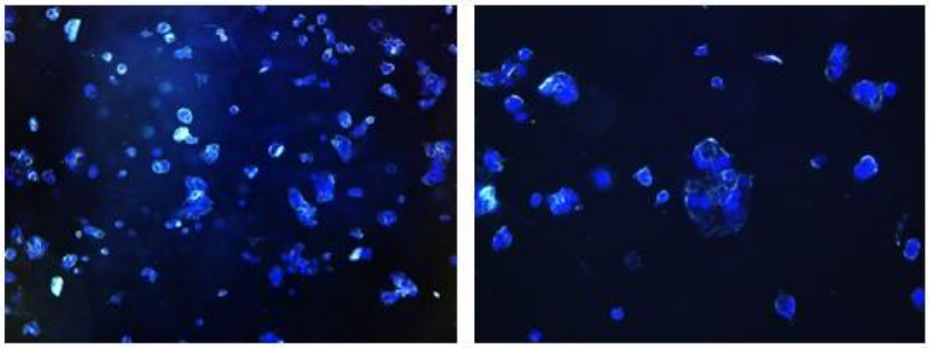

S8: MCF7 Cell Line Pre-Blocked with 1093 Peptide and Treated with GNR-1093

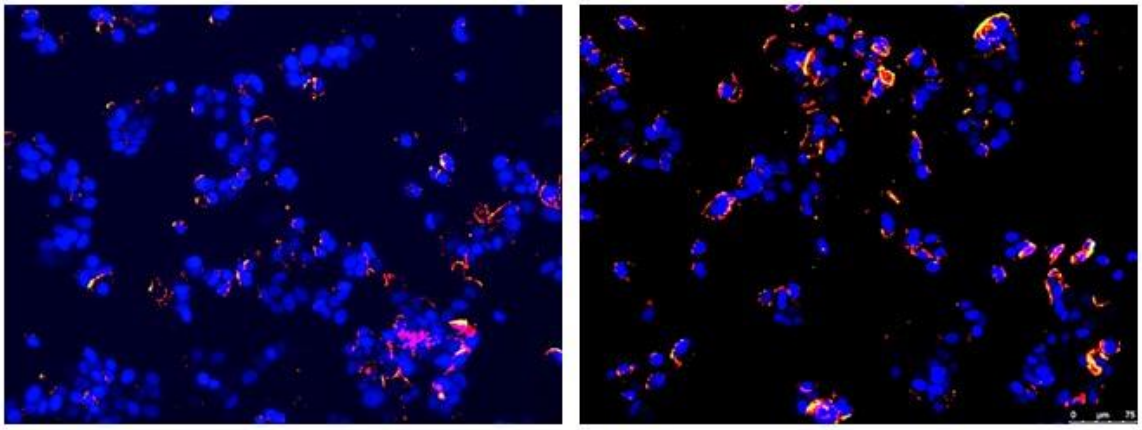

S9: H441 Cell Line Treated with GNR-1093

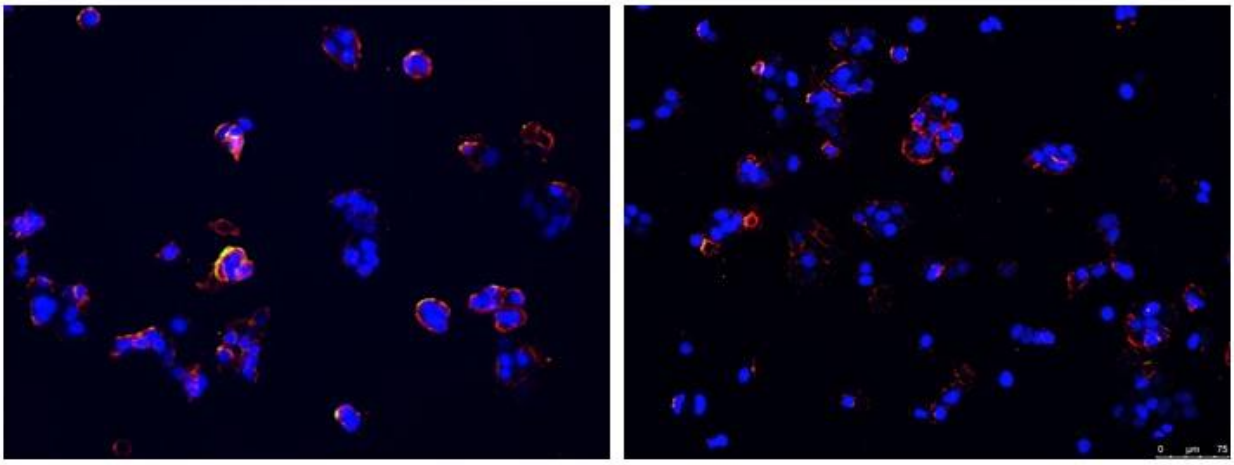

S10: cMET FFPE Cell Line Array

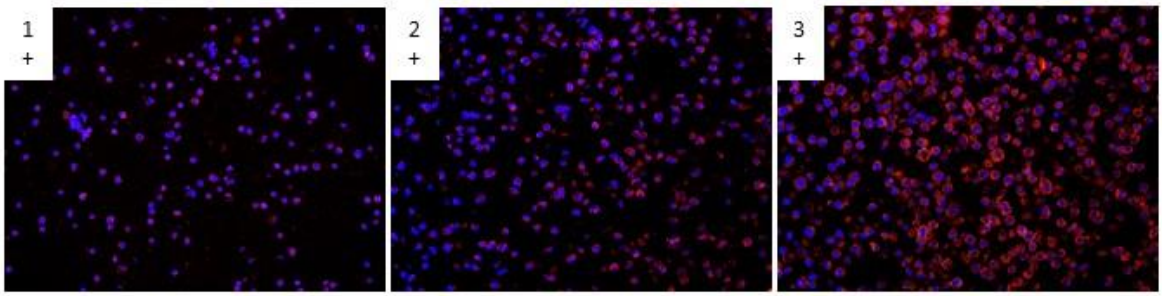

S11: GNR-1093 with Duodenum Tissue

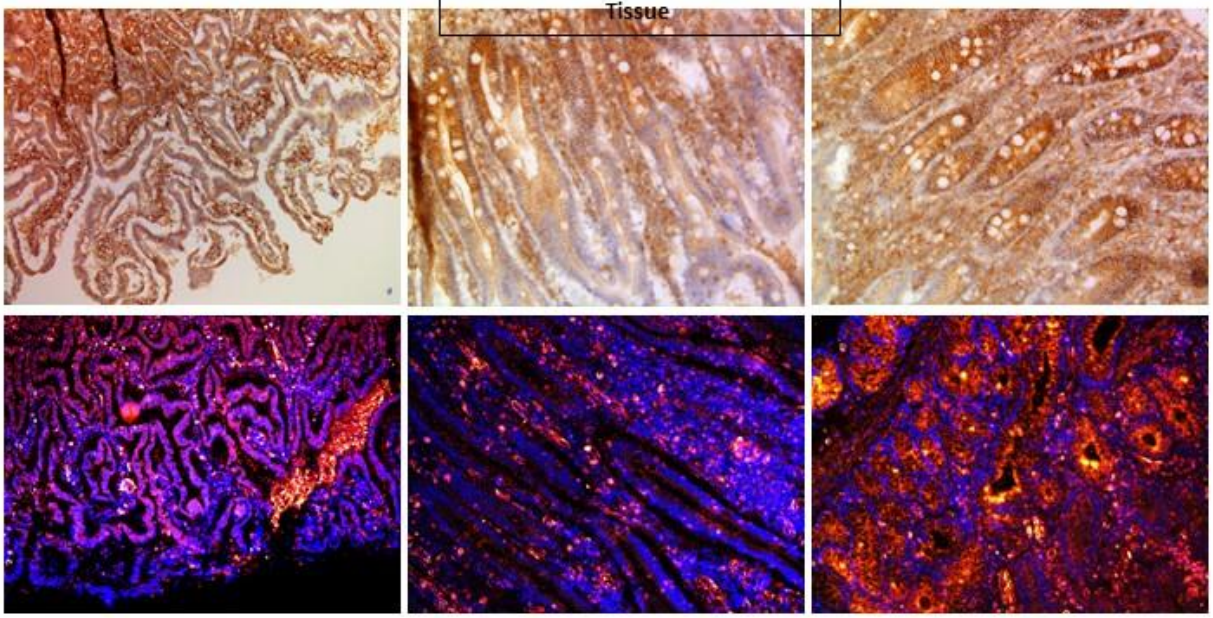

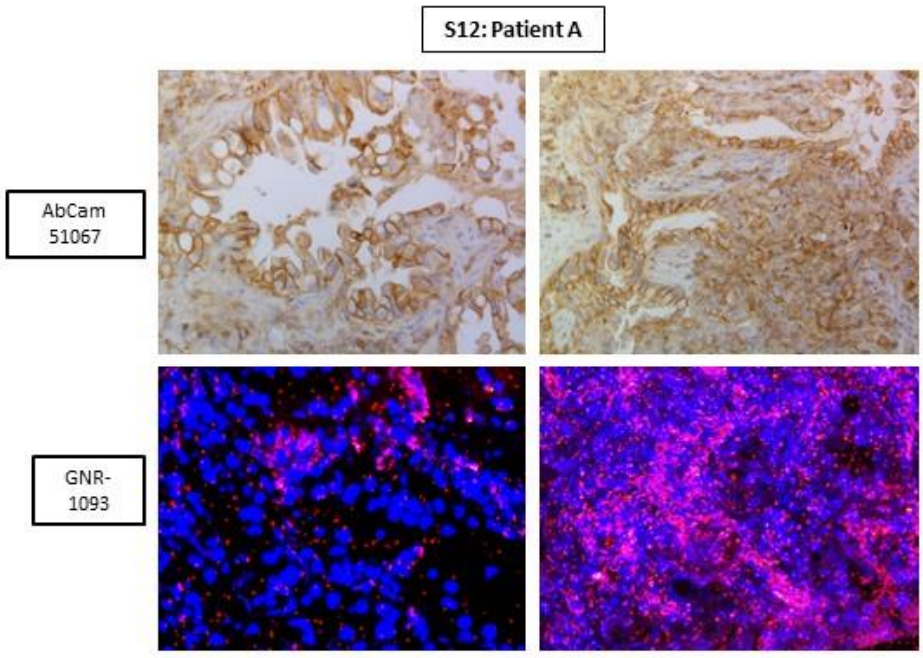
S12: Patient A
AbCam 51067
GNR-1093

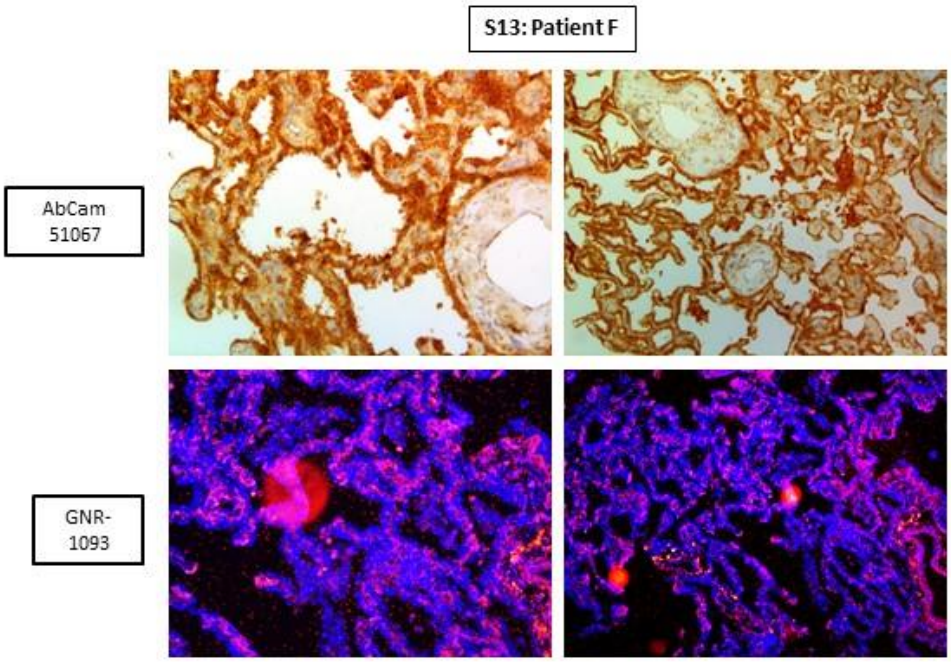
S13: Patient F
AbCam 51067
GNR-1093

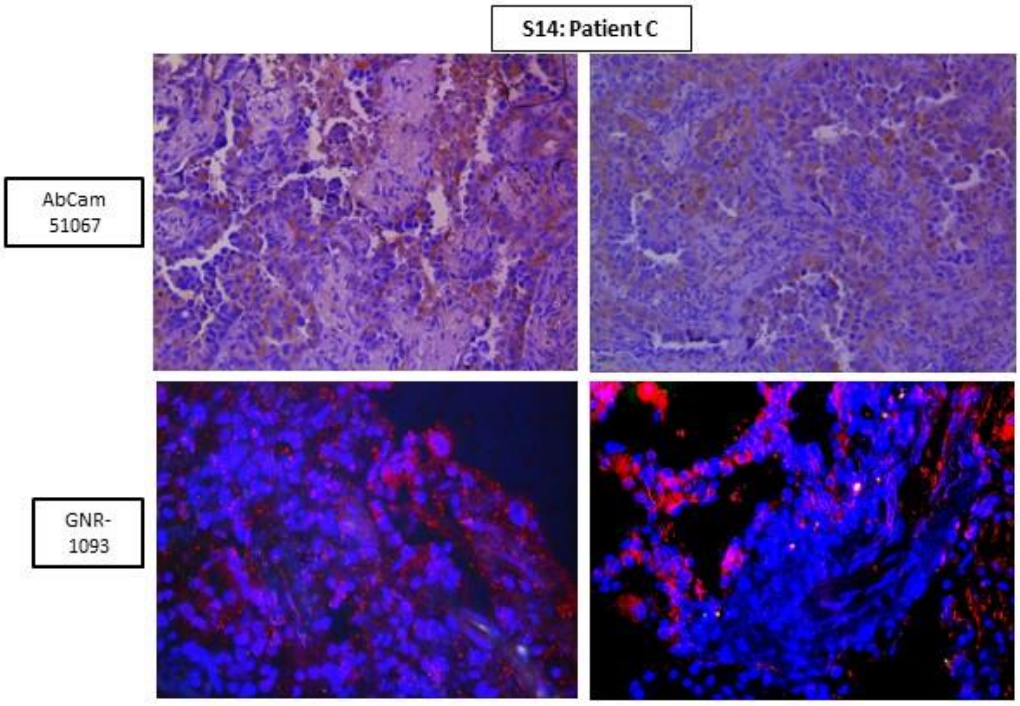
S14: Patient C
AbCam 51067
GNR-1093

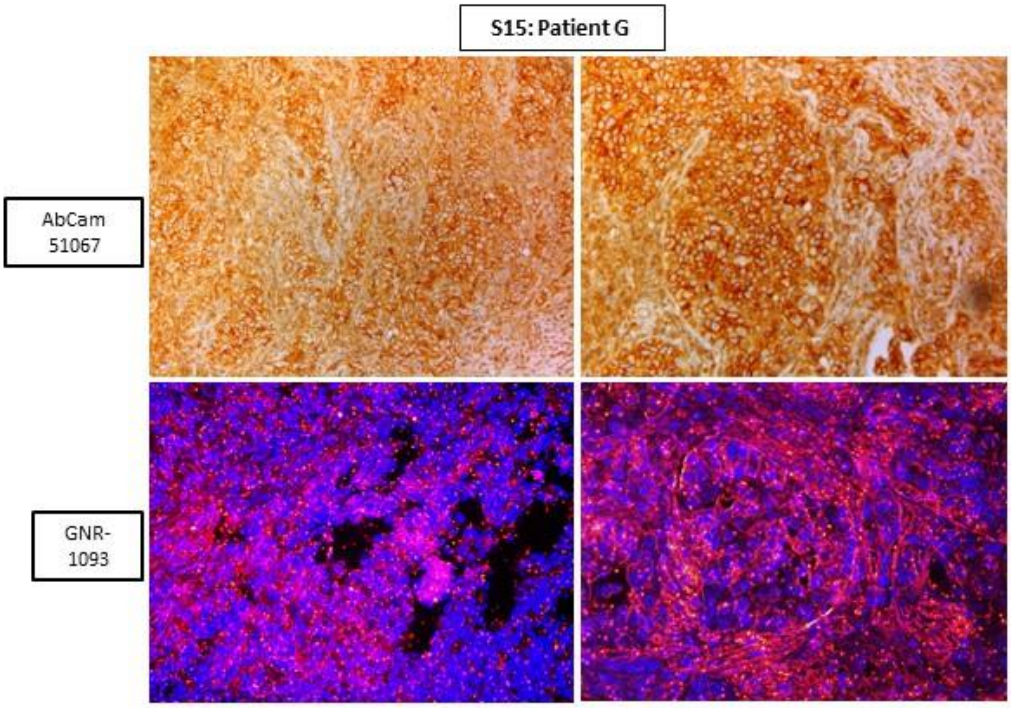
S15: Patient G
AbCam 51067
GNR-1093

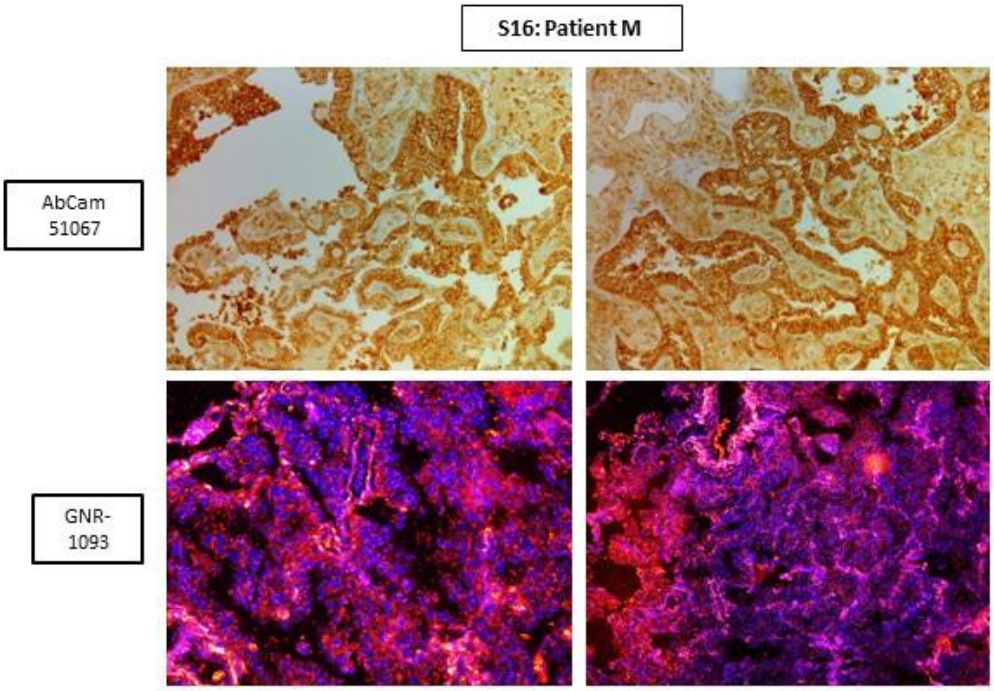
S16: Patient M
AbCam 51067
GNR-1093

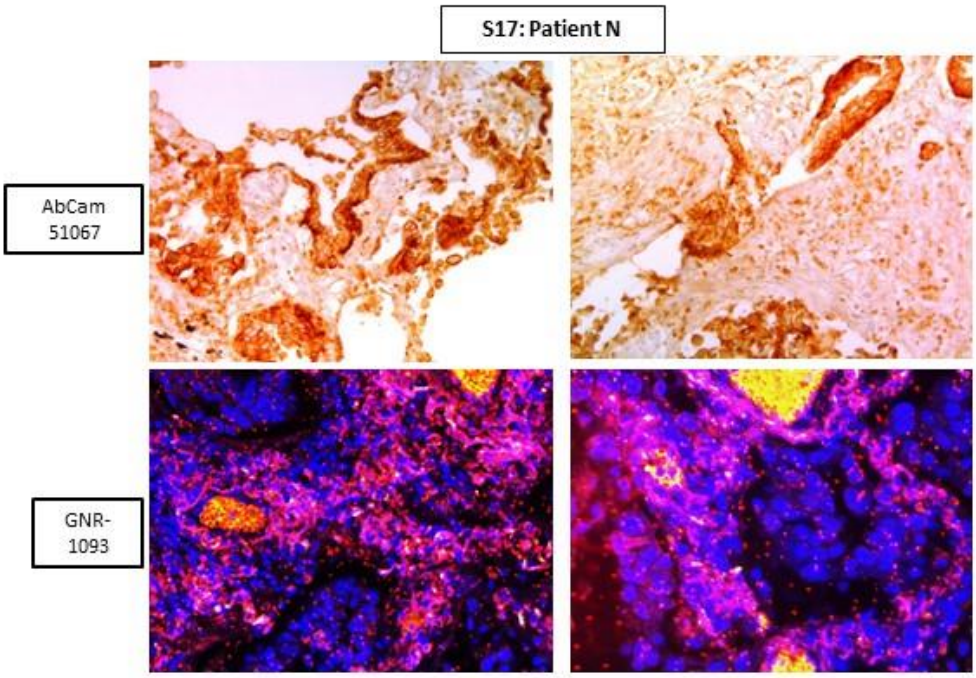
S17: Patient N
AbCam 51067
GNR-1093

S18: TMA A2

GNR-PEG

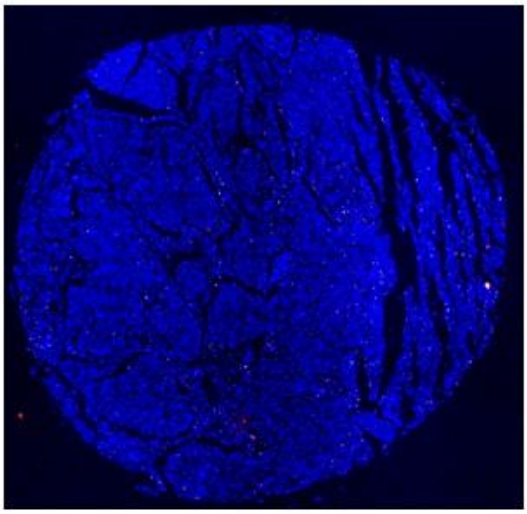

GNR-1070

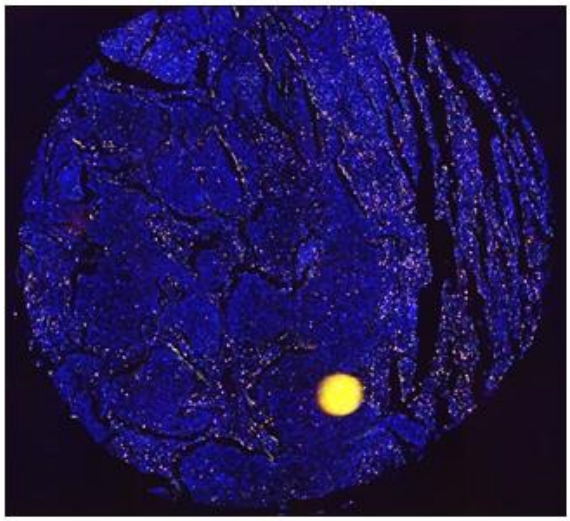

S19: TMA B2

GNR-PEG

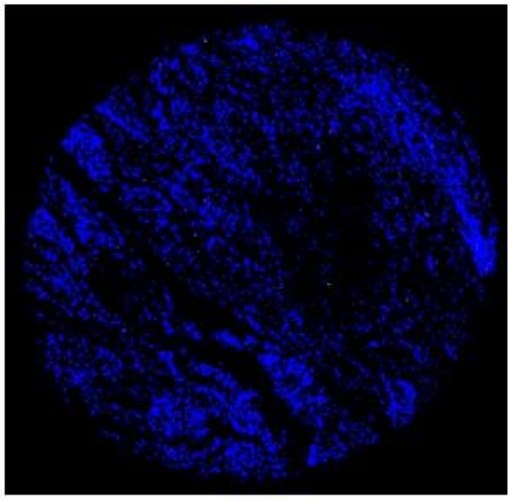

GNR-1070

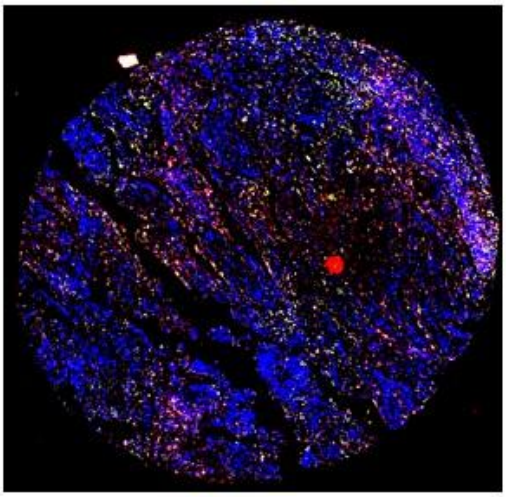

S20: TMA C2

GNR-PEG

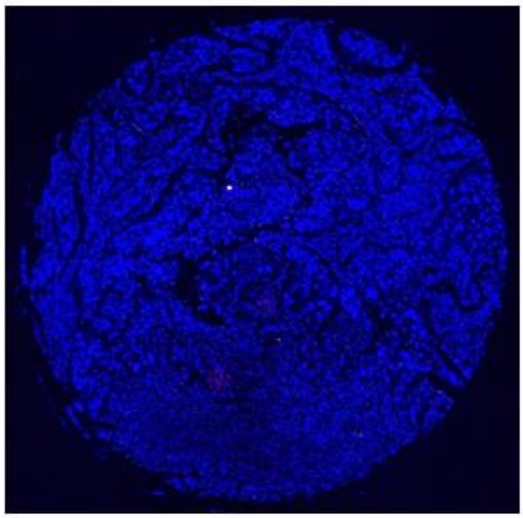

GNR-1070

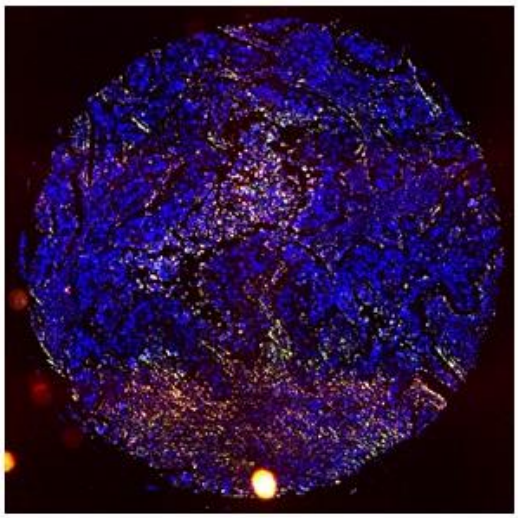

S21: TMAD2

GNR-PEG

GNR-1070

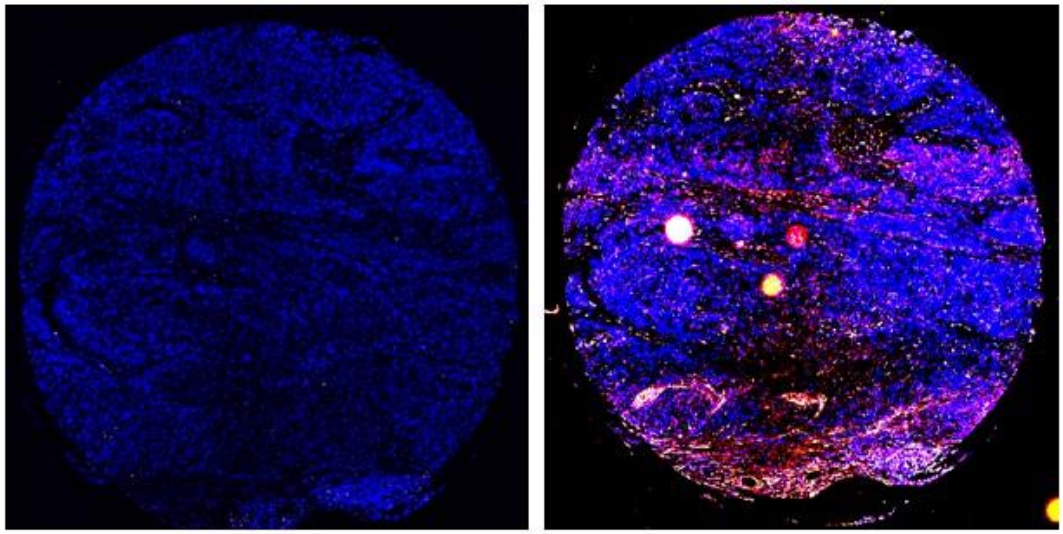

S22: TMA E2

GNR-PEG

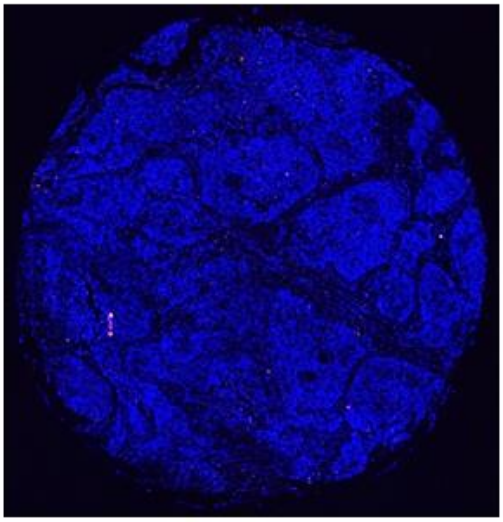

GNR-1070

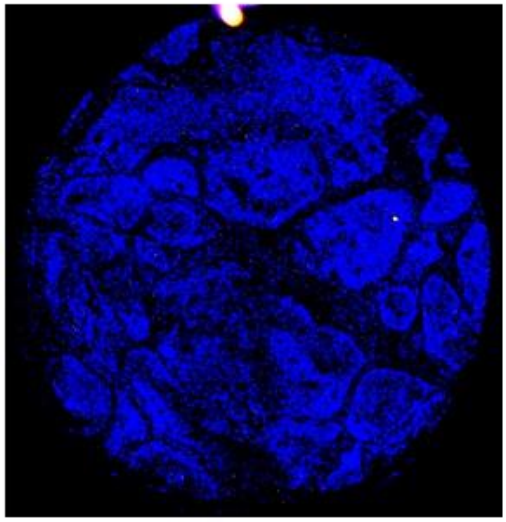

S23: TMAF2

GNR-PEG

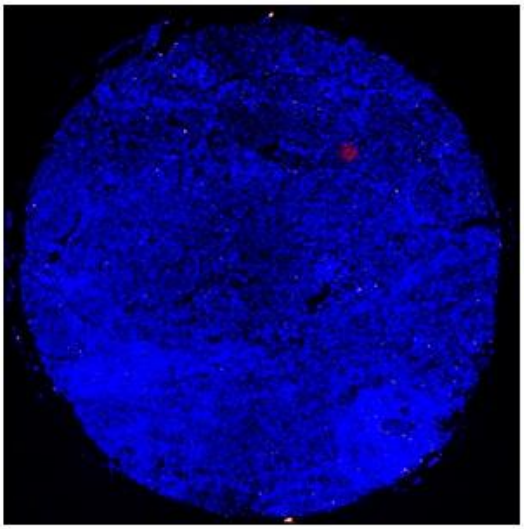

GNR-1070

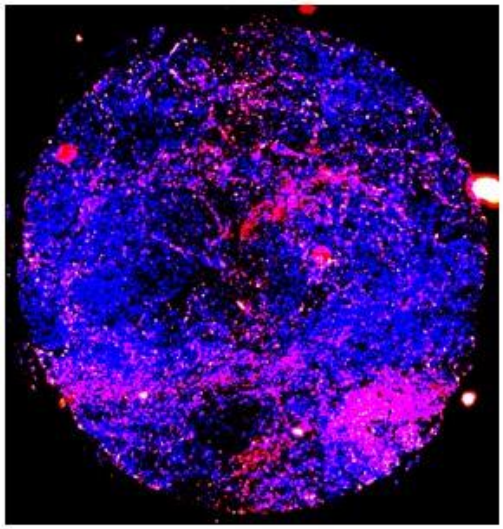

5.3 Supplementary Figures: Identification and Validation of a PD-L1 Binding Peptide for Determination of PDL1 Expression in Tumors

S1: Identification of PDL1 Binding Peptides

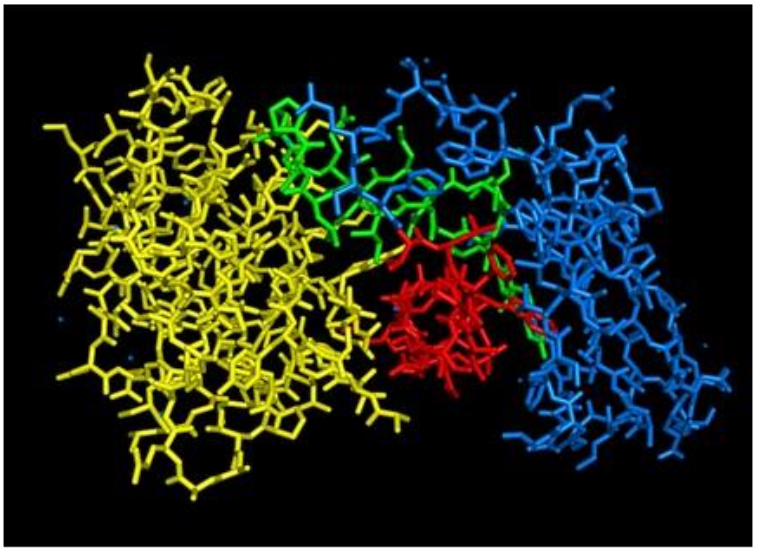

Chain A (PDL1) is shown in yellow. **Chain B** (PD1) is shown in blue, red and green.
Red and green corresponds to the sequence 1 and 2 suggested for synthesis which are in contact with PDL1. These two sequences were selected based on the contact criteria and extension beyond the contact residues to include extended chains to retain its secondary structure.

S2: Flow Cytometric Method

MDA-MB-231

FITC Expression (Cytokeratin)

Cy5 (PDL1) Expression

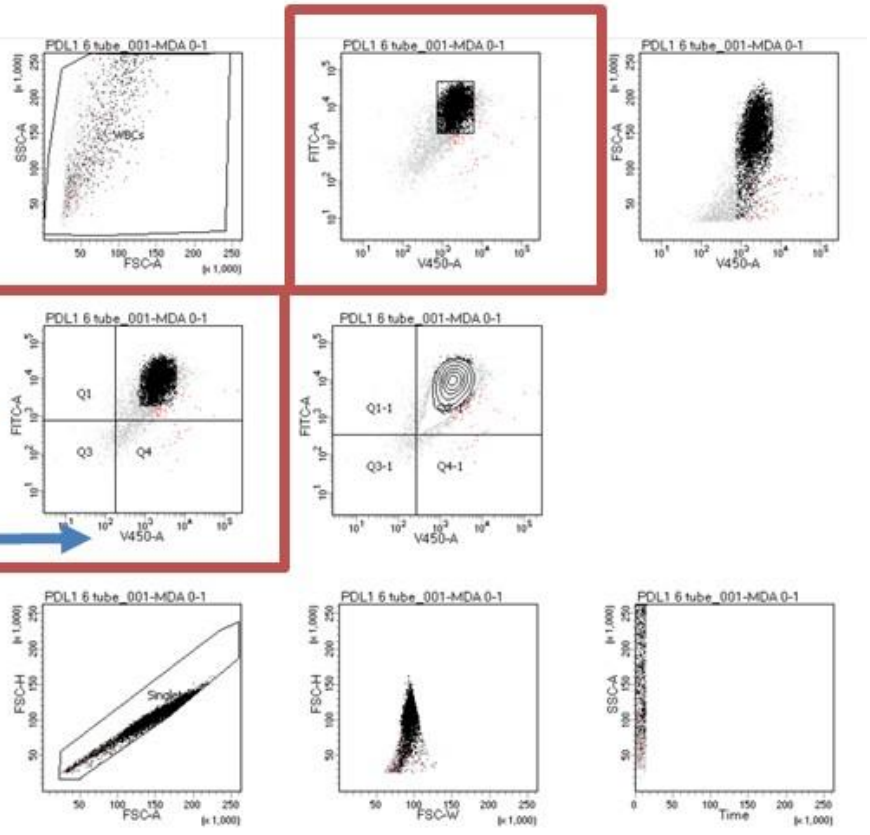

S3: RKC-10-Cy5 Titrations Using PDL1 Positive MDA-MB-231

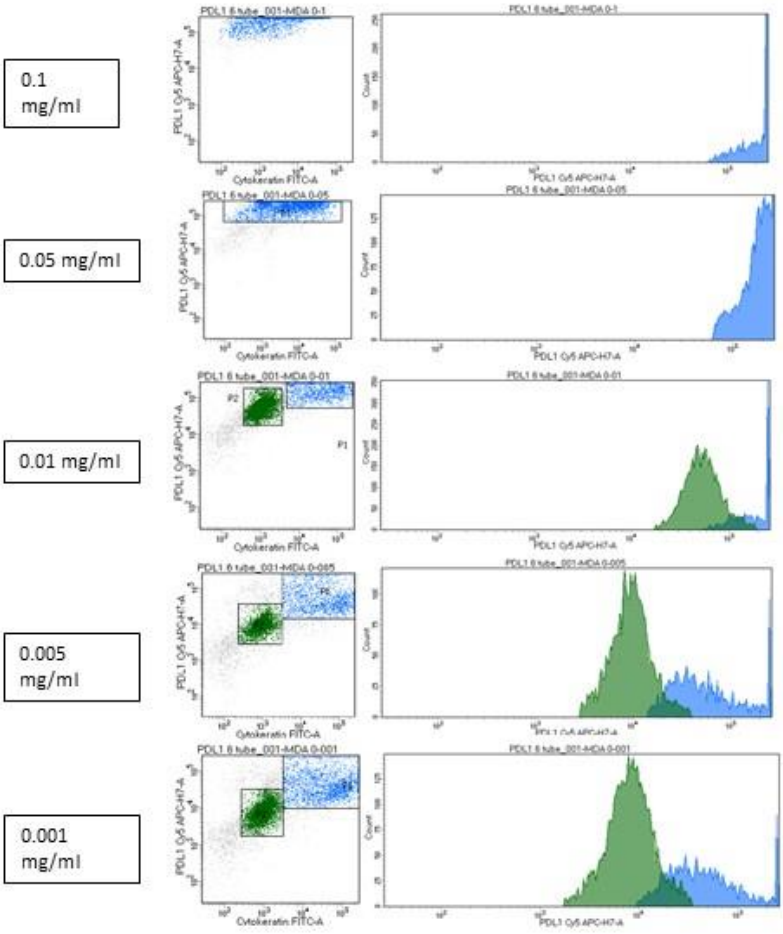

S4: MDA-MB-231 vs MCF7

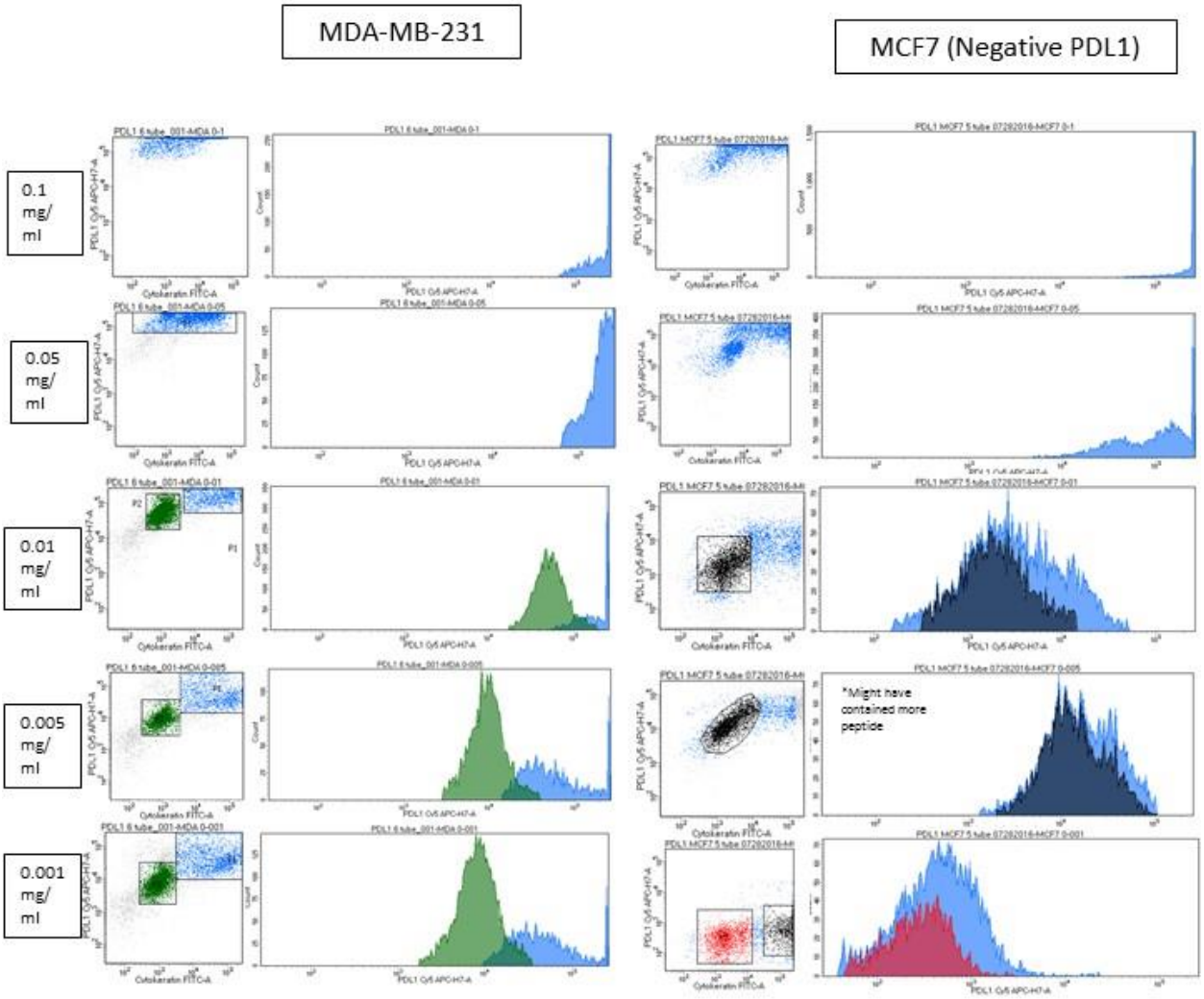

S5: MDA-MB-231 vsY79

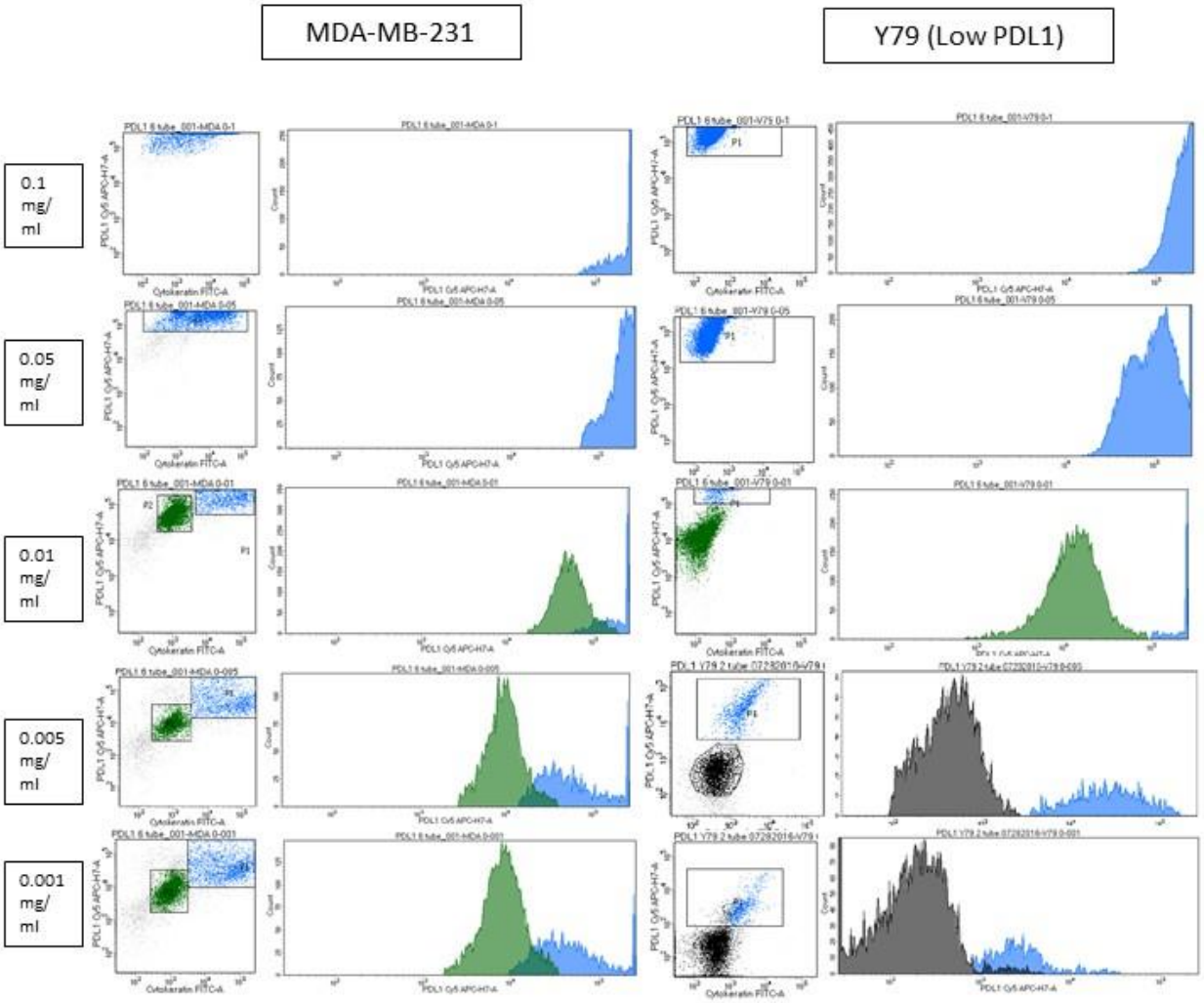

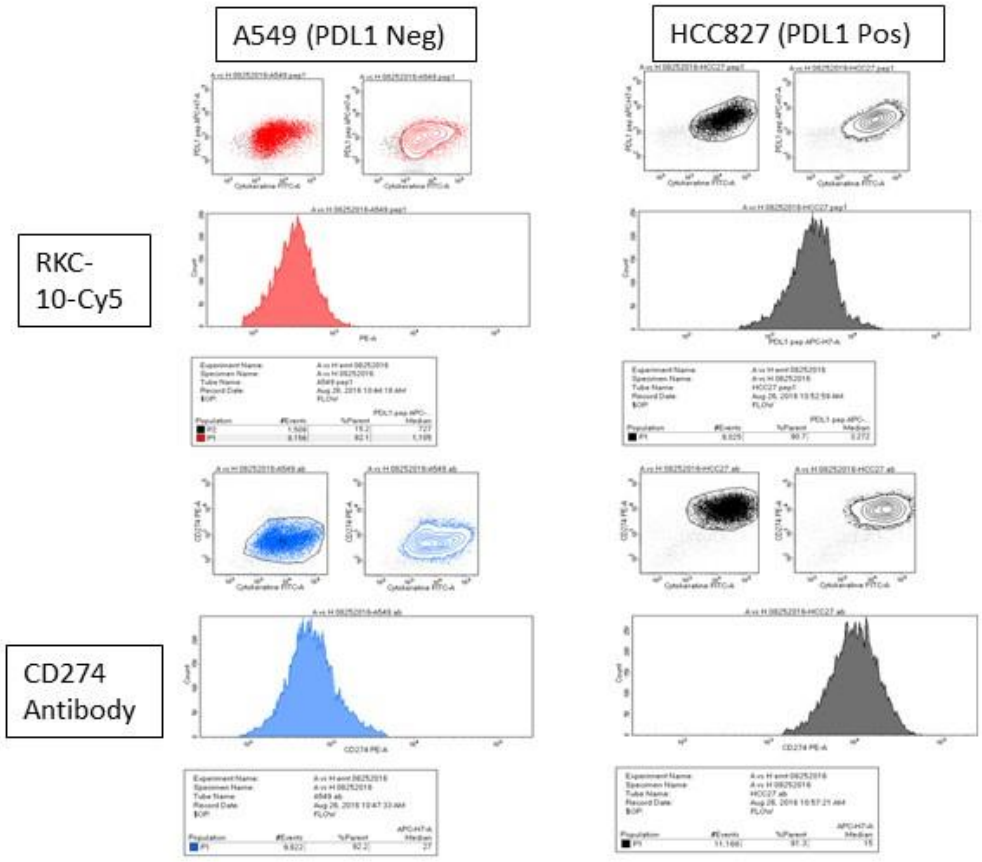

S6: PD-L1 Expression Evaluated by RKC-10-Cy5 and CD274 Flow Cytometry

S7: MDA-MB-231: Treated w/ Cy5-peptide and PE-Antibody (Anti-PDL1) Simultaneously

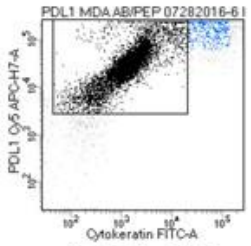

Cy5-Peptide (y-axis)

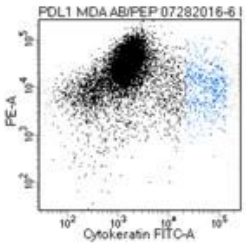

PE-Antibody (y-axis)

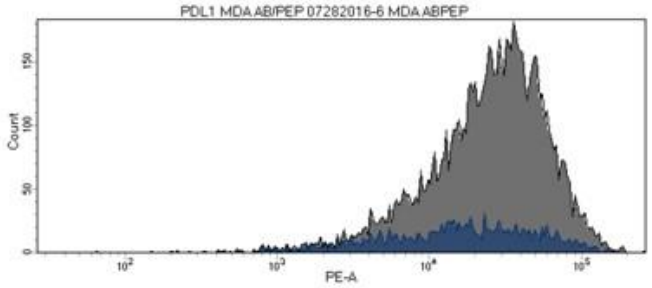

MCF7 (Neg): Treated w/ Cy5-peptide and PE-Antibody (Anti-PDL1) Simultaneously

Cy5-Peptide (y-axis)

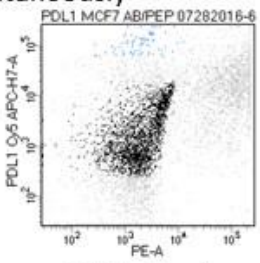

PE-Antibody (y-axis)

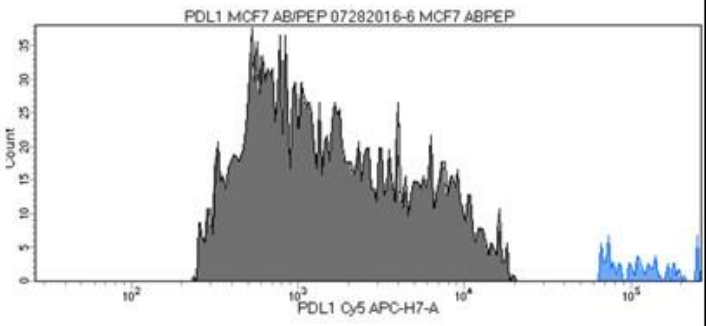

S8: MDA-MB-231: Treated w/ treated with Cy5 peptide 1 hour, treated with Anti-PDL1 antibody after

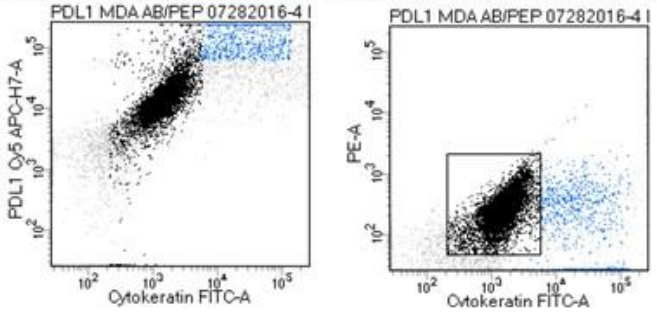

Cy5-Peptide (y-axis)

PE-Antibody (y-axis)

MCF7: Treated w/ treated with Cy5 peptide 1 hour, treated with Anti-PDL1 antibody after

Cy5-Peptide

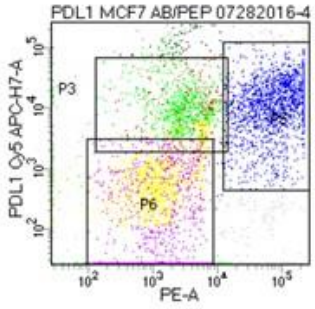

PE-Antibody

S9: Positive and Negative Controls

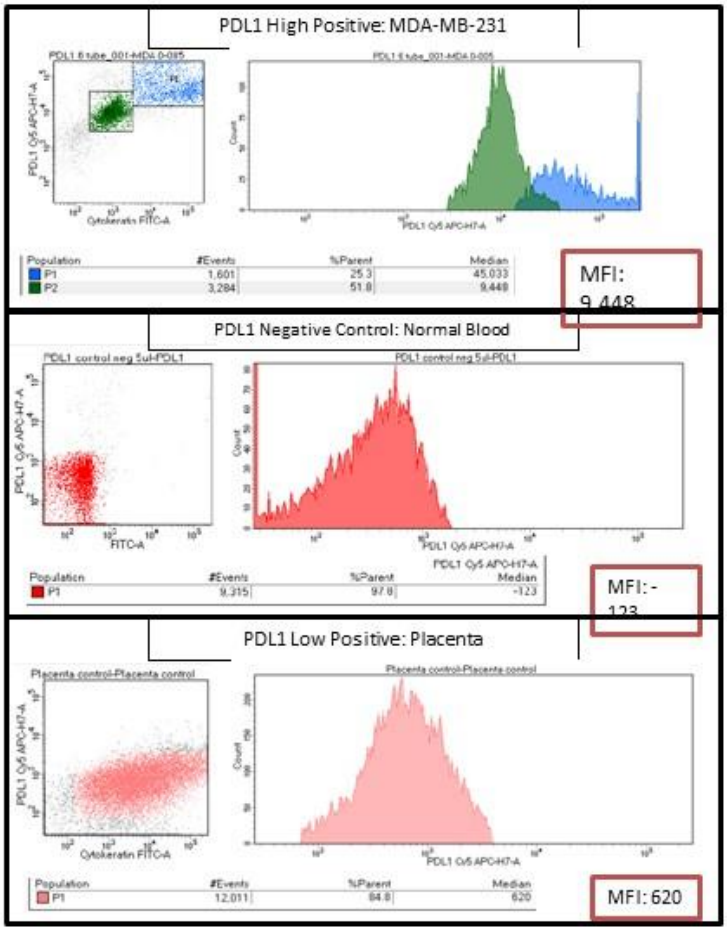

S10: Patient Tissue: Squamous Cell Carcinoma, 50 µL Peptide (0.05mg/mL)

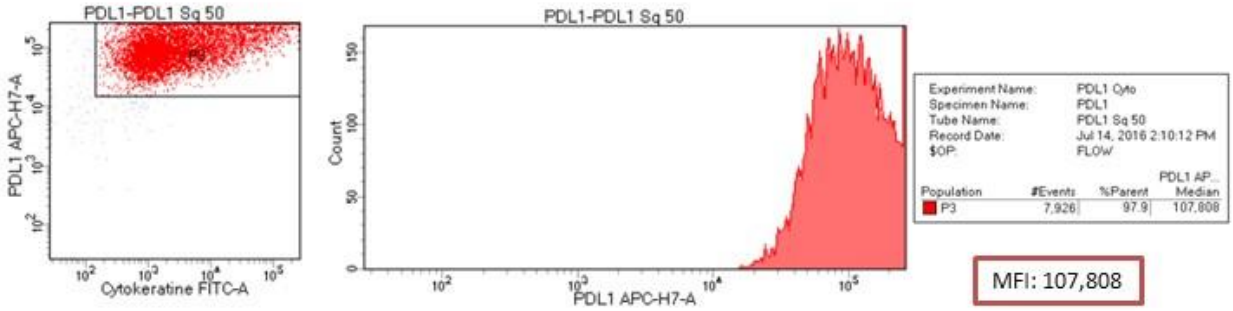

MFI: 107,808

Patient Tissue: Squamous Cell Carcinoma, 100 µL Peptide (0.05mg/mL)

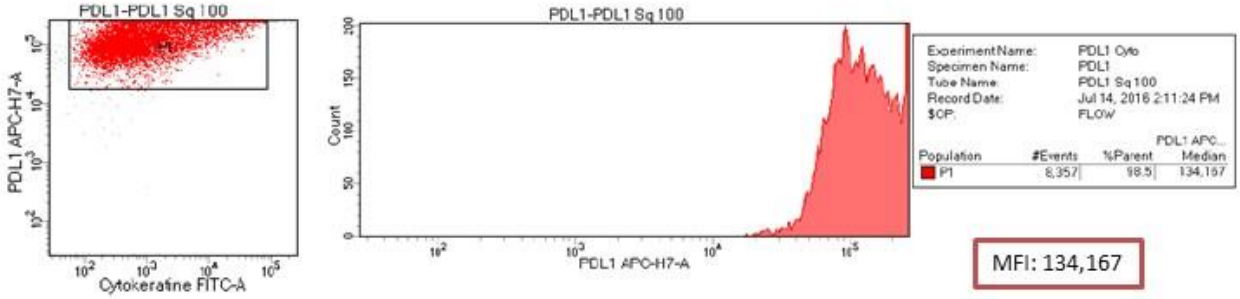

MFI: 134,167

S11: Cy5 PDL1 Flow Cytometry in Patient Melanoma

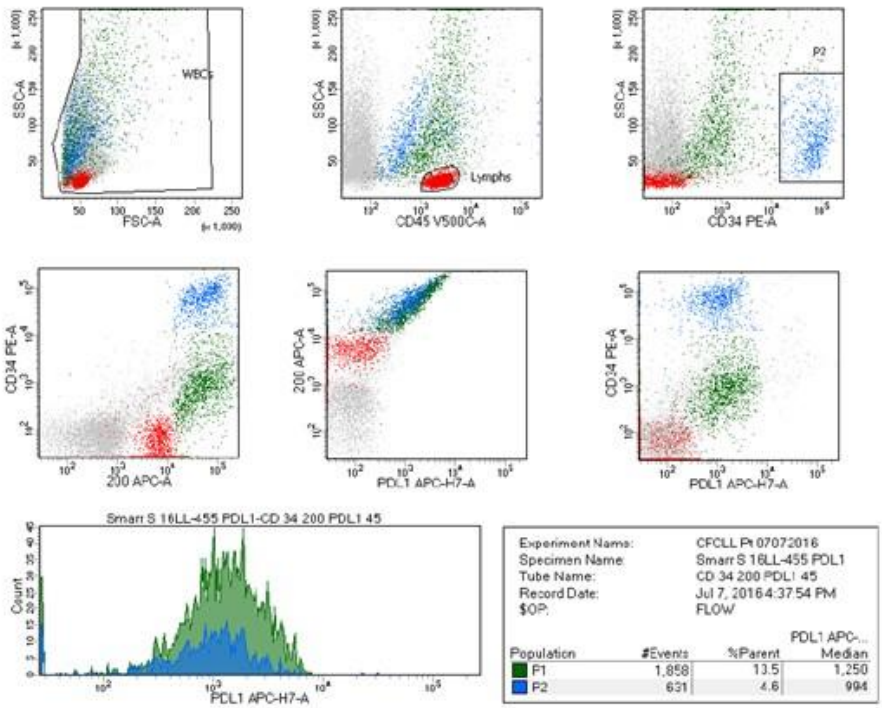

FLOW CYTOMETRIC IDENTIFICATION OF MELANOMA USING A STANDARD HEMATOPOETIC PANEL-A CLINICAL CASE AND REVIEW OF LITERATURE. (International Clinical Cytometry Society Meeting 2016 Abstract)

"...a distinct non-hematolymphoid population was identified with the unique phenotype of bright CD34, HLA-DR, moderated CD56 and negative CD45. **There was moderate PDL-1 using a proprietary peptide** and no expression of cytokeratin by flow cytometry. The tissue biopsy showed metastatic melanoma, which was positive for A103 and Sox 10 and negative for cytokeratin. The morphology, flow and phenotype were diagnostic of melanoma."

S12: Roche SP263 Antibody IHC – Placenta Tissue

10x Magnification

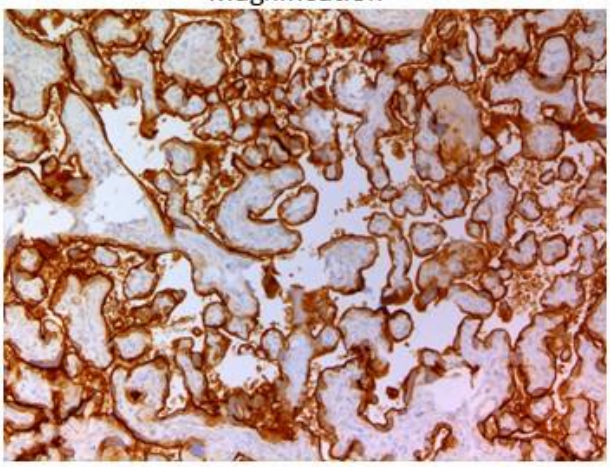

20x Magnification

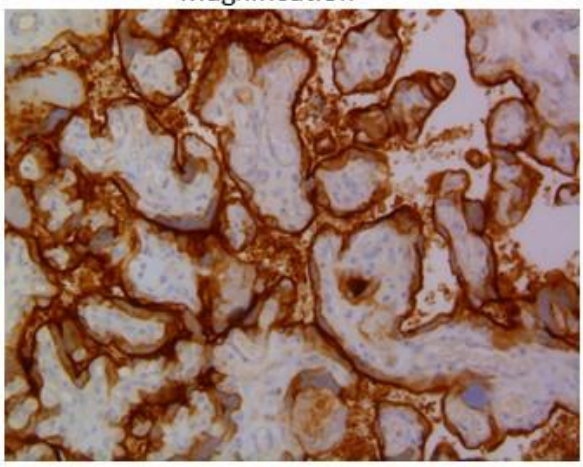

Placenta tissue obtained from Mizzou tissue bank is used as our positive control tissue since trophoblast cells will express PDL1

S13: Anti-PDL-1 Peptide RKC-10-Biotin

15µM Concentration

10x Magnification

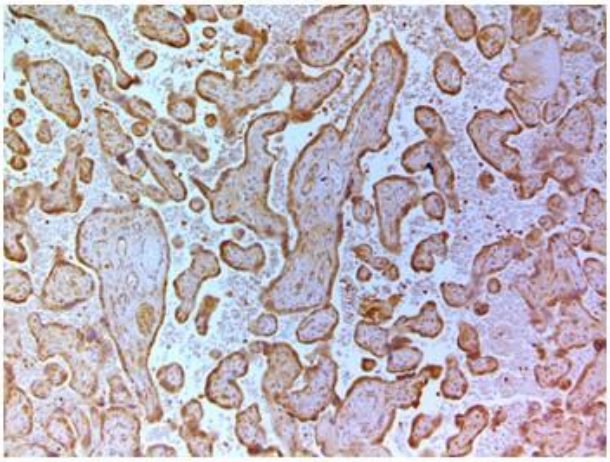

20x Magnification

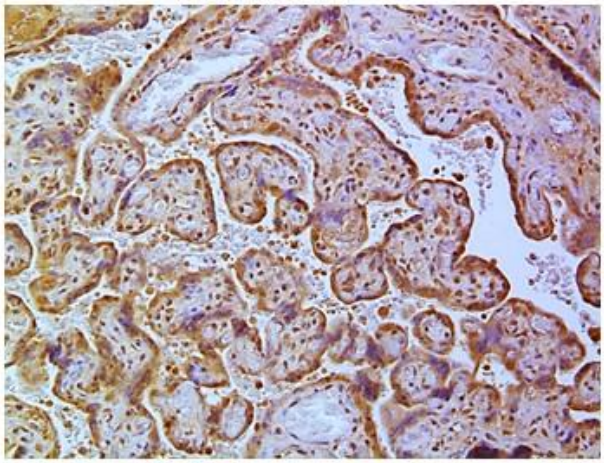

S14: High-Sensitivity Streptavidin-HRP

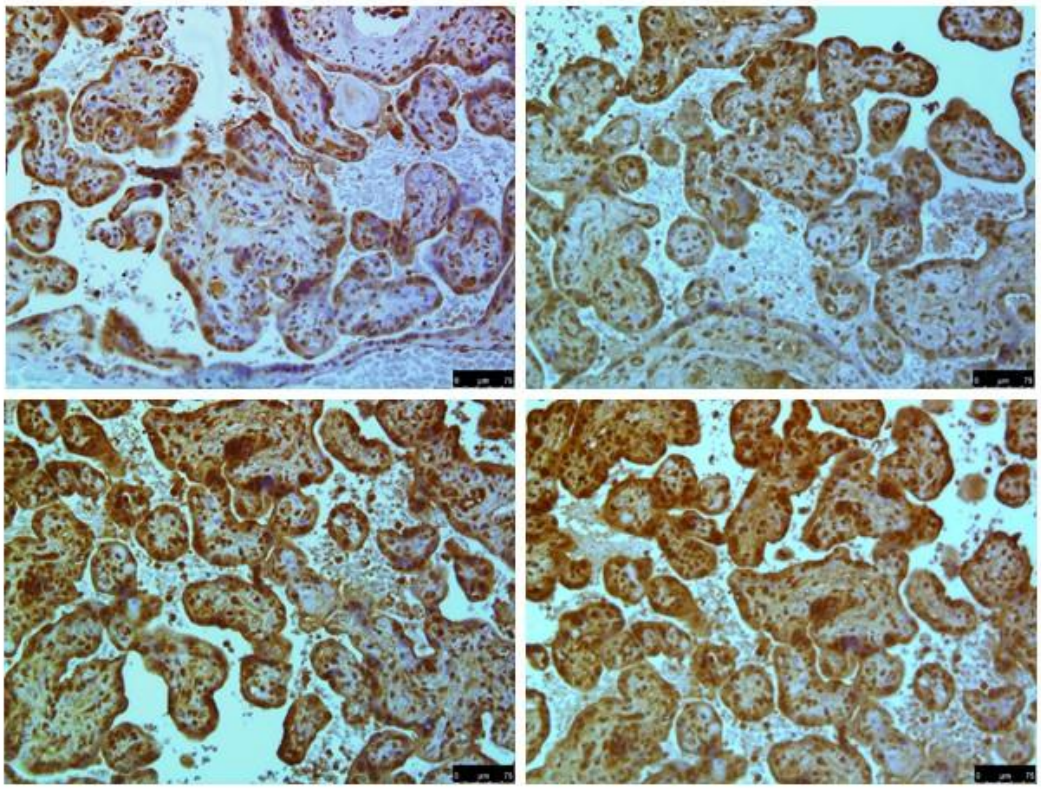

Peptide + Streptavidin-HRP Polymer, 15µM

S15: Mock peptide RKC-11-Biotin vs Anti-PDL-1 Peptide RKC-10-Biotin, Placental Tissue

Mock Peptide

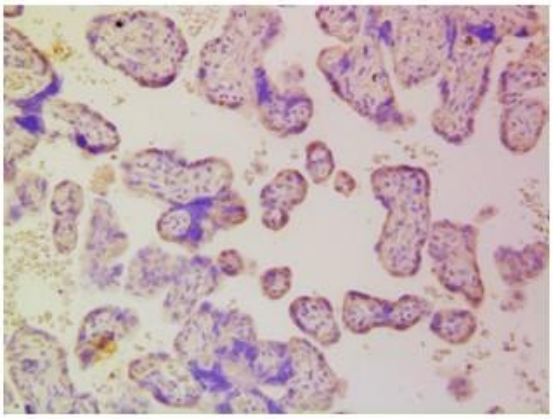

100µM Concentration

RKC-10-Biotin Peptide

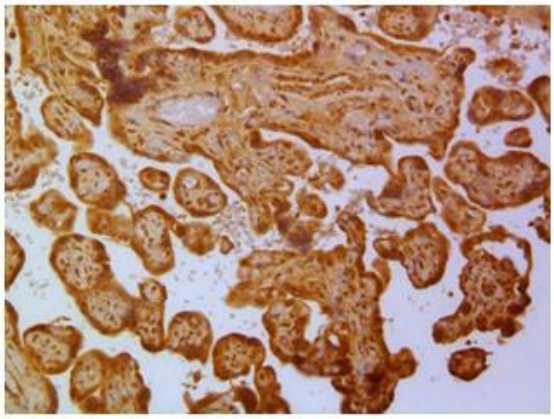

50µM Concentration

S16: Blocking of Roche Ab Using Anti-PDL1 Peptide

Pre-Blocked with Peptide, Treated with Roche kit on Roche Autostainer

Unblocked, treated with Roche kit on Roche Autostainer

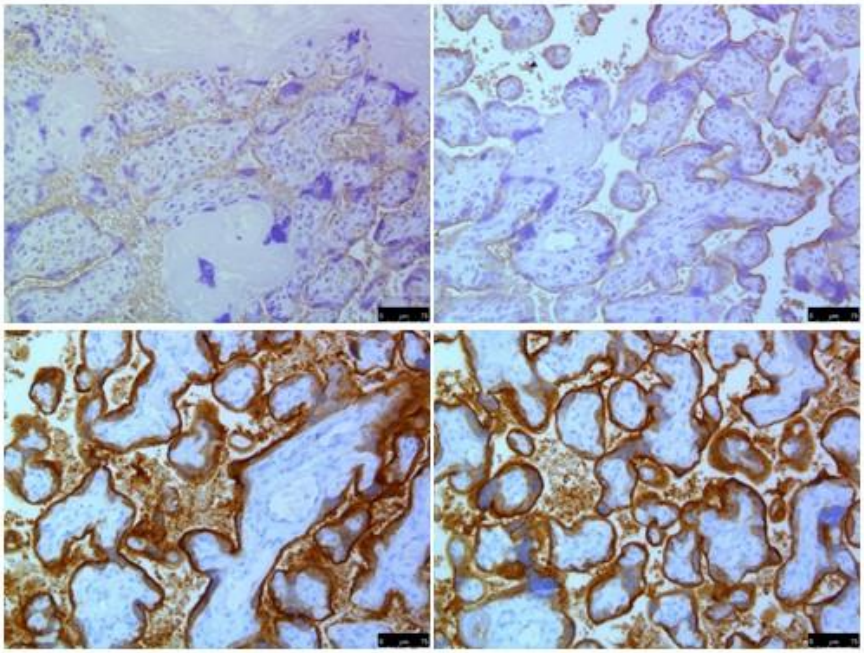

Placenta tissue was first blocked with 15µM peptide for 2h, washed, then put on the Roche autostainer with the Roche PDL-1 antibody IHC kit

S17: Blocking of PDL-1 Peptide Using Roche Ab

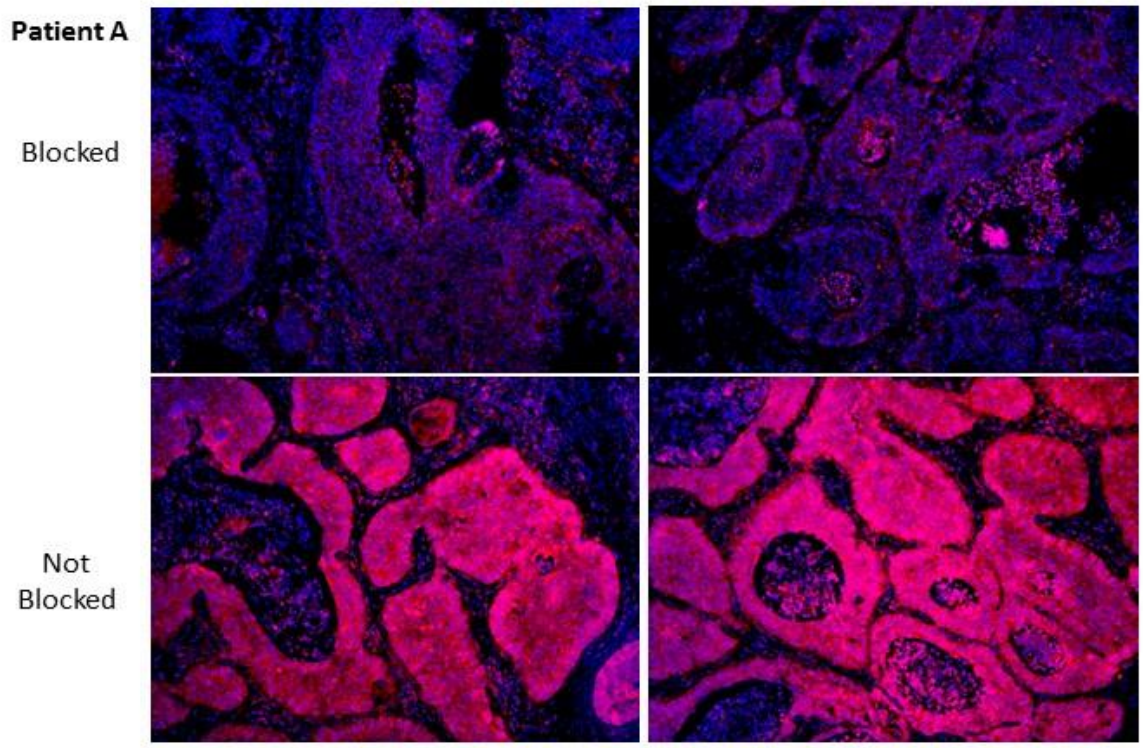

Images of Blocked and Not Blocked samples are taken under the same illumination conditions. No adjustments were made – leading to an overexposed Cy5 channel in the 'not blocked' sample

S18: Blocking of PDL-1 Peptide Using Roche Ab

Patient A

Blocked – Lower Sensitivity

Not Blocked – Lower Sensitivity

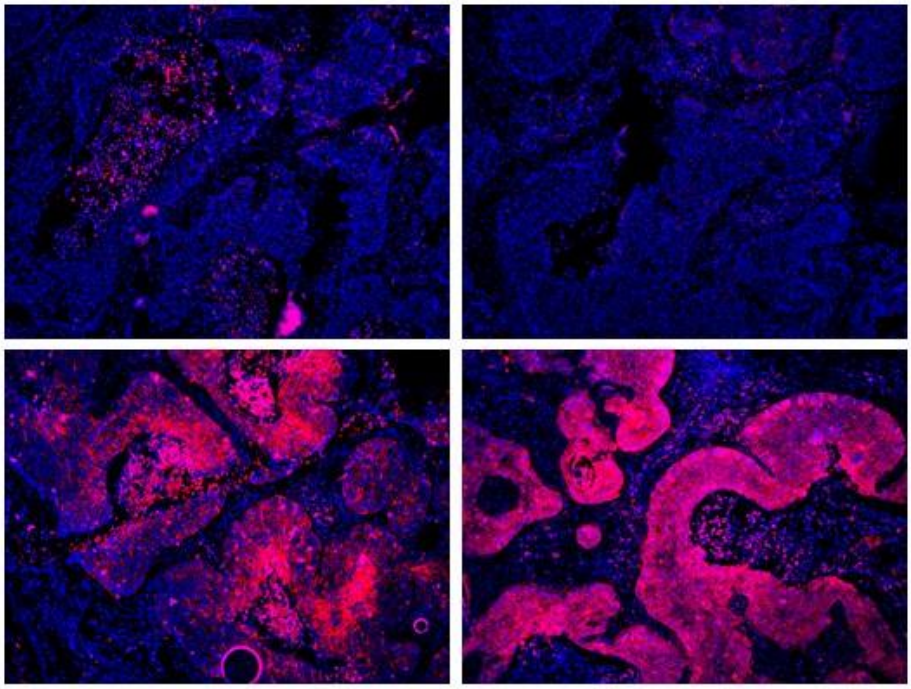

Cy5 Sensitivity was lowered until No Cy5 was seen in the Blocked Samples. The Unblocked samples still gave a strong Cy5 signal in the tumor. No illumination changes between the two samples were made.

S19: Fluorescent RKC-10-Cy5 Peptide (Cy5 Flurophore)

Roche Ab

Cy5 Peptide

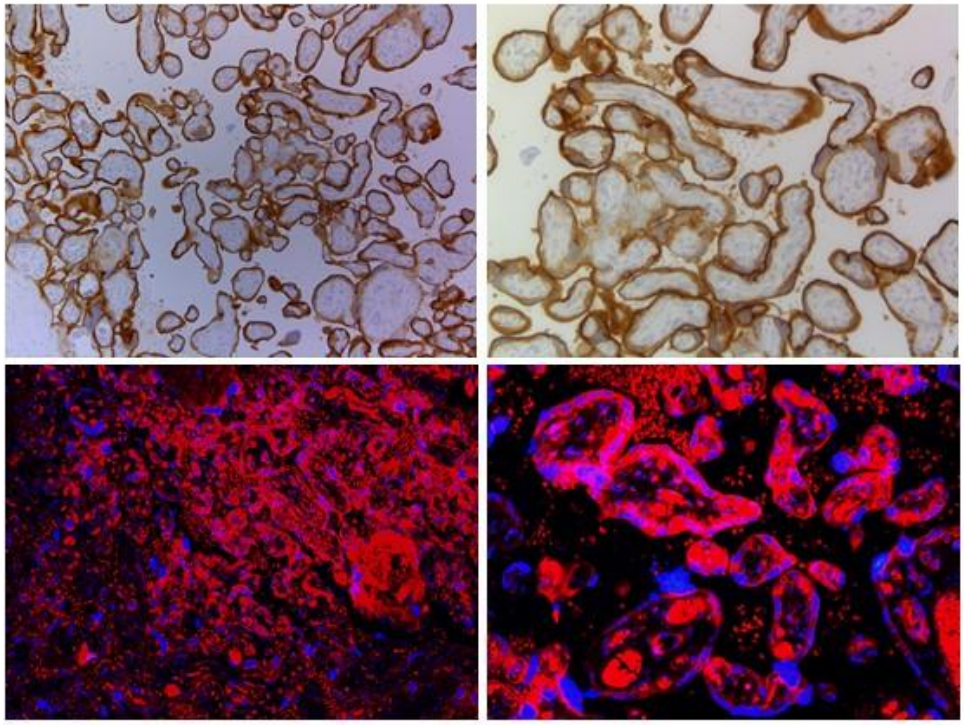

High sensitivity observed with the Fluorescent Peptide staining in Placental control tissue

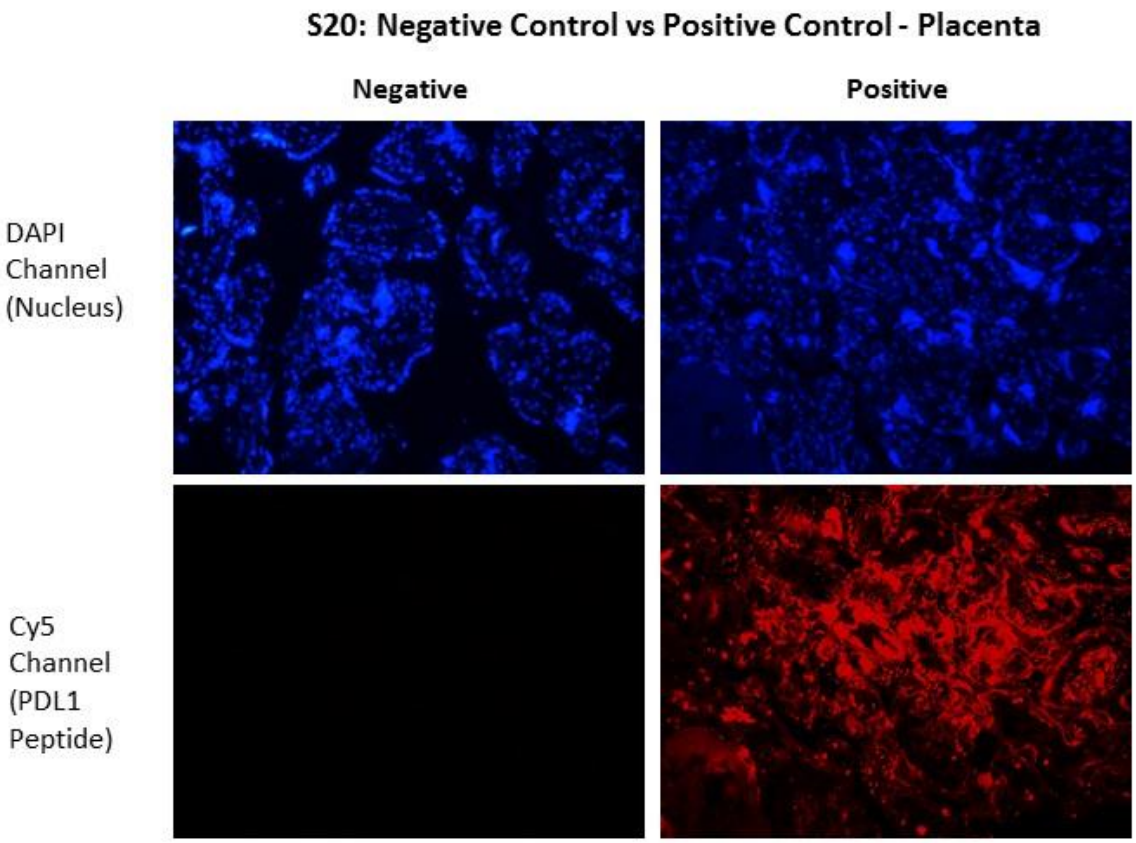
S20: Negative Control vs Positive Control - Placenta
Negative
Positive
DAPI Channel (Nucleus)
Cy5 Channel (PDL1 Peptide)

S21: PDL-1 Positive NSCLC Patient Tissue

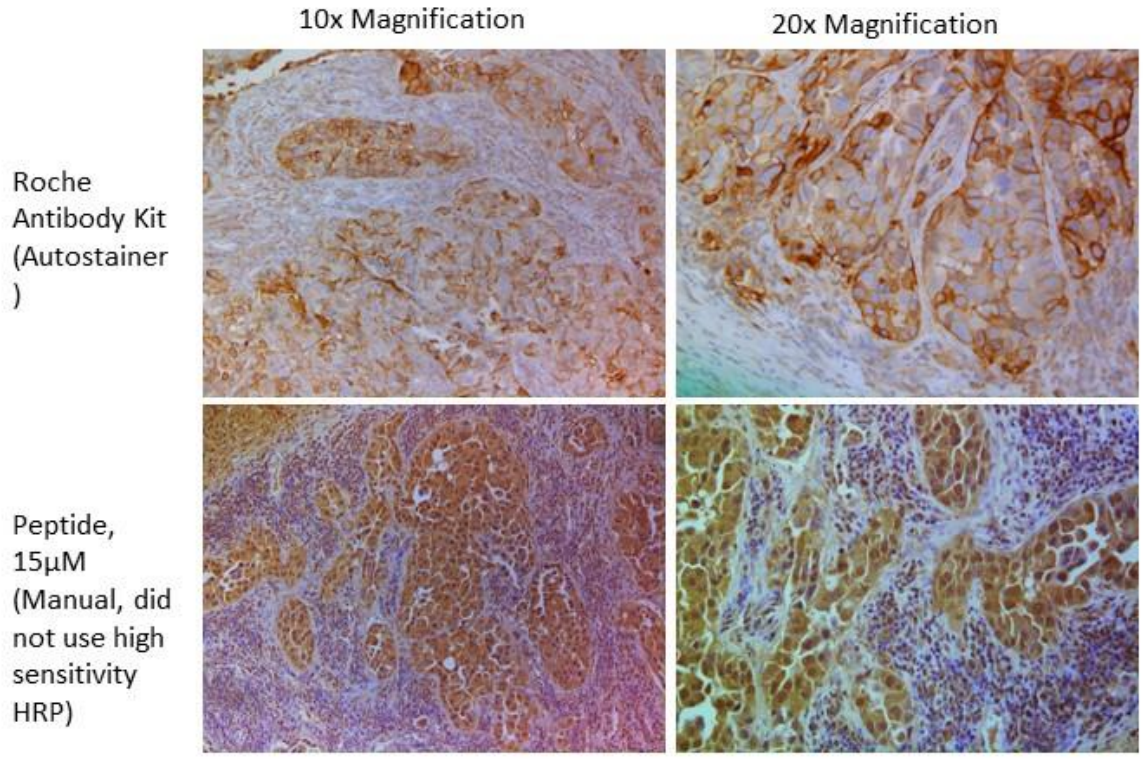

Patient Tissue from Mizzou clinical pathology lab was identified as tumor positive for PDL1 by both Roche antibody kit on autostainer and with peptide using manual IHC

S22: IHC Comparison: NSCLC 'Patient A'

Roche Kit, Autostained. Tumor (marked) Stains Very Faintly

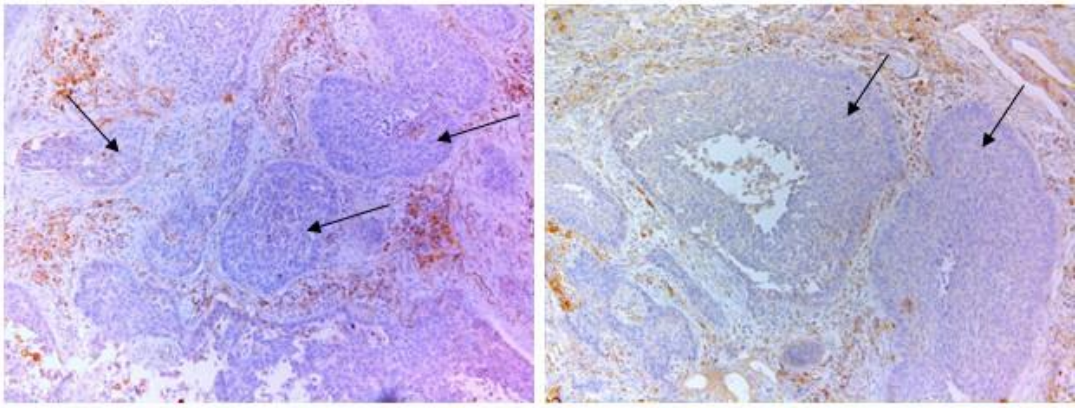

Peptide, Manual IHC. Heavy Tumor Staining.

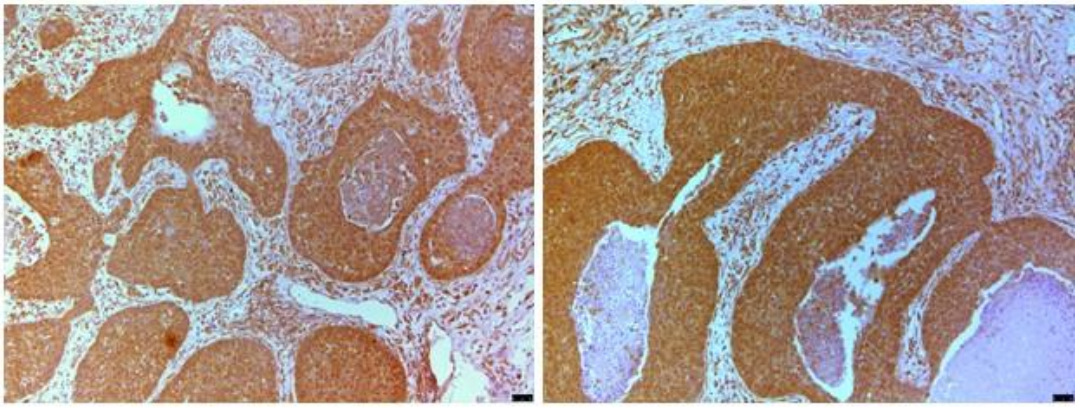

S23: Patient A IHC: Tissue Cut 3 Months Prior To Staining

Fresh Cut Tissue (24 hours) Stained with Anti-PDL1 Peptide

Tissue Cut 3 Months Prior to Staining (April-July)

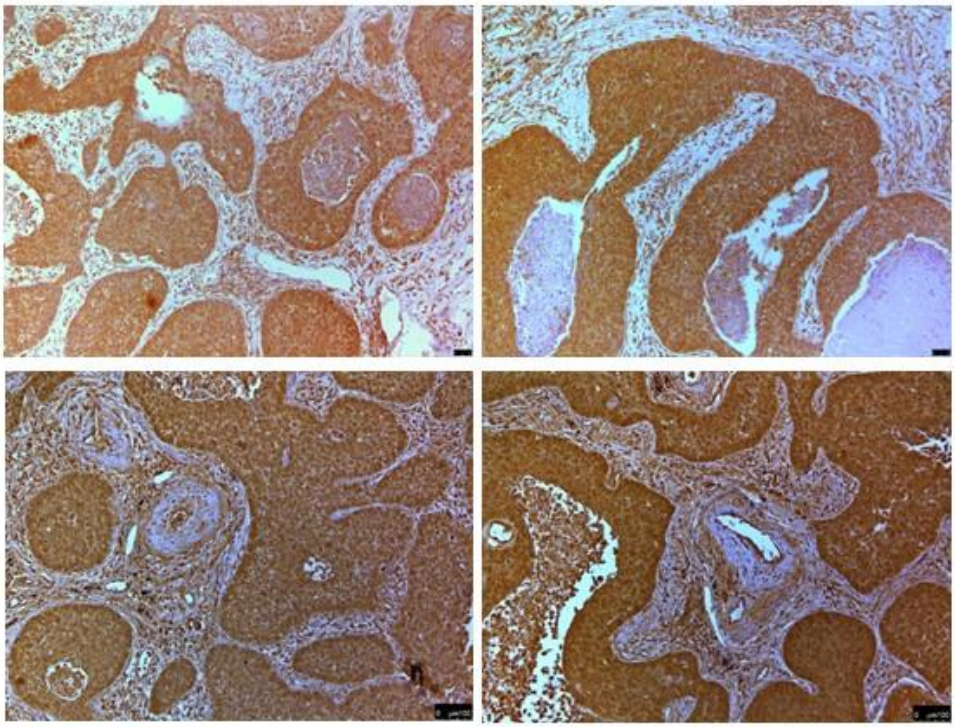

S24: IHC Comparison: NSCLC 'Patient B'

Roche Kit, Autostained. Faint/No Tumor staining

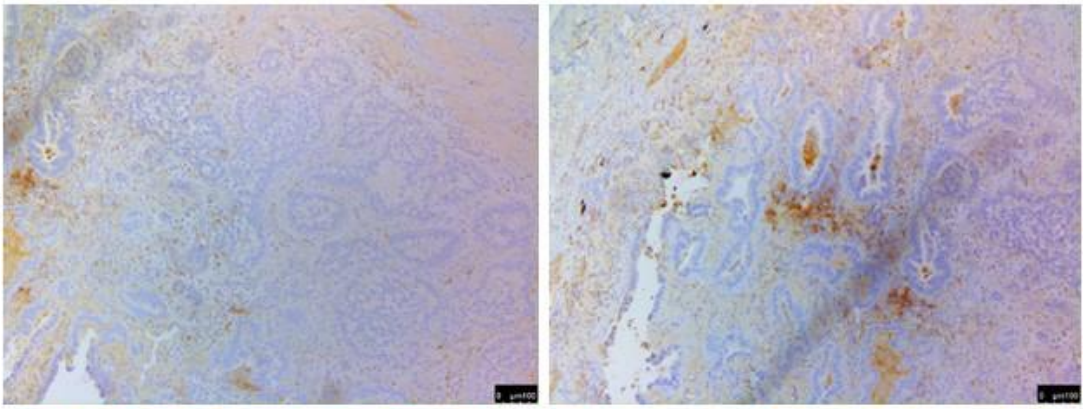

Peptide, Manual IHC. Good Tumor staining.

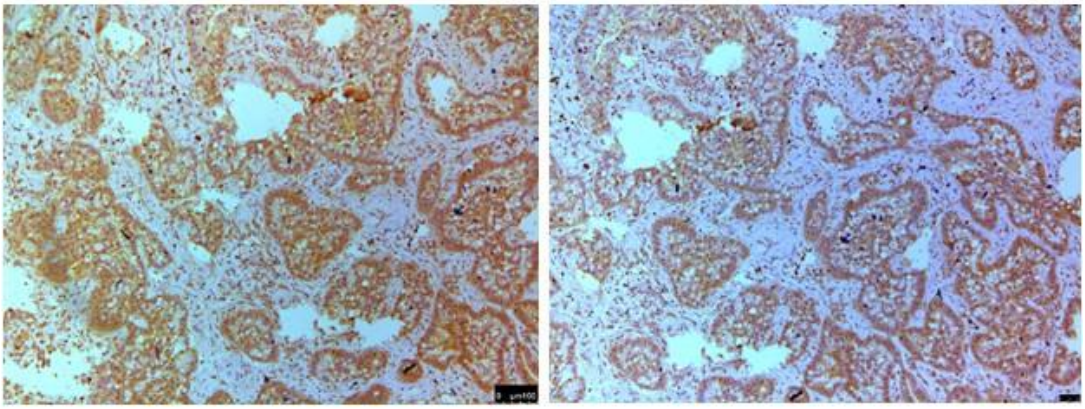

S25: IHC Comparison: NSCLC 'Patient C'

Roche Kit, Autostained. Some tumor areas stain

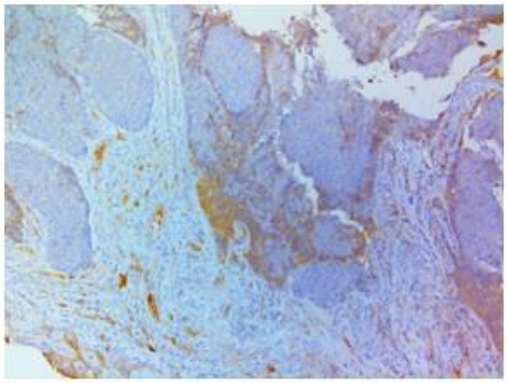

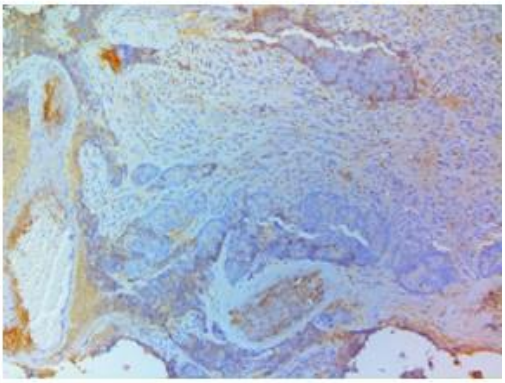

Peptide, Manual IHC. Consistent Tumor staining.

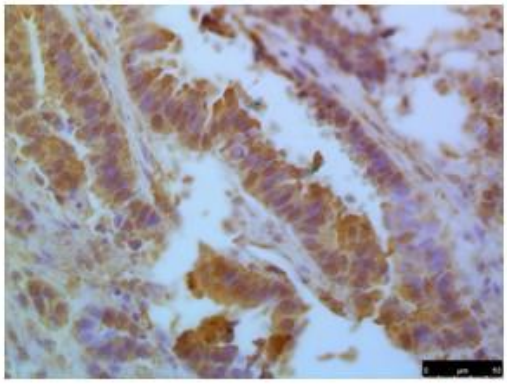

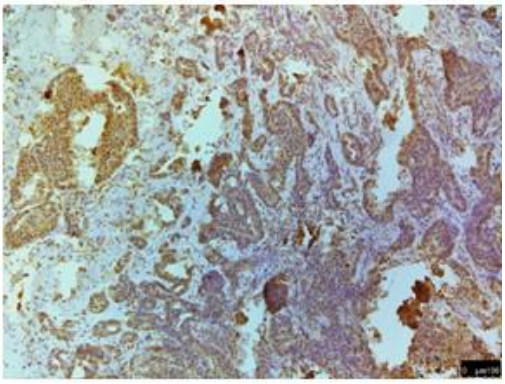

S26: IHC Comparison: NSCLC 'Patient D'

Roche Kit, Autostained. Faint/spotty tumor staining

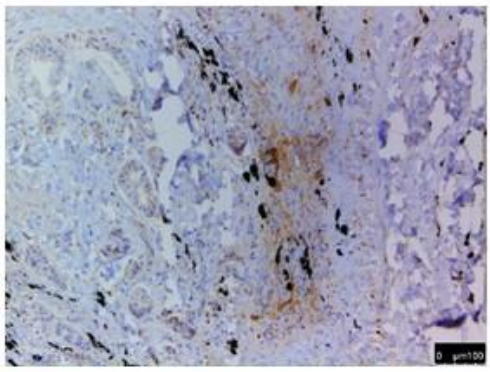

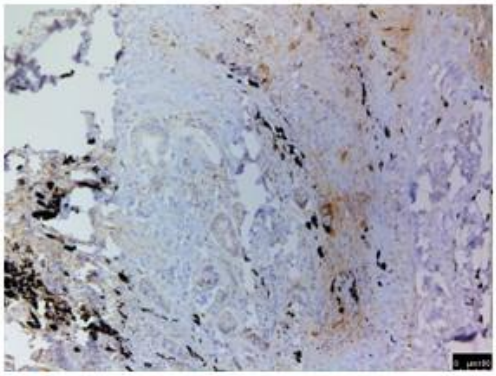

Peptide, Manual IHC. Good Tumor staining.

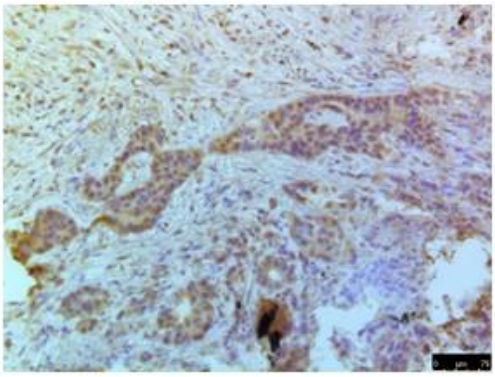

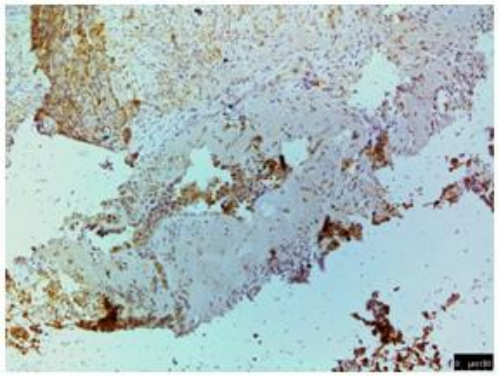

S27: IHC Comparison: NSCLC 'Patient E'

Roche Kit, Autostained. Faint/No Tumor staining

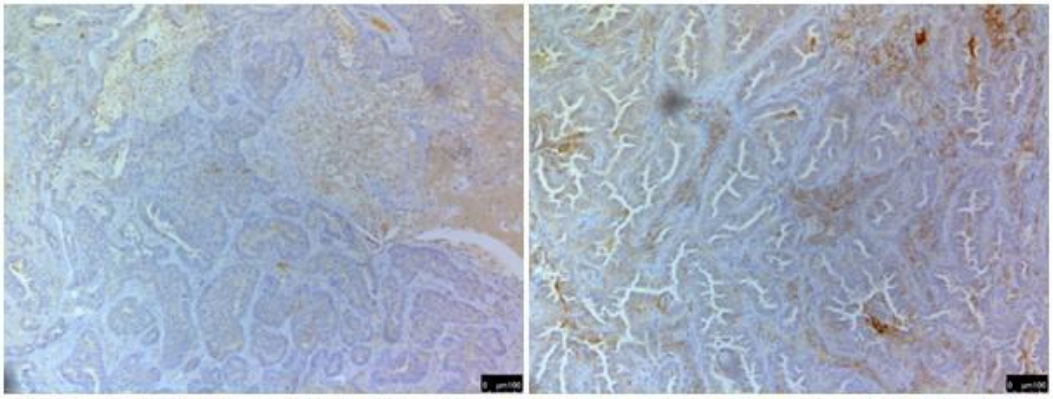

Peptide, Manual IHC. Good Tumor staining.

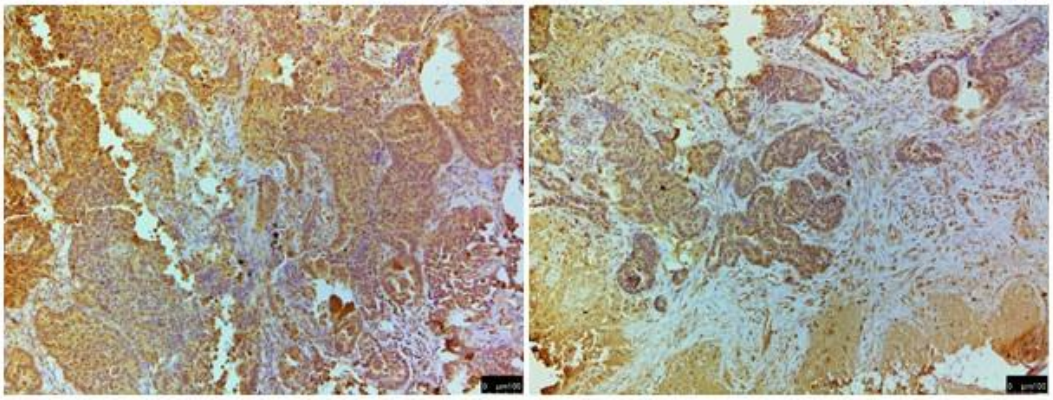

S28: IHC Comparison: NSCLC 'Patient F'

Roche Kit, Autostained. Very faint staining seen

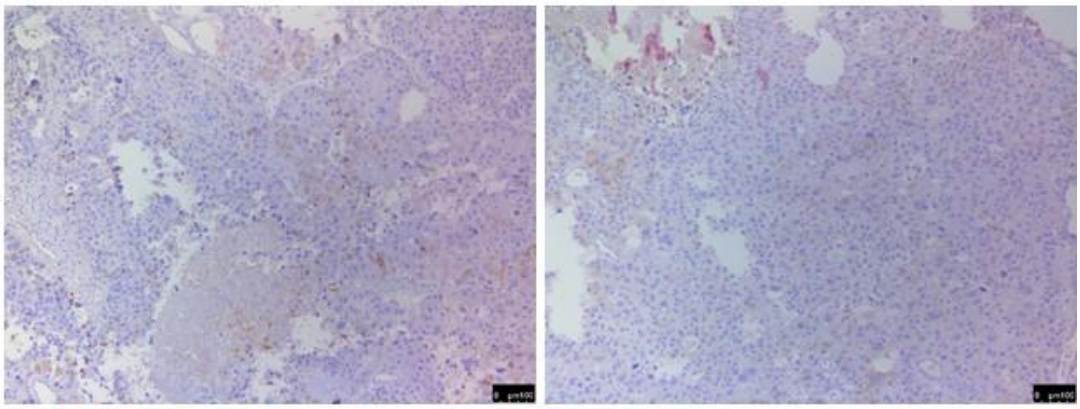

Peptide, Manual IHC. Tumor stains heavily.

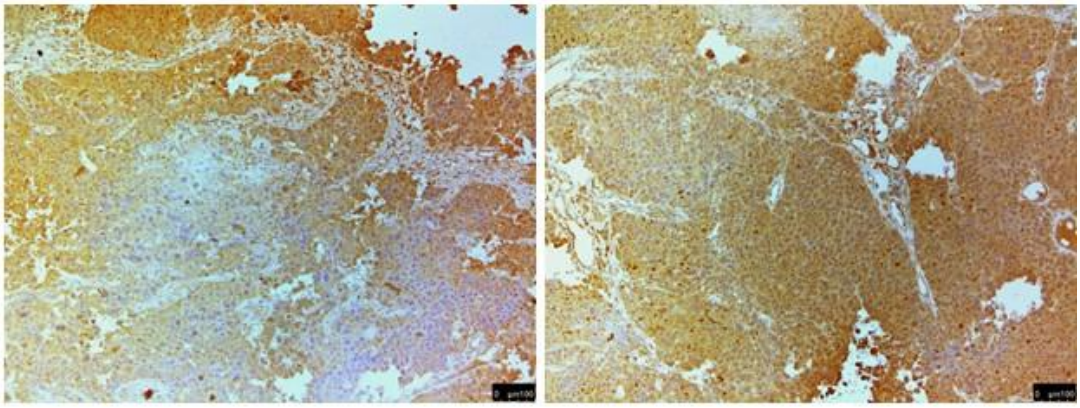

S29: IHC Comparison: NSCLC 'Patient G'

Roche Kit, Autostained. Tumor Stains reliably

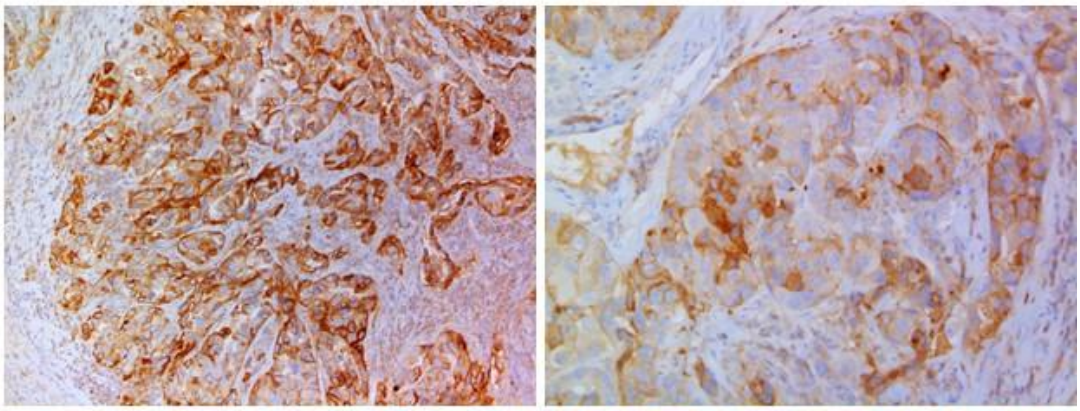

Peptide, Manual IHC. Tumor stains heavily.

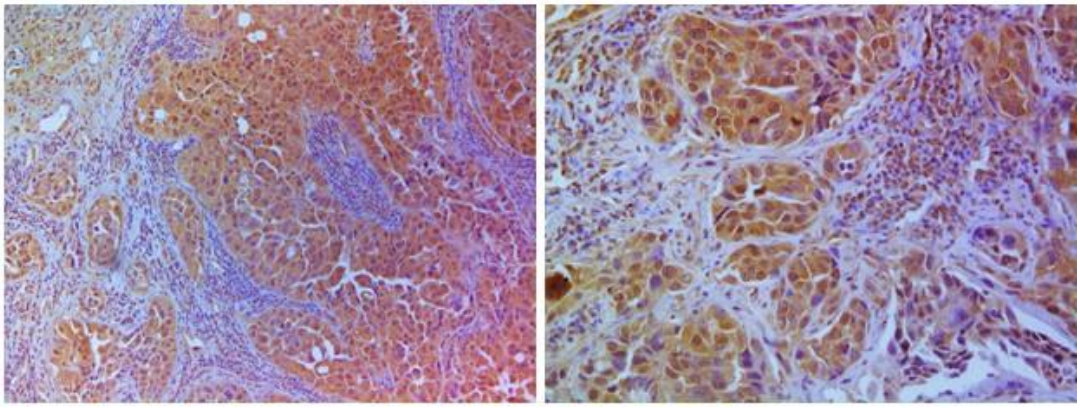

S30: Fluorescent IHC: NSCLC 'Patient A'

Roche Kit, Autostained. Faint/No Tumor staining

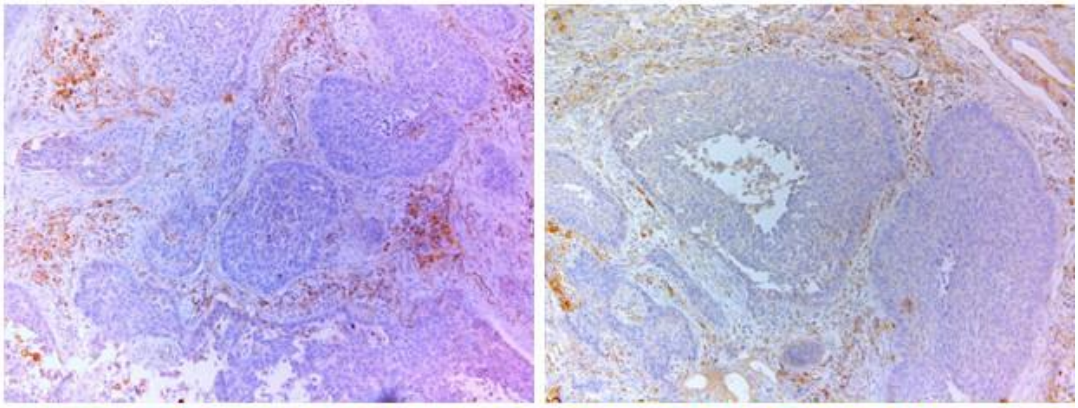

Peptide, Manual IHC. Very heavy tumor staining.

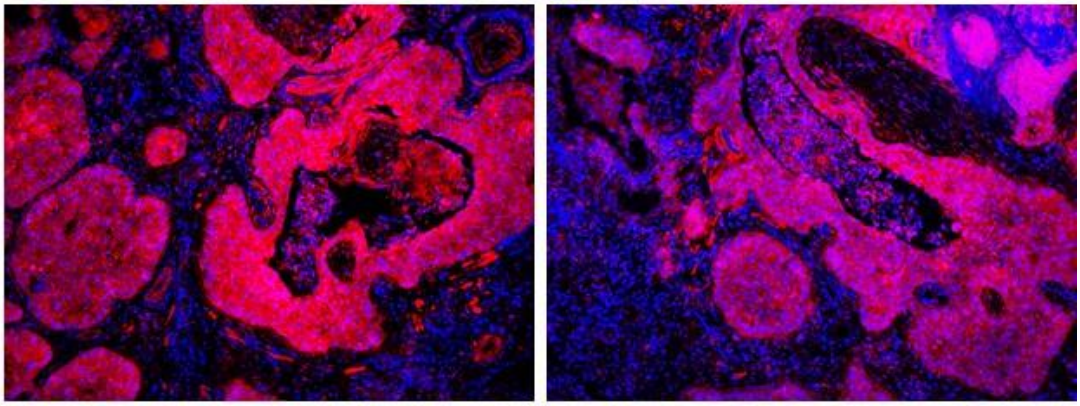

S31: Fluorescent IHC: NSCLC 'Patient A'

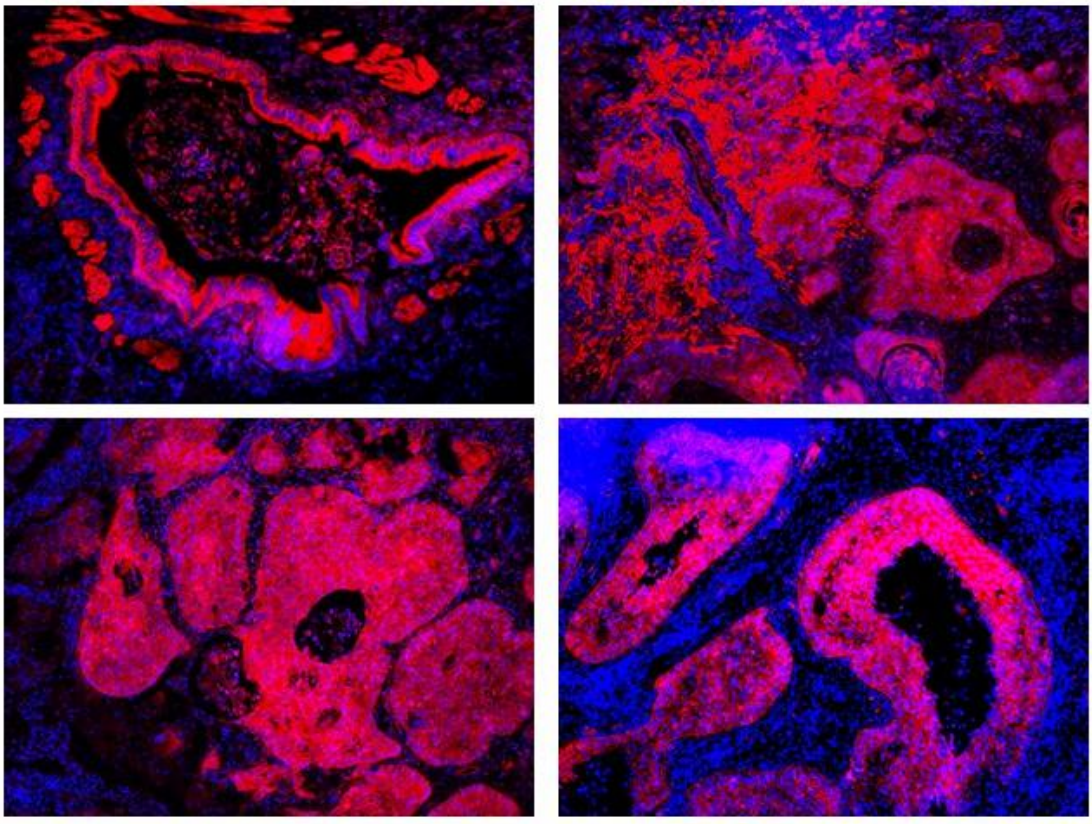

S32: Whole Slide Scan: NSCLC 'Patient A'

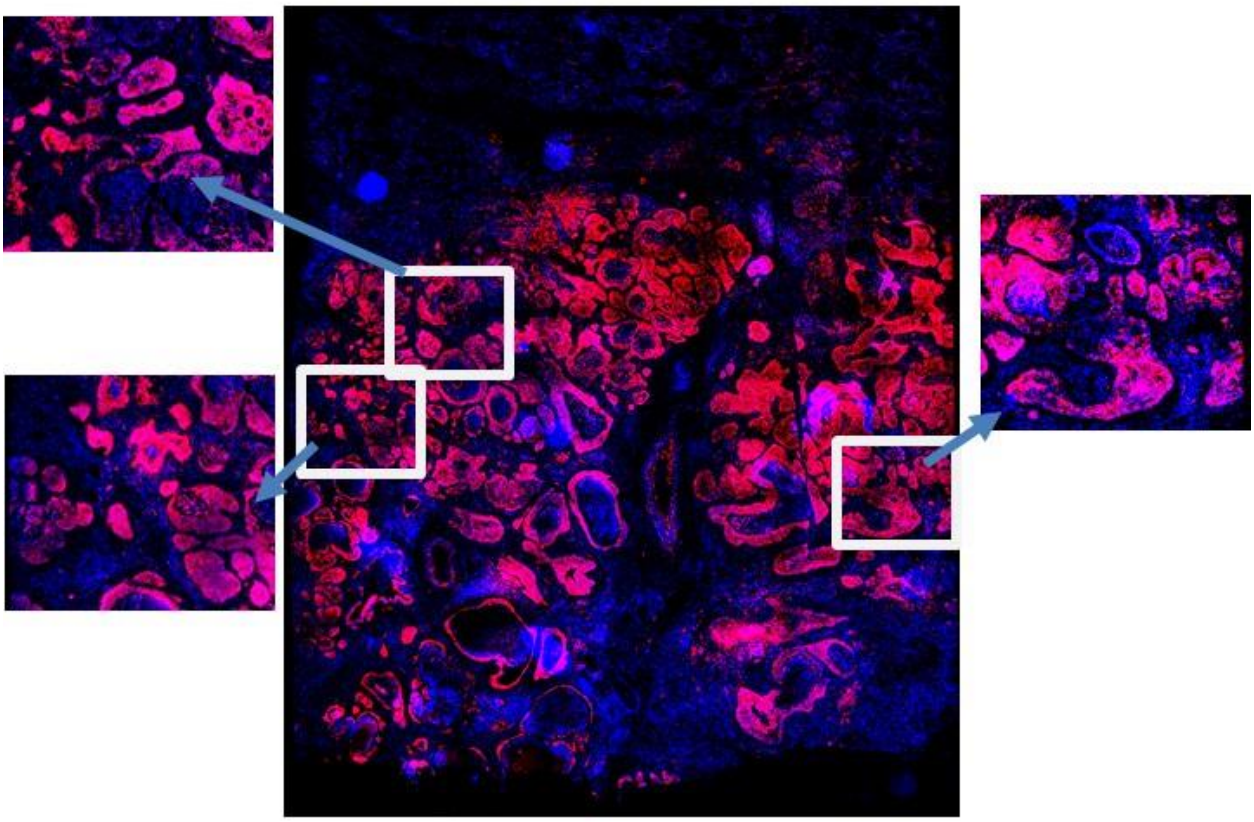

S33: Fluorescent IHC: NSCLC 'Patient B'

Roche Kit, Autostained. Faint/No Tumor staining

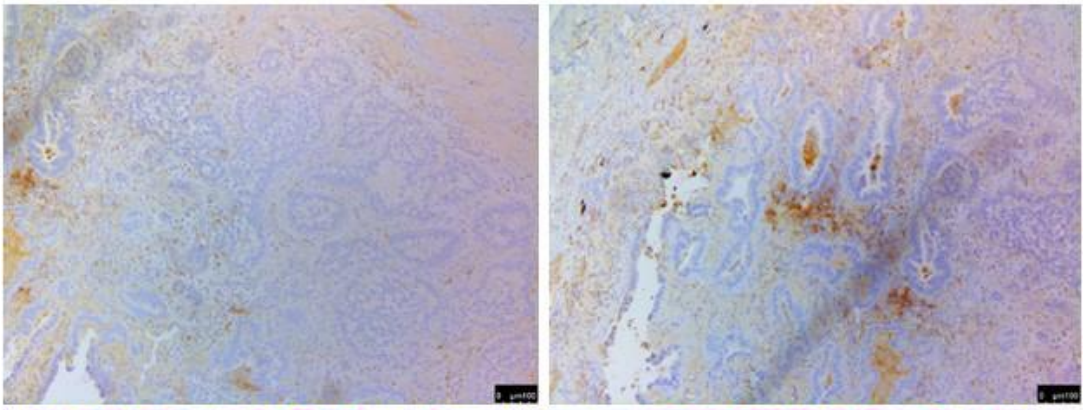

Peptide, Manual IHC

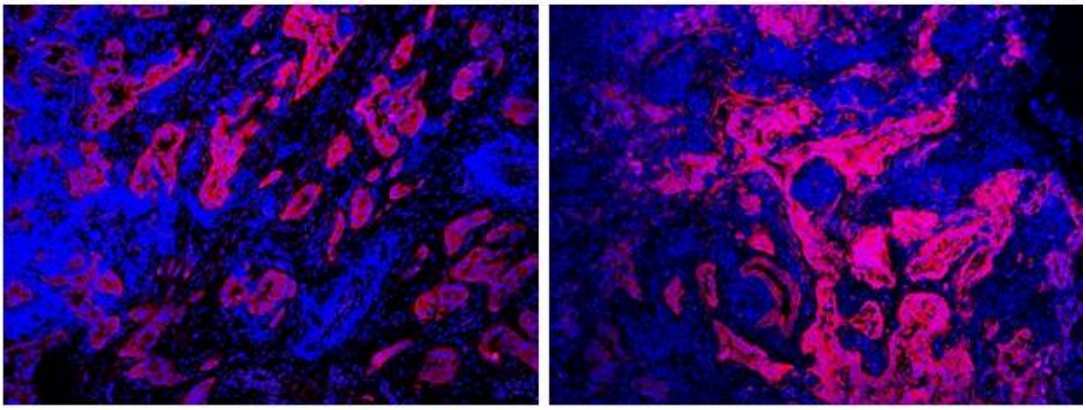

S34: Fluorescent IHC: NSCLC 'Patient B'

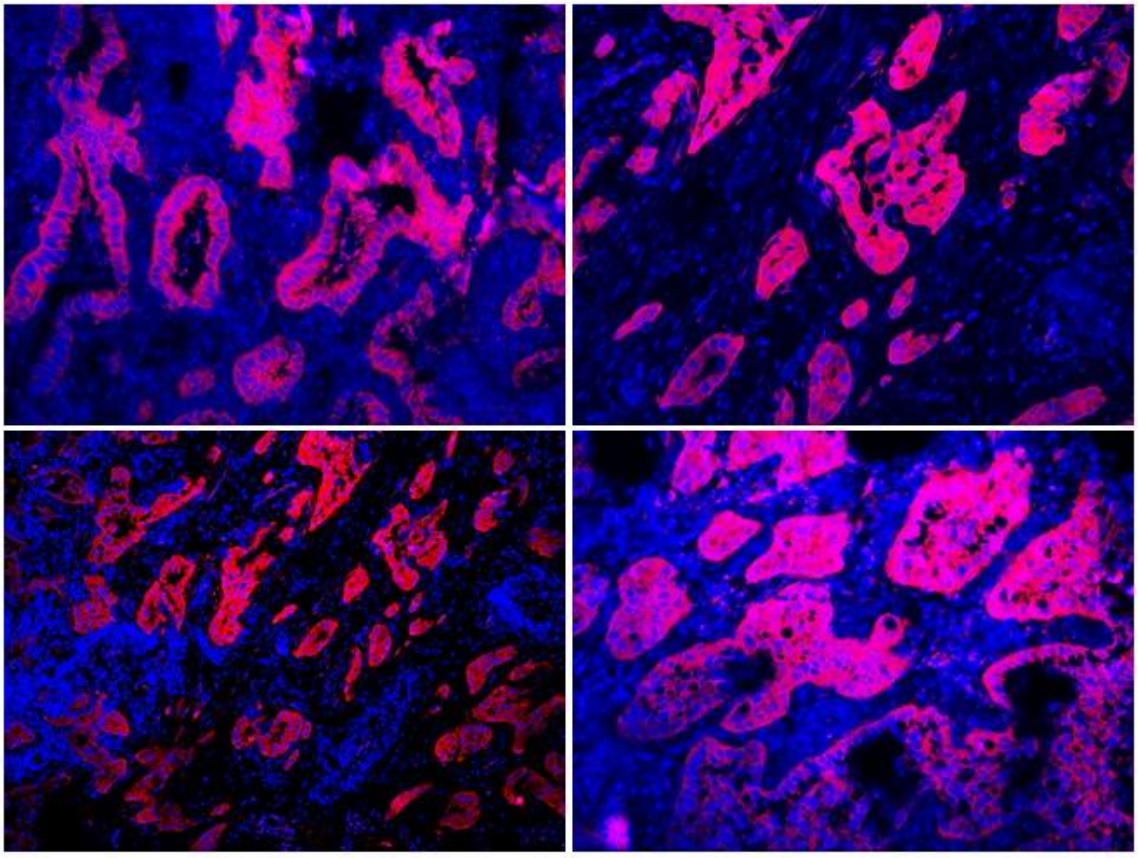

S35: Whole Slide Scan: NSCLC 'Patient B'

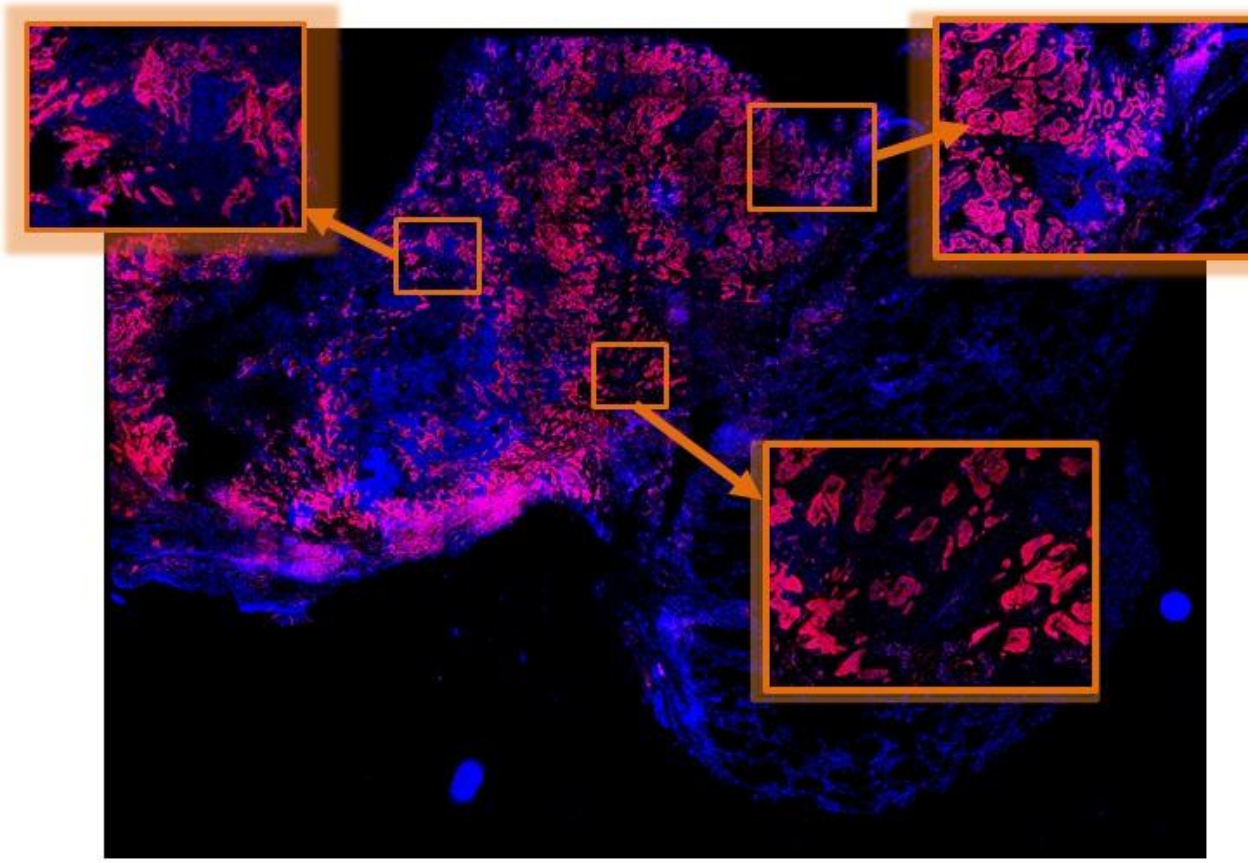

S36: Fluorescent IHC: NSCLC 'Patient C'

Roche Kit, Autostained. Faint/No Tumor staining

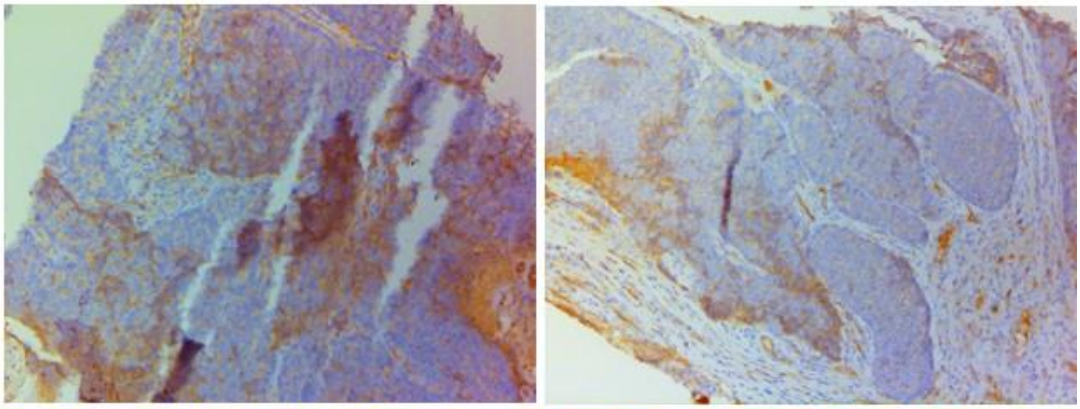

Peptide, Manual IHC

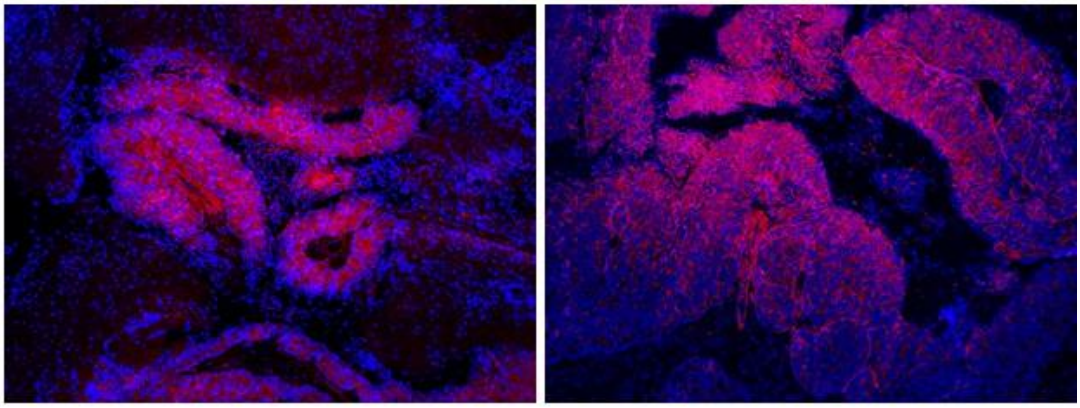

S37: Fluorescent IHC: NSCLC 'Patient C'

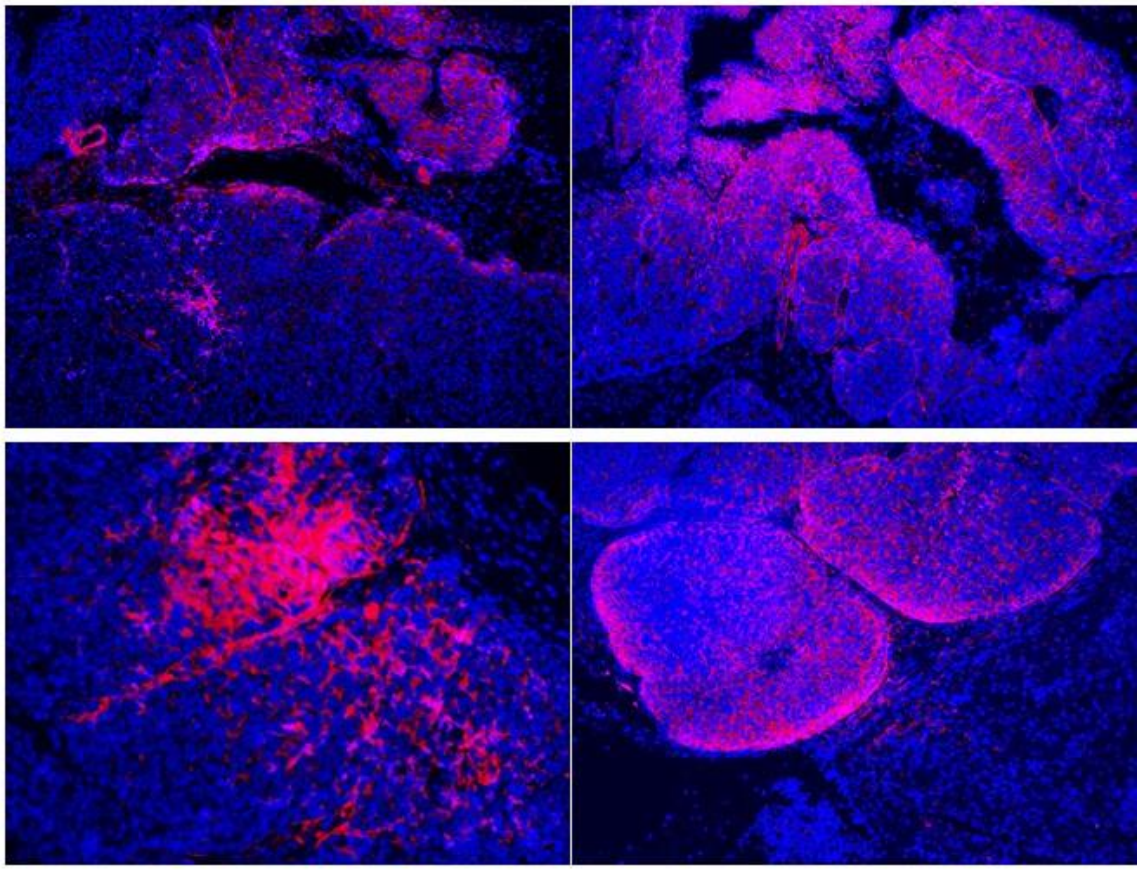

S38: Fluorescent IHC: NSCLC 'Patient D'

Roche Kit, Autostained.

Peptide, Manual IHC

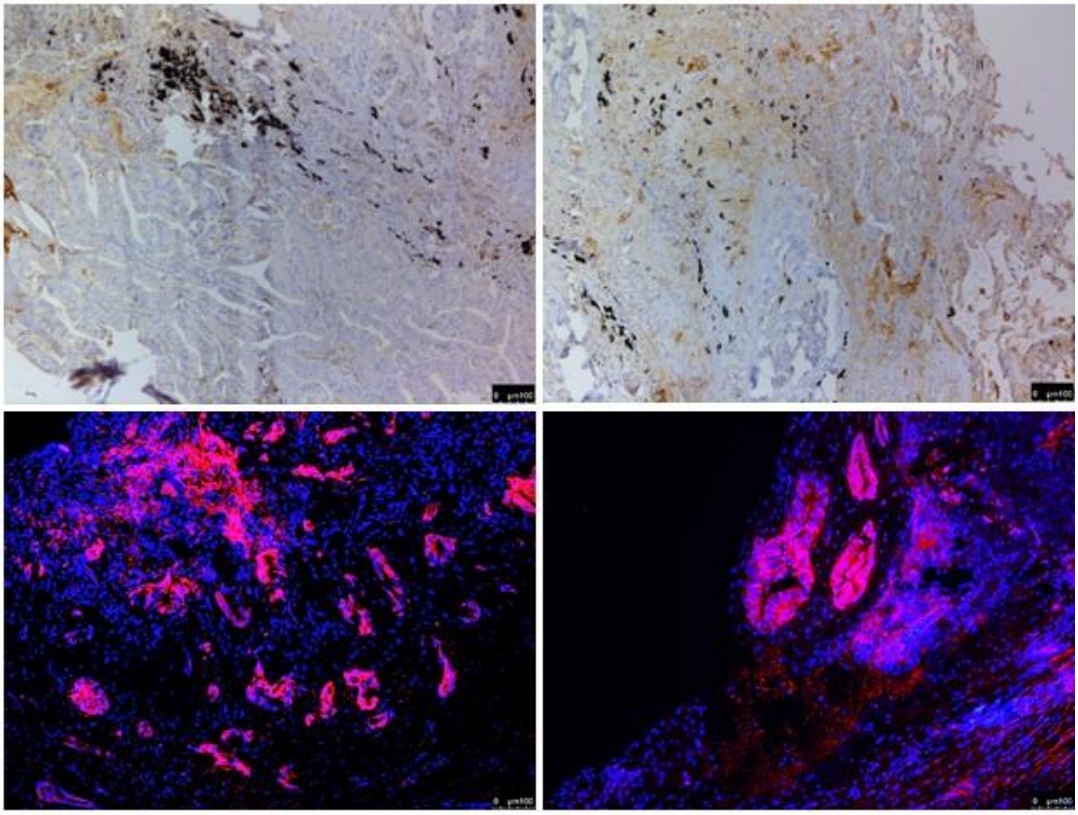

S39: Fluorescent IHC: NSCLC 'Patient D'

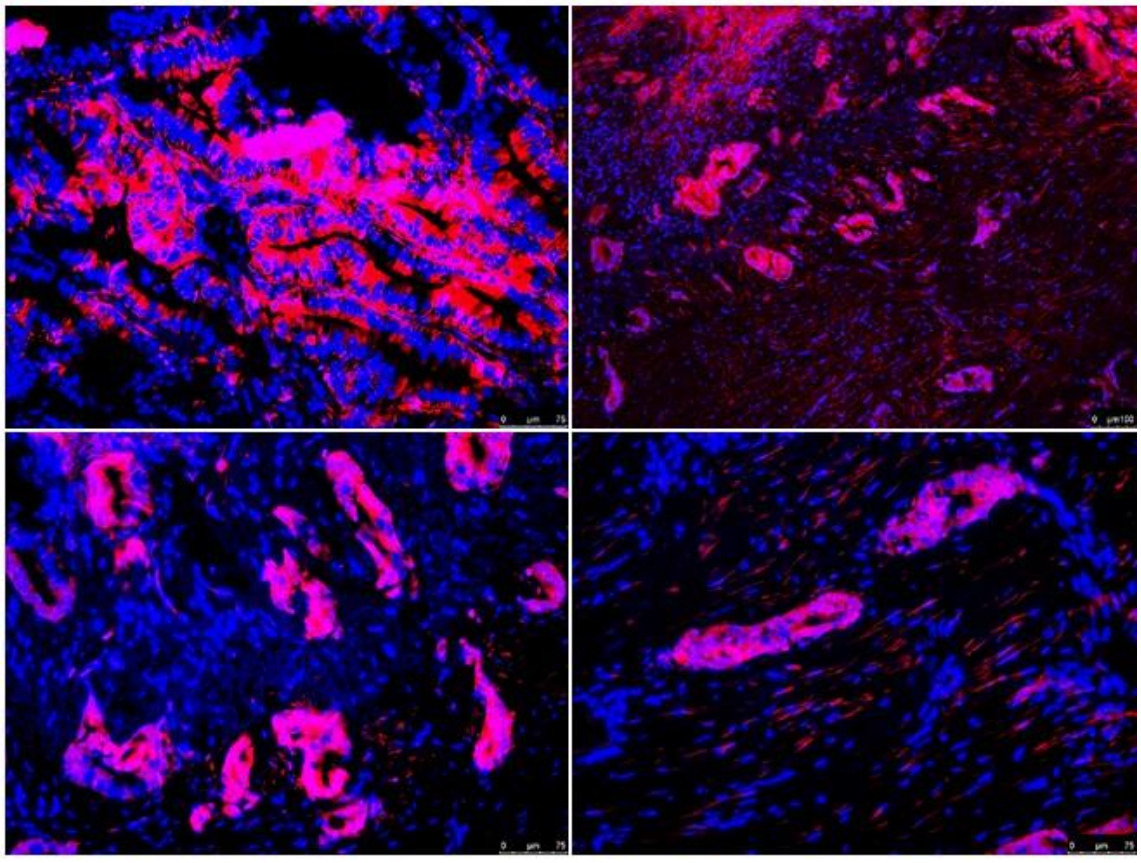

S40: Fluorescent IHC: NSCLC 'Patient E'

Roche Kit, Autostained. Faint/No Tumor staining

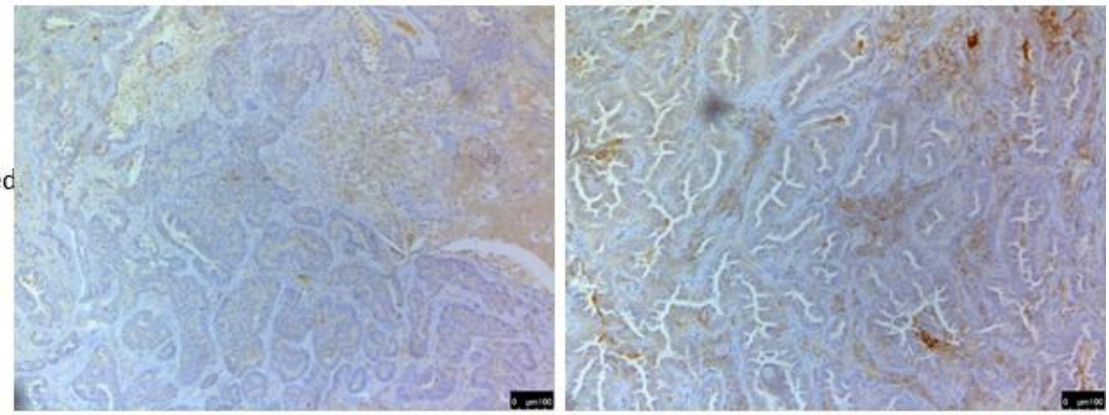

Peptide, Manual IHC

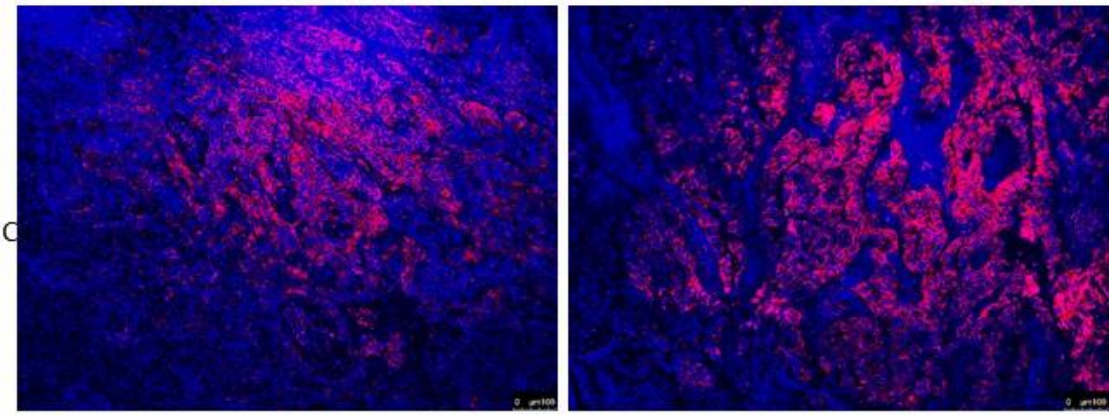

S41: Fluorescent IHC: NSCLC 'Patient E'

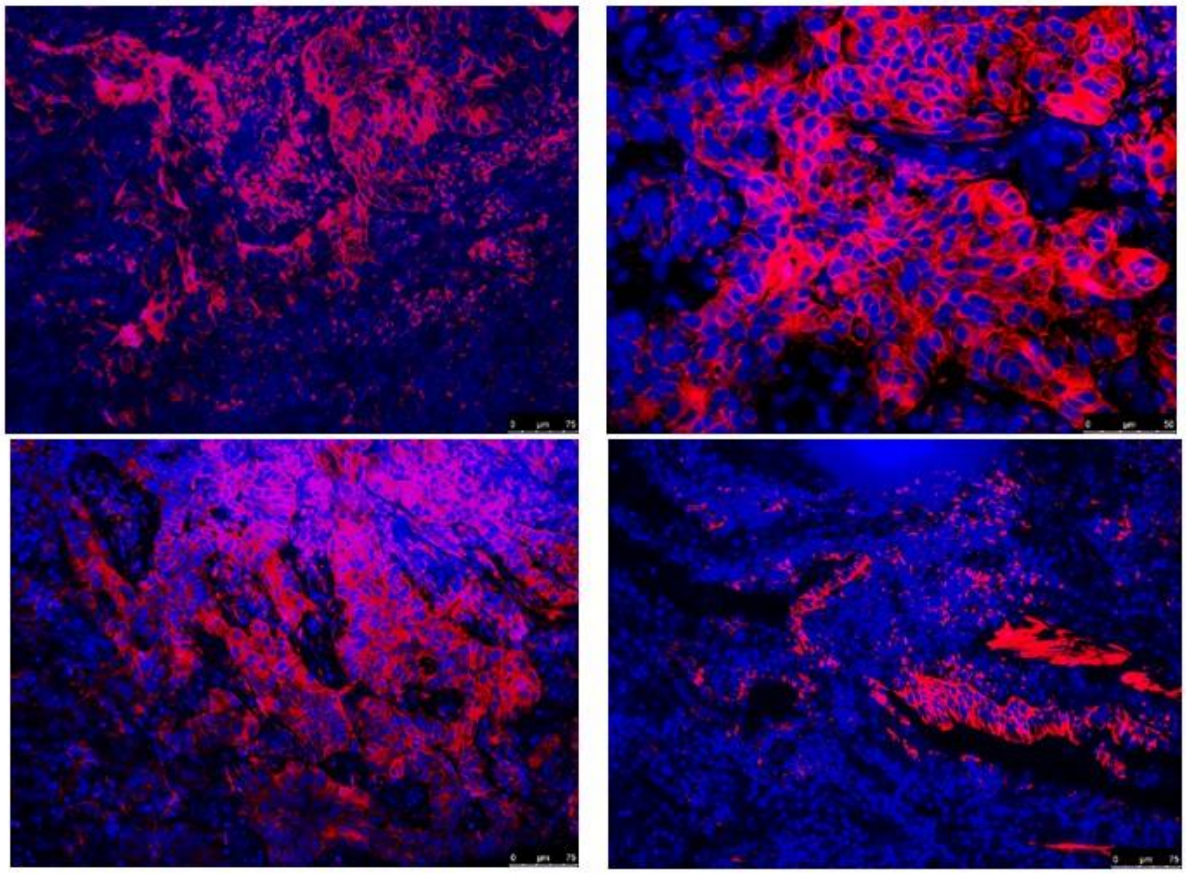

S42: Fluorescent IHC: NSCLC 'Patient F'

Roche Kit, Autostained .

Peptide, Manual IHC

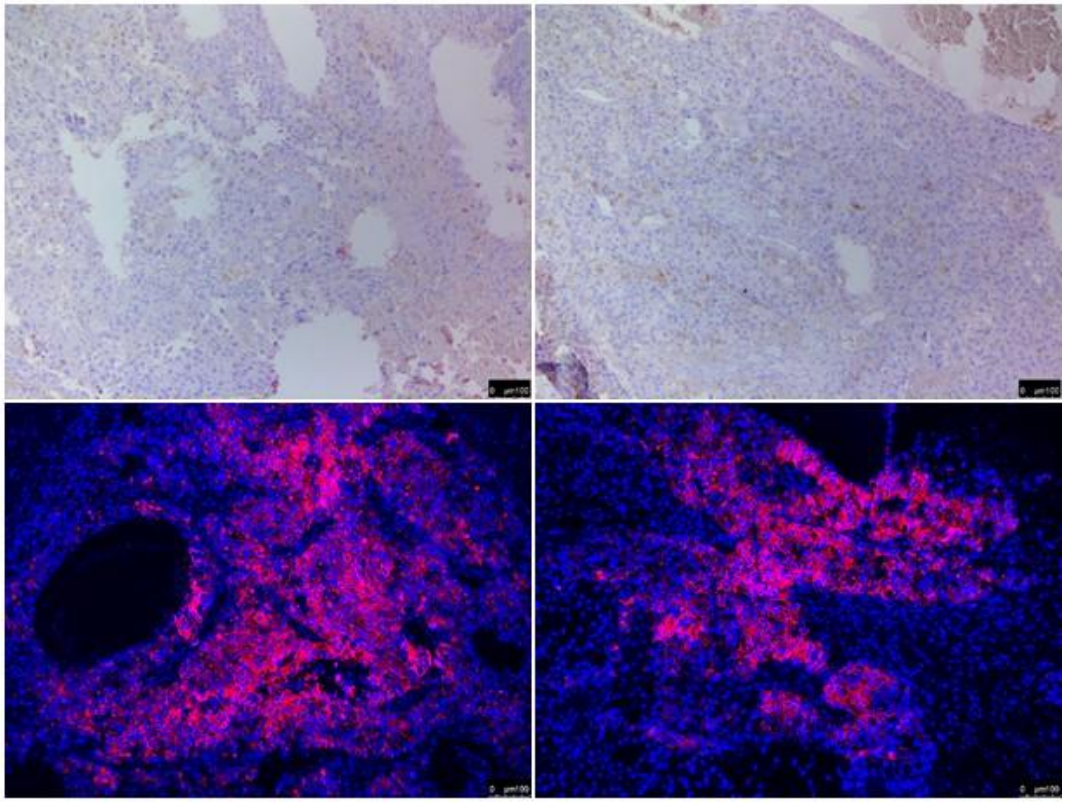

S43: Fluorescent IHC: NSCLC 'Patient F'

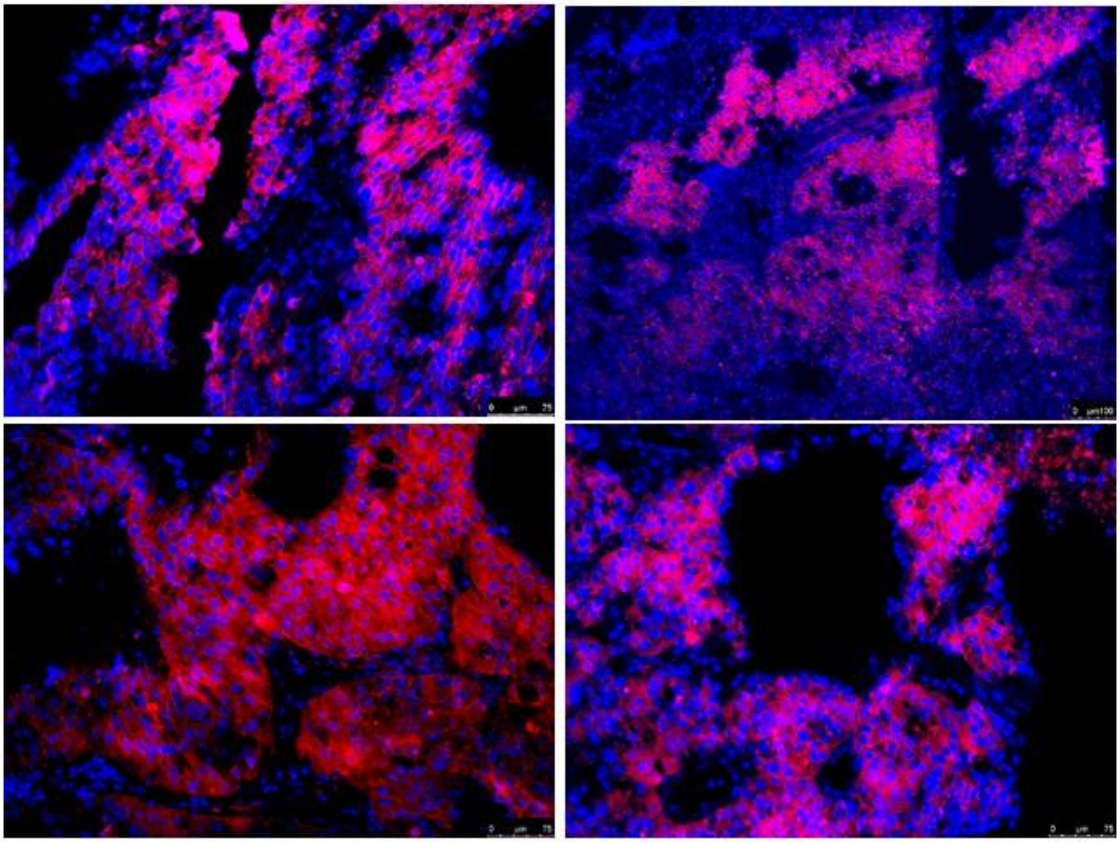

S44: Fluorescent IHC: NSCLC 'Patient G'

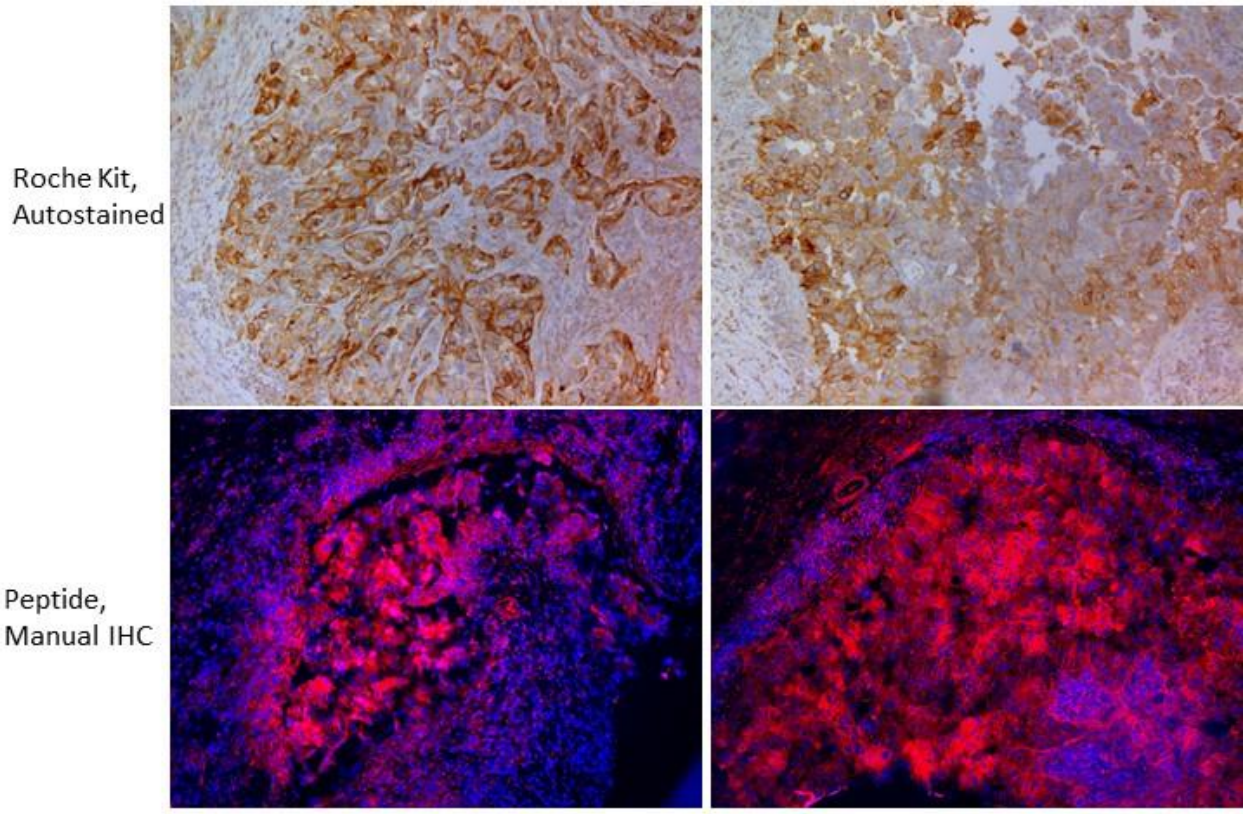

S45: Fluorescent IHC: NSCLC 'Patient G'

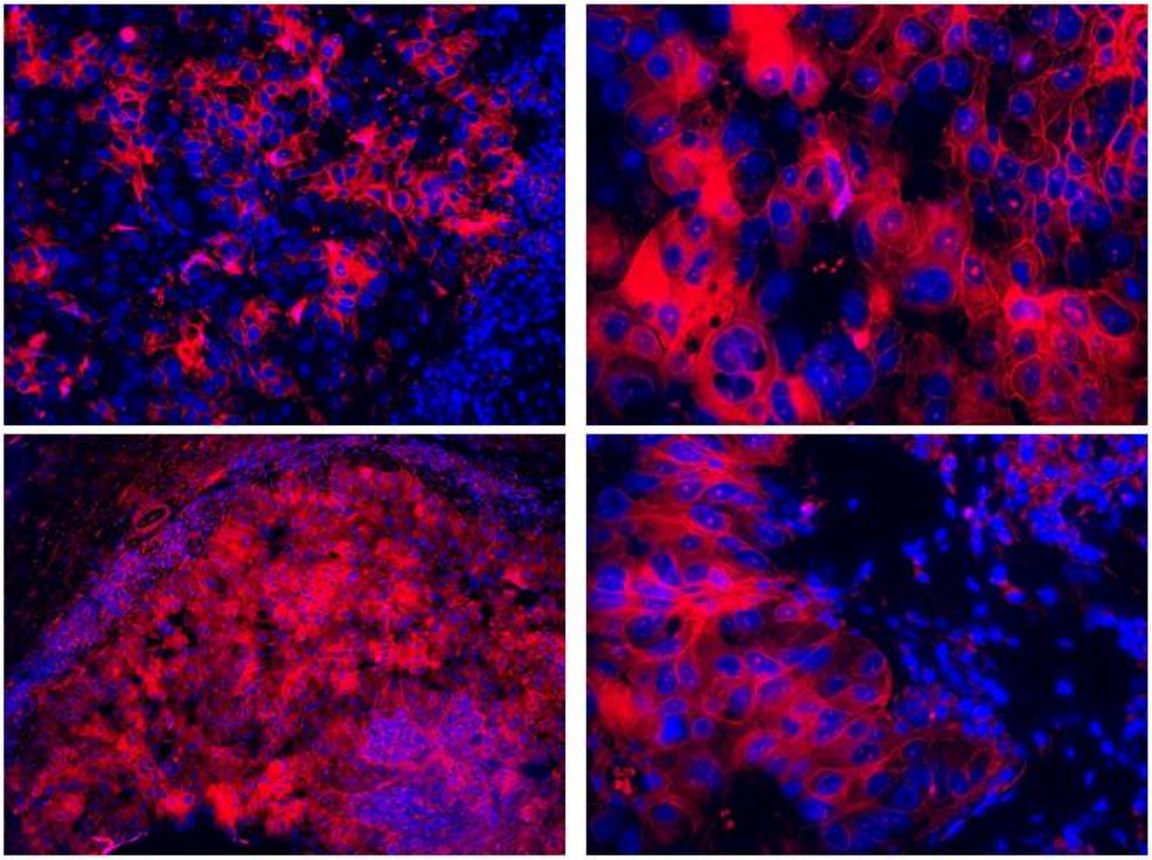

S46: Whole Slide Scan: NSCLC 'Patient G'

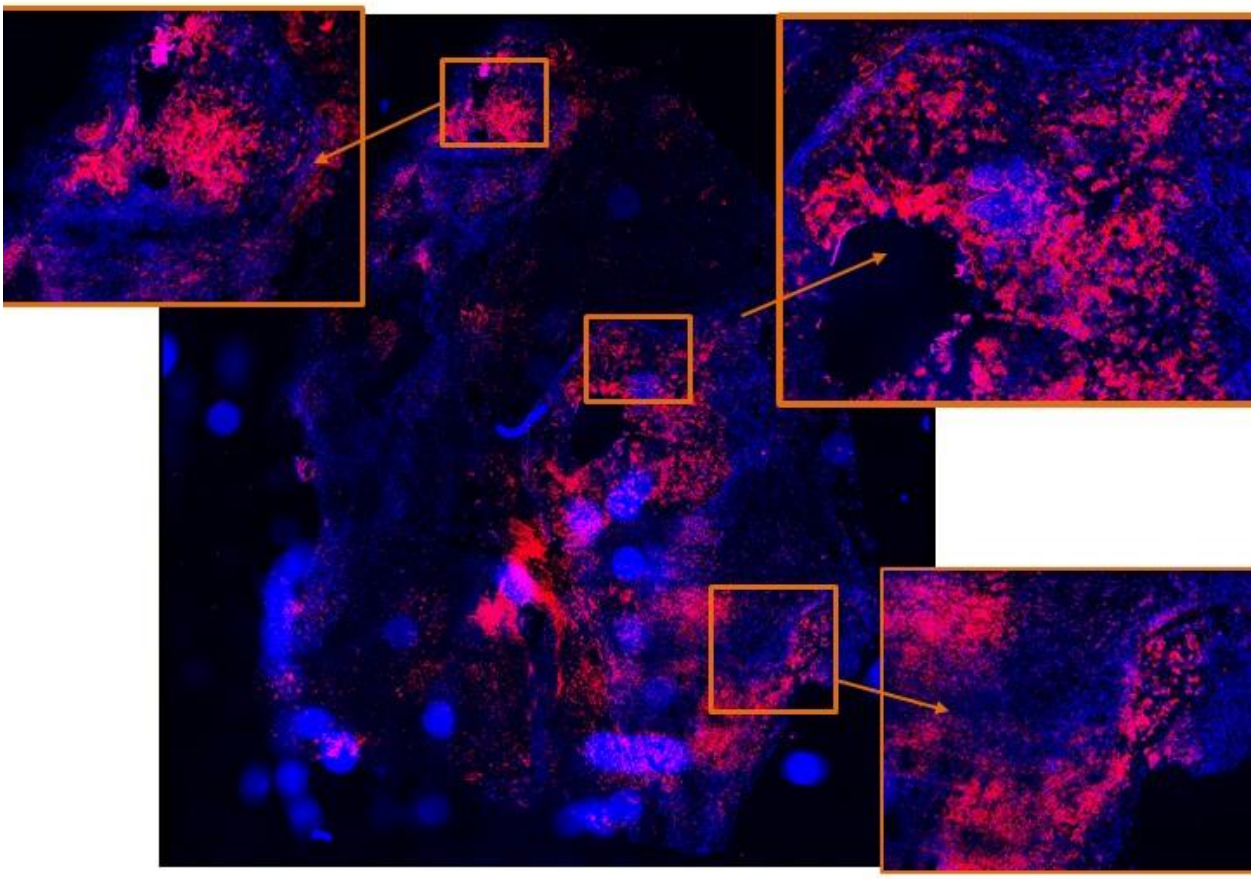

S47: TMA Used for Fluorescent IHC: LC1923

Microarray Panel Display

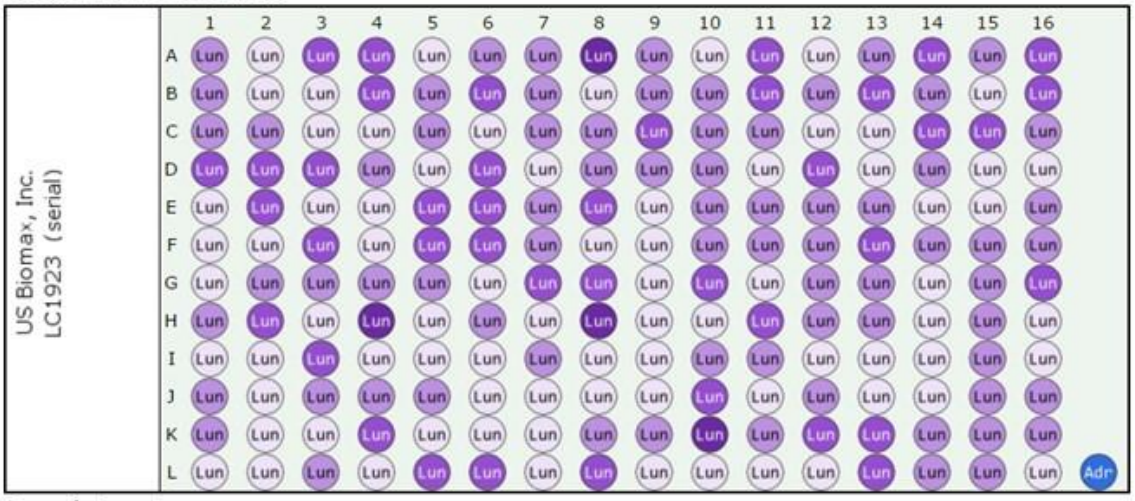

Legend: Lun - Lung
● - Malignant tumor, ● - Malignant tumor (stage I), ● - Malignant tumor (stage IA), ● - Malignant tumor (stage IB), ● - Malignant tumor (stage IIA), ● - Malignant tumor (stage IIB), ● - Malignant tumor (stage IIIA), ● - Malignant tumor (stage IIIB), ● - Malignant tumor (stage IV)

S48: 40x Image of NSCLC Tumor Spot

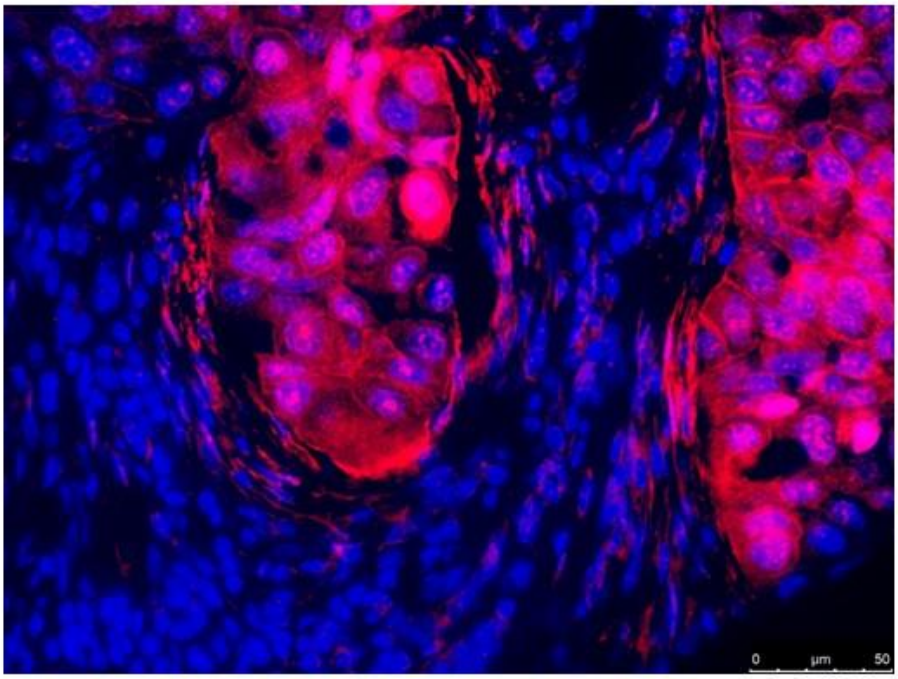

S49: Double Negative Spot

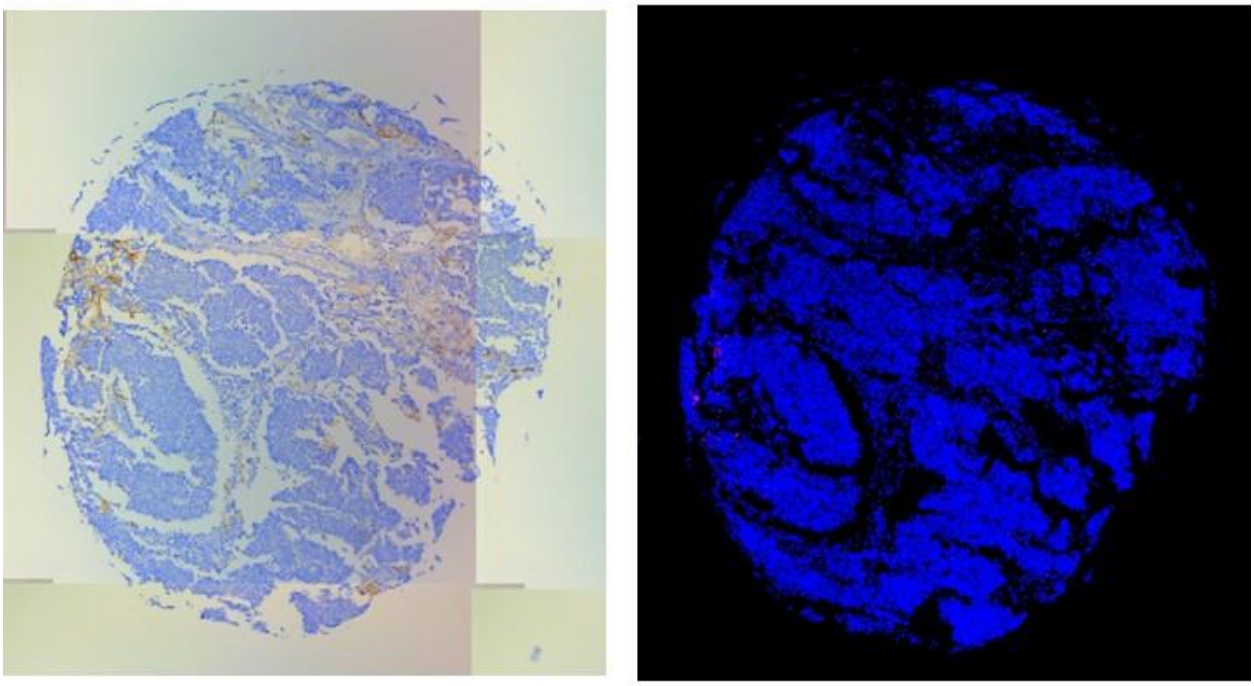

S50: Double Positive Spot

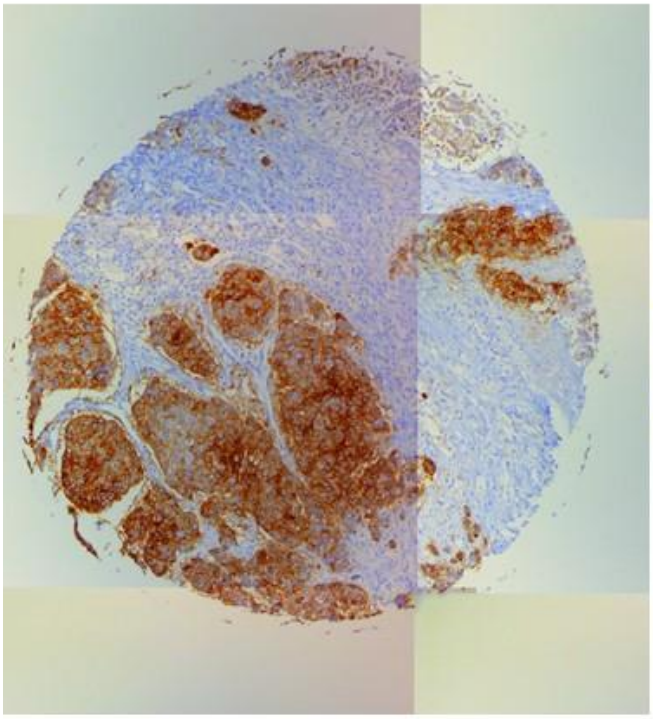

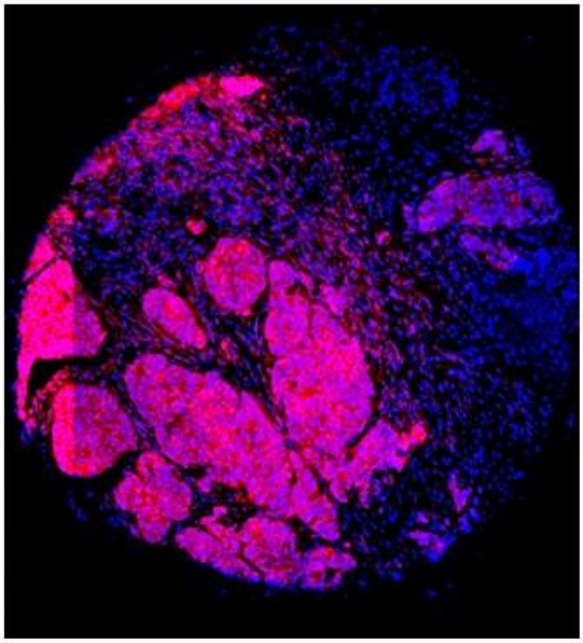

S51: Peptide Positive, Roche Negative

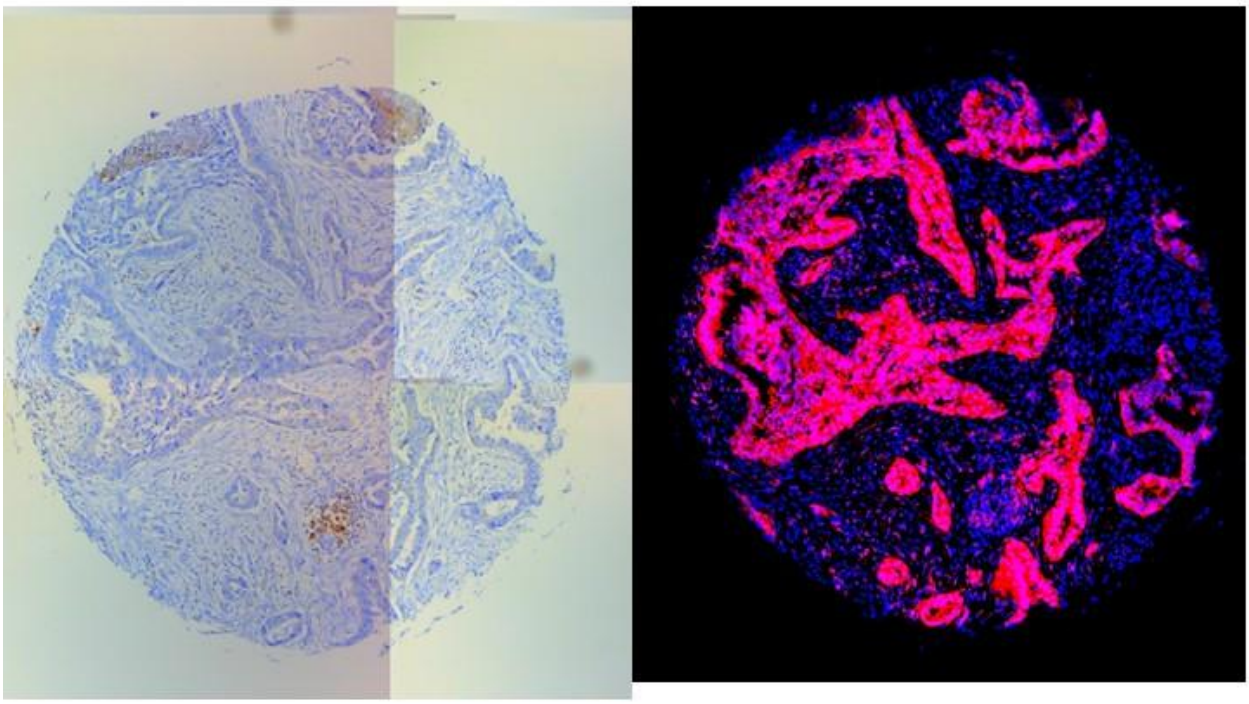

S52: Double Positive Spot

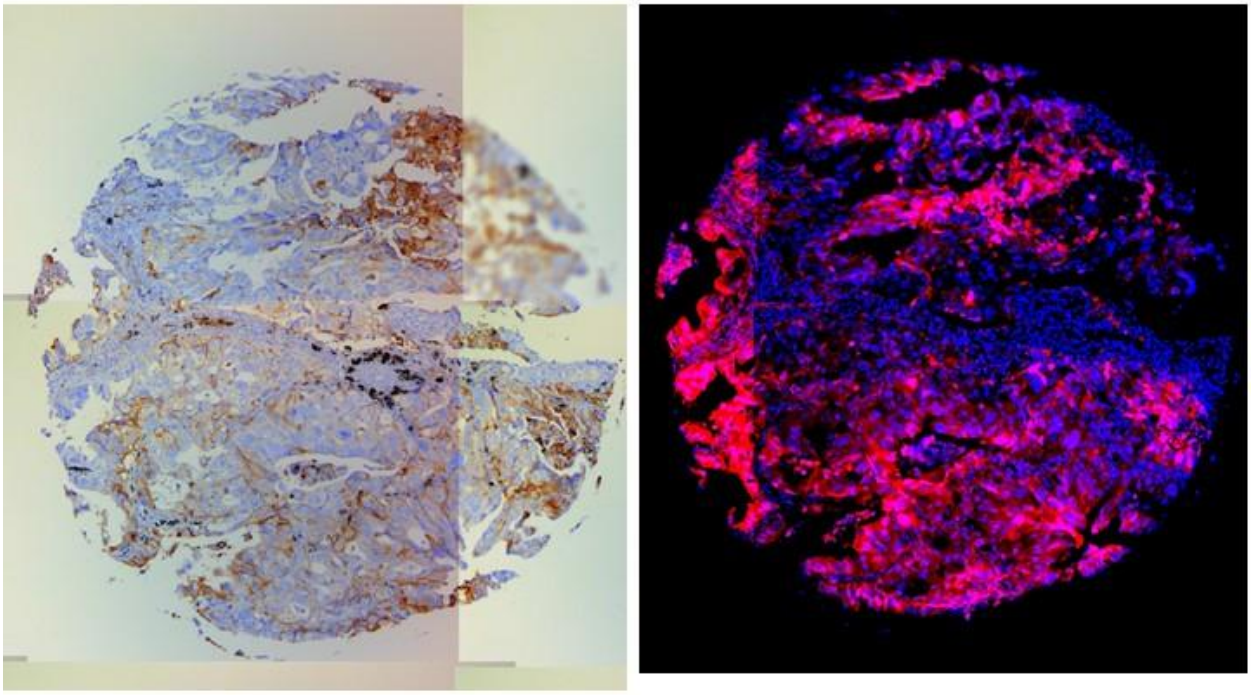

S53: Double Positive Spot

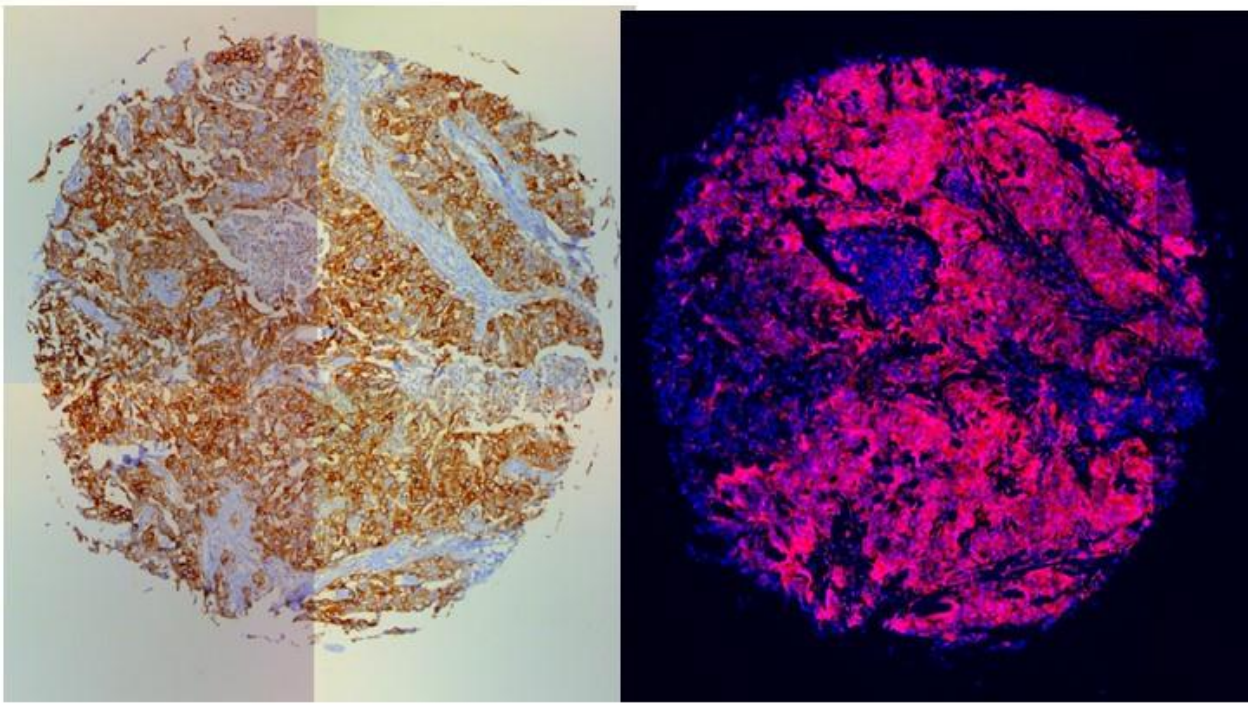

S54: Double Positive Spot

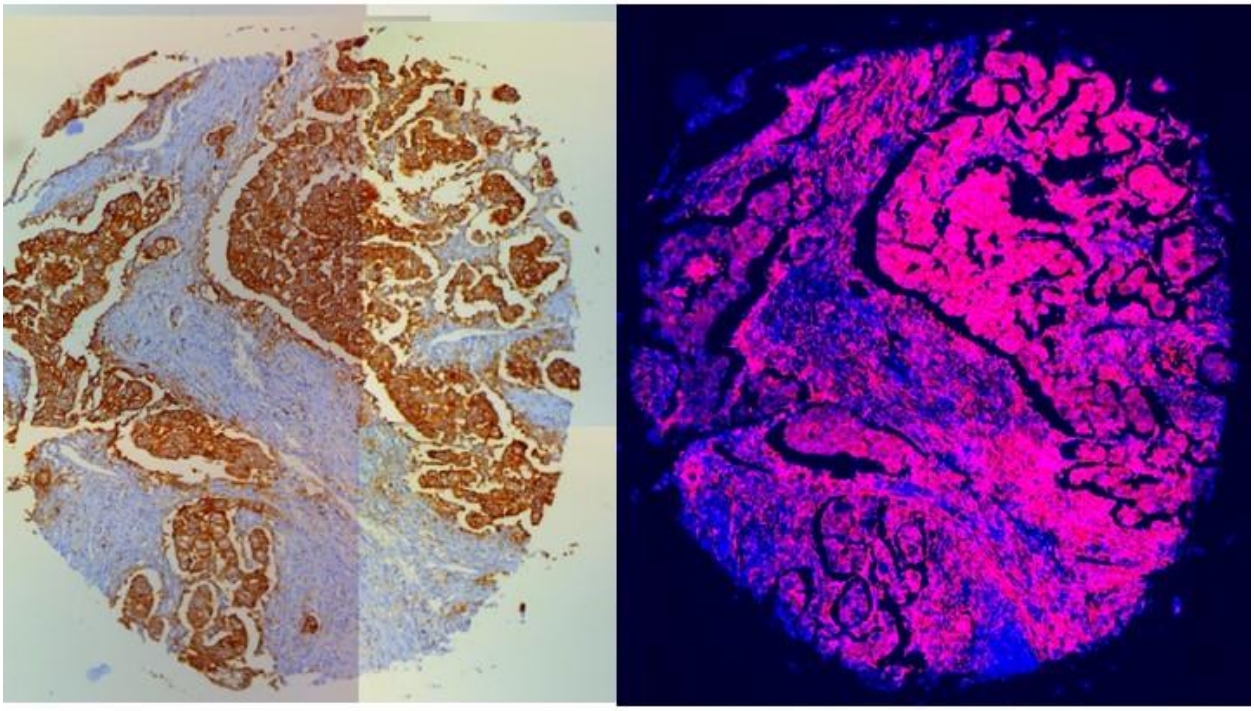

S55: Peptide Positive, Roche Negative

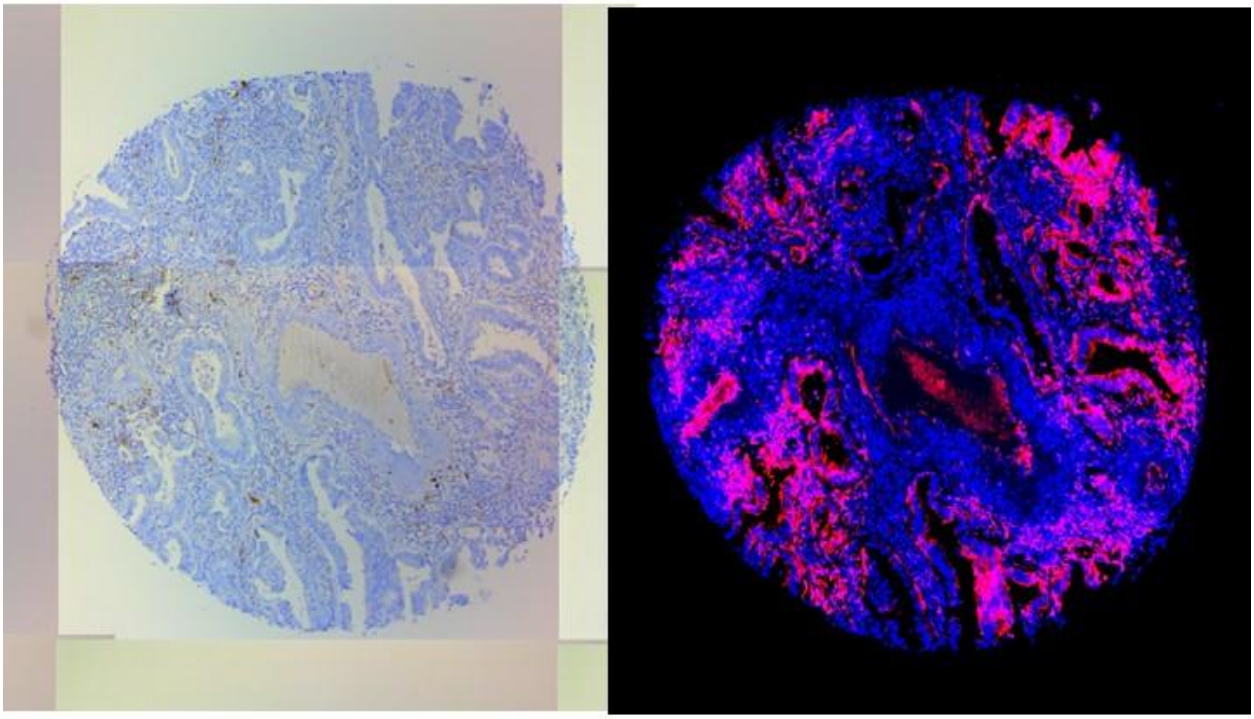

S47: Peptide Positive, Roche Negative

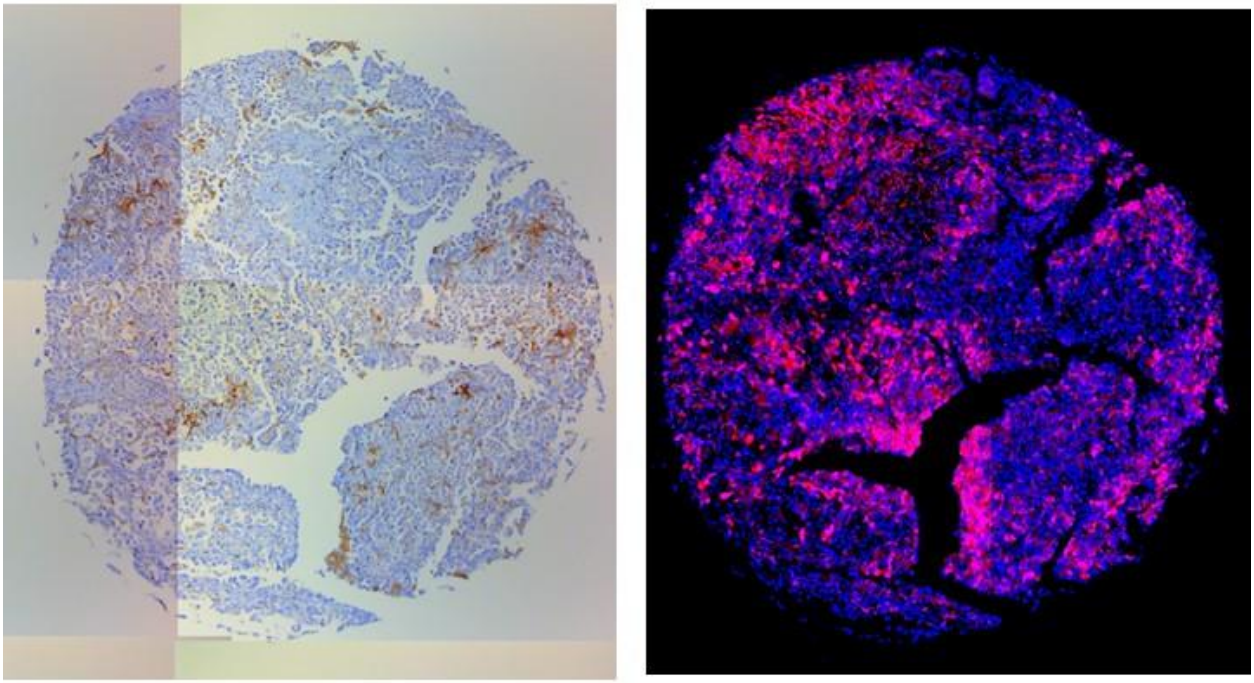

S56: Peptide Positive, Roche Negative

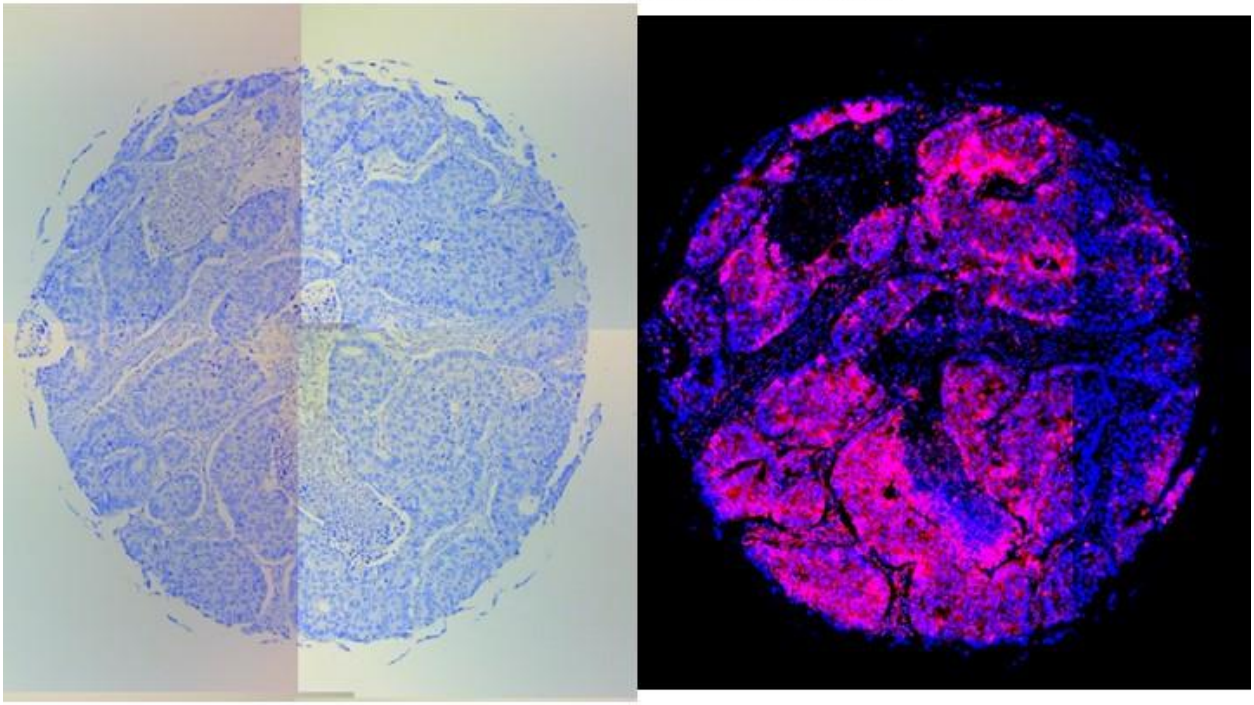

S57: Peptide Positive, Roche Negative

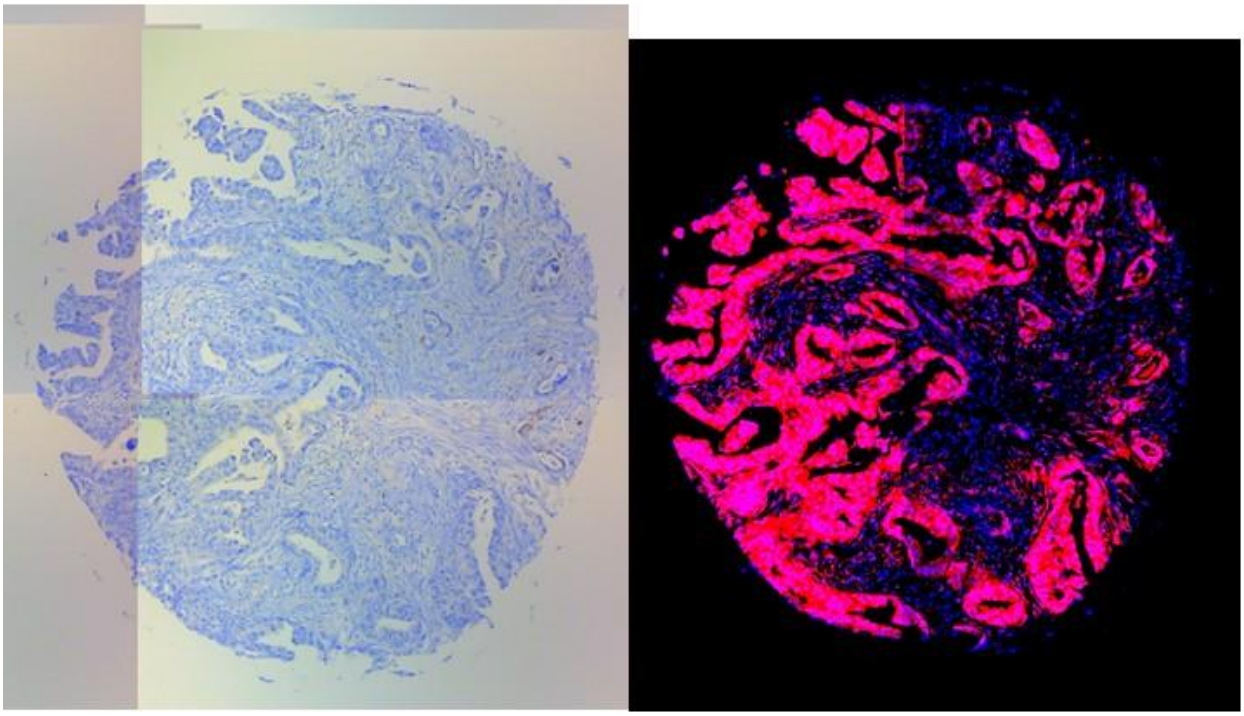

S58: Peptide Positive, Roche Negative

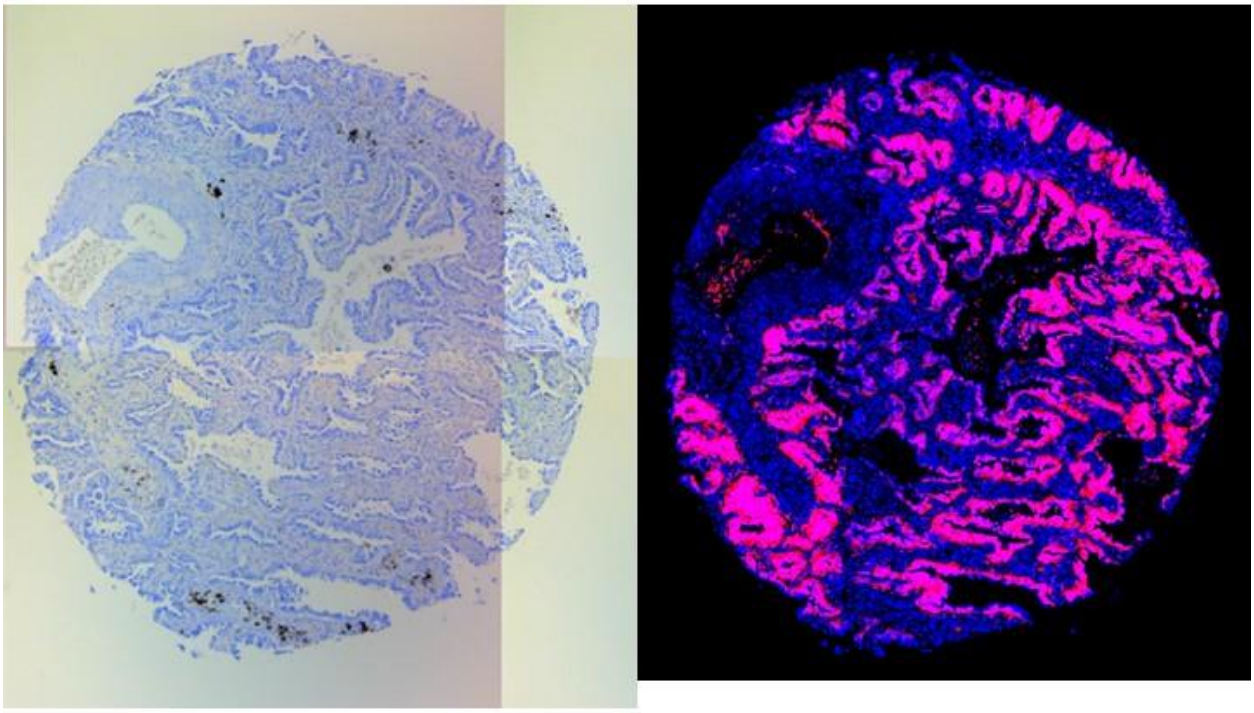

S59: Peptide Positive, Roche Negative

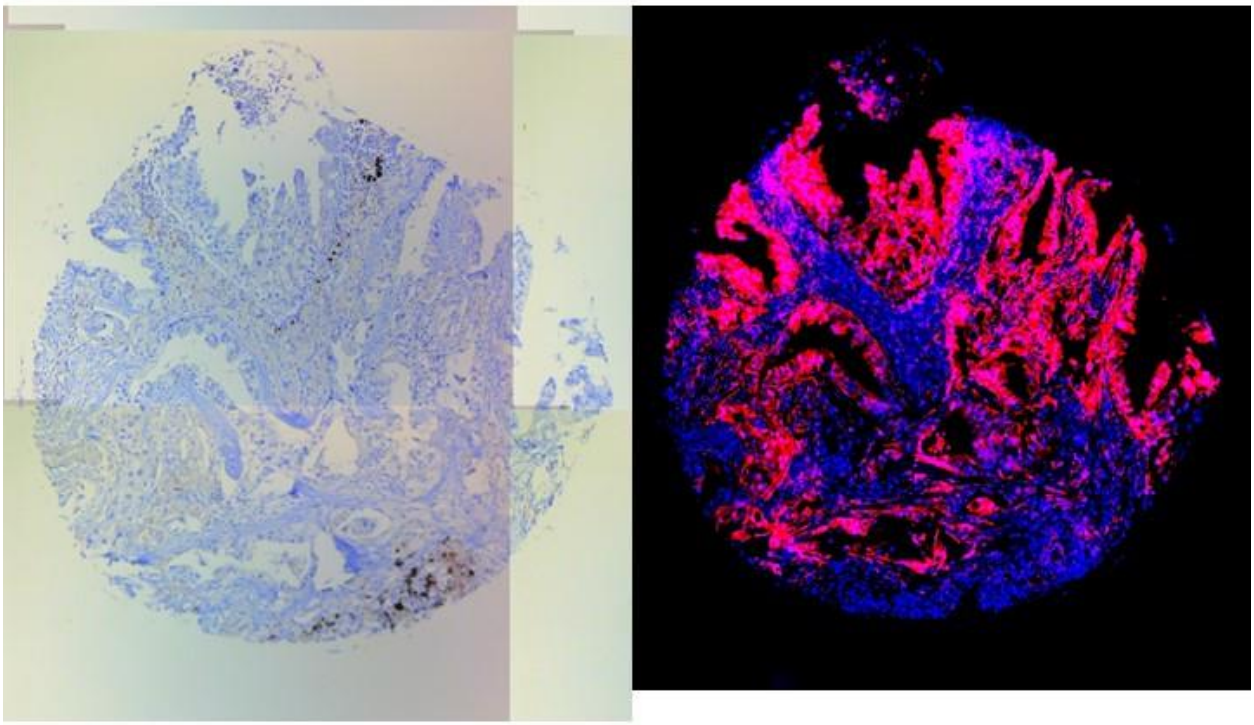

S52: Peptide Positive, Roche Negative

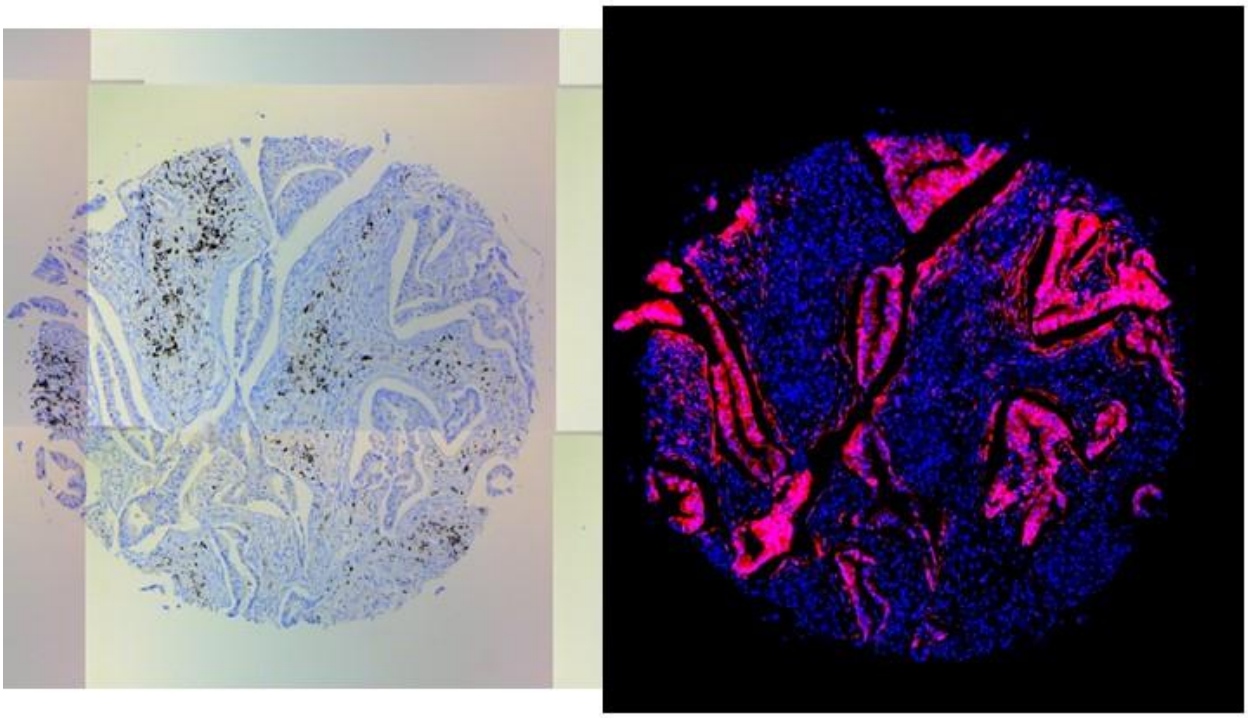

S53: Peptide Positive, Roche Negative

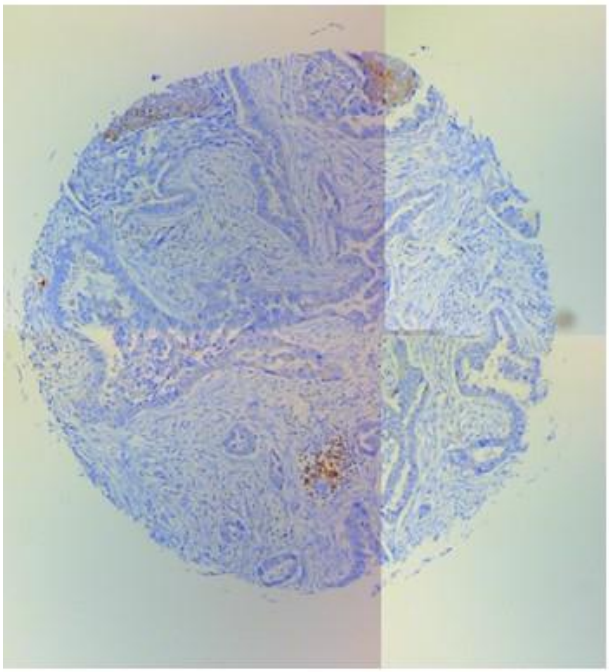

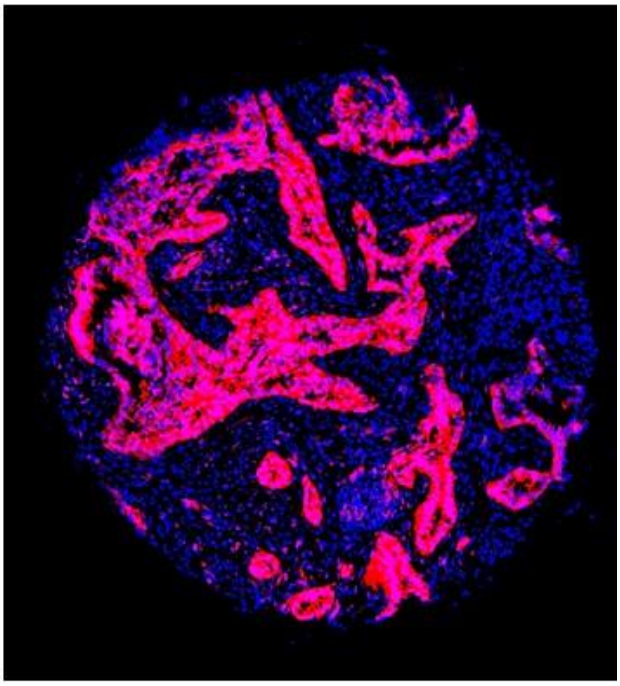

S54: Peptide Positive, Roche Negative

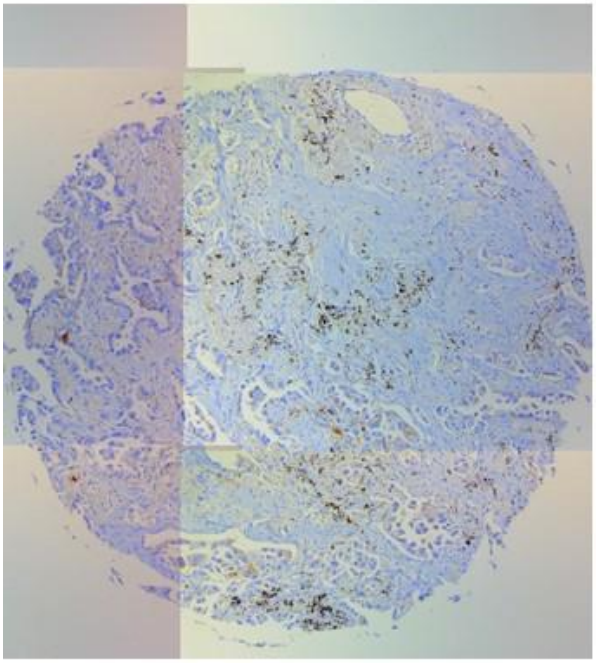

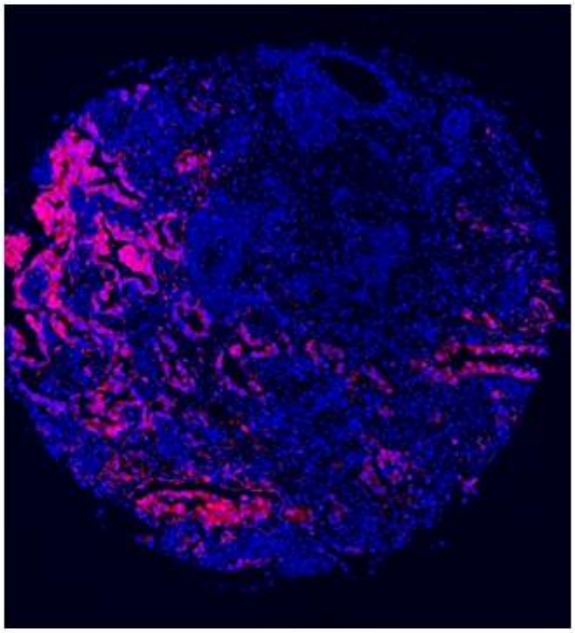

S55: Peptide Positive, Roche Negative

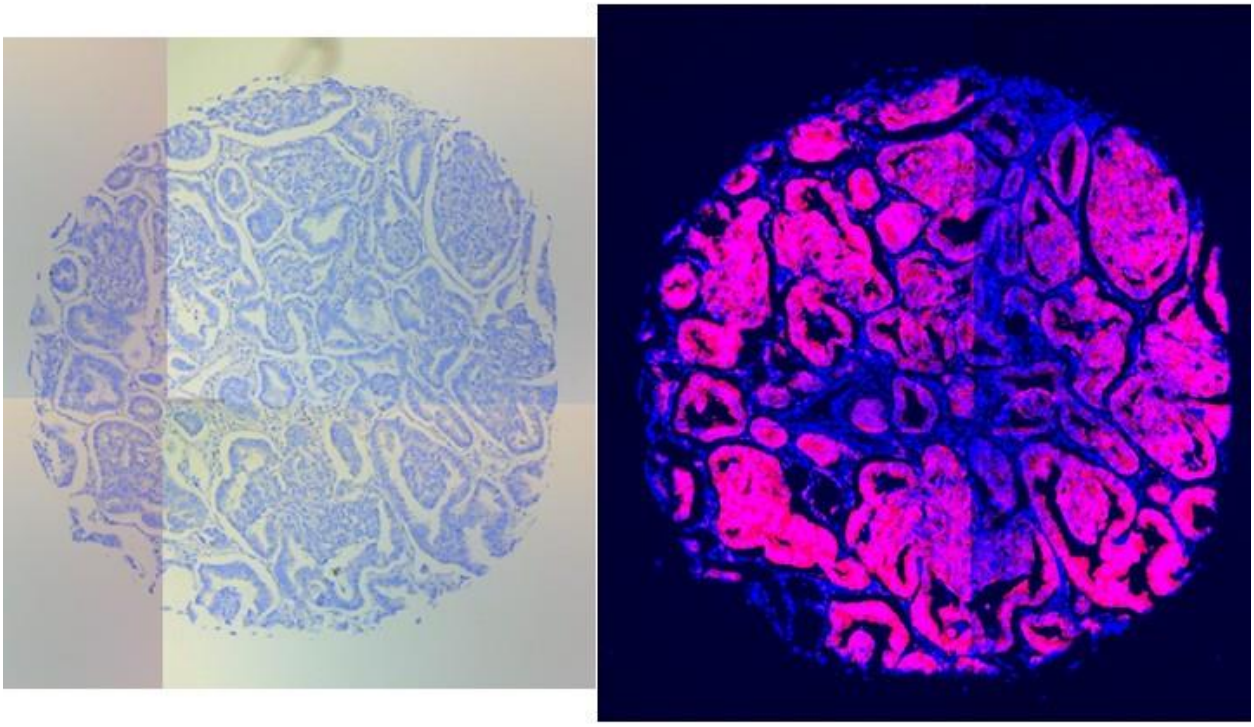

S56: Peptide Positive, Roche Negative

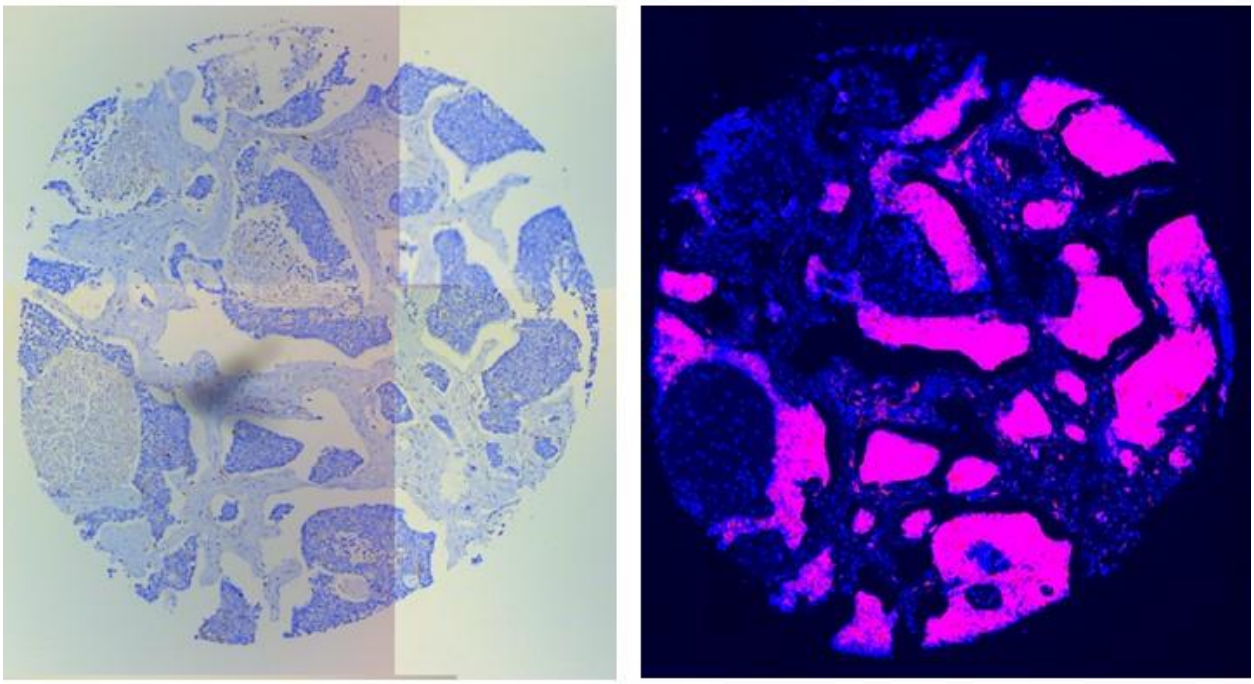

6.0 Vita

Charles “Chuck” Caldwell jr. was born in Columbia, MO on August 4th, 1987. He obtained his Bachelor of Science degree in Biological Engineering from the University of Missouri in December 2010. He joined Dr. Raghuraman Kannan’s group in August 2010 and began his work on novel tissue diagnostics in 2012. Upon graduation in December 2016 he will continue his work on tumor biomarker analysis at the University of Colorado Anschutz Medical Campus.